
THOMAS FRIEDRICH MOHR

2013

Phase Behavior
Of Colloidal Suspensions
With Critical Solvents



MAX-PLANCK-INSTITUT FÜR INTELLIGENTE SYSTEME
& UNIVERSITÄT STUTTGART

Phase behavior of colloidal suspensions with critical solvents

Von der Fakultät Mathematik und Physik der Universität
Stuttgart zur Erlangung der Würde eines Doktors der
Naturwissenschaften (Dr. rer. nat.) genehmigte Abhandlung

Vorgelegt von
Thomas F. Mohry
aus Leonberg

Hauptberichter: Prof. Dr. Siegfried Dietrich
Mitberichter: Prof. Dr. Christian Holm

Tag der Einreichung: 21. November 2012
Tag der mündlichen Prüfung: 04. Februar 2013

Max-Planck-Institut für Intelligente Systeme &
Institut für Theoretische Physik IV, Universität Stuttgart

2013

Erklärung

Stuttgart, den 21. November 2012

Hiermit erkläre ich gemäß § 5 Absatz (3) der Prüfungsordnung der Universität Stuttgart, dass ich, abgesehen von den ausdrücklich bezeichneten Hilfsmitteln und den Ratschlägen von jeweils namentlich aufgeführten Personen, die Dissertation selbständig verfasst habe.

Thomas F Mohry

Table of contents

Erklärung	3
Table of contents	5
1. Zusammenfassung	7
2. Introduction	15
3. Thermodynamics, phases, and critical phenomena	21
3.1. Phases and phase transitions	21
3.2. Bulk critical phenomena	23
3.3. Critical phenomena in inhomogeneous systems	28
3.4. The critical Casimir force	33
3.5. Theoretical approaches	38
4. Colloidal suspensions	45
4.1. Interactions	45
4.2. Structure	46
4.3. Thermodynamics	47
4.4. Stability	49
4.5. Density functional theory	50
5. Dependence of critical Casimir forces on bulk fields	53
5.1. Landau theory	53
5.2. Local functional approach	60
5.3. Dimensional comparison and approximation	63
5.4. Derjaguin approximation	67
6. Effective model	73
6.1. Range of parameters	74
6.2. Shapes of the effective potential	76
7. Structure and stability	79
7.1. Structure	79
7.2. Stability	82
7.3. Comparison with experiments	87

8. Thermodynamics	95
8.1. General discussion	95
8.2. Scaling of the critical point shift	98
8.3. Effective one-component approach	99
8.4. Phase diagrams	100
9. Conclusions	107
9.1. Outlook	107
9.2. Summary	111
Acknowledgments	117
A. Bulk critical properties within Landau theory	119
B. The critical Casimir force within the local functional approach	121
C. Properties of water lutidine mixtures	125
C.1. The non-universal amplitude of the order parameter	125
C.2. Permittivity	126
Technical tools	127
References	129

1. Zusammenfassung

Die typischen Längenskalen unseres (makroskopischen) Alltages erstrecken sich von einigen Millimetern bis zu mehreren Metern oder gar Kilometern. Bei dem menschlichen Streben, zu finden “was die Welt im Innersten zusammenhält”¹, fanden Physiker auf der mikroskopischen Skala, d.h. in der Größenordnung von Ångström (10^{-10}m), die Atome, welche die Bausteine der uns umgebenden Materie bilden. Auf noch kleineren Längenskalen wurden subatomare Teilchen gefunden, welche die Bausteine der Atome sind. Zwischen den mikroskopischen und den makroskopischen Längenskalen befindet sich “Die Welt der vernachlässigten Dimensionen”^{2,3} – so nannte W. Ostwald 1915 seine Einführung in die Kolloidchemie. Heutzutage wird der Forschungsbereich weiter gefasst (und nicht nur als Teilbereich der Chemie betrachtet) und kolloidale Systeme werden oft auch als weiche Materie oder komplexe Flüssigkeiten bezeichnet⁴. Kolloidale Systeme sind dadurch charakterisiert, dass einige ihrer Bestandteile eine typische Längenskala von einigen Nanometern (10^{-9}m) bis zu einigen Mikrometern (10^{-6}m) besitzen. Kolloidale Mischungen bestehen häufig aus Partikeln in einem flüssigen Lösungsmittel. Solche kolloidalen Dispersionen werden in dieser Arbeit betrachtet. Jedoch können kolloidale Systeme ebenso ein Gemisch aus gasförmigen, flüssigförmigen, und/oder festen Bestandteilen sein. Die Art der Bestandteile ist sehr vielfältig. Neben festen Partikeln können die Teilchen selbst aus kleineren Einheiten aufgebaut sein, wie etwa Polymere oder Mizellen. Eine frühe Abhandlung über die Vielfältigkeit von kolloidalen Systemen kann beispielsweise in dem Werk von Ostwald oder in der “Einführung in Kolloidchemie” von H. Staudinger⁵ gefunden werden. Wegen der Charakteristika von kolloidalen Mischungen sind in diesen innere Grenzflächen, d.h. deren Eigenschaften und ihr Beitrag zur freien Energie, von Bedeutung. Die Energieskala dieser Systeme ist im Bereich der thermischen Energie $k_B T$; T ist die Temperatur und $k_B = 1.38 \times 10^{-23} \text{J/K}$ ist die Boltzmann-Konstante⁶. Daher ist neben der Wechselwirkungsenergie zwischen den Bestandteilen in kolloidalen Systemen auch die Entropie dieser Systeme von Bedeutung, woraus sich ein interessantes

¹ Ausspruch der Hauptperson, dem Gelehrten Heinrich Faust, in J. W. von Goethe, *Faust*, J. G. Cotta (Tübingen), 1808.

² W. Ostwald, *Die Welt der vernachlässigten Dimensionen: eine Einführung in die moderne Kolloidchemie; mit besonderer Berücksichtigung ihrer Anwendungen*, Steinkopff (Dresden), 12. Aufl., 1944.

³ Auf eine ausführliche Referenzliste wird in dieser Zusammenfassung verzichtet. Es werden nur einige deutschsprachige Publikationen, zumeist allgemeine Übersichtsartikel, zitiert. Für eine umfassendere Referenzliste wird auf die Liste des Hauptteiles verwiesen.

⁴ H. Löwen, *Was ist hart an der Weichen Materie? Ein Streifzug durch das interdisziplinäre Gebiet der Kolloide und Polymere*, *Physik Journal* **7/8**, 51 (2003).

⁵ H. Staudinger, *Organische Kolloidchemie*, Vieweg (Braunschweig), 1940.

⁶ Zur Bestimmung des Wertes von k_B , siehe bspw.: PTB, *Erster Wert der PTB für die Boltzmann-Konstante* *PTBnews* **2**, 1 (2011).

Wechselspiel dieser Einflüsse ergibt⁷. Schon W. Ostwald relativierte die ‘Vernachlässigung’ in seinem Vorwort, in welchem er über die kolloidalen Systeme als “so lange schon existierende, aber so kurz erst wirklich erkannte Welt merkwürdiger Phänomene und eigenartiger Gedanken” schreibt. Eventuell produziert die Kolloidforschung weniger publikumsträchtige Schlagzeilen, dafür jedoch, wie schon W. Ostwald in dem Untertitel seines Buches andeutet, zahlreiche Anwendungen für unser alltägliches Leben. Hierzu zählen beispielsweise Farben, Zahnpasta oder die Gegenstände, für welche aktuell eine Mengenbeschränkung von 100ml in Flugzeugen gilt. Die zahlreichen Anwendungen resultieren unter anderem aus der Vielfältigkeit der möglichen Bestandteile von kolloidalen Systemen. Diese Variationsmöglichkeiten erlauben es, die effektiven Wechselwirkungen zwischen den (großen) Bestandteilen zielgerichtet zu manipulieren, beispielsweise für eine Anwendung zu optimieren. Diese effektiven Wechselwirkungen ergeben sich durch das Vorhandensein der weiteren Bestandteile und werden indirekt über diese vermittelt (siehe die Referenz in Fußnote 4). Zwar sind diese effektiven Wechselwirkungen im allgemeinen nicht paarweise additiv, jedoch ist häufig die Beschränkung auf das effektive Paar-Wechselwirkungspotential zulässig⁸. Wegen der kontrollierbaren Variabilität der effektiven Wechselwirkungen und ihrer guten experimentellen Untersuchbarkeit eignen sich kolloidale Systeme in einer herausstechenden Art und Weise als Modellsysteme für atomare Systeme und als paradigmatische Systeme der statistischen Physik⁹. Schließlich besitzen diese kolloidalen Systeme auch sehr spezifische, sie auszeichnende Eigenschaften, so dass sie selbst ein interessantes, herausforderndes Gebiet der Physik darstellen. Hiervon zeugt nicht zuletzt der Nobelpreis an P.-G. de Gennes, einen der ‘Gründerväter’ der theoretischen Kolloidforschung¹⁰.

Die dispergierten Kolloidteilchen verändern die Struktur des Lösungsmittels auf der Skala seiner Korrelationslänge. Für atomare oder molekulare Lösungsmittel, wie sie hier betrachtet werden, ist daher in vielen Situationen das Lösungsmittel nur in einer sehr dünnen, d.h. einige Ångström dicken, Schicht um die Kolloide herum durch deren Präsenz beeinflusst. Dies ändert sich fundamental, wenn die binäre Flüssigkeitsmischung, die als Lösungsmittel dient, in ihrer kritischen Konzentration mittels einer Veränderung der Temperatur an ihren kritischen Punkt eines Entmischungs-Phasenüberganges gebracht wird. Bei einem Phasenübergang wechselt das System von einem sogenannten ‘ungeordneten’ in einen ‘geordneten’ Zustand (oder vice versa)¹¹. Es gibt für den Phasenübergang eine quantitative Messgröße, den Ordnungsparameter Φ , dessen Wert von einem dazugehörigen Kontrollparameter \mathcal{C} abhängt. \mathcal{C} ist meistens die Temperatur T und der Ordnungsparameter Φ ist der Dichteunterschied ($\rho - \rho_c$) zur kritischen

⁷ C. Bechinger, H. H. von Grünberg, und P. Leiderer, *Entropische Kräfte*, *Phys. Blätt.*, **55**, 53 (1999); H. H. von Grünberg und C. Bechinger, *Die Attraktivität von Unordnung, Spektrum der Wissenschaft*, **6**, 16 (2000).

⁸ C. Bechinger und H. H. von Grünberg, *Wenn drei Körper mehr sind als drei Paare Mehrkörper-Wechselwirkungen in kolloidalen Systemen*, *Physik Journal* **11**, 33 (2004).

⁹ C. Bechinger, *Physik mit kolloidalen Suspensionen*, *Phys. Blätt.* **56**, 75 (2000).

¹⁰ T. Vilgis und K. Kremer, *Nachruf auf Pierre-Gilles de Gennes*, *Physik Journal* **8/9**, 116 (2007).

¹¹ W. Gebhardt und U. Krey, *Phasenübergänge und kritische Phänomene*, Vieweg (Braunschweig), 1980.

Dichte, die Differenz $(c_a - c_{a,c})$ der Konzentration von ihrem kritischen Wert oder die Magnetisierung m für einfache Flüssigkeiten, für binäre Flüssigkeitsmischungen beziehungsweise für uniaxiale Ferromagneten. An dem Phasenübergang ändert sich der Wert des Ordnungsparameter Φ qualitativ aufgrund einer kontinuierlichen Änderung des Kontrollparameters \mathcal{C} und zwar von $\Phi = 0$ in der ungeordneten Phase zu Werten $\Phi \neq 0$ in der geordneten Phase. An einem Phasenübergang erster Ordnung ist diese Änderung sprunghaft von $\Phi = 0$ zu einem endlichen Wert $|\Phi| > 0$. An einem kritischen Punkt (oder allgemeiner: an einem kontinuierlichen Phasenübergang) nimmt der Wert von Φ als Funktion des Kontrollparameters $\mathcal{C} = t$ kontinuierlich endliche Werte an und zwar gemäß $\Phi(t \leq 0) \sim (-t)^\beta$ und $\Phi(t > 0) = 0$. β ist dabei ein kritischer Exponent und $t = \pm (T - T_c^{(s)})/T_c^{(s)}$ ist die reduzierte Temperaturabweichung von der kritischen Temperatur $T_c^{(s)}$ für einen oberen ($\pm = +$) bzw. unteren ($\pm = -$) kritischen Punkt. Viele binäre Flüssigkeitsmischungen, wie beispielsweise Lutidin-Wasser-Mischungen, haben einen (unteren) kritischen Punkt bei Umgebungsdruck und ihre kritische Temperatur ist im Bereich $T_c^{(s)} \sim (20 \dots 70)^\circ \text{C}$. Daher lassen sich die kritischen Zustandsbedingungen sowohl in Experimenten als auch in möglichen Anwendungen ohne Großapparaturen einstellen. In der Nähe eines kritischen Punktes divergiert die Korrelationslänge $\xi \sim |t|^{-\nu}$ des kritischen Materials als Funktion der reduzierten Temperaturabweichung t . ν ist ein weiterer kritischer Exponent. Die langreichweitigen Korrelationen in dem kritischen Medium werden durch die kritischen Fluktuationen induziert, deren Verteilungsfunktion genau am kritischen Punkt keine charakteristische Länge besitzt. Folglich sind die Fluktuationen skaleninvariant und diese Symmetrie der Selbstähnlichkeit überträgt sich auf das gesamte System. (Fast-) kritische Systeme zeichnen sich desweiteren durch ihre sogenannte Universalität aus. Dies bedeutet, dass es irrelevant ist, welche konkrete physikalische Größe fluktuiert. Relevant sind nur drei Eigenschaften und zwar die räumliche Dimension d des Systems, die Dimension d_Φ des entsprechenden Ordnungsparameters sowie ob die Reichweite der Wechselwirkungen zwischen den Teilchen des kritischen Mediums lang- oder kurzreichweitig ist. Systeme, welche diese drei Eigenschaften gemeinsam haben, bilden eine sogenannte Universalitätsklasse (siehe die Referenz in Fußnote 11). Somit ist das kritische Verhalten der bereits oben erwähnten Phasenübergänge in einfachen Flüssigkeiten, in binären Flüssigkeitsmischungen und auch in uniaxialen Magneten, welche alle zur Ising-Universalitätsklasse gehören, nicht nur qualitativ dasselbe, sondern auch quantitativ (gemessen in entsprechenden, sogenannten SkalenvARIABLEN) gleich. Die eingeführten Exponenten β und ν sind universelle Größen und in $d = 3$ gilt für die Ising-Universalitätsklasse $\beta = 0.3265(3)$ und $\nu = 0.6301(4)$. Dieses universelle Verhalten kann mittels der Renormierungstheorie begründet werden¹²

Da die Korrelationslänge divergiert, beeinflussen begrenzende Oberflächen das kritische Verhalten des gesamten Systems und jede oben benannte Volumen-Universalitätsklasse spaltet sich in mehrere Oberflächen-Universalitätsklassen auf. So ist etwa der Wert des Ordnungsparameters an der Oberfläche gegeben durch $\Phi_s(t < 0) \sim (-t)^{\beta_s}$, wobei

¹² K. G. Wilson, *Die Renormierungsgruppe*, *Spektrum der Wissenschaft* **10**, 66 (1979); Übersetzung aus dem Englischen, Originalartikel erschienen im *Scientific American*.

der Wert, i. A. $\beta_s \neq \beta$, des kritischen Oberflächenexponenten β_s von der Oberflächen-Universalitätsklasse abhängt. Räumliche Beschränkungen verändern ebenso das kritische Verhalten. In einem Film der Dicke L , dessen Oberflächen die gleiche Phase adsorbieren, weicht die kritische Temperatur um $T_c(L) - T_c^{(s)} \sim L^{-1/\nu}$ von der kritischen Temperatur $T_c^{(s)}$ im unendlich ausgedehnten Volumen ab. In Filmen, deren Oberflächen unterschiedliche Phasen adsorbieren, ergibt sich ein komplizierteres Verhalten. Die räumlichen Beschränkungen des (fast-) kritischen Systems beeinflussen auch das Profil des Ordnungsparameters und beschränken das Spektrum der kritischen Fluktuationen. Daraus resultiert eine effektive Kraft, die sogenannte kritische Casimir Kraft f_C , welche auf die begrenzenden Oberflächen wirkt. Das Vorzeichen der kritischen Casimir Kraft hängt von den Oberflächen-Universalitätsklassen der Begrenzungen ab. Für symmetriebrechende Oberflächen ist die kritische Casimir Kraft attraktiv, wenn beide Oberflächen die gleiche Phase adsorbieren und repulsiv wenn die zwei Oberflächen je eine andere Phase adsorbieren. 30 Jahre nachdem M. E. Fisher und P.-G. de Gennes die kritische Casimir Kraft 1978 vorhersagten, wurde sie von C. Hertlein und Kollegen zwischen einem Kolloidteilchen und einer planaren Wand direkt gemessen¹³. Es kann erwartet werden, dass solch eine zusätzliche attraktive Kraft zwischen den Kolloidteilchen (der gleichen Sorte) deren Stabilität im Lösungsmittel beeinflusst. Andererseits werden die kolloidalen Partikel, die als Aussparungen im kritischen Medium wirken, das Phasenverhalten des kritischen Lösungsmittels beeinflussen. Schon 1985 beobachteten D. Beysens und D. Estève eine Aggregation¹⁴ von Kolloidteilchen in einer fast-kritischen Wasser-Lutidin Mischung. Darauf folgten weitere Experimente und theoretische Untersuchungen, um solche kolloidalen Dispersionen mit phasen-separierendem molekularem Lösungsmittel zu verstehen. Unter anderem wegen den unterschiedlichsten Mechanismen, welche in solchen Mischungen von Bedeutung sind, sowie weil verschiedenste Längenskalen, die mehrere Größenordnungen umspannen, relevant sind, ist bisher weder das beschriebene Aggregations-Experiment genau verstanden, noch gibt es ein klares Verständnis über das Phasenverhalten solcher Mischungen. Das Ziel dieser Arbeit ist es, zu diesen Aspekten einen Beitrag zu liefern.

Im ersten Teil der Resultate (Kap. 5) wird das vorhandene Wissen über die kritische Casimir Kraft f_C vertieft. Dabei wurde hauptsächlich die Filmgeometrie betrachtet und der Einfluss des äußeren Feldes h_b (konjugiert zum Ordnungsparameter Φ) berechnet. Für binäre Flüssigkeitsmischungen ist dieses äußere Feld $h_b \sim (\mu_a - \mu_b) - (\mu_a - \mu_b)_c$ der Wert von der Abweichung der Differenz $(\mu_a - \mu_b)$ von ihrem kritischen Wert $(\mu_a - \mu_b)_c$. μ_a und μ_b sind die chemischen Potentiale der Teilchensorten a und b . Für Filme, deren Oberfläche die gleiche Phase adsorbieren, stellt sich heraus, dass die Stärke $|f_C|$ der kritischen Casimir Kraft für kleine negative Werte von h_b merklich zunimmt. In den räumlichen Dimensionen $d = 4$ und $d = 3$ und für $t > 0$ nimmt die Stärke um einen Faktor von bis zu 7 beziehungsweise 10 zu, im Vergleich zu dem Wert von f_C bei $h_b = 0$. Für Temperaturen $t < 0$, bei welchen es im Volumen Phasen-Koexistenz gibt, kann

¹³ K. Mecke, *Die Kraft kritischer Fluktuationen*, *Physik Journal* **3**, 16 (2008).

¹⁴ Auf eine Ausdifferenzierung zwischen Aggregation, Koagulation, und Flokkulation wird hier vermieden. Hier werden sie gleichbedeutend als eine strukturelle Instabilität verwendet.

die effektive Kraft zwischen den zwei einschließenden Oberflächen sogar noch stärker werden. Für noch negativere Werte von t wird die effektive Kraft hauptsächlich im Bereich des Phasendiagramms zwischen der Film- und der Volumen-Phasenkoexistenzlinie extrem stark. Mittels der sogenannten Derjaguin-Näherung kann die kritische Casimir Kraft zwischen zwei großen kugelförmigen Teilchen aus den Ergebnissen für die kritische Casimir Kraft in der Filmgeometrie berechnet werden.

Im zweiten Teil (Kap. 7) wird untersucht, unter welchen Umständen die kolloidale Dispersion wegen der auftretenden stark attraktiven kritischen Casimir Kraft strukturell instabil wird. Bei solch einer strukturellen Instabilität bilden sich Aggregate, welche sich aus der Dispersion lösen und sedimentieren. Wegen der beschriebenen stärkeren kritischen Casimir Kraft bei $h_b \neq 0$ tritt diese Aggregation auf, wenn die binäre Flüssigkeitsmischung etwas ärmer (als in der kritische Konzentration) in der Komponente ist, die von den Kolloidteilchen adsorbiert wird. Dies ist ein Befund, der sowohl experimentell als auch theoretisch belegt ist. Es wurden zwei verschiedene Szenarien für die Aggregation identifiziert. In dem einen Fall ist die Stärke des (kurzreichweitigen) repulsiven Anteils in der effektiven Wechselwirkung zwischen den Kolloidpartikeln zwar stark genug, um die Dispersion für hinreichend große Werte $t > 0$ zu stabilisieren, jedoch ist die Stärke kleiner als jene der kritischen Casimir Kraft f_C . In diesem Falle kompensiert die attraktive Kraft f_C die gesamte Repulsion im effektiven Wechselwirkungspotential. Wegen der Attraktivität der kritischen Casimir Kräfte nähern sich die Kolloidpartikel an und berühren sich schließlich in den Aggregaten. In den Aggregaten werden die Kolloidpartikel durch Kräfte zwischen den Oberflächen, welche auf mikroskopischen Längenskalen wirken, zusammengehalten. Diese Oberflächenkräfte sind sehr materialspezifisch, so dass nur der Beginn dieses Aggregationprozesses den universellen Charakter kritischer Phänomene besitzt und der weitere Verlauf sowie die Struktur der gebildeten Aggregate stark von den speziellen Eigenschaften des Lösungsmittels und der Kolloidpartikel abhängen. Da die Oberflächenkräfte typischerweise sehr stark sind, bleiben die so gebildeten Aggregate auch bei einer Entfernung von der kritischen Temperatur bestehen. Zwar besitzt das effektive Wechselwirkungspotential dann, für große Werte von $t > 0$, wieder eine repulsive Barriere, jedoch hemmt diese (zusätzlich zu den starken Oberflächenkräften) ein Auseinanderbrechen der Aggregate.

Im zweiten Fall bleibt die repulsive Barriere im effektiven Paar-Wechselwirkungspotential auf kurzen Abständen zwischen den Kolloidpartikeln bestehen und bei etwas größeren Abständen bildet sich ein sogenanntes sekundäres Minimum heraus. Die Tiefe dieses Potentialminimumes kann einige Vielfache der thermischen Energie $k_B T$ betragen. Zwar ist auch in diesem Fall die genaue Abhängigkeit der Stärke des effektiven Wechselwirkungspotentials als Funktion des Abstandes von nicht-universellen Eigenschaften der Bestandteile der kolloidalen Dispersion abhängig, jedoch lassen sich diese Abhängigkeiten in guter Näherung in zwei relevante Parameter zusammenfassen. Diese sind eine charakteristische Stärke A des repulsiven Anteils sowie seine charakteristische Längenskala κ^{-1} . Auch in diesem Fall bilden sich Aggregate aus Kolloidpartikeln, welche sedimentieren. Entfernt man sich in diesem Fall jedoch wieder von der kritischen Temperatur, verschwindet das sekundäre Minimum im effektiven Wechselwirkungspotential und die Kolloid-Aggregate lösen sich wieder auf. D.h. man hat hier einen Mechanismus

für eine reversible Aggregation der Kolloidpartikel, der mittels kleiner (im Bereich von einigen Millikelvin bis zu ein paar Kelvin) Temperaturveränderungen reguliert werden kann.

Die Berechnungen zeigen, dass experimentell beide Szenarien der Aggregation realisierbar sein sollten. Die bisher berichteten Experimente fallen jedoch in die Kategorie des reversiblen Aggregationsmechanismus. Die Resultate der theoretischen Berechnungen und die experimentellen Daten aus der Literatur zeigen ein gleiches qualitatives und ein ähnliches quantitatives Verhalten. Quantitativ können die Berechnungen und die experimentellen Daten nur eingeschränkt verglichen werden, da zur genauen Beschreibung dynamische Effekte des Aggregationsprozesses mit einbezogen werden müssen. Des Weiteren sind die kritischen Casimir Kräfte nicht-additiv, d.h. es gibt starke Vielkörperwechselwirkungen. Diese müssen insbesondere bei der Berechnung der Struktur der Aggregate mit berücksichtigt werden. Für beide Aspekte gibt es bereits theoretische Ansätze und Resultate. Es bleiben aber noch Herausforderungen, diese in die Beschreibung des Aggregationsprozesses zu integrieren.

Wie bereits skizziert wurde, verändert sich das thermodynamische Verhalten von Systemen, welche räumlich eingeschränkt werden. In dem hier betrachteten Fall wird das kritische Verhalten des Lösungsmittels durch das Vorhandensein der kolloidalen Teilchen beeinflusst. Es kommt jedoch die weitere Komplikation hinzu, dass diese räumlichen Einschränkungen nicht fixiert sind, sondern selbst makroskopische Freiheitsgrade besitzen. Da die charakteristische Längenskala des Lösungsmittels, sprich die Korrelationslänge ξ , makroskopisch groß wird, wird für kolloidale Dispersionen mit (fast-) kritischem Lösungsmittel die Beschreibung mittels eines effektiven Paar-Wechselwirkungspotentials ungültig. Zwar könnte prinzipiell noch ein effektives Einkomponenten-System betrachtet werden, weil es eine exakte Abbildung eines Mehrkomponenten-Systems auf ein effektives Einkomponenten-System gibt, jedoch könnten die Vielkörper-Kräfte (zwischen $N > 2$ Teilchen) in solch einem System nicht mehr vernachlässigt werden und eventuell sogar die dominierende Rolle übernehmen. Daher ist ein solcher Ansatz nicht mehr praktikabel. Das Phasenverhalten solcher Mehrkomponenten-Systeme wird detailliert im dritten Teil dieser Arbeit (Kap. 8) diskutiert und die Grenzen des effektiven Ansatzes werden herausgearbeitet. Bei der Beschreibung des Phasenverhaltens der Mehrkomponenten-Mischung trifft man auf mehrere fundamentale Schwierigkeiten, welche u. a. in dem Größenunterschied der einzelnen Komponenten von mehreren Größenordnungen und der attraktiven Wechselwirkung zwischen den Teilchen des Lösungsmittels begründet liegen. Die kritische Temperatur T_c und das kritische Ordnungsfeld $h_{b,c}$ der kolloidalen Dispersion sind abhängig von der Teilchendichte ϱ an Kolloiden. Für kleine Werte von ϱ wurde ein generelles Skalenverhalten für die Relationen zwischen den kritischen Werten, $T_c = T_c(\varrho_c)$ und $h_{b,c} = h_{b,c}(\varrho_c)$, hergeleitet. In bestimmten Bereichen des thermodynamischen Raumes der kolloidalen Mischung kann der Ansatz mit einem effektiven Paar-Wechselwirkungspotential näherungsweise verwendet werden, um die Phasenkoexistenz zu bestimmen. In diesem Bereich wurde die Phasenkoexistenz mittels verschiedener theoretischer Ansätze berechnet.

Für eine kolloidale Dispersion, bestehend aus nanometer-großen Kolloidpartikeln und einem phasen-separierenden Lösungsmittel, wurde in Experimenten das Phasenverhal-

ten beobachtet. Für diese Mischung ist der Ansatz mit einem effektiven Paar-Wechselwirkungspotential nicht anwendbar. Durch eine Kombination der Resultate des effektiven Ansatzes und genereller Skalenargumente lässt sich jedoch der Wert der Abweichung der kritischen Temperatur $T_c(\varrho)$ in der Gegenwart von den Kolloidteilchen zu der kritischen Temperatur des reinen Lösungsmittels $T_c^{(s)} = T_c(\varrho = 0)$ abschätzen und man erhält, dass diese Abweichung bis zu 20 Kelvin in dieser Mischung betragen kann. Dieser Wert ist erstaunlich nahe an den experimentell beobachteten Werten, welche bis zu 25 Kelvin betragen können.

Die Arbeit schließt in Kapitel 9 mit einer Zusammenfassung und einer Einordnung der gewonnenen Resultate in den aktuellen Stand des Forschungsgebietes und einem Ausblick auf mögliche Ansätze und Perspektiven für weitere Arbeiten auf diesem Gebiet.

Teile dieser Arbeit wurden bereits vorab veröffentlicht:

- T. F. MOHRY, A. MACIOŁEK, UND S. DIETRICH,
Phase behavior of colloidal suspensions with critical solvents in terms of effective interactions,
J. Chem. Phys. **136**, 224902 (2012).
- T. F. MOHRY, A. MACIOŁEK, UND S. DIETRICH,
Structure and aggregation of colloids immersed in critical solvents,
J. Chem. Phys. **136**, 224903 (2012).

2. Introduction

Matter usually appears as a complex mixture of several components and only rarely as a pure substance. Colloidal suspensions are particular examples of such mixtures which we encounter in various applications in daily life, such as paint, toothpaste, or milk [1]. Studies on colloidal systems can be traced back earlier than the second half of the 18th century. [1, 2, 3]. T. Graham has designated a certain class of substances as colloids and distinguished their peculiar form of aggregation as colloidal condition of matter opposed to the crystalline condition [4]. To what extent colloidal suspensions can be regarded as a state of matter is disputable [2, 5]. Lacking a precise definition, colloidal suspensions are characterized as a mixture with at least one component of mesoscopic size, i.e., with an extension of $(10^{-9} \dots 10^{-5})$ m [3] or with the number of its constituting atoms in the range $10^3 \dots 10^9$ [6]. Colloidal mixtures can be subdivided according to the states of its components. There are dispersions in which solid particles are dispersed in a liquid, in aerosols solid particles or liquid droplets are dispersed in a gas, emulsions consist of liquid droplets dispersed in another liquid, and foams which are dispersions of gas in liquid or a solid [5]. The solvent in which colloidal particles are dissolved can itself be a mixture of molecular fluids. It may contain also surfactants, ions or smaller colloidal particles. Due to the large ratio of surface area to volume, the surface properties of colloidal particles and the properties of the interfaces between the constituents are preeminent for the behavior of colloidal systems.

The presence of the solvent and of the smaller components mediates effective interactions acting between large colloidal solute particles [7, 8, 9, 10]. The broad variety of solvents and colloidal particles that can be used in colloidal suspensions opens up the possibility to tailor these effective interactions between the large particles in a desired way. This tunability (see, e.g., the overview in Ref. [11]) in addition the micro- and nano- size of colloidal particles make colloidal system widely applicable. Further it allows to use colloidal suspensions as model systems of atomic systems and to study associated phenomena such as crystallization [12] or the kinetics of phase-transitions [13] on experimentally accessible time scales [14]. Also, colloidal systems are suitable, experimentally realizable model systems of the field of statistical physics. For example, a practical colloidal model of a ratchet cellular automaton is reported in Ref. [15]. Besides the mentioned applications, colloidal science has its research interests in its own rights as a challenging field at the border between physics and chemistry [2].

The effective forces between colloidal particles can be tailored by choosing the components of the solvent and their concentrations in the suspension. The prominent examples of such forces are screened electrostatic interactions and the attractive dispersion forces described by the Derjaguin-Landau-Verwey-Overbeek (DLVO) theory [16], or the depletion forces [17, 18]. The latter, entropy-driven effective force is induced by the presence

of smaller colloidal entities. The range and the strength of the depletion forces can be tuned by varying the size and the concentration of the small particles [19]. Depletion forces are predominantly attractive, however in certain systems the addition of small particles weakens the net attraction between the large particles [20].

The resulting phase diagrams of the colloidal particles are sensitive to changes in the effective pair potential between colloids [7, 9, 9, 21]. The phase behavior of colloidal suspensions is in general rather complicated and it is not easy to develop an appropriate theoretical description. Even for the simplest binary hard sphere mixture, the bare existence of a fluid-fluid demixing transition was a subject of a long debate, see the historical overview in Ref. [9]. Furthermore, for a binary mixture of species with very different sizes and the small ones interacting attractively among each other, the calculation of the free energy of solvation for the big particles is subtle. For a single big particle immersed in a sea of small ones, this solvation free energy can be calculated by means of density functional theory. It amounts to calculating the density profile of the small ones around a fixed big particle [22, 23]. However, there is no proper theory of a *bulk* mixture (consisting of the large solute particles and the particles of the solvent) available which would serve satisfactorily for this task [24].

For mixtures which contain very large (compared with the size of the particles of the solvent) particles, these solute particles confine locally the solvent. The confinement of a fluid changes its phase behavior and results in a fluid-mediated effective force acting on the confining surfaces [25]. This so-called solvation force depends on the thermodynamic state of the solvent. Solvation forces become particularly strong if the solvent exhibits fluctuations on large spatial scales. Associated with wetting phenomena near a first-order phase transition of the solvent such fluctuations are present close the surfaces of the colloidal particles [26, 27]. Another example, which is crucial for this study, are thermal fluctuations of the solvent order parameter near its second-order phase transition [28, 29, 30, 31, 32]. Upon approaching the critical point of a bulk system, the critical fluctuations drive the divergences of the bulk correlation length ξ of the solvent. An impressive experimental evidence of these large-scale fluctuations is observed in a liquid mixture close to its critical demixing point. The fluctuations are distributed over length scales of the order of the wave lengths of visible light. Accordingly, the light is scattered and a transparent mixture becomes opaque. This effect is known as critical opalescence, discovered experimentally by T. Andrews in 1869 [33] and theoretically described firstly by M. v. Smoluchowski in 1908 [34] and quantified by Einstein [35]. The characteristic length scale of the critical fluctuations is the bulk correlation length ξ , which governs the exponential decay of the bulk order parameter correlation function. Because of the divergence of ξ , right at the bulk critical point there is no characteristic length scale in the system. As a consequence, the free energy is a generalized homogeneous function of the relevant scaling fields, such as the reduced deviation t from the *bulk* critical temperature $T_{c,b}$ or the bulk ordering field h_b which couples to the order parameter. This self-similarity implies that physical quantities depend solely on the ratios of macroscopic relevant length scales through so-called scaling functions [36, 37]. Due to the self-similarity of critical fluctuations, for the critical behavior of the system the microscopic origin of these fluctuations is not relevant. The critical behavior depends solely on the spatial

dimension d , the symmetry of the order parameter, and whether the interactions between the particles are long-ranged or short-ranged [38, 39, 40]. This property is known as universality. As a consequence, the critical behavior of such different systems as binary liquid mixtures, simple fluids, or uniaxial ferromagnets is described by the same scaling functions.

Exposing the near-critical fluid to boundaries, e.g., by inserting colloidal particles acting as cavities, perturbs the fluctuating order parameter near the surfaces of the colloids on the scale of ξ and restricts the spectrum of its thermal fluctuations. Since these restrictions depend on the spatial configuration of the colloids, they result in an effective force between the particles, the critical Casimir force f_C [41, 42, 43]. Accordingly, the range of the critical Casimir forces is proportional to the bulk correlation length ξ . Therefore it can be tuned *continuously* by small changes of the temperature T . The range can also be controlled by varying the conjugate ordering field h_b , such as the chemical potential in the case of a simple fluid or the chemical potential difference of the two species forming a binary liquid mixture. The strength and the sign of f_C can be manipulated as well. This can be achieved by varying the temperature T or the field h_b and by suitable surface treatments, respectively [44, 45, 46]. The first experimental observation of critical Casimir forces has been indirect, by studying the thickness of the wetting films of ^4He near the fluid-superfluid transition [47, 48], of ^3He - ^4He mixtures close to the tricritical point [49], and of classical binary liquid mixtures near their critical demixing point [50, 51]. Development and improvement of the total internal reflection microscopy (TIRM) [52, 53] has allowed to measure colloidal interaction potentials with high accuracy, and in particular the critical Casimir forces between a colloidal particle and a wall could be measured directly [44, 45]. In the following, the measurements of the critical Casimir forces could be even used to probe sensitively chemical microstructures on surfaces [54, 55, 56, 57]. Compared with other effective forces, the critical Casimir force f_C offers two distinct features. First, due to the universality of critical phenomena, to a large extent critical Casimir forces do not depend on the microscopic details of the system. Second, whereas adding depletion agents or ions changes effective forces irreversibly, the tuning of f_C via T is fully and easily reversible. The tuning of the bulk correlation length ξ has been demonstrated experimentally in Ref. [58]. The critical Casimir forces, which result from the confinement of the critical fluctuations, are the “thermodynamical” analogs of the forces acting between objects induced by the vacuum (zero-point) fluctuations of the electromagnetic field. This QED force has been postulated by H. B. G. Casimir in 1948 [59] and has been experimentally verified nearly half a century later [60]. Indeed, these two forces are examples of the various kinds of effective forces induced by fluctuations. Such fluctuation induced forces act also between insertions of membranes [61] or between colloidal particles which are trapped at an interface [62], or in a confined Bose gas [63, 64]. A review is given in Ref. [65].

In colloidal systems with near-critical solvents, the critical Casimir force f_C adds an additional contribution to the effective interaction potential between the large solute particles. The critical Casimir forces successfully compete with direct dispersion forces [66] or electrostatic forces in determining the stability and phase behavior, which is the central issues of colloidal sciences [5]. In typical experiments, binary liquid mixtures

are used as solvent, which exhibit at ambient pressure a lower critical temperature $T_c^{(s)} \sim (20 \dots 70)^\circ \text{C}$ [45, 67]. Generically, colloidal particles adsorb one of these two species of the binary liquid mixture. Solute particles with equal preference for one of the two species realize equal boundary conditions for which the critical Casimir force is attractive. Upon approaching thermodynamically the critical point of the solvent, the additional attraction between the solute particles due to the emerging critical Casimir forces may alter the phase behavior of the colloidal suspension. Colloidal particles which in addition to their hard core repulsion interact attractively can phase separate into two thermodynamic phases, one being rich and the other being poor in colloidal particles. On the other hand, strong attractive interactions between the solute particles can result in the formation of *non-equilibrium* aggregates in which the colloidal particles stick together. In general, these aggregates may grow and shrink and their structure depends on the packing fraction of the colloidal particles in the aggregates and on the strength of the attraction among the colloidal particles [68, 69, 70]. In general the aggregates may consist of crystalline structures, gels, glasses, but also loose fractal aggregates may occur.

Beysens and Estève [71] have reported aggregation phenomena for silica spheres immersed in a binary liquid mixture of water and 2,6-lutidine which exhibits a miscibility gap with a lower critical point [67, 72]. Using light scattering these authors found that upon approaching the bulk coexistence region of demixing from the one-phase region of the binary liquid mixture at constant composition of the solvent, the silica spheres coagulate reversibly at rather well defined temperatures. Moving back the thermodynamic state deeply into the one-phase region the coagulated aggregates dissolve again. These observations, i.e., the formation of colloidal aggregates which sediment, have been confirmed later for silica and polystyrene particles immersed in the same solvent [73, 74, 75, 76, 77, 78, 79, 80, 81] and for various kinds of colloidal particles immersed in other solvents [78, 81, 82, 83, 84, 85, 86, 87, 88, 89, 90] (for reviews see Refs. [91, 92, 93]). Experimental studies on the aggregation of colloidal particles immersed in binary liquid mixtures which do not focus on the near-critical region of the solvent are reported in Ref. [94] and references therein. Suspensions containing micelles formed by surfactants can also phase separate [95] and immersed colloidal particles have been reported to cluster [96, 97]. The experimental findings have been interpreted as (the precursors of) a phase transition in the ternary mixture [82, 81, 83, 86] or as a (non-equilibrium) coagulation.

Several theoretical approaches have been used in order to study this aggregation phenomenon for colloids immersed in a solvent which is close to its phase separation focusing on the influence of the phase-separation itself [98, 99, 100, 101, 102], or on the influence of wetting layers and the modified electrostatic interactions between the colloidal particles due to the inhomogeneous solvent [103, 104, 105]. Most of these theoretical attempts, however, stay on a qualitative level of description, pointing out the possibility of coagulation.

The presentation is as follows. In Ch. 3 and 4 the concepts and used theoretical methods of critical phenomena and colloidal systems, respectively, are presented. The following chapters present the results of this study. In Ch. 5 the dependence of the critical Casimir force on the bulk ordering field h_b in spatial dimensions $d = 3, 4$ is considered.

In Ch. 6 an effective one-component description of colloidal particles immersed in near-critical solvents is introduced and discussed. This description is used in 7 in order to study the structure and stability of solute particles in near critical solvents. The results in Ch. 8 concern the phase behavior of colloidal suspensions with phase-separating solvents. In Ch. 9 the results are summarized and a brief outlook is given.

Parts of the results of this work have been published ahead:

- T. F. MOHRY, A. MACIOŁEK, AND S. DIETRICH,
Phase behavior of colloidal suspensions with critical solvents in terms of effective interactions,
J. Chem. Phys. **136**, 224902 (2012).
- T. F. MOHRY, A. MACIOŁEK, AND S. DIETRICH,
Structure and aggregation of colloids immersed in critical solvents,
J. Chem. Phys. **136**, 224903 (2012).

3. Thermodynamics, phases, and critical phenomena

3.1. Phases and phase transitions

Condensed matter systems appear in form of distinct (so-called) phases, e.g., simple liquids can occur as a liquid, a vapor, or a solid. Another example are mixtures, which can be either mixed or demixed. Despite their huge number of microscopical degrees of freedom (of the order of several N_A , where Avogadro's constant $N_A \simeq 6 \times 10^{23}$ [106, 107]), the macroscopic properties of these many-body systems depend on only a few thermodynamic variables and are fully described by a proper thermodynamic potential Π [108, 109, 110]. An open system consisting of several species is described by the grand potential $\Omega = \Omega(T, \{\mu_k\}_k, \mathcal{V})$ which depends on the temperature T , the chemical potentials $\{\mu_k\}_k$ of the particle reservoirs of the species k , and the volume \mathcal{V} . For a closed system at fixed numbers $\{N_k\}_k$ of particles, the appropriate thermodynamic potential is the Helmholtz free energy $\mathcal{A}(T, \{N_k\}_k, \mathcal{V}) = \Omega + \sum_k \mu_k N_k$. In the latter case, the chemical potentials are functions of the thermodynamic variables and are given by $\mu_k(T, \{N_k\}_k, \mathcal{V}) = (\partial \mathcal{A} / \partial N_k)_{T, \mathcal{V}, \mu_{k' \neq k}}$. The variables μ_k and N_k are called conjugated to each other. In general, for a system described by the thermodynamic potential Π , the pairs of conjugated variables are given by

$$Q_l = \pm \left(\frac{\partial \Pi}{\partial P_l} \right)_{i \neq l} \quad \text{or} \quad P_l = \mp \left(\frac{\partial \Pi}{\partial Q_l} \right)_{i \neq l}, \quad (3.1)$$

depending on whether Π depends on the thermodynamic variable P_l or Q_l , respectively, and $1 \leq l \leq \mathcal{N}$, where \mathcal{N} is the number of macroscopic degrees of freedom. The signs \pm and \mp depend on the particular pair of conjugated variables. The subscripts in Eq. (3.1) indicate that the partial derivative is taken at constant values of the other variables of Π . For simple substances the other two pairs of conjugated variables are the temperature T conjugated to the entropy \mathcal{S} and the pressure p conjugated to the volume \mathcal{V} . For more complex species additional macroscopic degrees of freedom are relevant, for example for magnetic or charged particles, these are the magnetic field and the magnetization, or the electrical field and the polarization, respectively. Each pair (P_l, Q_l) of conjugated variables, consists of one extensive P_l and one intensive Q_l variable. By resorting to the densities Π/P_1 and $P_{>1}/P_1$ the thermodynamic properties of a system are given in terms of intensive variables only, and the single extensive variable P_1 accounts for the size of the system [111]. Two phases I and II of a system differ in their corresponding values $(P_{>1}/P_1)^{(I)}$ and $(P_{>1}/P_1)^{(II)}$ of the densities. and can coexist only if their values

of the so-called fields Q_l are the same in both phases,

$$Q_l^{(I)} = Q_l^{(II)}, \quad 1 \leq i \leq \mathcal{N}. \quad (3.2)$$

Typical examples of phase transitions encompass the liquid-vapour transition and the liquid-solid and vapor-solid transitions in a simple fluid. The latter two phase transitions are accompanied by a break of the translational symmetry in the system, whereas the symmetries of the liquid and vapor phases are the same. These two phases differ in their values of the thermal averaged number densities, $\Delta\rho = \rho_l - \rho_v \leq 0$. The corresponding line of first order phase transitions ends at the bulk critical point $(T_{c,b}, \mu_{c,b})$ at which $\rho_l = \rho_v = \rho_{c,b} = 0$, and $\rho_{c,b}$ is the bulk critical density. A binary liquid mixture consisting of “A” and “B” species may, at fixed pressure p , phase segregate into two phases, one being rich in particles of species A and the other one being rich in particles of species B upon changing the difference $\Delta\mu = \mu_A - \mu_B$ in the chemical potentials of both species. At the critical demixing point, the concentration c_A of particles of species A attains its critical value $c_{A,c}$. For the potential richness of phase diagrams of binary liquid mixtures, beyond the sketch given here, see, e.g., Ref. [112]. As will be discussed below, the phase transition of a uniaxial magnet from para- to ferromagnetic with the critical temperature $T_{c,b}$, which in this context is called the Curie temperature, at vanishing magnetic field, $M = 0$, is to a certain degree similar to the ones mentioned above. There is a variety of other phase transitions, e.g., the isotropic-nematic transition in systems containing non-spherical particles, or phase transitions associated with quantum degrees of freedom, such as the fluid-superfluid transition [32, 113]. For the distinct phases the quantitative measure is the corresponding order parameter Φ . The order parameter Φ is the coarse-grained analog of a microscopic local quantity, i.e., Φ is the average of the latter over a subvolume, the extent of which is much larger than the typical size of the particles but much smaller than the total volume \mathcal{V} . In the cases of the liquid-vapor transition $\Phi \sim (\rho - \rho_{c,b})$, of the demixing transition $\Phi \sim (c_A - c_{A,c})$, and of the para-ferromagnetic transition $\Phi \sim M$, respectively. The order parameter is defined such¹ that in the one phase region its thermal average is $\Phi(h_b = 0, \hat{t} > 0) = 0$. In the two phase region at $h_b = 0$ the phases $\Phi(h_b = 0, \hat{t} < 0) = \pm\Phi_b \neq 0$ coexist. h_b is the conjugated bulk field to Φ and \hat{t} is the control parameter orthogonal to h_b in a two-dimensional thermodynamic (sub)space, such as $\{T, \mu\}$ in the case of a simple liquid or the $\{T, \Delta\mu = \mu_A - \mu_B, p = \text{const}\}$ subspace of the thermodynamic-space of a binary liquid mixture. In the latter case, the bulk ordering field $h_b \sim (\mu_A - \mu_B) - (\mu_A - \mu_B)_{c,b}$ is related to the deviation of the difference of the chemical potentials from the critical value of this difference and the control parameter $\hat{t} = t = \pm(T - T_{c,b})/T_{c,b}$ is the reduced temperature deviation from the upper ($\pm = +$) or lower ($\pm = -$) bulk critical temperature $T_{c,b}$ such that $t < 0$ in the two-phase region. A lower critical point in binary

¹ The definition of the order parameter is not unique. Its scale factor can be chosen quite arbitrarily. Further, for example in Ref. [32] the order parameter is defined such that in the two phase-region the phases with $\Phi = 0$ and $\Phi = \Phi_b > 0$ coexist. The formulations in terms of differently defined order parameters can be converted into each other and physical relevant quantities do not depend on the concrete definition.

liquid mixtures may emerge due to angular dependent interactions on top of attractive, spherical interactions [114, 115, 116, 117]. Actually, the control parameters h_b and \hat{t} are functions of the natural thermodynamic variables $\mu_{A,B}$ and T , known as field-mixing. \hat{t} corresponds in the thermodynamic space to the direction parallel to the coexistence line and h_b to the orthogonal direction. For a general discussion of this geometric point of view on phase transitions also for higher dimensional thermodynamic spaces, see Ref. [111]. For recent theoretical and experimental studies on the so-called complete scaling hypothesis, see, e.g., Refs. [118] and [119], respectively, and references therein. At a phase transition the value of the order parameter Φ changes non-analytically upon a continuous variation of one of the control parameters t or h_b . At a first-order transition² the order parameter exhibits a jump at the coexistence value $h_b^{(cx)}$, whereas at a continuous phase transitions the order parameter increases continuously as a function of t to values $\Phi \neq 0$ in the two phase region.

3.2. Bulk critical phenomena

Critical fluctuations and universality In general, the the thermal fluctuations decay within a microscopic length scale such as the correlation length amplitude $\xi^{(0)}$. As can be inferred from Fig. 3.1, for a simple fluid the slope p'_T of the pressure p along an isotherm $T = const$ as a function of the (number) density ϱ becomes small and at the bulk critical point $(T_{c,b}, \varrho_{c,b})$ it vanishes, $(\partial p(\varrho = \varrho_{c,b}) / \partial \varrho)_{T=T_{c,b}} = 0$. Accordingly, the isothermal compressibility χ_T diverges upon approaching the critical point,

$$\chi_T = \varrho^{-1} \frac{\partial \varrho}{\partial p} \xrightarrow[T \rightarrow T_{c,b}]{\varrho \rightarrow \varrho_{c,b}} \infty. \quad (3.3)$$

The divergences of χ_T implies that small fluctuations, e.g., of the pressure, result in large density fluctuations. The property of large fluctuations is common to all (near-)critical systems [28, 123, 30, 31, 36, 37]. These critical fluctuations drive the divergences of the correlation length ξ . and on length scales l with $\xi_0 \ll l \ll \xi$ the fluctuations are scale invariant. Accordingly, the whole critical system becomes self-similar. It turns out, for the critical behavior the particular nature of the critical fluctuations does not matter. For the critical behavior only the symmetry properties of the order parameter, i.e., for a vectorial order parameter its dimension d_Φ , the spatial dimension d of the system, and the range of the interparticle forces, whether they are long- or shorted-ranged, are relevant [38, 39, 40]. Therefore, all systems consisting of particles interacting via short-ranged forces with the same values $\mathbf{u} = (d, d_\Phi)$ share the common characteristic critical behavior and form a universality class. Accordingly, quite different systems, such as binary liquid mixtures close to their critical demixing point, simple fluids near the

²Ehrenfest classified the phase-transitions as first-, second-, etc. order phase-transitions depending on the highest ordered derivative of the chemical potential which is discontinuous [120]. However, at a continuous phase-transition, the second order derivative is not strictly discontinuous, but diverges. Therefore, it is now common to summarize all higher ordered phase transitions as continuous ones [32].

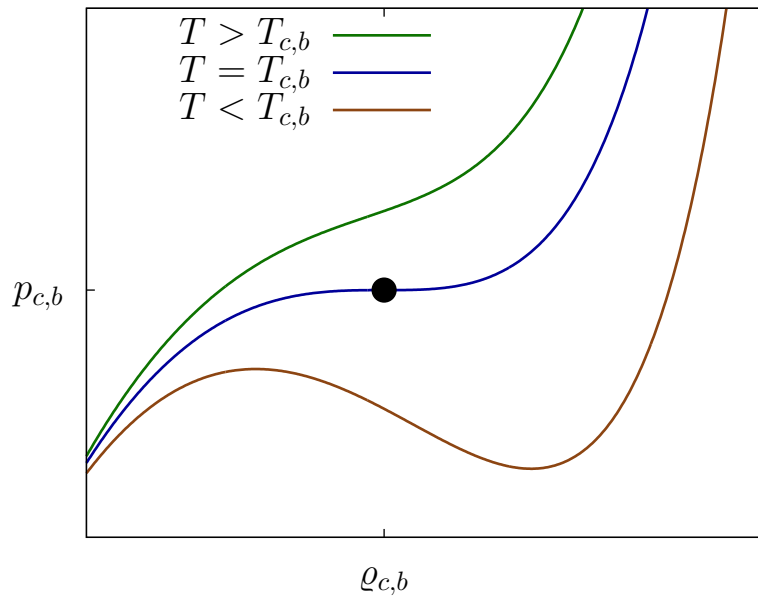


Figure 3.1.: Sketch of the isothermal pressure $p_T(\rho) = p(\rho, T = \text{const})$ curves as function of the number density ρ for a simple fluid. For temperatures $T > T_{c,b}$, the pressure p increases monotonically upon increasing ρ . For the bulk critical temperature $T_{c,b}$ the slope of the isothermal pressure curve is zero at the bulk critical density $\rho_{c,b}$. The critical point is indicated as black dot. For temperatures $T < T_{c,b}$ a vapor and a liquid phase with distinct densities $\rho_v < \rho_l$ coexist. The corresponding isothermals $p_{T < T_{c,b}}$ s exhibit within mean-field theory a van-der-Waals loop and the extrema of $p_{T < T_{c,b}}$ define the spinodals, which only occur within mean-field theory [121, 122].

critical point of the liquid-vapor transition, the uniaxial magnets close to the critical point of the para-ferromagnetic transition, or theoretical suitable models exhibit the same universal behavior, because they all are described by a scalar order parameter and thus belong to the d -dimensional Ising bulk universality class. Other common examples of bulk universality classes are the XY universality classes ($d_\Phi = 2$) to which, e.g., the fluid-superfluid transition in ${}^4\text{He}$ belongs to and the Heisenberg universality class ($d_\Phi = 3$). Of theoretical interest is also the so-called spherical model with $d_\Phi \rightarrow \infty$ for which analytic results can be obtained [124].

Scaling The scale invariance of a critical system manifests itself also in the thermodynamic potentials. The free energy F of a system splits into a *regular*, analytic contribution F_{reg} and a *singular* contribution F_{sgl} ,

$$F = F_{reg} + F_{sgl}. \quad (3.4)$$

At the critical point the singular free energy density f_{sgl} is a generalized homogeneous function of its variables [125, 36, 126, 123], i.e., for (every) $\lambda > 0$

$$f_{sgl}(\lambda^{\mathbf{p}_1} w_1, \lambda^{\mathbf{p}_2} w_2, \dots) = \lambda f_{sgl}(w_1, w_2, \dots). \quad (3.5)$$

In Eq. (3.5) w_i are the so-called scaling fields, which are functions of the thermodynamic variables and \mathbf{p}_i are their associated renormalization group dimension. The property given in Eq. (3.5) was first postulated by B. Widom as the so-called scaling hypothesis [127, 125] and can be derived within the renormalization group theory [128, 126, 37]. The variables w_i with $\mathbf{p}_i > 0$ are so-called relevant variables, whereas the so-called irrelevant variables w_j have the dimension $\mathbf{p}_j < 0$. Marginal variables w_k have a dimension $\mathbf{p}_k = 0$. Only the relevant variables influence the critical behavior. For bulk systems, in which t and h_b are the only two relevant fields, from Eq. (3.5) it follows for the singular bulk free energy density $f_{b,sgl}$ in units of $k_B T$,

$$f_{b,sgl}(t, h_b) = |t|^{2-\alpha} \tilde{f}_{b,sgl,\pm}^{(\mathbf{u})}(|t|^{-\Delta} h_b), \quad (3.6)$$

where \pm refers to the sign of t . In the notation of Eq. (3.5), the universal critical exponents are $\alpha = 2 - \mathbf{p}_t^{-1}$ and $\Delta = \mathbf{p}_{h_b}/\mathbf{p}_t$ and $\tilde{f}_{b,sgl,\pm}^{(\mathbf{u})}$ is a universal scaling function [up to metric factors, see c.f. Eq. (3.22)] the functional form of which only depends on the bulk universality class \mathbf{u} . Because in this thesis only the Ising universality class is considered, in the following it is omitted to write the dependence on \mathbf{u} explicitly. Corrections to scaling are described by an universal exponent [129]. Due to the self-similarity of critical system [see also Eq. (3.5)], asymptotically close to the critical point physical quantities depend on each other according to power laws with critical exponents. The critical exponent ϵ for a quantity $f(\mathcal{C})$ as function of the control parameter \mathcal{C} , which is typically the reduced temperature deviation $t = \pm (T - T_{c,b})/T_{c,b}$ or the bulk ordering field h_b (see Sec. 3.1), is defined as

$$\epsilon = \lim_{\mathcal{C} \rightarrow \mathcal{C}_c=0} \frac{\ln[f(\mathcal{C})]}{\ln[\mathcal{C}]}. \quad (3.7)$$

In general, one would have to distinguish the two different cases $\mathcal{C} \nearrow \mathcal{C}_c$ and $\mathcal{C} \searrow \mathcal{C}_c$. However, for the cases in which $f(\mathcal{C})$ is defined for both cases, the corresponding exponents are the same, $\mathbf{e}_{\nearrow} = \mathbf{e}_{\searrow} \equiv \mathbf{e}$. $\mathbf{e} = 0$ can either correspond to a discontinuity, a cusp, or a logarithmic divergence [29]. The critical exponents \mathbf{e} are universal, i.e., depend only on the universality class. At zero bulk field, $h_b = 0$, upon approaching the critical bulk temperature $T_{c,b}$ the specific heat C and the susceptibility χ diverge as

$$T_{c,b}C(t, h_b = 0) \sim A_{\pm} |t|^{-\alpha} \quad \text{and} \quad \chi(t, h_b = 0) \sim D_{\pm} |t|^{-\gamma}, \quad (3.8)$$

respectively, where A_{\pm} and D_{\pm} are non-universal, i.e., system specific, amplitudes which are different for $t > 0$ and $t < 0$. Depending on the thermodynamic path, the order parameter is asymptotically [in the sense of Eq. (3.7)] given by

$$\Phi(t \rightarrow 0^-, h_b = 0) \sim \mathcal{B}_t |t|^{\beta} \quad \text{and} \quad \Phi(t = 0, |h_b| \rightarrow 0) \sim \mathcal{B}_h \operatorname{sgn}(h_b) |h_b|^{1/\delta}, \quad (3.9)$$

where \mathcal{B}_t and \mathcal{B}_h are non-universal amplitudes. Two limiting cases of the true bulk correlation length $\xi = \xi(t, h_b)$, which governs the exponential decay of the bulk order parameter correlations function, can be identified,

$$\xi_t \equiv \xi(t, h_b = 0) = \xi_{\pm}^{(0)} |t|^{-\nu} \quad \text{and} \quad \xi_h \equiv \xi(t = 0, h_b) = \xi_h^{(0)} |h_b|^{-\nu/(\beta\delta)}, \quad (3.10)$$

with non-universal amplitudes $\xi_{\pm, h}^{(0)}$. For a general thermodynamic state point (t, h_b) the bulk correlation length $\xi = \xi(t, h_b)$ is given by

$$\xi(t, h_b) = \xi_t I(|\Sigma| = \xi_t/\xi_h), \quad (3.11)$$

where I is a universal scaling function with $I(|\Sigma| \rightarrow 0) = 1$ and $I(|\Sigma| \rightarrow \infty) = |\Sigma|^{-1}$. The bulk order parameter pair-correlation function $g(r) = \langle \Phi(0) \Phi(r) \rangle - \langle \Phi(0) \rangle \langle \Phi(r) \rangle$ at the critical point $(t = 0, h_b = 0)$ decays asymptotically as

$$g_c(r = |\mathbf{r}| \rightarrow \infty) \sim r^{-(d-2+\eta)}, \quad (3.12)$$

where the exponent η is a measure of the deviation to a purely Gaussian behavior. The surface tension ς between the coexisting phases for $t < 0$ close to criticality is

$$\varsigma = \varsigma_0 |t|^{\mu} \quad (3.13)$$

where ς_0 is a non-universal amplitude and, here³, μ is a universal critical exponent. Due to, inter alia, Eq. (3.6) the different critical exponents are not independent but are related by so-called scaling relations [123, 32, 37, 130],

$$\begin{aligned} \alpha + 2\beta + \gamma &= 2, & 2 - \alpha &= \beta(\delta + 1), & \gamma &= \nu(2 - \eta), \\ 2 - \alpha &= d\nu, & \Delta &= \delta\beta, \quad \text{and} & \mu &= (d - 1)\nu \end{aligned} \quad (3.14)$$

³ Because the standard notation for both the chemical potential and this critical exponent is μ this notation is adopted with the drawback of the double notation. The context in the use of μ should avoid confusion between these two meanings of μ .

such that there are only two independent bulk critical exponents. The hyperscaling relation $2 - \alpha = d\nu$ is valid only for $d \leq d_>$, where $d_>$ is the upper critical dimension. For $d \geq d_>$ mean-field theory is exact; (for $d = d_>$ there are logarithmic corrections). For the Ising universality class $d_> (d_\Phi = 1) = 4$. The values of the critical exponents are in $d = 4$ (see Appendix A)

$$\beta(d = 4) = 1/2 \quad \text{and} \quad \nu(d = 4) = 1/2, \quad (3.15a)$$

and for $d = 3$ accurate estimates from Monte-Carlo simulations and field-theoretical approaches are available [130]

$$\beta(d = 3) = 0.3265(3) \quad \text{and} \quad \nu(d = 3) = 0.6301(4). \quad (3.15b)$$

Also not all introduced non-universal amplitudes are independent. It can be shown that there are only two non-universal amplitudes. In summary of the said above, the specific properties of the particular critical system are captured solely by these two amplitudes [131]. Among others, there are the universal amplitude ratios [130, 132]

$$\begin{aligned} U_\xi &= \xi_+^{(0)}/\xi_-^{(0)}, & R_\chi &= D_+ \mathcal{B}_t^{\delta-1} \mathcal{B}_h^{-\delta}, & R_\sigma^+ &= \frac{s_0}{k_B T_{c,b}} \left(\xi_+^{(0)} \right)^{d-1}, \\ Q_c &= \mathcal{B}_t^2 \left(\xi_+^{(0)} \right)^d / D_+, & Q^+ &= \alpha A_+ \left(\xi_+^{(0)} \right)^d, & Q_2^* &= \left(\xi_h^{(0)}/\xi_+^{(0)} \right)^{2-\eta} (D_+/D_h) \end{aligned} \quad (3.16)$$

where D_h is defined by $\chi(t = 0, |h_b| \rightarrow 0) \sim D_h |h_b|^{(1-\delta)/\delta}$ and turns out to be $D_h = \mathcal{B}_h/\delta$. Note, that in Eq. (3.16) Q_2^* and the other amplitude ratios are given in terms of the amplitudes $\xi_+^{(0)}$ and $\xi_h^{(0)}$ of the true correlation lengths. In Ref. [130] Q_2 and the other amplitude ratios are defined in terms of the amplitudes $\xi_+^{(2nd)}$ and $\xi_h^{(2nd)}$ of the correlation lengths as defined by the second moment of the order parameter pair correlation function. Both kinds of amplitudes are related by the universal ratios $Q_\xi^+ = \xi_+^{(0)}/\xi_+^{(2nd)}$ and $Q_\xi^c = \xi_h^{(0)}/\xi_h^{(2nd)}$. For the ($d = 3$)-Ising universality class $Q_\xi^+ \simeq Q_\xi^c \simeq 1$. The values $U_\xi (d_\Phi = 1, d = 3) \simeq 1.9$, $R_\chi (d_\Phi = 1, d = 3) \simeq 0.4$, and $Q_2 (d_\Phi = 1, d = 3) \simeq 1.2$ [130] are adopted.

The critical equation of state The order parameter Φ (which is not uniquely defined) is related to the ordering field h_b by the equation of state, which for a near-critical system exhibits the homogeneity property [130]

$$h_b = (\mathcal{B}_h)^{-\delta} \text{sgn}(\Phi) |\Phi|^\delta F \left[t |\mathcal{B}_t/\Phi|^{1/\beta} \right], \quad (3.17)$$

or equivalently

$$\Phi = \text{sgn}(h_b) \mathcal{B}_t |t|^\beta G \left[(\mathcal{B}_t/\mathcal{B}_h)^{1/\beta} t |h_b|^{-1/(\delta\beta)} \right]. \quad (3.18)$$

$F(\hat{X})$ and $G(Y)$ are universal scaling functions with $F(\hat{X} \rightarrow 0) = 1$, $G(Y \rightarrow \infty) = 1$, and $G(Y \rightarrow 0) = |Y|^{-\beta}$. For certain limits, results on the expansion of F and G are

available and the corresponding coefficients are known formally [130]. Within mean-field theory G is known, see Appendix A. In the lowest order in its argument $\hat{X} = t |\mathcal{B}_t/\Phi|^{1/\beta}$, the universal scaling function F has the functional form $F(\hat{X}) = 1 + \hat{X}$ [130], which captures the crossover between the critical behavior at $t = 0$ and at $h_b = 0$, respectively, compare Eq. (3.9). At the coexistence curve one has $t < 0$ and $h_b = 0$; therefore $\hat{X} = -1$ in agreement with $\Phi_b = \mathcal{B}_t |t|^\beta$. Along the critical isotherm $t = 0$ one has $\hat{X} = 0$ and thus $\Phi_b = \text{sgn}(h_b) \mathcal{B}_h |h_b|^{1/\delta}$. For the present purpose of fluid systems exposed to surfaces the sign of Φ matters and the appropriate scaling variables are

$$X = \text{sgn}(\Phi) |t| |\mathcal{B}_t/\Phi|^{1/\beta} \quad (3.19a)$$

and

$$\Sigma = \text{sgn}(h_b t) \xi_t/\xi_h = \text{sgn}(h_b t) \left(\xi_\pm^{(0)}/\xi_h^{(0)} \right) |h_b|^{\nu/(\beta\delta)} |t|^{-\nu}. \quad (3.19b)$$

In terms of these scaling variables the equation of state, Eq. (3.17), takes the scaling form

$$\text{sgn}(\Sigma) |\Sigma|^{\beta\delta/\nu} = (R_\chi \delta / Q_2^*)^{\delta/(\delta-1)} \text{sgn}(X) |X|^{-\beta\delta} F_\pm(|X|), \quad (3.20)$$

where $F_\pm(X) = |X| \pm 1$ and \pm refers to the sign of t . R_χ and Q_2^* are universal amplitude ratios, see Eqs. (3.16). The condition $\Sigma = \text{const}$ corresponds to different paths (depending on the constant value) in the thermodynamic space which all pass through the bulk critical point ($\tau = 0, h_b = 0$). In the limits $\Sigma = 0$ and $|\Sigma| = \infty$, these paths are the critical ‘isochor’ ($h_b = 0$) and the critical isotherm ($t = 0$), respectively. Varying the value of Σ from one of these limits to the other one allows to smoothly transform these two specific critical thermodynamic paths into each other. These expressions shall be used in order to calculate the variation of several experimentally accessible quantities along experimentally realizable thermodynamic paths.

3.3. Critical phenomena in inhomogeneous systems

Surface critical phenomena

The presence of a macroscopic large surface breaks the translational invariance of the system, resulting in a non-uniform profile of the order parameter, $\Phi = \Phi(\mathbf{r})$. In addition to this geometrical constraint, the interactions between particles close to the wall are modified and there are specific interactions of the particles with the wall. These alterations are captured by a surface contribution F_s to the free energy and lead to a wealth of phenomena both in the d -dimensional system and at the $(d-1)$ -dimensional surface. There are surface phase transitions, at which F_s is non-analytic, but the bulk free-energy density f_b is analytic. The effects of these transitions may occur on macroscopically large spatial scales. For example, close to a phase coexistence of a fluid in contact with the surface, wetting phenomena of various kinds are present [133, 26]. The influence of the surface propagates into the bulk of the system on the scale of the bulk

correlation length ξ . Therefore, except for certain conditions [134], the presence of colloidal particles affects the structure of their molecular solvent only on the scale of several Ångströms. One of such conditions is the divergence of the bulk correlation length ξ upon approaching the bulk critical point. This results in the importance of boundaries to critical phenomena [135, 136, 137] with the boundary conditions being, in a certain sense, scale dependent [137]. As for bulk systems, for the critical behavior only few macroscopic properties of the surfaces are of relevance and each bulk universality class u splits into several surface universality classes [138, 139]. Due to missing neighboring particles, modified interactions at the surface, etc., the tendency to order at the surface might be enhanced or suppressed w.r.t. the bulk, corresponding to the extraordinary transition and the ordinary transition, respectively, [140, 141]. For surfaces belonging to the extraordinary surface universality class, i.e., at which the order is favored, the surface orders already for temperatures $t > 0$, with the surface transition temperature $T^{(sf)} > T_{c,b}$ (for an upper bulk critical temperature $T_{c,b}$). In the surface phase diagram [133, 138, 139] the lines of the ordinary transition and extraordinary transition meet in the multicritical point of the special transition, at which both the bulk and the surface are critical [141]. Generically, the surface of a colloidal particle adsorbs one of the species forming the binary liquid mixture which serves as solvent. Such an adsorption preference is described by a surface ordering field h_s , which is the surface analog of the bulk ordering field h_b , and the corresponding transition is called the normal transition [142]. The corresponding boundary conditions for strong surface fields are denoted by (+) and (-) for $h_s > 0$ and $h_s < 0$, respectively. The extraordinary transition and normal transition turn out to be (asymptotically) equivalent [143, 142]. Early studies of surface critical phenomena concerned magnetic systems, for theoretical ones see, e.g., Refs. [144, 145] and for early measurements of surface critical exponents using spin-polarized low-energy electron diffraction see Ref. [146]. For an extensive overview see Refs. [138, 139]. The critical behavior of local surface quantities and excess over bulk properties is characterized by a variety of surface critical exponents (some of which have corresponding bulk counterparts, Sec. 3.2) [138, 139]. These exponents are related by scaling relations and it turns out, that all surface exponents can be expressed in terms of two bulk exponents and one surface exponent [147, 148]. Theoretical studies of the order parameter profile in the semi-infinite geometry, beyond the mean-field theory [149, 140], encompass scaling arguments, field-theoretical methods, and Monte-Carlo simulations, see, in particular for the crossover behavior between the normal and ordinary transition, Refs. [150, 151, 152, 153] and references therein. The rich interplay of the various length scales associated with surface criticality are discussed in detail in Refs. [154, 137]. In Ref. [155] results on universal amplitudes of critical adsorption are presented and compared with experimental data. Concerning critical adsorption at and wetting of curved surfaces, see, e.g., Refs. [156] and [157], respectively. The critical adsorption at geometrically structured surfaces has been studied within mean-field theory in Ref. [158] and at chemically structured surfaces in $d = 4$ [159, 160] and in $d = 3$ [161].

Finite systems

Generals: The confinement of a system has a significant influence not only on the structure but also on the phase behavior of the system, see, e.g., Ref. [25, 162, 163] and references therein. Changing the spatial confinement of a system allows one to tune continuously between the various $0 \leq d \leq 3$ -dimensional bulk phase diagrams of the system and thereby accessing new phases (which are not present in any bulk system) on intermediate scales of the confinement [164, 165]. For example, between two particles, which both prefer the ‘+’ phase and are located in an environment which is rich in the ‘(-)’ phase, close to bulk coexistence of the ‘(-)’ and ‘+’ phases the ‘bridging’ transition occurs. At the bridging transition a bridge-like configuration rich in the ‘+’ phase between the two spherical particles builds up, see Refs. [27, 166, 167] and references therein. The confinement shifts (w.r.t. the bulk) also locations of first order transitions and critical points. These alterations of the phase diagrams of confined systems are a result of the geometrical constraints and the interactions with the boundaries. For sufficiently large confined systems, the free energy F can be decomposed into terms proportional to the volume \mathcal{V} and the confining surface area \mathcal{S} [138, 139, 168],

$$F = \mathcal{V}f_b + \mathcal{S}f_s + \dots + \delta F. \quad (3.21)$$

$f_b = \lim_{\mathcal{V} \rightarrow \infty} F/\mathcal{V}$ and $f_s = \lim_{\mathcal{V}, \mathcal{S} \rightarrow \infty} (F - \mathcal{V}f_b)/\mathcal{S}$ are the bulk and the surface free energy densities, respectively [169]. The periods in Eq. (3.21) stand for contributions in more complex geometries, like curvature, line, or edge contributions. δF is the finite-size contribution to the free energy.

Film geometry: Paradigmatic examples for finite size systems are films. A d -dimensional film has a mesoscopically large width L and is in the $(d - 1)$ other dimensions macroscopically large extended. In the following some aspects of the phase diagrams of films are discussed, the intricate interplay between wetting transitions and the phase behavior in films is reviewed in Ref. [170]. For $(+, +)$ boundary conditions⁴, i.e., equal adsorption preferences of the confining surfaces, the phase diagrams of films are shown in Fig. 3.2. For $(+, +)$ boundary conditions, the ‘+’ phase is favored due to the surface fields and the coexistence line is shifted to negative bulk fields, $h_{b,cx}^{(++)} < 0$, and the critical temperature $T_{c,++}(L) < T_{c,b}$ for finite width L is shifted to lower values than the upper bulk critical temperature $T_{c,b}$ [171, 172]; see also the detailed discussion of the thermodynamics of a liquid film confined between two adsorbing walls in Ref. [173]. For $(+, -)$ boundary conditions, i.e., competing adsorption preferences of the confining surfaces, the symmetry w.r.t. the exchange $h_b \rightarrow -h_b$ is preserved and therefore the coexistence line is located at $h_{b,cx}^{(+-)} = 0$. The corresponding critical temperature is shifted to lower values than in the bulk and even below the wetting temperature $T_{c,w}$ of a corresponding single wall, $T_{c,+-(L)} < T_{c,w}$ [174, 175]. For a more detailed discussion of

⁴ The universal properties of films with $(-, -)$ boundary conditions are derived from the ones of films with $(+, +)$ boundary conditions by a change of sign of both the order parameter profile and the corresponding bulk field, i.e., $\Phi_{(+,+)}(z; t, h_b) = -\Phi_{(-,-)}(z; t, -h_b)$.

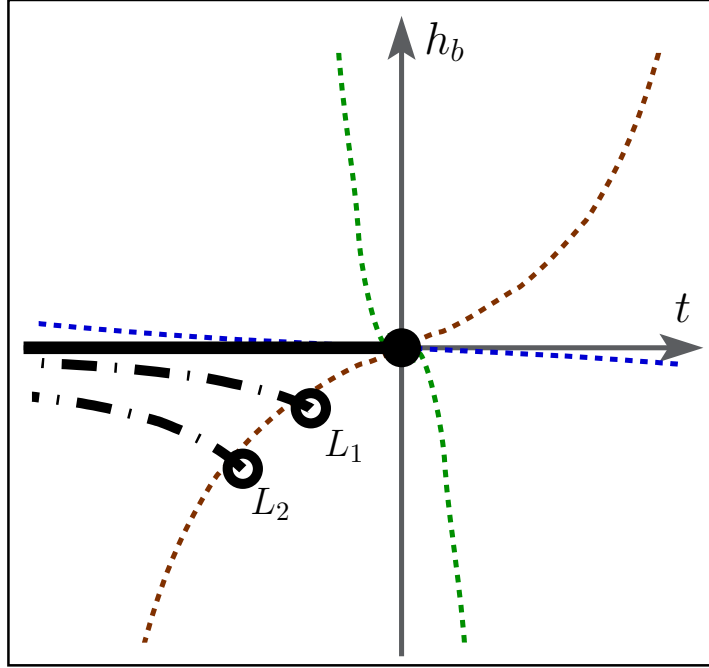


Figure 3.2.: Generic phase diagrams of bulk systems and films belonging to the Ising bulk universality class, such as uniaxial ferromagnets, simple fluids, or binary liquid mixtures in terms of the reduced temperature deviation $t = (T - T_{c,b})/T_{c,b}$ from the bulk critical temperature $T_{c,b}$ and the bulk ordering field h_b conjugated to the order parameter (see the last paragraph of Sec. 3.1). In the bulk there is a first order transition line (thick black line) at $t < 0$ and $h_b = 0$ with the bulk critical point (black full dot) at $(t = 0, h_b = 0)$. For films with equal adsorption preferences, i.e., $(+, +)$ boundary conditions, and thicknesses $L_2 < L_1 < \infty$ the first order transition line (thick black dashed-dotted lines) of capillary condensation is shifted to negative values of the bulk field and the corresponding critical point in the film (black open circles) is located at lower temperatures $T_{c,++}(L_2) < T_{c,++}(L_1) < T_{c,b}$ than in the bulk. The blue, green, and brown shorted-dashed lines correspond to thermodynamic paths of constant value of the bulk scaling variable $\Sigma = \text{sgn}(th_b) \xi_t/\xi_h \sim \text{sgn}(th_b) |t|^{-\nu} |h_b|^{\nu/(\beta\delta)}$, compare Eq. (3.19), along which the influence of both control parameters relative to each other does not vary. ξ_t and ξ_h are the bulk correlation lengths along the critical isochor ($h_b = 0$) and the critical isotherm ($t = 0$), respectively, see Eq. (3.10). ν , β , and δ are standard bulk critical exponents [Eqs. (3.9), (3.10), and (3.14)]. The green and blue line correspond to a small ($|\Sigma| \ll 1$) and a large ($|\Sigma| \gg 1$) negative value of Σ , respectively, and the brown line corresponds to an intermediate positive value $\Sigma \sim 1$.

this intricate phase diagram of $(+, -)$ films see the seminal Refs. [174, 175] and the review in Ref. [170]. Early Monte-Carlo simulation results are reported in Refs. [176, 177]. In a recent study a film consisting of particles interacting via long-ranged forces subjected to competing surfaces has been concerned [178]. Films with competing surface fields of unequal strength, have been also studied [179]. Ising spin films with competing surface fields in the presence of gravity have been studied within the density matrix renormalization approach [180, 181] and by means of Monte-Carlo simulations and within an effective phenomenological theory [182]. Structural and thermodynamic properties of films with equal confining surfaces, both corresponding to the crossover between the normal and the ordinary transition have been studied by means of transfer-matrix methods, Monte-Carlo simulations, and within density functional theory [183, 184]. In these references, the potential realization of ‘neutral’ walls has been discussed as well as the field-mixing of the surface parameters in fluids (analogous to the field-mixing of bulk fluids). The pseudo-transition in $(d = 2)$ -dimensional films is investigated and discussed, e.g., in Ref. [185]. The universal properties of critical films corresponding to several bulk universality classes and subject to various boundary conditions have been thoroughly discussed in Refs. [186, 187]. The singular contribution to the two-point correlation function of critical films subject to ordinary-ordinary boundary conditions has been determined by field-theoretic renormalization-group theory and the connection to potential scattering experiments has been drawn in Ref. [188]. Recently, the fluid-fluid demixing of a colloid-polymer mixture between two parallel opposing walls, both with the same adsorption preference, has been studied experimentally [189].

Finite-size scaling: As for bulk systems, the free energy $F = F_{reg} + F_{sgl}$ of a confined system is a sum of a *regular* and a *singular* contribution, Eq. (3.4). Finite-size scaling theory [190, 168] predicts for the singular part of the free energy density

$$f_{sgl} = L^{-d} \mathfrak{f}(\text{sgn}(t) L/\xi_t, \text{sgn}(h_b) L/\xi_h). \quad (3.22)$$

\mathfrak{f} is an universal function which depends on the corresponding bulk universality class, the surface universality class(es) of the confining surface(es), and the geometry. L is a characteristic measure for the confinement, such as the film thickness L . The significance of Eq. (3.22) is that there occurs no additional non-universal amplitude associated with the confined geometry. Finite-size scaling [Eq. (3.5)], like the homogeneous property of the bulk free energy density, cannot be proven rigorously but can be rationalized within the renormalization group approach [191]. Note, that in the limit $L \rightarrow \infty$ at $\xi_t/\xi_h = \text{const}$, the scaling of the bulk free energy density, Eq. (3.5), is derived with the metric factors (which have been dropped in Eq. (3.5)) being fixed. From the finite-size scaling theory one derives for the shift of the critical temperature and the critical value of the bulk field in films of large thickness L with $(+, +)$ boundary conditions,

$$T_{c,b} - T_{c,++}(L) \sim L^{-1/\nu} \quad \text{and} \quad -h_{b,cx}^{(++)}(L) \sim L^{-\beta\delta/\nu}, \quad (3.23)$$

respectively [171, 172].

3.4. The critical Casimir force

Definition

As discussed in the previous section, boundaries alter the structure of a critical medium. Moreover the confinement restricts the spectrum of the thermal fluctuations. These modifications depend on the relative configuration and the shape of the boundaries resulting in effective, so-called critical Casimir forces acting on the confining surfaces [41, 42]. Because their origin are the critical fluctuations, the critical Casimir forces exhibit the scaling property and universality, too.

For a film of width L and the macroscopically large cross area \mathcal{S} the critical Casimir force acting between the two confining surfaces is given by

$$f_C^{(\parallel)} / (k_B T) = -\frac{\partial \mathbf{F}_{sgl}^{(ex)}}{\partial L} = -\frac{\partial (\mathbf{F}_{sgl} - \mathcal{V} \mathbf{f}_{b,sgl})}{\partial L}, \quad (3.24)$$

where \mathbf{F}_{sgl} is the singular contribution to the free energy of the film and $\mathbf{f}_{b,sgl}$ is the singular bulk free energy density, compare Eqs. (3.4) and Eq. (3.21); $\mathcal{V} = L\mathcal{S}$ is the volume of the film and $k_B T$ is the thermal energy. Finite-size scaling theory (Sec. 3.3) predicts for the critical Casimir force per unit area [192, 186, 187]

$$f_C^{(\parallel)} / \mathcal{S} = k_B T L^{-d} \vartheta_{\parallel, \text{I}}^{(d)} (\mathcal{Y} = \text{sgn}(t) L / \xi_t, \Lambda = \text{sgn}(h_b) L / \xi_h), \quad (3.25a)$$

where ξ_t and ξ_h are the true correlation lengths along the critical isochor and the critical isotherm, respectively, see Eqs. (3.10). $\vartheta_{\parallel, \text{I}}^{(d)}$ is a universal scaling function the functional form of which depends on the bulk universality class of the phase transition occurring in the bulk and the boundary conditions set by the two confining surfaces, i.e., on their corresponding surface universality classes. In the present study only the Ising bulk universality class and surfaces with equal adsorption properties in the so-called strong adsorption limit, denoted as (+, +) boundary conditions (Sec. 3.3), are considered. Therefore it is omitted to write explicitly the dependence of $\vartheta_{\parallel, \text{I}}^{(d)}$ on the bulk universality class and the boundary conditions. $\vartheta_{\parallel, \text{I}}^{(d)}$ depends on the sign of $\Lambda = \text{sgn}(h_b) L / \xi_h$ because the confining surfaces break the bulk symmetry w.r.t. $h_b \rightarrow -h_b$.

Depending on the particular purpose other, equivalent, representations of the scaling function of the critical Casimir force can be appropriate, such as

$$\frac{L^d}{\mathcal{S} k_B T} f_C^{(\parallel)} = \vartheta_{\parallel, \text{II}}^{(d)} (\mathcal{Y} = \text{sgn}(t) L / \xi_t, \Sigma = \text{sgn}(th_b) \xi_t / \xi_h) \quad (3.25b)$$

$$= \vartheta_{\parallel, \text{III}}^{(d)} (\mathcal{Y} = \text{sgn}(t) L / \xi(t, h_b), \Sigma = \text{sgn}(th_b) \xi_t / \xi_h), \quad (3.25c)$$

where in Eq. (3.25b) $\Sigma = \Lambda / \mathcal{Y}$ and in Eq. (3.25c) $\mathcal{Y} = \mathcal{V} / I (|\Sigma|)$ have been used, compare the general expression for the bulk correlation length in Eq. (3.11). Although the three representations $\vartheta_{\parallel, \text{I-III}}^{(d)}$ are different functions, they describe the same quantity, see the lhs of Eq. (3.25b). Therefore, in favor of a better readability, the indices I, II, and III will be dropped whenever the particular dependency on the scaling variables is either

not important or given explicitly, i.e., $\vartheta_{\parallel}^{(d)}(\mathcal{Y}, \Lambda) = \vartheta_{\parallel, \text{I}}^{(d)}(\mathcal{Y}, \Lambda)$, $\vartheta_{\parallel}^{(d)}(\mathcal{Y}, \Sigma) = \vartheta_{\parallel, \text{II}}^{(d)}(\mathcal{Y}, \Sigma)$, and $\vartheta_{\parallel}^{(d)}(\mathcal{Y}, \Sigma) = \vartheta_{\parallel, \text{III}}^{(d)}(\mathcal{Y}, \Sigma)$. The representation I, $\vartheta_{\parallel}^{(d)}(\mathcal{Y}, \Lambda)$, is most intuitive and for fixed \mathcal{Y} (or Λ) the variation of $\vartheta_{\parallel}^{(d)}$ as function of Λ (of \mathcal{Y}) corresponds to the variation of the critical Casimir force along an isotherm, $t = \text{const}$, (an isochor, $h_b = \text{const}$). The strength of the critical Casimir force at a particular thermodynamic state point depends on its distance to the bulk critical point and the distinct influences of the two control parameters t and h_b . In order to get an insight to these two mechanisms, the representation III, i.e., $\vartheta_{\parallel}^{(d)}(\mathcal{Y}, \Sigma)$, is appropriate. The significance of the influences of t and h_b relative to each other (as measured by their corresponding length scales) is captured by $|\Sigma| = \xi_t/\xi_h$. Thus Σ provides information about the corresponding bulk thermodynamic state and its value varies smoothly from 0 at the critical isochor to $\pm\infty$ at the critical isotherm. Complementary, the scaling variable $|\mathcal{Y}| = L/\xi(t, h_b)$ is a measure for the spatial range of the confinement and for the distance to the bulk critical point, which corresponds to $\mathcal{Y} = 0$. Note, that for the two limiting cases $\Sigma = 0$ and $\Sigma = \pm\infty$ one has $\mathcal{Y}(\Sigma = 0) = \mathcal{Y} = \text{sgn}(t) L/\xi_t$ and⁵ $|\mathcal{Y}(\Sigma = \pm\infty)| = |\Lambda| = L/\xi_h$, respectively. This representation, $\vartheta_{\parallel}^{(d)}(\mathcal{Y}, \Sigma)$, has the drawback that the bulk correlation length $\xi(t, h_b)$ is often not known for an arbitrary thermodynamic state ($t \neq 0, h_b \neq 0$); for the mean-field expression for the corresponding scaling function $I(|\Sigma|)$ [Eq. (3.11)] see Eq. (A.8). In order to get around this lack of knowledge but retaining (to a certain extent) the property that each of the scaling variables accounts for the confinement and for the bulk thermodynamic state, respectively, in Eq. (3.25b) the representation $\vartheta_{\parallel}^{(d)}(\mathcal{Y}, \Sigma)$ is given. Within this representation the corresponding bulk thermodynamic state is encoded in Σ (as for the representation III) and $\mathcal{Y} = \text{sgn}(t) L/\xi_t$ is a measure for the distance to the critical isotherm. Concerning the variation of $\vartheta_{\parallel}^{(d)}$ along thermodynamic paths corresponding to $|\Sigma| = \text{const} \gg 1$, i.e., close to the critical isotherm, $\vartheta_{\parallel}^{(d)}(\mathcal{Y}, \Sigma)$ attains notable values only for small values of \mathcal{Y} . Therefore, in this limit it is useful to consider the scaling function as function of $\Lambda = \mathcal{Y}\Sigma = \text{sgn}(h_b) L/\xi_h$, i.e., $\vartheta_{\parallel}^{(d)} = \vartheta_{\parallel, \text{II}}^{(d)}(\mathcal{Y} = \Lambda/\Sigma, \Sigma)$. In this way, the variation of the scaling function $\vartheta_{\parallel}^{(d)}$ along the critical isotherm (corresponding to $\mathcal{Y} = 0$ and $|\Sigma| = \infty$) can be inferred from the representation II, too, namely in the simultaneous limit $\mathcal{Y}, \Sigma^{-1} \rightarrow 0$ with $\Lambda = \mathcal{Y}\Sigma = \text{const}$, i.e., $\vartheta_{\parallel}^{(d)}(\mathcal{Y} = 0, \Lambda) = \vartheta_{\parallel, \text{II}}^{(d)}(\mathcal{Y} \rightarrow 0, \Sigma = \Lambda/\mathcal{Y})$.

Theoretical results for films

There is a rich accumulated knowledge about the critical Casimir force for the Ising bulk universality class ($d_{\Phi} = 1$) in spatial dimensions $d = 2, 3$, and $d \geq 4$, see also the reviews in Refs. [193, 124, 43]. Results obtained within mean-field theory correspond to $d \geq d_{>}$, with the upper critical dimension $d_{>} = 4$ for the Ising universality class. Logarithmic corrections are present at the upper critical dimension $d = d_{>}$, see, e.g.,

⁵In order to avoid a tedious, but not worthwhile discussion of the corresponding signs for the limits $\Sigma \rightarrow \pm\infty$, only the absolute values are considered and $|\text{sgn}(t = 0)| = 1$ is assigned. Taking care about the signs, one obtains $\mathcal{Y}(|\Sigma| = \infty) = \text{sgn}(\Sigma) \Lambda$, with the assignment $\text{sgn}(t = 0) = \text{sgn}(t \rightarrow 0^{\pm})$.

Ref. [194] for a study of the critical Casimir forces at a tricritical point for which $d_> = 3$. Theoretical studies encompass analytic results, quasi-exact numerical calculations and Monte-Carlo simulation results. For $h_b = 0$ the scaling function $\vartheta_{\parallel, (\mathbf{u}_{s,1}, \mathbf{u}_{s,2})}^{(d=2,4)}(\mathcal{Y}, \Lambda = 0)$ is known analytically in $d = 4$ for the various combinations $(\mathbf{u}_{s,1}, \mathbf{u}_{s,2})$ of the different surface universality classes $\mathbf{u}_{s,i} \in \{\text{ordinary, special, and normal } (\pm)\}$ [195, 196] and in $d = 2$ for $(+, \pm)$ boundary conditions [197] and for free (corresponding to the ordinary transition), fixed, periodic, and antiperiodic boundary conditions [198]. In the latter reference also results for an effective force in $d = 1 < d_<$, with the lower critical dimension $d_< = 2$ for the Ising universality class, are presented which, to some extent, can be seen analogous to critical Casimir forces and with a critical temperature $T_{c,b} = 0$. In $d = 2$ and for long-ranged (i.e., decaying with a power law) wall-fluid interactions the critical Casimir force has been calculated in Ref. [199]. In $d = 3$ and for various combinations of the ordinary and normal (\pm) boundary conditions the critical Casimir force has been obtained by means of Monte-Carlo simulations [195, 200, 201, 202]. For symmetry breaking boundary conditions (the normal surface universality class), results have also been obtained by field-theoretical studies [195] and by the extended de Gennes-Fisher local-functional method [203, 204, 205, 206]. A method of a ‘renormalized’ field-theory which has some similarities with the local functional approach has been proposed in Ref. [207]. The crossover behavior of $\vartheta_{\parallel}^{(d)}(\mathcal{Y}, \Lambda = 0)$ between various surface universality classes has been studied in $d = 2$ via transfer matrix calculations [208, 209, 210] and at $T = T_{c,b}$ by making use of a variational principle [211], in $d = 3$ by Monte-Carlo simulations [212, 213], in $d = 4$ within Landau theory [214], and in $\epsilon = 4 - d$ dimension at $T = T_{c,b}$ for symmetry preserving boundary conditions by renormalization group calculations [215, 216]. The critical Casimir force between chemically structured, planar surfaces has been studied in $d = 4$ [217, 160] and in $d = 3$ [161] and between geometrically structured surfaces in $d = 4$ [158]. For $h_b \neq 0$, in $d = 2$ the critical Casimir force has been calculated at the bulk critical temperature, $T = T_{c,b}$, for symmetric boundary conditions with both surfaces belonging to the ordinary transition or the normal transition [218], and for the crossover between these transitions [219]. Results for temperatures around the bulk critical one, $T \gtrless T_{c,b}$ for $(+, +)$ boundary conditions [220, 185] and for identical walls, both exposing algebraically decaying potentials [221] are also available. Within mean-field theory, for $h_b \neq 0$ and $(+, +)$ boundary conditions the scaling function $\vartheta_{\parallel}^{(d=4)}(\mathcal{Y}, \Lambda)$ of the critical Casimir force has been calculated numerically [222]. In $d = 3$, close to the bulk critical point and for $h_b \neq 0$ the effective force between symmetric, strongly adsorbing walls has been calculated from a density functional approach [96, 97].

Experimental studies

Experimentally, it is difficult to adjust two planar plates parallel to each other. An elegant way to realize the film geometry is by wetting films. The critical Casimir forces have been observed indirectly via measurements of the wetting film thickness of pure ^4He at the fluid-superfluid transition (corresponding to ordinary-ordinary boundary conditions)

[47, 48] and of ^3He - ^4He mixtures close to the tricritical point (corresponding to ordinary-normal boundary conditions) [49]. These systems belong to the XY universality class ($d_\Phi = 2$) and corresponding theoretical results are available [194, 196, 223, 200, 201, 224]. Experiments on wetting films of classical binary liquid mixtures close to their demixing critical point [corresponding to $(+, -)$ boundary conditions] have been also performed [50, 51]. A colloidal particle in front of a planar substrate has been proven to be a rewarding experimental setup in order to measure the critical Casimir forces directly. By making use of total internal reflection microscopy the Brownian motion of a colloidal particle close to a wall can be observed [52]. From the histogram of the positions of a polystyrene sphere suspended in a near-critical water-2,6 lutidine mixture the corresponding potential of the critical Casimir force between a spherical colloidal particle and a planar wall for $(+, \pm)$ boundary conditions has been deduced in good agreement with theoretical predictions [44, 45]. Earlier theoretical results for the sphere-plane geometry have been reported in Ref. [225]. This configuration has the additional advantage, that the boundary conditions of the substrate can be changed locally by tuning the chemical composition of a monomolecular overlayer only. By making use of this property, in subsequent experimental studies, the potential between a spherical particle and a substrate corresponding to the crossover between $(+)$ and $(-)$ boundary conditions [46] and chemically patterned substrates [226, 56] could be measured. Whereas for the crossover behavior theoretical results are only available for the film geometry (see above), for chemically patterned substrates corresponding theoretical results, which are based on the Derjaguin approximation, (see below) are available [54, 55, 56]. These references provide also a detailed comparison between the experimental and theoretical results, which are in remarkably agreement. Only recently, Monte-Carlo simulation results in $d = 3$ for the critical Casimir force between a spherical particle and a planar, homogeneous wall, both with fixed (\pm) boundary conditions, have been reported [227]. On ellipsoidal particles in front of a planar wall not only the critical Casimir force but also a corresponding torque acts. These have been studied for $h_b = 0$ and $(+, \pm)$ boundary conditions within mean-field theory [228].

Non-planar geometries

In colloidal suspensions with near-critical solvents the colloidal solute particles act as cavities in the fluctuating medium, and the critical Casimir forces between these particles is of interest. Analogously to the critical Casimir force in the film, Eq. (3.25), the corresponding pair potential $V_c = k_B T U_c$ of the critical Casimir force between two spherical particles (denoted as $\circ\circ$) in spatial dimension $d = 3$ exhibits scaling [225, 228, 222, 55],

$$\begin{aligned}
 V_c(D; R, T, h_b) &= k_B T \frac{R}{D} \Theta_{\circ\circ, \text{I}}^{(d=3)}(\mathcal{Y}_\bullet = \text{sgn}(t) D/\xi_t, \Delta = D/R, \Lambda = \text{sgn}(h_b) D/\xi_h), \\
 &= k_B T \frac{R}{D} \Theta_{\circ\circ, \text{II}}^{(d=3)}(\mathcal{Y}_\bullet = \text{sgn}(t) D/\xi_t, \Delta = D/R, \Sigma = \text{sgn}(th_b) \xi_t/\xi_h),
 \end{aligned}
 \tag{3.26}$$

where D is the surface-to-surface distance between the spherical colloidal particles, each of radius R , and ξ_t and ξ_h are the bulk correlation lengths along the critical isochor and the critical isotherm, respectively, Eqs. (3.10). $\Theta_{\circ\circ,\text{I}}^{(d)}$ and $\Theta_{\circ\circ,\text{II}}^{(d)}$ are universal scaling functions. As for the scaling function $\vartheta_{\parallel}^{(d)}$ of the critical Casimir force in the film, in the following the indices I and II are omitted; concerning the different representations of the scaling functions see the discussion around Eqs. (3.25). Theoretical results for the universal scaling function $\vartheta_{\circ\circ}^{(d)}$ of the critical Casimir force between two d -dimensional spheres in the full range of the scaling variables \mathcal{Y}_{\bullet} , Δ , and Λ are available only within mean-field theory, $d = 4$, for equal adsorption preferences of both spheres (denoted as $\oplus\oplus$) [222]. At the bulk critical point, i.e., $T = T_{c,b}$ and $h_b = 0$, the critical Casimir force $f_C^{(\circ\circ)}$ between two spheres is long-ranged and its asymptotic behaviors are known [229]. In the so-called protein limit of small spheres far apart, i.e., $\xi \gg D \gg R$, the so-called small-sphere expansion renders $f_C^{(\circ\circ)}(D; T_{c,b}, h_b = 0, R) / (k_B T_{c,b}) \sim R^{d-2+\eta} D^{-(d-1+\eta)}$, where η is the standard bulk critical exponent for the two-point correlation function, Eq. (3.12). In the opposite, so-called Derjaguin limit $D \ll R$ one has $f_C^{(\circ\circ)}(D; T_{c,b}, h_b = 0, R) / (k_B T_{c,b}) \sim R^{(d-1)/2} D^{-(d+1)/2}$. In Refs. [225] and [227] for the sphere-plane geometry both limiting behaviors are compared with results of the corresponding numerical calculation and of Monte-Carlo simulations, respectively, in the full geometry. From the form of the decay of the critical Casimir forces it follows that these forces can indeed successfully compete with direct dispersion [66] or electrostatic forces in determining the stability and phase behavior of colloidal systems.

For sufficiently large particles, $D/R \ll 1$, the Derjaguin approximation [230] allows one to express the the critical Casimir force between two particles in terms of the scaling function $\vartheta_{\parallel}^{(d)}$ of the critical Casimir force between two planar, parallel walls, see, e.g., Ref. [45]. Within the Derjaguin approximation the curved, smooth surfaces are approximated by stepped surfaces. Between the opposing flat pieces of such surfaces a force like in the slab geometry is assumed to act and the total force is taken to be the sum of the forces between the single pieces of the stepped surfaces. Here, the cases of ($d_{\circ} = 3$)-dimensional ‘spheres’ (denoted as \circ) in spatial dimensions $d = 3$ (corresponding to experimental realizations) and $d = 4$ (corresponding to the spatial dimension in which, up to logarithmic corrections, mean-field theory is exact) are of interest. For $d > d_{\circ}$ these ‘spheres’ are actually hypercylinders with a $(d - d_{\circ})$ dimensional hyper-axis, see the detailed discussion in Ref. [228]. For $d_{\circ} = 3$ and in $d = 3$ and $d = 4$, the Derjaguin approximation renders for the scaling functions $\vartheta_{\circ\circ}^{(d,d_{\circ})}$ and $\Theta_{\circ\circ}^{(d,d_{\circ})}$ [compare with Eq. (3.26) and $\Theta_{\circ\circ}^{(d)} \equiv \Theta_{\circ\circ}^{(d,d_{\circ}=d)}$] of the critical Casimir force $f_C^{(\circ\circ)} = k_B T \frac{R}{D^2} D^{d_{\circ}-d} \vartheta_{\circ\circ}^{(d,d_{\circ})}$ and the corresponding potential $V_c = k_B T \frac{R}{D} D^{d_{\circ}-d} \Theta_{\circ\circ}^{(d,d_{\circ})}$ (for $d = d_{\circ} + 1$ both quantities are the ones per unit length of the, in one dimension infinitely large, hypercylinder), [225, 228, 222, 55]

$$\vartheta_{\circ\circ,Derj}^{(d,d_{\circ}=3)}(\Delta, \mathcal{Y}_{\bullet}, \Sigma) = \pi \int_1^{\infty} x^{-d} \vartheta_{\parallel}^{(d)}(x \mathcal{Y}_{\bullet}, \Sigma) dx \quad (3.27)$$

and

$$\Theta_{\infty, Derj}^{(d, d_o=3)}(\Delta, \mathcal{Y}_\bullet, \Sigma) = \pi \int_1^\infty (x^{1-d} - x^{-d}) \vartheta_{\parallel}^{(d)}(x \mathcal{Y}_\bullet, \Sigma) dx, \quad (3.28)$$

respectively. It is pointed out that within the Derjaguin approximation the scaling function $\Theta_{\infty, Derj}^{(d, d_o)}$ does not depend on $\Delta = D/R$, which therefore enters into Eq. (3.26) only as a prefactor, Δ^{-1} . For $d = d_o = 4$ this prefactor in the potential is $\Delta^{-3/2}$ and in Ref. [222] for $(+, +)$ boundary conditions the results of the Derjaguin approximation are compared with the numerical calculations of the critical Casimir force in the full geometry. For hypercylindrical particles in front of a planar wall in Ref. [228] the general expression for the Derjaguin approximation is given and the corresponding results are tested within mean-field theory for $(+, \pm)$ boundary conditions with the calculations in the full geometry. Note, that within the Derjaguin approximation the scaling functions for the sphere-sphere geometry and the plane-sphere geometry $(\bullet|)$ are related by a factor of 2, i.e., $\Theta_{\bullet|, Derj} = 2\Theta_{\infty, Derj}$ and $\vartheta_{\bullet|, Derj} = 2\vartheta_{\infty, Derj}$. In $d = 4$ for the sphere-plane geometry and cylinders in front of a planar wall, in both cases for chemically homogeneous and patterned walls, the Derjaguin approximation has been tested against corresponding full calculations [54, 55, 56, 231]. It has been observed, that this approximation for homogeneous walls works surprisingly well even for $D \lesssim R/3$. In Ref. [227], for $d = d_o = 3$ the results of Monte-Carlo simulations are compared with the results of the Derjaguin approximation and the small sphere expansion.

3.5. Theoretical approaches

There is a variety of theoretical approaches to critical phenomena. The two-dimensional bulk Ising model is exactly solvable [232] and also in confined ($d = 2$) geometries there are numerous analytic results. For $d = 2$ Ising strips, transfer matrix calculations and density matrix renormalization-group methods are suitable [183]. The conformal invariance of critical systems can be exploited in $d = 2$. In higher spatial dimensions the number of associated transformations is however too large to gain results [233]. The field-theoretical approach allows for different treatments. Within the mean-field approximation, exact results can be obtained for $d > d_>$, with the upper critical dimension $d_> = 4$ for the Ising bulk universality class. Applying renormalization group techniques allows for a deeper understanding of critical phenomena, general results and in particular for an improved perturbation theory in $\epsilon = d_> - d$ dimensions [234, 128, 36, 37, 235]. Quantitative results in the experimentally relevant case $d = 3$ are available via Monte-Carlo simulations, see, e.g., the reviews in Refs. [236, 237, 238, 239] and references therein. Close to criticality these simulations are computationally demanding and time consuming. Therefore only small systems can be simulated and careful finite-size analysis are required. In order to study inhomogeneous ($d = 3$)-dimensional systems, semi-empirical local functionals have been constructed [240, 41, 205, 206, 241] which require the bulk critical properties as an input. In $d = 2$ there is an exact variational principle [242, 243]. Within the so-called parametric representation, the critical bulk equation of state can be cast in a form which by construction fulfills several analyticity requirements [244, 245, 29].

Concerning classical near-critical fluids, a hierarchy of integro-differential equations in momenta space has been proposed accompanied by suitable approximations [246].

3.5.1. Field-theoretical approach

Within the field-theoretical renormalization group theory the leading behavior of the singular contribution F_s for a confined system is captured by the effective Landau-Ginzburg Hamiltonian \mathcal{H} [247, 248]. For a critical medium in the film geometry the order parameter field $\Phi(z)$ depends solely on the position z perpendicular to the surfaces and \mathcal{H} is given by

$$\mathcal{H}[\Phi(z)] / (k_B T \mathcal{S}) = \int_{-L/2}^{L/2} \mathfrak{h}(\Phi) dz + \mathcal{H}_S(\Phi_1, \Phi_2), \quad (3.29a)$$

with the Hamiltonian density

$$\mathfrak{h}(\Phi) = \frac{1}{2} \left(\frac{\partial \Phi(z)}{\partial z} \right)^2 + \frac{\tau}{2} [\Phi(z)]^2 + \frac{g}{4!} [\Phi(z)]^4 - h_b \Phi(z). \quad (3.29b)$$

$\tau \propto t = \pm(T - T_{c,b})/T_{c,b}$, changes sign at the upper ($\pm = +$) or lower ($\pm = -$) bulk critical temperature $T_{c,b}$ and the quartic term with the coupling constant g stabilizes the Hamiltonian in the two phase region, i.e., for $\tau < 0$. The surface contribution is

$$\mathcal{H}_S = \frac{c_1}{2} \Phi_1^2 - h_{s,1} \Phi_1 + \frac{c_2}{2} \Phi_2^2 - h_{s,2} \Phi_2, \quad (3.29c)$$

where $\Phi_1 = \Phi(z = -L/2)$ and $\Phi_2 = \Phi(z = L/2)$. The so-called surface enhancements $c_{(1,2)}$ account for a different tendency to order at the surfaces and the symmetry breaking surface fields $h_{s(1,2)}$ capture the preference of the surfaces for one of the two phases [138, 139, 137]. The $(+, +)$ boundary conditions are given by $c_1 = c_2 \geq 0$ and $h_{s1} = h_{s2} = \infty$ rendering $\Phi_1 = \Phi_2 = \infty$. In Ref. [249] microscopic expressions for h_s and c are derived by using density functional theory.

In a systematic perturbation theory in terms of $\epsilon = d_{>} - d$, with the upper critical dimension $d_{>} = 4$ for the Ising universality class, the fluctuations are taken into account with a statistical weight $\sim \exp\{-\mathcal{H}[\Phi]/(k_B T)\}$. Mean-field theory corresponds to the lowest order ($d = 4$). Accordingly, the mean-field equilibrium configuration Φ_{MFT} minimizes \mathcal{H} . Within mean-field theory for the Hamiltonian given in Eqs. (3.29), one has [222] $\xi_t(t > 0) = |\tau|^{-1/2}$ and $\xi_h = 3^{-1/2} |\sqrt{g/6} h_b|^{-1/3}$, see Appendix A.

In order to calculate the critical Casimir force for a given configuration Φ_{MFT} the so-called stress-tensor \mathcal{T} is suitable [250]. For the slab geometry one has $f_{C\parallel}^{(MFT)}/\mathcal{S} = k_B T \langle \mathcal{T}_{z,z}[\Phi_{MFT}] - \mathcal{T}_{z,z}[\Phi_{b,MFT}] \rangle$, where $\langle \dots \rangle$ denotes the thermal average and the (z, z) component of the stress tensor is

$$\mathcal{T}_{z,z}[\Phi((z))] = \frac{1}{2} \Phi'^2 - \frac{\tau}{2} \Phi^2 - \frac{g}{4!} \Phi^4 + h_b \Phi. \quad (3.30)$$

3.5.2. Local functional approach

Fisher and de Gennes proposed for $T = T_{c,b}$ a local functional in terms of the order parameter field $\Phi(z)$ the minimal value of which corresponds to the singular free energy contribution F_s [41]. After an early attempt by Au-Yang and Fisher [251], Fisher and Upton extended this ansatz for a near-critical medium, i.e., $T \neq T_{c,b}$, in the presence of a wall [205, 206]. Later Borjan and Upton extended the functional in order to calculate the order parameter profile in a slab, the critical Casimir amplitudes [203] and to study critical adsorption both, on the critical isochor as well as on the critical isotherm [241]. The functional is constructed in such a way that it exhibits the proper scaling and analyticity properties. For temperatures $T \neq T_{c,b}$ and vanishing bulk ordering field, $h_b = 0$, the scaling function $\vartheta_{\parallel\pm}^{(d=3)}$ of the critical Casimir force in a ($d = 3$)-dimensional slab with $(+, +)$ boundary conditions as obtained by the local functional approach agrees surprisingly well with the scaling function determined from Monte-Carlo simulations [204]. For the film geometry the local ansatz for the functional is

$$F[\Phi(z)] = \int_{-L/2}^{L/2} \mathbf{f}(\Phi, \Phi', t, h_b) dz + \mathbf{f}_1(\Phi_1, h_{s,1}) + \mathbf{f}_2(\Phi_2, h_{s,2}) \quad (3.31)$$

where $\Phi' = \partial\Phi/\partial z$. The surface terms \mathbf{f}_i are the same as given in Eq. (3.29c), i.e., $\mathbf{f}_1 + \mathbf{f}_2 = \mathcal{H}_S$. The integrand \mathbf{f} is assumed to depend on bulk critical quantities only and is postulated to be

$$\mathbf{f}(\Phi, \Phi', t, h_b) = \{J(\Phi) \mathcal{G}(\Lambda(\Phi, t, h_b) \Phi') + 1\} \mathcal{W}(\Phi, t, h_b), \quad (3.32)$$

where

$$\mathcal{W}(\Phi; t, h_b) = \mathcal{A}(\Phi, t) - \mathcal{A}(\Phi_b, t) - (\Phi - \Phi_b) h_b \quad (3.33)$$

is the excess over bulk free energy density (in terms of $k_B T$) and $\mathcal{A}(\Phi, t)$ is its conjugated free energy density. The function \mathcal{G} has to fulfill several requirements [205, 206]. It has been shown, that appropriate choices are

$$J(\Phi) = 1 \quad \text{and} \quad \Lambda(\Phi, t, h_b) = \xi(\Phi; t) [2\chi(\Phi; t) \mathcal{W}(\Phi, t, h_b)]^{-1/2}, \quad (3.34)$$

where $\xi(\Phi; t)$ and $\chi(\Phi; t)$ are the bulk correlation length and the susceptibility of a bulk homogeneous system at the thermodynamic state point (t, Φ) , respectively [205, 206]. \mathcal{G} can be approximated by $\mathcal{G}(x) \simeq x^2$ [206, 203]. In the scaling limit $t \rightarrow 0^\pm$ and $\Phi \rightarrow 0$ the bulk quantities take the following analytic scaling forms

$$\mathcal{W}(\Phi; t, h_b) = |\Phi|^{\delta+1} Y_\pm(\Psi, \Sigma) \quad (3.35a)$$

and

$$(\xi^2/(2\chi))(\Phi; t) = |\Phi|^{\eta\nu/\beta} Z_\pm(\Psi), \quad (3.35b)$$

where $\Psi = \Phi/\Phi_b(-|t|) = \text{sgn} \Phi |X|^{-\beta}$ [compare Eq. (3.19)]. $\tilde{Y}_\pm(\Psi, \Sigma) = Y_\pm(\Psi, \Sigma)/Y_+(\infty, 0)$ and $\tilde{Z}_\pm(\Psi) = Z_\pm(\Psi)/Z_+(\infty)$ are universal scaling functions. The functions Y_\pm and Z_\pm (which describe bulk critical properties) as well as the values of the bulk critical exponents are required as additional input for the local functional approach.

3.5.3. The parametric representation of the critical equation of state

Generals: The basic idea of the parametric representation is to perform a coordinate transformation such that certain analyticity and scaling properties of the critical equation of state are manifest, i.e., build in, in that representation [244, 245]; the theoretical background is worked out in Ref. [29]. This framework provides an elegant way for the the description of bulk critical systems and their properties and (as shall be discussed below) the unknown functions of that approach can be approximated by simple (elementary) functions. However, the drawbacks of this approach are that the central properties of critical systems, i.e., universality and scaling, are incorporated a priori and are not explained as being an outcome (in contrast to, e.g., the renormalization treatment), as well as that the universal values of certain quantities, which are specific to critical systems, such as critical exponents or universal amplitude ratios cannot be calculated within the parametric framework, but are needed as input. Explicitly, the parametric representation is formulated in terms of pseudo-‘polar’ coordinates ($\mathbf{s} \geq 0, \mathfrak{z}$),

$$t = \mathbf{s}k(\mathfrak{z}), \quad h_b = \mathbf{s}^{\delta\beta}l(\mathfrak{z}), \quad \text{and} \quad \Phi = \mathbf{s}^{\beta}m(\mathfrak{z}), \quad (3.36)$$

where the ‘radial’ variable $\mathbf{s} \geq 0$ is a measure of the distance to the critical point ($t = 0, h_b = 0$) which corresponds to $\mathbf{s} = 0$. The ‘angular’ variable \mathfrak{z} , with $|\mathfrak{z}| \leq \mathfrak{z}_x$, measures the location on the coordinate curves $\mathbf{s} = \text{const}$. Particular lines in the phase diagram are specified by corresponding values of \mathfrak{z} ; for the critical isochor ($t > 0, h_b = 0$) $\mathfrak{z} = \mathfrak{z}_0 = 0$, for the critical isotherm ($t = 0, h_b \geq 0$) $\mathfrak{z} = \pm\mathfrak{z}_c$, and for the coexistence curve ($t < 0, h_b = 0$) $\mathfrak{z} = \pm\mathfrak{z}_x$. (Actually, in order to satisfy the assignments, these values have to be the zeros of the functions in Eq. (3.36), $m(\mathfrak{z}_0) = 0$, $k(\pm\mathfrak{z}_c) = 0$, and $l(\mathfrak{z}_0) = l(\pm\mathfrak{z}_x) = 0$.) For a phase diagram in these coordinates see, e.g., Fig. 1 in Ref. [252]. The non-analyticity of the thermodynamic functions is captured entirely by \mathbf{s} , whereas their dependence on \mathfrak{z} is analytic throughout. The functions $k(\mathfrak{z})$, $l(\mathfrak{z})$, and $m(\mathfrak{z})$ are analytic in their argument and to a certain extent arbitrary, in the sense, that there are no further requirements available which these functions have to fulfill [29, 130]. The singular part of the conjugated free-energy density takes the form [252]:

$$\mathbf{a}(\Phi, t) = \mathbf{s}^{2-\alpha}n(\mathfrak{z}). \quad (3.37)$$

Out of the four functions $k(\mathfrak{z})$, $l(\mathfrak{z})$, $m(\mathfrak{z})$, and $n(\mathfrak{z})$ introduced in the Eqs. (3.36) and (3.37), respectively, only three of them has to be constructed and the fourth one follows by thermodynamic relations [252]. If one in addition *requires* that the mean-field equation of state is reproduced for the classical values of the critical exponents one additional relation has to be fulfilled [29, 252] and accordingly then only two out of these four functions are independent. The angular functions of other bulk thermodynamic properties can be expressed in terms of these above introduced ones [29, 252, 253], such as the inverse susceptibility

$$1/\chi = \mathbf{s}^{\gamma}p(\mathfrak{z}) = \mathbf{s}^{\gamma} \frac{\beta\delta k'(\mathfrak{z})l(\mathfrak{z}) - k(\mathfrak{z})l'(\mathfrak{z})}{\beta k'(\mathfrak{z})m(\mathfrak{z}) - k(\mathfrak{z})m'(\mathfrak{z})}, \quad (3.38)$$

where the prime denotes the differentiation w.r.t. \mathfrak{z} , or the singular excess over bulk free energy density [Eq. (3.33)]

$$\mathcal{W}(\Phi; t, h_b) = \mathfrak{s}^{2-\alpha} w(\mathfrak{z}, \mathfrak{z}_b), \quad (3.39a)$$

with $h_b = \mathfrak{s}_b^\Delta l(\mathfrak{z}_b)$, $\Phi = \mathfrak{s}^\beta m(\mathfrak{z})$, and $t = \mathfrak{s}_b k(\mathfrak{z}_b) = \mathfrak{s} k(\mathfrak{z})$ [Eq. (3.36)] and according to Eq. (3.37)

$$w(\mathfrak{z}, \mathfrak{z}_b) = n(\mathfrak{z}) - l(\mathfrak{z}_b) m(\mathfrak{z}) |k(\mathfrak{z})/k(\mathfrak{z}_b)|^\Delta - [n(\mathfrak{z}_b) - l(\mathfrak{z}_b) m(\mathfrak{z}_b)] |k(\mathfrak{z})/k(\mathfrak{z}_b)|^{(2-\alpha)}. \quad (3.39b)$$

Concerning the structure of the bulk system an additional function needs to be introduced [254]. The correlation length is usually given as

$$\xi^2 / (2\chi) = \mathfrak{s}^{-\eta\nu} a(\mathfrak{z}). \quad (3.40)$$

Within the parametric representation the scaling variable Σ [Eq. (3.19)] is solely a function of \mathfrak{z} [compare Eqs. (3.10), (3.14), (3.36), and (3.38) from which one derives and $\xi_\pm^{(0)} = |k(\mathfrak{z}_\pm)|^\nu [2a(\mathfrak{z}_\pm)/p(\mathfrak{z}_\pm)]^{1/2}$ and $\xi_h^{(0)} = |l(\mathfrak{z}_c)|^{\nu/(\beta\delta)} [2a(\mathfrak{z}_c)/p(\mathfrak{z}_c)]^{1/2}$],

$$\Sigma = \text{sgn}(h_b t) \xi_t / \xi_h = \text{sgn}[l(\mathfrak{z}) k(\mathfrak{z})] \sqrt{\frac{a(\mathfrak{z}_\pm) p(\mathfrak{z}_c)}{a(\mathfrak{z}_c) p(\mathfrak{z}_\pm)}} \left| \frac{k(\mathfrak{z}_\pm)}{k(\mathfrak{z})} \right|^\nu \left| \frac{l(\mathfrak{z})}{l(\mathfrak{z}_c)} \right|^{\nu/(\beta\delta)}, \quad (3.41)$$

where $\mathfrak{z}_+ = \mathfrak{z}_0$ corresponds to $t > 0$ and $\mathfrak{z}_- = \mathfrak{z}_x$ corresponds to $t < 0$, respectively.

The linear parametric model One way to obtain explicit expressions for the functions $k(\mathfrak{z})$, $l(\mathfrak{z})$, $m(\mathfrak{z})$, and $a(\mathfrak{z})$ [Eqs. (3.36) and (3.37), respectively] is to expand these functions, consistently with the present symmetries, in powers of their argument. Indeed, it can be shown, that for $m(\mathfrak{z}) = \mathfrak{z}$ and $l(\mathfrak{z}) = \mathfrak{z} + \sum_{i=1}^m l_{2i+1} \mathfrak{z}^{2i+1}$ there are coefficients l_{2i+1} such that this specification of the parametric representation is exact up to order ϵ^{m+2} , see Ref. [255, 130] and references therein. To the lowest orders necessary to fulfill the conditions to reproduce correctly the phase diagram the so-called linear parametric model is obtained [29, 130], given by [244]

$$k(\mathfrak{z}) = 1 - \mathfrak{b}^2 \mathfrak{z}^2, \quad (3.42a)$$

$$l(\mathfrak{z}) = l_0 \mathfrak{z} (1 - \mathfrak{z}^2), \quad (3.42b)$$

$$m(\mathfrak{z}) = m_0 \mathfrak{z}. \quad (3.42c)$$

and

$$a(\mathfrak{z}) = a_0 (1 + a_2 \mathfrak{z}^2). \quad (3.42d)$$

The name of the linear model obviously stems from the Eq. (3.42c), which, despite its simplicity, resembles quite well experimental data [244, 256]. The coefficients l_0 , m_0 , and a_0 in the Eqs. (3.42) are metric factors. According to the universality of critical

phenomena, the constants $\mathbf{b} > 1$ and a_2 are assumed to be universal. They are fixed, for example, by matching the universal ratios as obtained within the linear parametric model to the values obtained by Monte-Carlo simulations or by field-theoretical renormalization group treatments. Within the present study the values used in Ref. [204] are adopted,

$$\mathbf{b}^2 = 1.30 \qquad \text{and} \qquad a_2 = 0.28. \qquad (3.43)$$

Concerning a discussion on the dependence of resulting scaling functions, in particular $\nu_{\parallel\pm}^{d=3}(\mathcal{Y}, \Sigma = 0)$, on the choice of \mathbf{b} and a_2 see, e.g., Ref. [257].

The ‘angular’ function $n(\mathfrak{z})$ of the free-energy density [Eq. (3.37)] is obtained by integrating the equation of state, which can be done analytically within the linear representation [Eqs. (3.42)] yielding [252, 257]

$$n(\mathfrak{z}) = m_0 l_0 (c_0 + c_1 k(\mathfrak{z}) + c_2 [k(\mathfrak{z})]^2) \qquad (3.44a)$$

with the coefficients

$$c_0 = \frac{\beta(\mathbf{b}^2 - 1)}{(2 - \alpha)\mathbf{b}^4}, \quad c_1 = \frac{(4\beta - 1) + (1 - 2\beta)\mathbf{b}^2}{2(1 - \alpha)\mathbf{b}^4}, \quad \text{and} \quad c_2 = \frac{2\beta - 1}{2\mathbf{b}^4\alpha}. \qquad (3.44b)$$

For $\alpha = 0$ the coefficient c_2 has to be modified and is finite; in particular, within mean-field theory, for which $\alpha = 0$ and $\beta = 1/2$, $(c_2)_{MFT} = 0$ [252]. For the critical exponents taking their classical values and $a_2 = 0$ the linear parametric model reduces to the common mean-field Landau free energy [29].

There are also other specifications of the parametric representation, such as employing trigonometric functions [258, 252, 253]. Within these trigonometric models the free energy does exhibit a van-der-Waals loop in the coexistence region, in contrast to the linear parametric model.

4. Colloidal suspensions

4.1. Interactions

In order to cope with the large size difference between the molecular solvent particles and the solute colloidal particles, it is suitable to adopt an effective approach. In Ref. [9] exact, but implicit, formulas for the effective potentials between particles of one species due to the presence of particles of another species have been derived. However, the advantage of the effective approach is, that the effective pair-potential between two large particles can be derived from a theory for the solvent alone, and the large particles act as *external* potential to the solvent. The effective interactions between colloidal particles are rich, subtle, and specific due to the diversity of materials and solvents which can be used. The goal of the present study is to provide a general view of the effects a critical solvent has on dissolved colloids due to the emerging *universal* critical Casimir forces. Therefore for the background interaction potential between the colloids which is present also away from the critical temperature $T_c^{(s)}$ of the solvent a generic potential is adopted. It captures the essential features of a stable suspension on the relevant, i.e., mesoscopic, length scale. These features are the hard core repulsion for center-to-center distances $r < 2R$ and a soft, repulsive contribution

$$V_{rep}(r)/(k_B T) = U_{rep}(r) = A \exp(-\kappa D), \quad D = r - 2R > 0, \quad (4.1)$$

which prevents coagulation favored by effectively attractive dispersion forces. The main mechanisms providing $U_{rep}(r)$ are either electrostatic or steric repulsion, which are both described by the generic functional form given by Eq. (4.1) [1, 259]. The steric repulsion is achieved by a polymer coverage of the colloidal surface. If two such covered colloids come close to each other the polymer layers overlap, which leads to a decrease in their configurational entropy and thus to an effective repulsion. Concerning the electrostatic repulsion, for large values of the surface-to-surface distance D the effective interaction between the corresponding electrical double-layers at the colloid surfaces dominates; this leads to a repulsion. The range κ^{-1} of the repulsion is associated with the Debye screening length in the case of electrostatic repulsion and with the polymer length in the case of the steric repulsion. The strength A of the repulsion depends on the colloidal surface charge density and on the polymer density, respectively. For the effective Coulomb interaction screened by counterions A is given by [1]

$$A = 2\pi (\epsilon\epsilon_0)^{-1} \Upsilon^2 \kappa^{-2} R / (k_B T), \quad (4.2)$$

where ϵ is the permittivity of the solvent relative to vacuum, ϵ_0 is the permittivity of the vacuum, Υ is the surface charge density of the colloid, and κ is the inverse

Debye screening length. Indeed the interaction potential of two charged spheres in a dielectric medium containing counter ions does not depend purely exponentially on the surface-to-surface distance D but, within the linearized Debye-Hückel theory, as $\exp(-\kappa D)/(D + 2R)$, where R is the radius of the spherical particles [259, 16] For the cases considered in the present study $\kappa R \gg 1$ and thus only for surface-to-surface distances $D < R$ the soft repulsive contribution is relevant. However, in this range of values of D one can approximate the denominator by $2R$, which renders the generic form given in Eq. (4.1). The results presented in Ch. 7 have been calculated using the generic potential given in Eq. (4.1) as well as using the full form of the Debye-Hückel potential quoted above. The differences are hardly visible.

Wetting phenomena [26] are also important for the aggregation in colloidal suspensions and hydrodynamic interactions [70, 260] influence the character of aggregation. In order to focus on the *universal* aspects connected with the critical Casimir forces, these former, system specific, influences are in the present study neglected.

4.2. Structure

The bulk structure of a colloidal suspension is characterized by its radial distribution function $g(r)$ which can be interpreted as the probability to find a colloidal particle a distance r apart from another particle fixed at the origin. The total correlation function $h(r)$ is related to the former one according to $h(r) = g(r) - 1$. The Ornstein-Zernicke equation expresses $h(r)$ in terms of the direct correlation function direct correlation function $c(r)$ and the number density ϱ [261, 262],

$$h(r) = c(r) + \varrho \int h(r') c(|\mathbf{r} - \mathbf{r}'|) d^d \mathbf{r}', \quad (4.3)$$

or equivalently in Fourier space

$$\hat{h}(q) = \hat{c}(q) / (1 - \varrho \hat{c}(q)), \quad (4.4)$$

with $\hat{h}(\mathbf{q}) = \int e^{i\mathbf{q}\mathbf{r}} h(\mathbf{r}) d^d \mathbf{r}$, analogously for $\hat{c}(\mathbf{q})$, and $q = |\mathbf{q}|$. In order to determine the two unknown functions $c(r)$ and $h(r)$ a second equation is required. This is the so-called closure equation which in its most general form is given by

$$h(r) + 1 = \exp \{-U(r) + h(r) - c(r) + b(r)\} \quad (4.5)$$

where $b(r)$ is the so-called bridge function, which in general is not known. The most common approximations for the bridge function are the so-called Percus-Yevick approximation (PY),

$$b_{PY}(r) = \ln [h(r) - c(r) + 1] - h(r) + c(r), \quad (4.6)$$

and the so-called hypernetted-chain approximation (HNC),

$$b_{HNC}(r) = 0. \quad (4.7)$$

For practical reasons, in order to handle the hard core $U(r < 2R) = \infty$, it is useful to introduce the function

$$k(r) = h(r) - c(r). \quad (4.8)$$

In terms of $k(r)$ the Percus-Yevick closure (Eq. (4.6)) can be written as

$$c_{PY}(r) = [\exp\{-U(r)\} - 1](k(r) + 1) \quad (4.9)$$

and the hypernetted-chain closure (Eq. (4.7)) as

$$c_{HNC}(r) = \exp\{-U(r) + k(r)\} - k(r) - 1. \quad (4.10)$$

The correlation functions can be calculated iteratively [262, 263]. For a given approximate $c_i(r)$ one calculates the total correlation function $h_i(r)$ according to Eq. (4.4). By using a closure, i.e., by choosing a bridge function, Eq. (4.5) renders a direct correlation function c_{i+1} which typically differs from c_i . This procedure is continued until satisfactory convergence is achieved. The initial guess $c_{i=1}(r)$ is guided by the shape of the direct interaction potential.

The applicability and reliability of this integral equation approach is discussed in detail in Ref. [264]. There has been an attempt to improve the performance of this approach in the critical region [265]. For comparison with Monte Carlo simulations in the case of a pair potential with attractive and repulsive parts see, e.g., Ref. [266], which discusses particles interacting with a pair potential containing attractive and repulsive Yukawa-like contributions $\epsilon_i e^{-\kappa_i r}/r$. The integral equation approach is capable to reveal the rich phase behavior of such systems.

The structure factor

$$S(q) = 1 + \rho \hat{h}(q) = 1 / (1 - \rho \hat{c}(q)) \quad (4.11)$$

can be determined by scattering experiments.

4.3. Thermodynamics

Determining the thermodynamic properties of a system from the underlying pair potential $V(r)$ of its constituents is a central issue of statistical physics [262]. In principle the thermodynamic properties of a system can be determined from its correlation functions [262, 264]. For example, the so-called virial equation provides the pressure p of the homogeneous system in terms of the radial distribution function $g(r)$ (see Sec. 4.2):

$$p/(\rho k_B T) = 1 - \frac{2}{3} \pi \rho \int_0^\infty U'(r) g(r) r^3 dr. \quad (4.12)$$

The isothermal compressibility χ_T follows from the sum rule [262]

$$\lim_{q \rightarrow 0} S(q) = \rho k_B T \chi_T \quad (4.13)$$

with the structure factor $S(q)$ given in Eq. (4.11). The system becomes unstable for $\chi_T \rightarrow \infty$, corresponding to the critical point and, within mean-field theory, to the spinodals in the phase diagram (see, e.g., Refs. [121, 122]).

There are further relations expressing thermodynamic quantities in terms of correlation functions which are exact from the formal point of view. However, because the bridge function is not known exactly, the set of equations (4.3) and (4.5) may have no solution in the full one-phase region of the thermodynamic phase space; moreover the resulting thermodynamic quantities depend on the scheme taken. This is the well known thermodynamic inconsistency of this approach (although there are more sophisticated schemes trying to cope with this problem) [264]. Moreover, for the kind of systems considered here, the determination of phase equilibria is even more subtle because due to the adsorption phenomena, which are state dependent, the effective potential between the colloids depends on the thermodynamic state itself. Inter alia this implies that the effective potential acting between the particles should be different in coexisting phases. This feature is not captured by the effective potential approach presented above. Therefore within the integral equation approach only certain estimates for the coexistence curve can be obtained. For a reliable phase diagram actually the full many component mixture (such as the binary solvent plus the colloidal particles) has to be considered.

Another useful first insight into the collective behavior of attractive (spherical) particles is provided by the second virial coefficient [262]

$$B_2 = 2\pi \int_0^\infty (1 - \exp\{-U(r)\}) r^2 dr. \quad (4.14)$$

Beyond the ideal gas contribution it determines the leading non-trivial term in the expansion of the pressure $p(\rho) / (k_B T \rho) = 1 + B_2 \rho + \dots$ in terms of powers of the number density ρ . Measurements of B_2 for colloids immersed in near-critical solvents have been reported in Refs. [79, 80]. Vliegenthart and Lekkerkerker [267] and Noro and Frenkel [268] (VLNF) proposed an extended law of corresponding states according to which the value of the reduced second virial coefficient $B_2^* \equiv B_2 / B_2^{(HS)}$ at the critical point is the same for all systems composed of particles with short-ranged attractions, regardless of the details of these interactions. $B_2^{(HS)} = \frac{2\pi}{3} \sigma^3$ is the second virial coefficient of a suitable reference system of hard spheres (HS) with diameter σ . This (approximate) empirical rule is supported by experimental data [267] and by theoretical results [21]. The critical value $B_{2,c}^*$ can be obtained in particular from the Baxter model for adhesive hard spheres, for which the interaction is given by $\exp\{-U(r)\} = H(r - \sigma) + \frac{\sigma}{12\mathcal{S}} \delta(r - \sigma)$ [269] where $H(r)$ is the Heaviside function and $\delta(r)$ is the delta function. The reduced second virial coefficient is related to the so-called stickiness parameter \mathcal{S} by

$$B_2^* \equiv B_2 / \left(\frac{2\pi}{3} \sigma^3 \right) = 1 - \frac{1}{4\mathcal{S}}. \quad (4.15)$$

This model exhibits a liquid-vapor phase transition as function of \mathcal{S} with the critical value $\mathcal{S}_c \simeq 0.113$, so that $B_{2,c}^* \simeq -1.212$ [270].

In order to obtain a suitable hard sphere reference system, following Weeks, Chandler, and Andersen [271, 272] the pair potential U is split, as it is commonly done [262], into

a purely attractive contribution

$$U_a(r) = \begin{cases} U(r_{min}), & r \leq r_{min} \\ U(r), & r_{min} < r, \end{cases} \quad (4.16)$$

where U has its minimum at r_{min} , and into an effective core, $\exp\{-U_{HS}(r)\} = H(r - \sigma)$, with the diameter σ defined by

$$\sigma = \int_0^{r_0} (1 - \exp\{-U(r)\}) dr, \quad (4.17)$$

where $U(r = r_0) = 0$. It has been checked that for the potential U considered here [c.f., Eq. (6.1)] and for its split potential

$$U_s(r) = U_{HS}(r) + U_a(r), \quad (4.18)$$

as given by Eqs. (4.16) and (4.17), the resulting values of B_2 are almost the same.

4.4. Stability

The stability of colloidal suspensions and the aggregation of colloids are related to kinetic processes, see Refs. [1, 69, 70] and references therein. In these references structural instabilities are subdivided into flocculation, aggregation, or coagulation. However, the notation is not consistent and transparent throughout the literature. In the present work these terms are used as synonyms. They are based on the diffusion of single particles in the presence of other particles of the same kind, interacting with them via interaction potentials which contain both attractive and repulsive contributions. For a review of different mechanisms and experimental results using small angle light scattering see Ref. [68] and references therein. Because multiple scattering between colloidal particles (or in strongly fluctuating media) substantially complicates the analysis of scattering data, this method is limited to suspensions dilute in colloidal particles in which multiple scattering can be neglected. An alternative experimental way to access information about the interactions between and the structure of the colloidal particles is the turbidity method [273, 274]. The concept of the stability ratio W , introduced by Fuchs, makes use of static properties only in order to access the rate of aggregation in a suspension [275]. For interacting particles, which in addition irreversibly stick together once their surfaces touch each other, W can be calculated using Smulochowski's theory [275]

$$W = 2R \int_{2R}^{\infty} \frac{\exp\{U(r)\}}{r^2} dr. \quad (4.19)$$

For hard spheres $W = 1$, while for $W > 1$ ($W < 1$) the repulsive (attractive) part of the interaction potential U dominates. If there is a potential barrier, i.e., $U(r) \gg 1$ for a certain range of distances $r > 2R$, which leads to $W > 1$, on intermediate time scales the suspension will equilibrate into a (meta)stable homogeneous state. Only on very

large time scales cluster formation sets in slowly. It turns out that W is proportional to the ratio between the characteristic times for diffusion of a single particle, \mathfrak{t}_{diff} , and for the formation of a pair of particles, \mathfrak{t}_{pair} [1]:

$$\mathfrak{t}_{diff}/\mathfrak{t}_{pair} = 3\eta/W, \quad (4.20)$$

with the packing fraction $\eta = (4\pi/3)R^3\rho$; ρ is the number density of the colloidal particles. Concerning the importance of hydrodynamic interactions, see e.g., early consideration in Refs. [276, 277], and the review in Ref. [70].

4.5. Density functional theory

Density functional theory is based on the fact that there is a one-to-one correspondence between the local equilibrium number density $\rho(\mathbf{r})$ of a fluid and a spatially varying external potential acting on it. It follows that there exists a unique functional $F[\rho]$ which is minimized by the equilibrium one-particle number density and that the equilibrium free energy of the system is equal to the minimal value of the functional [278, 279]. Since for static properties the absolute size of the particles does not matter, density functional theory has turned out to be very successful not only in describing simple fluids but also colloidal suspensions, see, e.g., Ref. [280]. The ideal gas contribution to the functional F is known exactly, $F_{id}[\rho]/(k_B T) = \int d\mathbf{r} \rho(\mathbf{r}) \{\ln[\lambda^3 \rho(\mathbf{r})] - 1\}$, where $\lambda = h/\sqrt{2\pi m k_B T}$ is the thermal wavelength, m is the mass of the particles and h is Planck's constant. For the expression of the excess contribution $F_{ex} = F - F_{id}$ only approximate ones are available.

As a first step, for a liquid in a volume \mathcal{V} the simple functional

$$F_{ex}[\rho] = F_{HS}([\rho]; \sigma) + \frac{k_B T}{2} \iint_{\mathcal{V}} d^3\mathbf{r}_1 d^3\mathbf{r}_2 \rho(\mathbf{r}_1) U_a(r_{12}) \rho(\mathbf{r}_2), \quad (4.21)$$

where $r_{12} = |\mathbf{r}_1 - \mathbf{r}_2|$, renders the direct correlation as within the random phase approximation. For the attractive contribution U_a to the interaction potential entering into Eq. (4.21), the expression in Eq. (4.16) is employed. $F_{HS}([\rho]; \sigma)$ is the excess functional for the hard sphere system for which the effective hard sphere diameter σ as given by Eq. (4.17) is taken. For F_{HS} various sophisticated functionals are available [281, 282, 283, 279]. For the present purposes, however, it is sufficient to determine the *bulk* free energy density. According to Eq. (4.21) the so-called random phase approximation for F is given by

$$\frac{\pi\sigma^3/6}{v} F_{RPA}/(k_B T) = \eta_\sigma \left(\ln \left(\frac{\eta_\sigma}{1 - \eta_\sigma} \right) - \frac{2 - 10\eta_\sigma + 5\eta_\sigma^2}{2(1 - \eta_\sigma)^2} \right) + \frac{1}{2} \eta_\sigma^2 \tilde{U}_{a,0} \quad (4.22)$$

where for the hard sphere-contribution in Eq. (4.22) the Percus-Yevick approximation (as obtained via the compressibility equation) has been adopted [262]; $\tilde{U}_{a,0} = \frac{6}{\pi\sigma^3} \hat{U}_a(q=0)$ with $\hat{U}_a(q)$ as the Fourier transform of the potential. The packing fraction η_σ used in

Eq. (4.22) corresponds to the effective hard sphere system, i.e., $\eta_\sigma = \frac{\pi}{6}\sigma^3\rho = \left(\frac{\sigma}{2R}\right)^3\eta$. In Eq. (4.22) $F_{id}/(k_B T) = v\rho(\ln(\eta_\sigma) - \ln(\frac{\pi}{6}(\sigma/\lambda)^3) - 1)$ is incorporated, except for the term $v\rho\ln(\frac{\pi}{6}(\sigma/\lambda)^3)$ which accounts only for a shift of F linear in ρ and therefore is irrelevant for determining phase coexistence. For the free energy given in Eq. (4.22) the critical point is given implicitly by $\eta_{\sigma,c}^{(RPA)} = 0.129$ and $\left(\tilde{U}_{a,0}\right)_c = -21.3$. By choosing the Percus-Yevick approximation the results obtained by density functional theory and by the integral equation approach are on the same footing.

5. Dependence of critical Casimir forces on bulk fields

5.1. Landau theory

The critical Casimir forces at $h_b \neq 0$ in a slab with $(+, +)$ boundary conditions are given in terms of the scaling function $\vartheta_{\parallel+}^{(d)}$. For its dependence on two scaling variables, there are different representations, see Eqs. (3.25) and the discussion thereafter. In an earlier study of mean-field results, the dependence of $\vartheta_{\parallel+}^{(d=4)}$ on $\mathcal{Y} = \text{sgn}(t) L/\xi_t$ and $\Lambda = \text{sgn}(h_b) L/\xi_h$ has been considered. L is the width of the film and $\xi_t = \xi(t, h_b = 0)$ and $\xi_h = \xi(t = 0, h_b)$ are the true bulk correlations lengths along the critical isochor and the critical isotherm, respectively [Eq. (3.10)]. t is the reduced temperature deviation from the critical temperature and h_b is the bulk ordering field conjugated to the order parameter. Within mean-field theory the expression for the true bulk correlation $\xi(t, h_b) = \xi_t I(\xi_t/\xi_h)$ at the thermodynamic state point (t, h_b) is known, see Eq. (A.8). In the following, the dependence of $\vartheta_{\parallel+}^{(d=4)}$ on the scaling variables $\Sigma = \text{sgn}(th_b) \xi_t/\xi_h$, Eq. (3.19b), and $\mathcal{Y} = \text{sgn}(t) L/\xi(t, h_b)$ is considered, because the effective model discussed in c.f. Ch. 6 is formulated in terms of Σ . In principle the behavior of $\vartheta_{\parallel+, \text{III}}^{(d)}$ (\mathcal{Y}, Σ) can be inferred from the study of $\vartheta_{\parallel+, \text{I}}^{(d)}$ (\mathcal{Y}, Λ), too, see the equivalence given in Eq. (3.25). Nonetheless, the study of $\vartheta_{\parallel+, \text{III}}^{(d)}$ (\mathcal{Y}, Σ) itself may broaden the knowledge by setting a different point of view. The scaling variable $\Sigma = \text{sgn}(th_b) \xi_t/\xi_h$ depends solely on the corresponding bulk thermodynamic state point and the scaling variable $\mathcal{Y} = \text{sgn}(t) L/\xi(t, h_b)$ is a measure of the confinement. Therefore, the use of these two scaling variables Σ and \mathcal{Y} allows to study the effect of the interplay between the two distinct control parameters t and h_b on one hand and the effect of confinement on the other hand separately by keeping one of these two scaling variables constant. The scaling function $\vartheta_{\parallel+}^{(d=4)}$ has been obtained by minimizing the effective Hamiltonian given in Eqs. (3.29) and by making use of the stress tensor which is given in Eq. (3.30).

In Fig. 5.1 contour lines of constant ‘distance’ $|\mathcal{Y}| = L/\xi(t, h_b) = 3, 4, \dots, 10$ are shown in the thermodynamic space spanned by t and h_b . Along these curves the modulus of the scaling variable $|\Sigma| = \xi_t/\xi_h \sim |t|^{-\nu} |h_b|^{\nu/(\beta\delta)}$ varies from ∞ at the critical isotherm ($t = 0$) to 0 at the critical isochore ($h_b = 0$) and its sign $\text{sgn}(\Sigma)$ changes upon crossing one of these lines, compare also the phase diagram shown in Fig. 3.2. The $|\mathcal{Y}|$ -contour lines exhibit a kink at the bulk coexistence line ($t < 0, h_b = 0$) because of their bulk

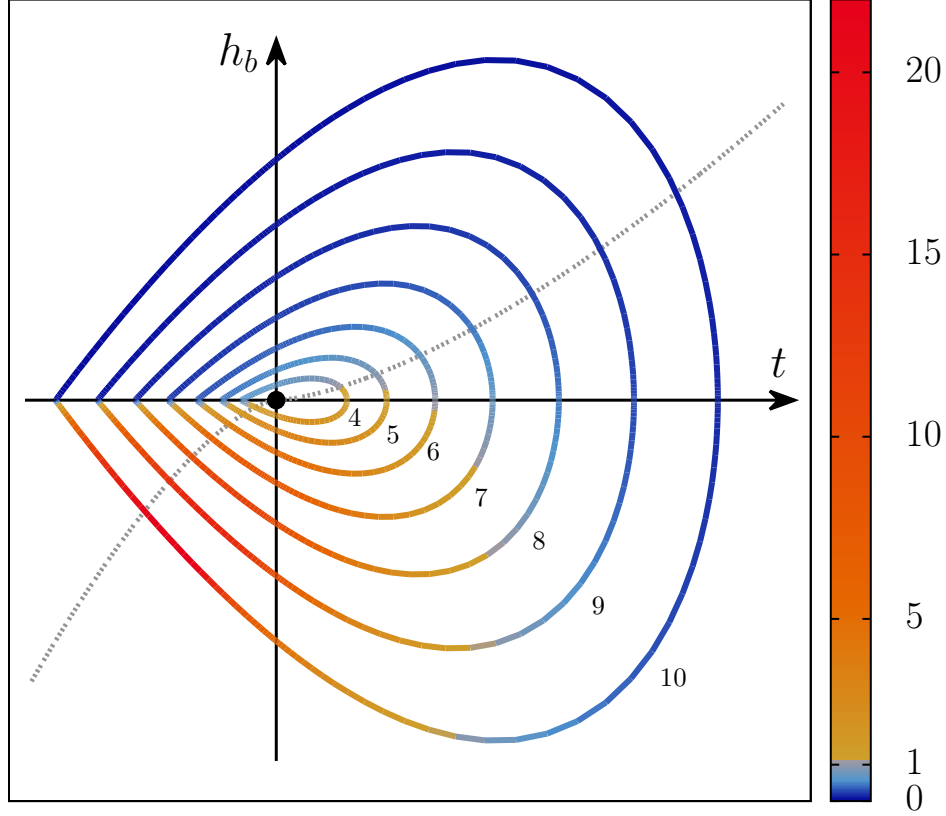


Figure 5.1.: Contour lines of constant ‘distance’ $|Y| = L/\xi(t, h_b) = 4, 5, \dots, 10$ (from the inner to the outer most ring), where $\xi(t, h_b)$ is the bulk correlation length at the thermodynamic state point (t, h_b) , Eqs. (3.11) and (A.8). $t = (T - T_{c,b})/T_{c,b}$ is the reduced temperature deviation from the upper critical temperature $T_{c,b}$ and h_b is the bulk ordering field (Sec. 3.1). Along the critical isochore, i.e., $h_b = 0$, one has $|Y| = L/\xi_t = \frac{L}{\xi_{\pm}^{(0)}} |t|^\nu$ and along the critical isotherm, i.e., for $t = 0$, $|Y| = L/\xi_h = \frac{L}{\xi_h^{(0)}} |h_b|^{\nu/(\delta\beta)}$, Eqs. (3.10). The bulk critical point $(t, h_b) = (0, 0)$ is indicated as full black dot, \bullet . The color along the $|Y|$ -contour lines corresponds to the absolute value $|\vartheta_{\parallel+}^{(4)}|$ at the particular thermodynamic state point. $\vartheta_{\parallel+}^{(4)}$ is the scaling function of the critical Casimir force in a $(d = 4)$ -dimensional film of width L with $(+, +)$ boundary conditions, i.e., both confining surfaces adsorb strongly the same species of a binary liquid mixture, Eq. (3.25). For such films the critical Casimir forces are attractive and $\vartheta_{\parallel+}^{(4)} < 0$. Along each $|Y|$ -contour line the strength $|\vartheta_{\parallel+}^{(4)}|$ attains its minimal value at the bulk coexistence curve ($t < 0, h_b = 0$). The critical Casimir forces are strongest for negative bulk fields $h_b < 0$. For $|Y| < 6.3$ (for $|Y| > 6.3$) the maximal strength of $|\vartheta_{\parallel+}^{(4)}|$ along the corresponding $|Y|$ -contour line occurs at $t > 0$ (at $t < 0$). In the region $t < 0$ and $h_b < 0$ capillary condensation occurs, however for larger values of $|Y| = L/\xi(t, h_b)$ than the shown ones. The dotted line is the thermodynamic path corresponding to $\Sigma = \text{sgn}(th_b) \xi_t/\xi_h = 1$. This mean-field results for the Ising universality class ($d_\Phi = 1$) correspond to spatial dimension $d = 4$ for which $\nu(d = 4) = 1/2$, $\beta(d = 4) = 1/2$, and $\delta(d = 4) = 3$ [Eqs. (3.14) and (3.15a)] and $U_\xi(d = 4) = \xi_+^{(0)}/\xi_-^{(0)} = \sqrt{2}$ [Eqs. (3.16) and (A.7)]. The non-universal amplitudes $\xi_+^{(0)}$ and $\xi_h^{(0)}$ depend on the microscopic details of the particular system.

symmetry w.r.t. $h_b \rightarrow -h_b$ and the dependence of $\xi(t, h_b)$ on the bulk order parameter Φ_b , for the mean-field expression see Eq. (A.6). The color of these contour curves represents the strength $|\vartheta_{\parallel\pm}^{(4)}|$ of the scaling function of the critical Casimir force. Because of the symmetry breaking surface fields $|\vartheta_{\parallel\pm}^{(d)}|$ clearly does not obey the bulk symmetry.

Complementary, in Fig. 5.2 the curves $\vartheta_{\parallel\pm}^{(4)}$ as functions of $Y = \text{sgn}(t) L/\xi(t, h_b)$ for various fixed values of $\Sigma = \text{sgn}(th_b) \xi_t/\xi_h$ are shown. The variation of the scaling variable Y at constant value of Σ corresponds either to moving along the thermodynamic path specified by Σ at fixed film width L , or, equivalently, varying the width L of the film at a fixed bulk thermodynamic state point given by $\Sigma = \text{sgn}(th_b) \xi_t/\xi_h$; see also Fig. 3.2 and Eq. (3.19). Note, that within the former interpretation the phase boundary and the critical point (which are both shifted w.r.t. the bulk) are fixed and the thermodynamic state point in that particular phase diagram is varied, whereas within the latter interpretation the bulk thermodynamic state point is fixed but due to the variation of L the phase diagrams corresponding to different values of $Y = \text{sgn}(t) L/\xi$ are different.

For $(+, +)$ boundary conditions the critical Casimir force in a slab is attractive and accordingly $\vartheta_{\parallel\pm} < 0$ for all values of t and h_b . Along each $|Y|$ -contour line the minimum of the strength $|\vartheta_{\parallel\pm}^{(4)}|$ occurs at the bulk coexistence curve, i.e., for $Y < 0$ and $\Sigma = 0$, corresponding to $t < 0$ and $h_b = 0$. For $Y = \text{sgn}(t) L/\xi < 0$ and upon decreasing the value of $\Sigma = \text{sgn}(th_b) \xi_t/\xi_h$ from 0, which corresponds to the critical isochor, towards $-\infty$ at the critical isotherm, i.e., upon moving clockwise along the $|Y|$ -contour lines in Fig. 5.1, the value of $\vartheta_{\parallel\pm}^{(4)}$ becomes more negative. However in this region of the thermodynamic space, i.e., for $h_b \geq 0$ and $t \leq 0$, the value of $\vartheta_{\parallel\pm}^{(4)}$ depends only mildly on Σ , see the hardly varying color along the $|Y|$ -contour lines in Fig. 5.1 and in Fig. 5.2 the corresponding curves for different values of $\Sigma < 0$. For a shown, fixed value of $Y < 0$ the value of $|\vartheta_{\parallel\pm}^{(4)}(Y, \Sigma)|$ increases by not more than 20% upon decreasing Σ from 0 to $-\infty$. Accordingly, the monotonic decay of $|\vartheta_{\parallel\pm}^{(4)}(Y, \Sigma)|$ towards 0 upon decreasing the value of $Y < 0$ is quite similar (on the scale of Fig. 5.2) for different (fixed) values $-\infty \leq \Sigma \leq 0$.

Recall, that $Y = \text{sgn}(t) L/\xi$ and $\Sigma = \text{sgn}(th_b) \xi_t/\xi_h$ change their sign upon crossing the critical isotherm $t = 0$, corresponding to $|\Sigma| = \infty$, see their definitions in Eq. (3.25). Accordingly $\vartheta_{\parallel\pm}^{(d)}(Y, \Sigma \rightarrow \infty) = \vartheta_{\parallel\pm}^{(d)}(-Y, \Sigma \rightarrow -\infty)$, see the magenta and red curves corresponding to $\Sigma = -15$ and $\Sigma = 15$, respectively. These two curves are merely mirrored w.r.t. $Y \rightarrow -Y$. Both closely represent the behavior of $\vartheta_{\parallel\pm}^{(4)}$ along the critical isotherm.

The increase of the value of $|\vartheta_{\parallel\pm}^{(4)}|$ becomes more pronounced on the other side of the critical isotherm, i.e., for $Y = \text{sgn}(t) L/\xi > 0$ and upon decreasing $\Sigma = \text{sgn}(th_b) \xi_t/\xi_h$ from $+\infty$, see Figs. 5.1 and 5.2. Along the $|Y|$ -contour lines $|\vartheta_{\parallel\pm}^{(4)}|$ attains its maximum value for $h_b < 0$. For $|Y| \simeq 6.3$ this maximum is positioned at $|\Sigma| = \infty$, i.e., $t = 0$ and

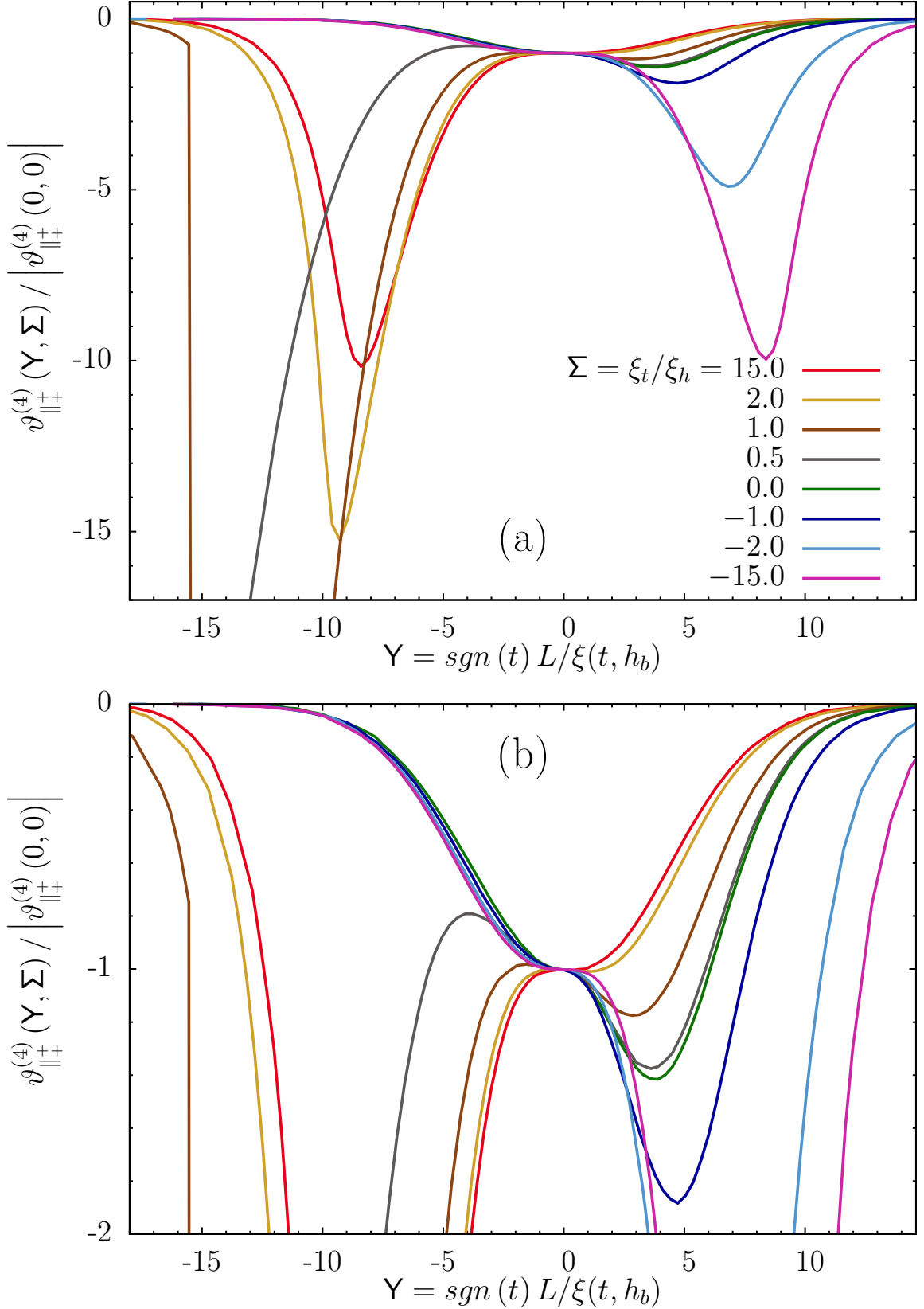


Figure 5.2.: The scaling function $\vartheta_{\parallel+}^{(d=4)}(\Upsilon, \Sigma = \text{const})$ of the critical Casimir force in a $(d = 4)$ -dimensional film subject to $(+, +)$ boundary conditions, Eqs. (3.25), as function of

the scaling variable $Y = \text{sgn}(t) L/\xi(t, h_b)$ which is a measure for the confinement. L is the film width and $\xi(t, h_b)$ is the bulk correlation length [Eqs. (3.10) and (A.8)] at the thermodynamic state point (t, h_b) , which is given by the reduced temperature deviation $t = (T - T_{c,b})/T_{c,b}$ from the upper bulk critical temperature $T_{c,b}$ and the bulk ordering field h_b conjugated to the order parameter. The scaling variable $\Sigma = \text{sgn}(th_b) \xi_t/\xi_h$ specifies the corresponding bulk thermodynamic state point. The condition $\Sigma = \text{const}$ defines thermodynamic paths which pass all through the bulk critical point $(t = 0, h_b = 0)$, corresponding to $Y = 0$, along which the influences of the two control parameters t and h_b , as measured by their associated bulk correlation lengths $\xi_t = \xi(t, h_b = 0)$ and $\xi_h = \xi(t = 0, h_b)$ [Eq. (3.10)], respectively, relative to each other are constant. Panel (b) zooms to values around 1 of the ordinate. In the high-temperature region $Y = \text{sgn}(t) L/\xi(t, h_b) > 0$ the strength $|\vartheta_{\parallel+}^{(d=4)}|$ of the scaling function increases in general upon decreasing the value of $\Sigma = \text{sgn}(th_b) \xi_t/\xi_h$. [An exception is given for small values of Y and large negative values of Σ , see the bright blue curve, corresponding to $\Sigma = -2.0$, and the violet curve, corresponding to $\Sigma = -15.0$, in the range $0 < Y < 5$ in panel (b)]. The minimum along the critical isochore, corresponding to $|\Sigma| = \infty$ is about seven times deeper than the one along the critical isotherm, corresponding to $\Sigma = 0$. Due to the definitions of the scaling variables $Y = \text{sgn}(t) L/\xi(t, h_b)$ and $\Sigma = \text{sgn}(th_b) \xi_t/\xi_h$ the curves for $|\Sigma| \rightarrow \infty$ resemble the behavior of the scaling function $\vartheta_{\parallel+}^{(d)}$ along the critical isochore ($t = 0$) and exhibit the symmetry $\vartheta_{\parallel+}^{(d)}(Y, \Sigma \rightarrow \infty) = \vartheta_{\parallel+}^{(d)}(-Y, \Sigma \rightarrow -\infty)$, see the red and the violet curves corresponding to $\Sigma = \pm 15$. In the low-temperature region, $Y < 0$, the decay of $\vartheta_{\parallel+}^{(4)}$ upon decreasing the value of Y hardly depends on the fixed value $\Sigma \leq 0$, see panel (b). In contrast, for negative bulk fields, i.e., for $\Sigma = \text{sgn}(th_b) \xi_t/\xi_h > 0$, the presence of the capillary condensation amplifies strongly the strength $|\vartheta_{\parallel+}^{(4)}|$, see the curves for $\Sigma > 0$ and $Y < 0$ in panel (a). At the capillary condensation transition, which occurs for $0 < \Sigma \leq 1.6$ and $Y \leq 13$, the effective force between the walls exhibits a jump, see the brown curve corresponding to $\Sigma = 1.0$ at $Y \simeq 15.5$.

$h_b < 0$, whereas for smaller or larger values of $|\mathbf{Y}| = L/\xi_t$ this maximum is located at values $t > 0$ (corresponding to $\mathbf{Y} > 0$ and $\Sigma < 0$) and $t < 0$ (corresponding to $\mathbf{Y} < 0$ and $\Sigma > 0$), respectively. The increase of the value of $\left| \vartheta_{\parallel\pm}^{(4)} \right|$ for $\mathbf{Y} = \text{sgn}(t) L/\xi > 0$ upon decreasing the value of $\Sigma = \text{sgn}(th_b) \xi_t/\xi_h$ is also seen for the curves shown in Fig. 5.2. At about $\Sigma \simeq 3$ a local minimum (which is larger than the numerical accuracy) for values $\mathbf{Y} > 0$ in the curves $\vartheta_{\parallel\pm,III}^{(4)}$ develops. Upon decreasing the value of $\Sigma = \text{sgn}(th_b) \xi_t/\xi_h$ the depth of this minimum deepens and its position shifts towards larger values of \mathbf{Y} . For small (fixed) values of $\mathbf{Y} > 0$ the value of $\vartheta_{\parallel\pm}^{(4)}$ attains a maximum upon decreasing Σ and decreases again upon further decreasing the value of Σ , see for an example the bright blue and violet curves, corresponding to $\Sigma = -2.0$ and $= -15.0$, respectively, in the range $\mathbf{Y} = \text{sgn}(t) L/\xi < 5$ in Fig. 5.2. In order to put the behavior of the described minimum of the curves $\vartheta_{\parallel\pm}^{(4)}$ ($\mathbf{Y} > 0, \Sigma < 3$) in a quantitative context, the depths $\vartheta_{\parallel\pm}^{(4)}(\mathbf{Y}_{min}, \Sigma = 0) = 1.4\vartheta_{\parallel\pm}^{(4)}(0, 0)$ and $\vartheta_{\parallel\pm}^{(4)}(\mathbf{Y}_{min}, \Sigma = \infty) = 10\vartheta_{\parallel\pm}^{(4)}(0, 0)$ as well as the positions $\mathbf{Y}_{min}(\Sigma = 0) \simeq 3.8$ and $\mathbf{Y}_{min}(\Sigma = \infty) \simeq 8.4$ of the *minimas* along the particular pathes $\Sigma = 0$ (i.e., the critical isochore) and $\Sigma = \infty$ (i.e., the critical isotherm), respectively, are given.

For negative bulk fields and below the upper bulk critical temperature, i.e., for $\Sigma = \text{sgn}(th_b) \xi_t/\xi_h > 0$ and $\mathbf{Y} = \text{sgn}(t) L/\xi < 0$, the trends observed in the high temperature region, $\mathbf{Y} > 0$, continue. That is, the curves $\vartheta_{\parallel\pm}^{(4)}(\mathbf{Y}, \Sigma = \text{const})$ exhibit a local minimum at a value $\mathbf{Y}_{min}(\Sigma > 0) < 0$. This minimum becomes deeper and its position \mathbf{Y}_{min} becomes more negative along thermodynamic pathes which lie closer to the bulk coexistence curve. The closer the corresponding thermodynamic path lies to the bulk coexistence curve, i.e., for $\Sigma = \text{sgn}(th_b) \xi_t/\xi_h > 0$ decreasing to 0, the deeper the minimum becomes and it shifts towards more negative values of \mathbf{Y} . Whereas for $\Sigma = \text{sgn}(th_b) \xi_t/\xi_h > 0$ and $\mathbf{Y} = \text{sgn}(t) L/\xi > 0$ the local minimum smoothly emerges, see the discussion above, for $\mathbf{Y} < 0$ and decreasing $\Sigma > 0$ towards 0, i.e., $\Sigma \searrow 0$ the position \mathbf{Y}_{min} of the local minimum shifts, within the present approach, towards $-\infty$ and does not appear for $\Sigma = 0$. In order to calculate properly the effective force between the walls in the thermodynamic region corresponding to large negative values of \mathbf{Y} another approach is needed, because this Landau theory used here applies only for the near-critical region.

For less negative values of $\mathbf{Y} = \text{sgn}(t) L/\xi < 0$ the curves $\vartheta_{\parallel\pm}^{(4)}(\mathbf{Y}, \Sigma = \text{const})$ merge with the curve $\vartheta_{\parallel\pm}^{(4)}(\mathbf{Y}, \Sigma = 0)$. In Fig. 5.2 the deepening of the minima is seen for all curves corresponding to values $\Sigma > 0$. The merging of the curves for temperatures not too far below the bulk critical temperature, i.e., for small negative values of $\mathbf{Y} = \text{sgn}(t) L/\xi(t, h_b)$, is especially seen for the dark brown and dark grey curves, corresponding to $\Sigma = 1.0$ and $\Sigma = 0.5$, respectively, in the range $-5 \lesssim \mathbf{Y}$, see Fig. 5.2 (b). For sufficiently small values $0 < \Sigma < \dots \sim 1.6$ the corresponding thermodynamic path crosses the film phase boundary $\mathbf{Y}_{cx}(\Sigma)$ of coexisting phases. At the capillary condensation the solvation force (within this context this general term is more appropriate than

the term critical Casimir force) exhibits a jump to a significantly smaller value in the $(-)$ phase than in the $(+)$ phase and the local minimum of $\vartheta_{\parallel\pm}^{(d)}$ becomes a cusp.

The reason for the two described trends, the merging of the curve $\vartheta_{\parallel\pm}^{(d)}$ ($Y < 0, \Sigma > 0$) with the curve corresponding to $\Sigma = \text{sgn}(th_b)\xi_t/\xi_h = 0$ for less negative values of $Y = \text{sgn}(t)L/\xi$ on one hand and, contrary, the deepening of the minimum at more negative values of Y , is the interplay of three relevant length scales ξ_t , ξ_h , and L . As described above, varying the value of Y at constant value of Σ can be seen as varying the value of L at fixed values of ξ_t and ξ_h . For $|\Sigma| = \xi_t/\xi_h \rightarrow 0$ one has $Y = \frac{L}{\xi_t I(\Sigma)} \approx L/\xi_t$, see Eq. (3.11). Accordingly, for small values of $|Y|$ one has $L \sim \xi_t \ll \xi_h$ and the behavior as for $h_b = 0$ is observed, whereas upon increasing the value of $|Y|$, L becomes comparable and even larger than ξ_h . Therefore, as $\xi_h, \xi_t \ll L$ the influence of the surfaces with the $(+)$ boundary conditions diminishes and in the film (with the large width L) the predominantly $(-)$ phase becomes favourable and the system crosses the phase boundary Y_{cx} . Obviously, for $\Sigma \rightarrow 0$ it follows that $Y_{cx} \rightarrow -\infty$ in order to obtain $L > \xi_h$.

In Ref. [185], the solvation force f_{solv} in the region of the thermodynamic space close to the capillary condensation has been analysed. Based on the argument that for sufficiently large values of the width L , the L -dependent contribution to the excess free energy density in the film is approximately the (corresponding) bulk excess free energy density, the expression for the solvation force in that region of the thermodynamic space $f_{solv}(t, h_b^{(cx)} < h_b < 0) \simeq 2h_b\Phi_b(t)$ has been derived. Also the jump of f_{solv} at $h_b^{(cx)}$ has been obtained and estimated. The value of the shifted coexistence bulk field has been obtained as $-h_b^{(cx)}(L) \simeq [\varsigma/\Phi_b(t)] \left[L - l_0 l(t, h_b^{(cx)}) \right]^{-1}$, where ς is the surface tension between $(+)$ and $(-)$ phases, see Eqs. (3.13), (3.14), and (3.16), l is the thickness of the adsorbed wetting film of $(+)$ phase, and l_0 is a constant which depends on the spatial dimension d and the range of the wall-fluid and fluid-fluid interactions. In terms of the scaling variables \mathcal{Y} and Σ these expressions read

$$\vartheta_{\parallel\pm}(\mathcal{Y}, \Sigma) \sim -|\mathcal{Y}|^d |\Sigma|^{\beta\delta/\nu} \quad \text{and} \quad (\Sigma^{(cx)})^{-\nu/(\beta\delta)} \sim \mathcal{Y}(1 - l_0 l/L), \quad (5.1)$$

where $\beta\delta/\nu = 3$ within mean-field theory [Eqs. (3.14) and (3.15a)]. These expressions hold also within the present description as has been already mentioned in Ref. [222]. Upon decreasing the value of $\mathcal{Y} = \text{sgn}(t)L/\xi_t < 0$ for small values of $|\Sigma|$ and about $\ln(-\mathcal{Y}|\Sigma|^{1/3}) \approx 1.5$ the curve $\vartheta_{\parallel\pm}^{(4)}$ crosses over to the expression given in Eq. (5.1). The jump of the effective force occurs for small values of $|\Sigma|$ at around $\ln(-\mathcal{Y}|\Sigma|^3) \approx 2.5$.

The expressions reported in Ref. [185] and given in Eq. (5.1), which are model independent and are derived from general thermodynamic arguments, are valid for the thermodynamic region around the first order transition. It is quite interesting that the results obtained within the mean-field theory of the Landau-Ginzburg Hamiltonian satisfy these expressions, too. Nonetheless, these results should be taken with care, because this Landau approach is appropriate for critical phenomena. It may capture certain qualitative features of the first order transition but fails for a detailed and quantitatively correct description. Furthermore, although the general expressions can be written

in terms of the scaling variables [Eq. (5.1)], for that region of the thermodynamic space, i.e., close to the capillary condensation, the scaling (and the universality) property is not expected to hold. The fact that the curves as obtained from the mean-field theory of the Landau-Ginzburg-Wilson Hamiltonian obey scaling is an artifact of this theory. The scaling regime can not be reached for these thermodynamic state points, because for these $|\mathcal{Y}| = L/\xi_t \gg 1$ is required in contrast to the requirement for critical scaling that ξ is the dominating length scale. For the $d = 2$ Ising film the failure of scaling has been reported in Refs. [185, 221].

5.2. Local functional approach

In Ref. [204] it has been shown that for $d = 3$ and $h_b = 0$ the scaling function $\vartheta_{\parallel+}^{(d=3)}(y, \Sigma = 0)$ of the critical Casimir force in a slab with $(+, +)$ boundary conditions as obtained from the semi-empirical local functional approach (Sec. 3.5.2) combined with the linear parametric model (Sec. 3.5.3), compares well with Monte-Carlo simulation data. Here, the results of this approach in the high temperature regime, $t > 0$, and for general values $h_b \neq 0$ of the bulk ordering are evaluated. For $h_b < 0$ and $t < 0$, i.e., in the region of the thermodynamic space where capillary condensation occurs this approach may be not valid as discussed in Appendix B. This issue has been not investigated within the present study, because the range of values $t > 0$ has been sufficient for studying critical Casimir forces in colloidal suspensions. The detailed calculations, which follow the ones presented in Ref. [257], are given in Appendix B. The solvation force and the order parameter profile are obtained by integrating the corresponding Euler-Lagrange equation. For $(+, +)$ boundary conditions the order parameter profile exhibits a minimum $\Phi_{min} = \Psi_{min} \Phi_b(-|t|, h_b = 0^+)$. Within the local functional approach as given in Eq. (3.31) and specified in Eqs. (3.32) and (3.34), the scaling variables Ψ_{min} and $\mathcal{Y} = \text{sgn}(t) L/\xi_t$ are related in the strong adsorption limit for $t > 0$ via [see Eq. (B.7)]

$$A_2 \mathcal{Y} = \int_{\Psi_{min}}^{\infty} du \left[\frac{u^{-2(1+\nu/\beta)} \tilde{Z}_{\pm}(u)}{\tilde{Y}_{\pm}(u, \Sigma) - (\Psi_{min}/u)^{1+\delta} \tilde{Y}_{\pm}(\Psi_{min}, \Sigma)} \right]^{1/2}, \quad (5.2)$$

where $A_2 = [2\delta(\delta + 1)]^{-1/2} \left(\frac{\delta R_{\chi}}{Q_2} \right)^{\nu/\gamma}$ is a universal amplitude, compare with Eqs. (3.14) and (3.16), $\tilde{Z}_{\pm}(\Psi) = Z_{\pm}(\Psi)/Z_{\pm}(\infty)$ and $\tilde{Y}_{\pm}(\Psi, \Sigma) = Y_{\pm}(\Psi, \Sigma)/Y_{\pm}(\infty, 0)$ are the universal scaling functions of the ratio $\frac{\xi^2}{2\chi}$ of the bulk correlation length and the susceptibility and of the excess over bulk conjugated free energy density \mathcal{W} , respectively, see Eqs. (3.35), and the approximation $\hat{\mathcal{G}}^{-1}(x) \simeq \sqrt{x}$ (see Appendix B) has been adopted. For $t > 0$ the scaling function $\vartheta_{\parallel+}^{(d)}$ is obtained as [compare Eq. (B.5)]

$$\vartheta_{\parallel+}^{(d)}(\mathcal{Y} > 0, \Sigma) = -A_1 \mathcal{Y}^d \Psi_{min}^{(1+\delta)} \tilde{Y}_{\pm}(\Psi_{min}, \Sigma) \quad (5.3)$$

with the universal amplitude $A_1 = R_{\chi} Q_c / (\delta + 1)$, compare with Eqs. (3.14) and (3.16). In terms of the variables $\{\mathbf{s}, \mathfrak{z}\}$ and the functions of the parametric representation

(Sec. 3.5.3) these expressions are, see Eqs. (B.10) and (B.9), respectively,

$$\vartheta_{\parallel+}^{(d)} = -\frac{Q_+}{\alpha} \mathcal{Y}^d |\mathbf{k}(\mathfrak{z}_{min})|^{-d\nu} w(\mathfrak{z}_{min}; \mathfrak{z}_b) / (A_+) \quad (5.4)$$

and

$$\mathcal{Y} = \frac{2}{\xi_+^{(0)}} \int_{\mathfrak{z}_{min}}^{\mathfrak{z}_c} d\hat{\mathfrak{z}} \frac{|\mathbf{k}(\hat{\mathfrak{z}})|^\nu [m'(\hat{\mathfrak{z}}) - \beta m(\hat{\mathfrak{z}}) k'(\hat{\mathfrak{z}}) / k(\hat{\mathfrak{z}})] \sqrt{a(\hat{\mathfrak{z}}) / w(\hat{\mathfrak{z}}, \mathfrak{z}_b)}}{\sqrt{1 - \left(\frac{k(\hat{\mathfrak{z}})}{k(\mathfrak{z}_{min})}\right)^{2-\alpha} w(\mathfrak{z}_{min}; \mathfrak{z}_b) / w(\hat{\mathfrak{z}}; \mathfrak{z}_b)}}, \quad (5.5)$$

where Q_+ is a universal amplitude ratio [Eq. (3.16)]. In Eq. (5.4) the ratio of w and A_+ is a universal function [see Eq. (3.8) and Appendix B] and in Eq. (5.5) the non-universal metric factor $\xi_+^{(0)} = |\mathbf{k}(0)|^\nu [2a(0)/p(0)]^{1/2}$ cancels with the non-universal metric factors of the integrand (compare with Sec. 3.5.3) such that for both equations the right hand sides are indeed universal. The ‘‘radial’’ variable \mathfrak{z} of the parametric model is related to Σ by Eq. (3.41). \mathfrak{z}_b and \mathfrak{z}_{min} correspond to the corresponding bulk thermodynamic state (t, h_b) and to Ψ_{min} , respectively. The functions \mathbf{k} , w , m , and a describe the dependence of t , \mathcal{W} , Φ , and $\frac{\xi^2}{2\chi}$ on \mathfrak{z} , see Eqs. (3.36), (3.39a), (3.36), and (3.40), respectively, and m' and k' are corresponding derivatives w.r.t. \mathfrak{z} .

In Fig. 5.3, for various fixed values of $\Sigma = \text{sgn}(th_b) \xi_t / \xi_h$ [Eq. (3.19b)], the variation of the scaling functions $\vartheta_{\parallel+,\text{II}}^{(3)} = \vartheta_{\parallel+}^{(3)}(\mathcal{Y}, \Sigma)$ upon changing $\mathcal{Y} = \text{sgn}(t) L / \xi_t$ as resulting from Eqs. (5.4) and (5.5) within the linear parametric model, Eqs. (3.42), (3.43), and (3.44), are shown. It was chosen to present $\vartheta_{\parallel+,\text{II}}^{(3)}$, in order to enable a direct comparison with the scaling functions resulting from the proposed approximation (Sec. 5.3), which is formulated in terms of $\vartheta_{\parallel+,\text{II}}^{(d)}$ and is based on both Monte-Carlo simulation data and the mean-field theory. In order to compare with the corresponding results obtained within mean-field theory and presented in Fig. 5.2 in terms of $\vartheta_{\parallel+,\text{III}}^{(4)} = \vartheta_{\parallel+}^{(4)}(\mathbf{Y} = \text{sgn}(t) L / \xi(t, h_b), \Sigma)$, recall the definitions of these scaling variables given in Eqs. (3.25). $\mathbf{Y} = \mathcal{Y} I(|\Sigma|)$, where I interpolates between the two limiting cases $I(|\Sigma| \rightarrow 0) = 1$ and $I(|\Sigma| \rightarrow \infty) = |\Sigma|^{-1}$, see Eq. (3.11). Accordingly the abscissae \mathcal{Y} and $\mathcal{Y}\Sigma$ in Figs. 5.3 a) and b), respectively, correspond to these limiting cases of the abscissa \mathbf{Y} in Fig. 5.2.

The scaling functions $\vartheta_{\parallel+}^{(3)}$ obtained from the local functional approach within the linear parametric model exhibit the same qualitative features as the ones calculated within Landau theory see Fig. 5.3 and Fig. 5.2, respectively. The curves $\vartheta_{\parallel+,\text{II}}^{(3)}$ as functions of $\mathcal{Y} = \text{sgn}(t) L / \xi_t$ exhibit a minimum which deepens upon decreasing the value of $\Sigma = \text{sgn}(th_b) \xi_t / \xi_h$. For large negative values of Σ , the minimum is about ten times deeper than for $\Sigma = 0$. Thus the increase of the the strength $|\vartheta_{\parallel+}^{(d)}|$ is stronger for $d = 3$ than within mean-field theory ($d = 4$). For latter, the depth of the minimum becomes deeper by a factor of about 7. These values are, however, quite similar and rather small, compared to $d = 2$ for which the minimum along the critical isochore is of the order of $\sim 100 \vartheta_{\parallel+}^{(d)}(0, 0)$ [218]. For not too negative values of

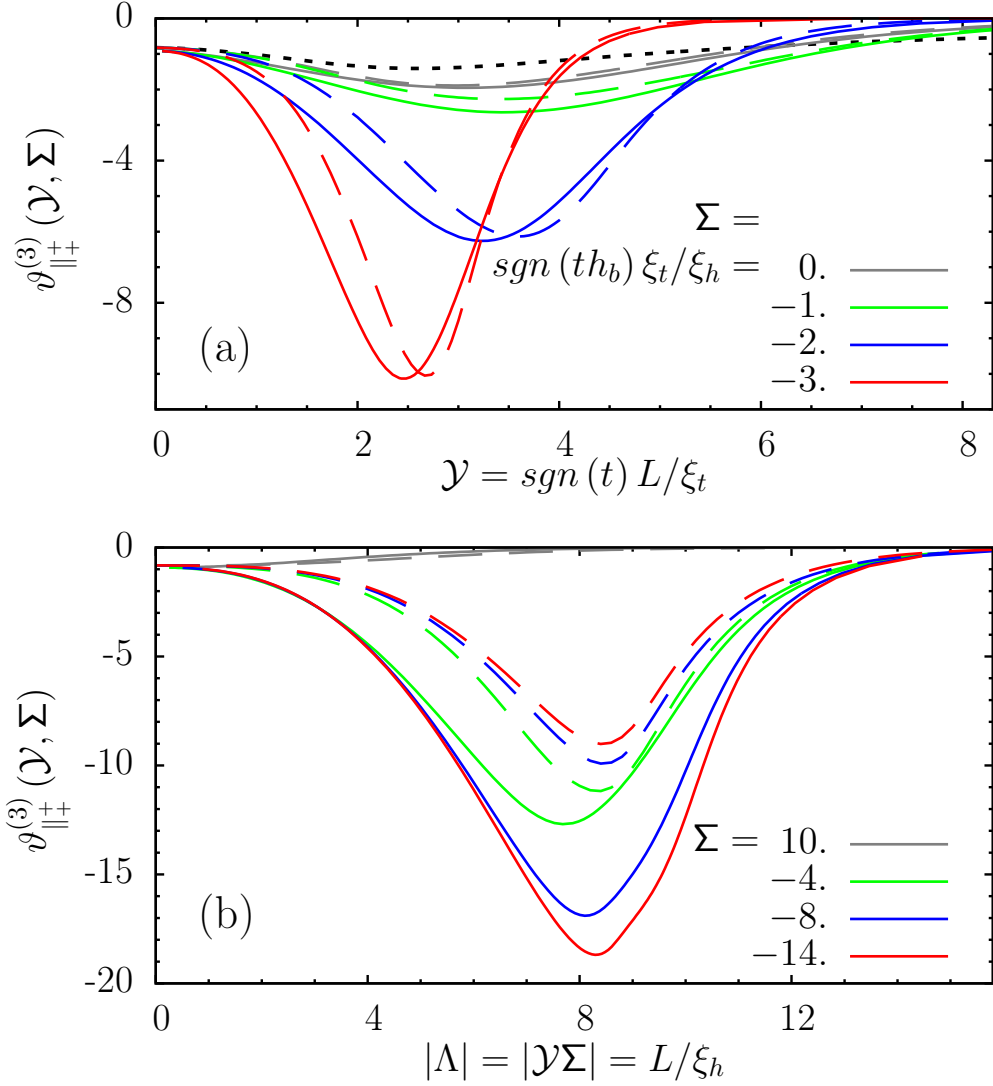


Figure 5.3.: The scaling functions $\vartheta_{\parallel+}^{(d=3)}(\mathcal{Y}, \Sigma)$ of the critical Casimir force in a $(d=3)$ -dimensional film subject to $(+, +)$ boundary conditions, Eq. (3.25), in the high-temperature regime, i.e., $t = (T - T_{c,b})/T_{c,b} > 0$, where $T_{c,b}$ is the upper bulk critical temperature. The full lines are obtained from the local functional approach and the linear parametric model, Eqs. (5.3) and (5.4). The dashed lines are obtained from the dimensional approximation Eq. (5.6) within which the dependence on the bulk field is taken into account from the corresponding scaling function in $d' = 4$. The scaling variables are $\mathcal{Y} = \text{sgn}(t) L/\xi_t$ and $\Sigma = \text{sgn}(th_b) \xi_t/\xi_h$, where L is the film width and ξ_t and ξ_h are the true bulk correlations associated to the reduced temperature deviation t and the bulk ordering field h_b conjugated to the order parameter, Eqs. (3.10). $\Sigma = \text{const}$ defines thermodynamic paths which pass through the bulk critical point, corresponding to $\mathcal{Y} = 0$, and along which the strength of the influences of these two control parameters relative to each other, measured in terms of their correlation lengths, are constant. The critical isochor ($h_b = 0$) corresponds to $\Sigma = 0$ and the critical isotherm ($t = 0$) to $|\Sigma| = \infty$. For large values $|\Sigma| = \xi_t/\xi_h \gg 1$ the corresponding thermodynamic paths lie close to the critical isotherm and the scaling function $\vartheta_{\parallel+}^{(d=3)}$ attains notable values only for small values $t \ll 1$. For such thermodynamic paths

the proper scaling variable is $|\Lambda| = |\Sigma\mathcal{Y}| = L/\xi_h$, see panel (b). Upon decreasing the bulk ordering field, i.e., decreasing the value of Σ , the strength $|\vartheta_{\parallel\pm}^{(d=3)}|$ increase remarkably. The minimum at the critical isotherm is about ten times deeper than the one at the critical isochor. For not too strong bulk ordering field, i.e., for $|\Sigma| \lesssim 3$, the curves from the two different approaches compare well, see panel (a). The largest deviations are observed close to the bulk critical point, i.e., for small values of $\mathcal{Y} = \text{sgn}(t) L/\xi_t$. Right at the bulk critical point, $\mathcal{Y} = \text{sgn}(t) L/\xi_t \sim |t|^\nu = 0$, the values of the curves of each approach are the same regardless the value of $|\Sigma| = \xi_t/\xi_h \sim |t|^{-\nu} |t|^{\nu/(\beta\delta)}$, because $\mathcal{Y} = 0$ and $|\Sigma| < 0$ implies $t = 0$ and $h_b = 0$. For strong bulk fields, i.e., $\Sigma < -4$ the resulting curves of the dimensional approximation exhibit even the opposite trend, i.e., the strength $|\vartheta_{\parallel\pm}^{(d=3,d'=4)}|$ decreases for more negative values of Σ . In order to explain this failure one has to resort to the ratio $\vartheta_{\parallel\pm}^{(d=3)}(\mathcal{Y}, \Sigma = 0) / \vartheta_{\parallel\pm}^{(d'=4)}(\mathcal{Y}, \Sigma = 0)$ of the scaling functions in the spatial dimensions d and d' along the critical isochore. The black dotted curve in panel (a) represents the negative values of this ratio. Within the approximation, this ratio accounts for the behavior in spatial dimension d . However, for large values $|\Sigma| \gg 1$ only its value at $\mathcal{Y} = 0$ but not its full shape enters the approximation. For more details see the main text.

$\Sigma = \text{sgn}(th_b) \xi_t/\xi_h$, the position $\mathcal{Y}_{min}(\Sigma)$ of the minimum increases upon decreasing the value of Σ , see Fig. 5.3 a). For large values of $|\Sigma| = \xi_t/\xi_h$ the relevant part of the corresponding thermodynamic path is close to the critical isotherm and accordingly $\mathcal{Y}_{min}(\Sigma \rightarrow -\infty) \sim |t|^\nu \rightarrow 0$. For negative values of $\Sigma = \text{sgn}(th_b) \xi_t/\xi_h$ the corresponding position $|\Lambda|_{min} = |\Sigma\mathcal{Y}_{min}(\Sigma)| = (L/\xi_h)_{min}$ increases upon decreasing the value of Σ , see Fig. 5.3 b). This behavior of the minimum is in line with the monotonous increase of $|\mathcal{Y}(\Sigma)|_{min} = [L/\xi(t, h_b)]_{min}$ as observed within mean-field theory (Sec. 5.1). The position $\mathcal{Y}_{min}(\Sigma)$ of the minimum as obtained from the present local functional theory shifts from $\mathcal{Y}_{min}(\Sigma = 0) = \mathcal{Y}_{min}(\Sigma = 0) = \text{sgn}(t) L/\xi_t \simeq 3.1$ at the critical isochor towards $\mathcal{Y}_{min}(\Sigma = -\infty) = \Lambda_{min}(\Sigma = -\infty) = \text{sgn}(h_b) L/\xi_h \simeq 8.4$ at the critical isotherm. These values are similar to the ones obtained from mean-field theory, see Sec. 5.1.

5.3. Dimensional comparison and approximation

$\vartheta_{\parallel\pm}^{(d)}$ depends nontrivially on the spatial dimension d . It turns out that qualitative features are often the same in $d = 2, 3, 4$ (for examples of exceptions see, e.g., Ref. [188]) but there are significant quantitative differences, see Sec. 5.1 and Sec. 5.2 and the references given in Sec. 3.4. Beside the interest in its own rights, the dependence on spatial dimension d can be used to estimate the behavior in the experimental relevant case $d = 3$ from the cases $d = 2$ and $d = 4$, for which (quasi-)exact results for many situations are available, see e.g. Refs. [225, 195]. Systematically, this can be done within the ϵ -expansion [235], where $\epsilon = d_{>} - d$ and the upper critical dimension $d_{>} = 4$ for the Ising universality class. Because $\vartheta_{\parallel\pm}^{(d=3)}(\mathcal{Y}, \Sigma = 0)$ is rather accurately known from Monte-Carlo simulations, the

dependence of $\vartheta_{\parallel}^{(d)}$ on Σ can be approximated by

$$\vartheta_{\parallel}^{(d)}(\mathcal{Y}, \Sigma) \simeq \vartheta_{\parallel}^{(d)}(\mathcal{Y}, \Sigma = 0) \frac{\vartheta_{\parallel}^{(d')}(\mathcal{Y}, \Sigma)}{\vartheta_{\parallel}^{(d')}(\mathcal{Y}, \Sigma = 0)} \equiv \vartheta_{\parallel}^{(d)}(\mathcal{Y}, \Sigma = 0) \varpi_{\vartheta_{\parallel}}^{(d')}(\mathcal{Y}, \Sigma). \quad (5.6)$$

Obviously, for $d = d'$ in Eq. (5.6) the lhs and rhs are equal. For $d \neq d'$ Eq. (5.6) is an approximation, which can be motivated by the observation that typically the qualitative features of the shape of the corresponding scaling functions depend on d only mildly, see, e.g., the comparison of results as obtained within mean-field theory with corresponding results obtained by Monte-Carlo simulations for $d = 3$ or with exact results for $d = 2$ in Refs. [200, 201, 214]. Notice that for $\Sigma \rightarrow 0$ the lhs and rhs of Eq. (5.6) become equal for all values of d, d' , and \mathcal{Y} . Thus, in this sense, this approximation is concentrated on the dependence on h_b . For $d' = 4$ the approximation given in Eq. (5.6) can be understood as the lowest order contribution, $\mathcal{O}(\epsilon^0)$, in the systematic ϵ -expansion of $\varpi_{\vartheta_{\parallel}}^{(d)}(\mathcal{Y}, \Sigma)$ which carries the Σ -dependence of the critical Casimir force. Due to the normalization, a mean-field treatment of $\varpi_{\vartheta_{\parallel}}^{(d)} = \vartheta_{\parallel}^{(d)}(\mathcal{Y}, \Sigma)/\vartheta_{\parallel}^{(d)}(\mathcal{Y}, \Sigma = 0)$ does not suffer from the undetermined amplitude of $\vartheta_{\parallel}^{(d=4)}$.

In the expression for $\varpi_{\vartheta_{\parallel}}^{(d')}$ in Eq. (5.6) the scaling variables $\mathcal{Y} = \text{sgn}(t) L/\xi_t$ and $\Sigma = \text{sgn}(th_b) \xi_t/\xi_h$ are taken with the bulk critical exponents corresponding to the spatial dimension d . Thus the proposed approximation concerns only the shape of the scaling function $\varpi_{\vartheta_{\parallel}}^{(d)}$. The use of bulk critical exponents corresponding to the spatial dimension d in the scaling variables which are arguments of the scaling function in spatial dimension $d' \neq d$, may lead to a deviation from the proper asymptotic behavior [284]. For example, for $|\Sigma| = \xi_t/\xi_h = 0$ in the limit $\mathcal{Y} = \text{sgn}(t) L/\xi_t \rightarrow \infty$ both within mean-field theory and within the local functional approach for $d = 3$ the asymptotic behavior $\vartheta_{\parallel}^{(d)}(\mathcal{Y} \rightarrow \infty) \sim \mathcal{Y}^{2-\alpha} \exp(-\mathcal{Y})$ has been found, see Refs. [195] and [204], respectively. Thus, because the value of α depends on d , for $L \rightarrow \infty$ the asymptotic behavior of the critical Casimir force is indeed different for different values of d . However, this potential violation of the proper asymptotic behavior might occur for large values of the arguments of the scaling function where its value is (exponentially) small and it might not matter quantitatively in the range of values of \mathcal{Y} and Σ for which the scaling function $\vartheta_{\parallel}^{(d)}$ is large.

In Fig. 5.4 the scaling function $\vartheta_{\parallel, \pm, \Gamma}^{(d=2)}$ of the critical Casimir force for the fixed value $\mathcal{Y} = \text{sgn}(t) L/\xi_t = 1.67$ as a function of $\Lambda = \text{sgn}(h_b) L/\xi_h$ is shown. The exact results are taken from Fig. 2 b) of Ref. [185]. In $d = 2$ the bulk critical exponents $\nu(d = 2, d_{\Phi} = 1) = 1$ and $\Delta(d = 2, d_{\Phi} = 1) = \beta\delta = 15/8$ are exactly known. The non-universal amplitudes of the bulk correlation lengths of the two-dimensional square lattice are $\xi_{+} = 1/[2\text{arcsinh}(1)]$ and $\xi_h^{(0)} \simeq 0.233$ [254]. The exact results are compared with the results of the approximation given in Eq. (5.6) with $d' = 4$. By construction of the approximation, the value for $\Lambda = 0$ is for both curves the same. Both curves exhibit a rather deep minimum which is located at negative values of Λ . However, the depth as obtained by the approximation is less than half of the depth of the exact results. More-

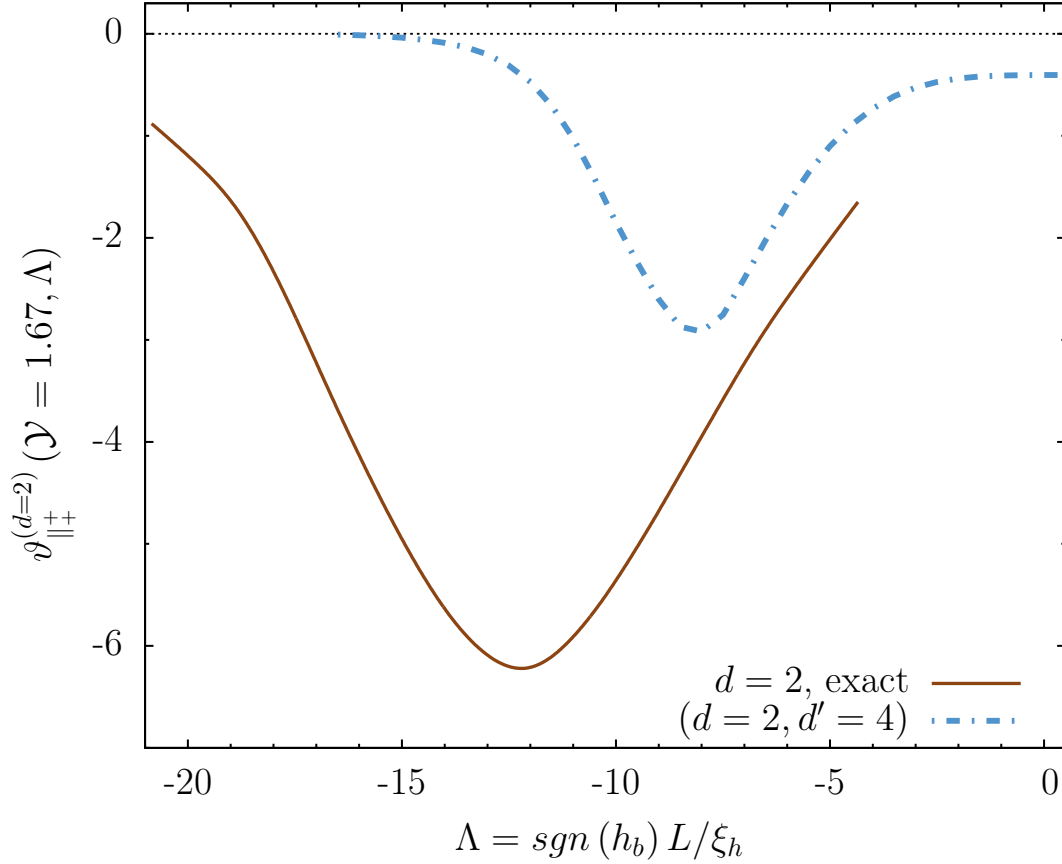


Figure 5.4.: Comparison of the exact scaling function $\vartheta_{\parallel+}^{(2)}(\mathcal{Y} = 1.67, \Lambda)$ of the critical Casimir force in a ($d = 2$)-dimensional film subject to $(+, +)$ boundary conditions with the corresponding curve as obtained from the dimensional approximation given in Eq. (5.6) for $d = 2$ and $d' = 4$. The exact results is taken from Fig. 2 b) of Ref. [185]. Varying the scaling variable $\Lambda = \text{sgn}(h_b) L/\xi_h$ at fixed value of the scaling variable $\mathcal{Y} = \text{sgn}(t) L/\xi_t$ corresponds to vary the bulk ordering field h_b at fixed value of the reduced temperature deviation $t = (T - T_{c,b})/T_{c,b}$; $T_{c,b}$ is the upper critical temperature. The dimensional approximation is able to reproduce the qualitative features of the exact result, i.e., the pronounced minimum at a negative value of Λ . However, the dimensional approximation fails quantitatively. The position of the minimum is at a too less negative value of Λ and its depth is only about half of the exact one. Also, whereas the value of the approximate function has reached 0 already for $\Lambda \approx -15$, the exact scaling function $\vartheta_{\parallel+}^{(2)}(\mathcal{Y} = 1.67, \Lambda)$ has large values even for $\Lambda < -20$.

over the position of the minimum is $\Lambda_{min} = -12$ for the exact results but $\Lambda_{min} = -8$ within the approximation. The comparison with other exact results for $d = 2$ which are available [185, 221] reveals, that the proposed approximation in Eq. (5.6) for $d = 2$ and $d' = 4$ does not hold quantitatively. Although the approximation captures the qualitative trend that the depth of the minima becomes significantly deeper upon decreasing the value of t , the actual value of the depth is however clearly underestimated; for $t < 0$ even by one or several orders of magnitude.

For $d = 3$ and $h_b \neq 0$ there are no (quasi-)exact results or Monte Carlo simulation data available with which the results for $d = 2$ and 4 could be compared with. But the results obtained from the local functional approach presented in Sec. 5.2 can be compared with the approximation given in Eq. (5.6). As can be inferred from Fig. 5.3, for $d = 3$ and $d' = 4$ the approximation given in Eq. (5.6) compares to a certain extent even quantitatively well with the results obtained from the local functional approach. In Fig. 5.3, curves $\vartheta_{\parallel+}^{(3)}(\mathcal{Y} = \text{sgn}(t) L/\xi_t, \Sigma = \text{const})$ are shown for various values of $\Sigma = \text{sgn}(th_b) \xi_t/\xi_h$. For the approximation the function $\vartheta_{\parallel+}^{(d=3)}(\mathcal{Y}, \Sigma = 0)$ from Monte Carlo simulations [201] has been used. Therefore a slight difference between the curves for $\Sigma = 0$ occurs, because $\vartheta_{\parallel+}^{(d=3)}$ from the local functional approach and from the Monte Carlo simulations differ slightly. At $\Sigma = \text{sgn}(th_b) \xi_t/\xi_h = 0$ the minimal value of $\vartheta_{\parallel+}(\mathcal{Y}, \Sigma = 0)$ occurs for $d = 4$ at a larger value \mathcal{Y}_{min} of $\mathcal{Y} = \text{sgn}(t) L/\xi_t$ than for $d = 3$. This property transfers to values $\Sigma \neq 0$, where \mathcal{Y}_{min} is moderately larger within the dimensional approximation than within the local functional approach. The depth of the minima of the curves $\vartheta_{\parallel+}^{(3)}(\mathcal{Y}, \Sigma = \text{const})$ for moderate negative values of Σ is notably deeper within the local functional approach than for the dimensional approximation, see the green curves in Fig. 5.3 a) corresponding to $\Sigma = -1$. Upon further decreasing the value of Σ this difference in the values of the minimas becomes quite small, see the blue and the red curves in Fig. 5.3 a) corresponding to $\Sigma = -2$ and -3 , respectively. For all values of Σ corresponding to the curves shown in Fig. 5.3 a) the largest deviations between the results of the local functional approach and of the dimensional approximation occurs for values of \mathcal{Y} which are larger than 0 and smaller than \mathcal{Y}_{min} . For values of \mathcal{Y} larger than \mathcal{Y}_{min} the curves obtained from the two different approaches and corresponding to the same value of Σ become comparable.

For values of $\Sigma < -4$ the curves as obtained from the dimensional approximation clearly deviate from the curves obtained from the local functional approach, see Fig. 5.3 b). The simultaneous limit $\Sigma^{-1}, \mathcal{Y} \rightarrow 0$ with $\Lambda = \mathcal{Y}\Sigma = \text{sgn}(h_b) L/\xi_h = \text{const}$, corresponds to the critical isotherm (i.e., $t = 0$ and $h_b \neq 0$). Along the critical isotherm, the curve from the dimensional approximation, Eq. (5.6), attains the shape corresponding to d' . Accordingly, the curves shown in Fig. 5.3 b) reflect the quantitative differences of the scaling functions $\vartheta_{\parallel+}^{(d)}$ for $d = 4$ and $d = 3$ upon approaching the critical isotherm (see also Secs. 5.1 and 5.2 and in particular recall that the minimum at the critical isotherm is by a factor 7 and 10, respectively, deeper than at the critical isochor). For $\Sigma < -4$ the minimum in the curves $\vartheta_{\parallel+}^{(d)}(\mathcal{Y}, \Sigma = \text{const})$ from the dimensional approxi-

mation becomes shallower upon decreasing Σ , see Fig. 5.3 b). This is in stark contrast to the behavior seen for the curves corresponding to $d = 3$ and $d = 4$ from mean-field theory and the local functional approach, respectively. That reason lies in the behavior of the ratio $\vartheta_{\parallel+}^{(3)}(\mathcal{Y}, \Sigma = 0) / \vartheta_{\parallel+}^{(4)}(\mathcal{Y}, \Sigma = 0)$, see the black dotted line in Fig. 5.3 a). The curve resulting from the dimensional approximation [Eq. (5.6)] for $\Sigma \neq 0$ is the corresponding curve $\vartheta_{\parallel+}^{(4)}(\mathcal{Y}, \Sigma)$ obtained from the Landau theory weighted with the ratio $\vartheta_{\parallel+}^{(3)}(\mathcal{Y}, \Sigma = 0) / \vartheta_{\parallel+}^{(4)}(\mathcal{Y}, \Sigma = 0)$ of the scaling functions for $\Sigma = 0$ in $d = 3$ and $d = 4$. This ratio attains its maximal value for $\mathcal{Y}_{max}^{rat} \simeq 2.6$, and thus for a smaller value of \mathcal{Y} than the ones for which $\vartheta_{\parallel+}^{(3)}(\mathcal{Y}, \Sigma = 0)$ and $\vartheta_{\parallel+}^{(4)}(\mathcal{Y}, \Sigma = 0)$ attain their extremal values. (In Fig. 5.3 a) the negative values of this ratio are plotted and therefore the corresponding curve has a minimum.) Upon decreasing the value of $\Sigma < 0$, the minima corresponding to the curve $\vartheta_{\parallel+}^{(4)}(\mathcal{Y}, \Sigma)$ moves towards smaller values of \mathcal{Y} . Accordingly, there is a value of Σ , for which the curve $\vartheta_{\parallel+}^{(4)}(\mathcal{Y}, \Sigma)$ happens to attain its extremal value precisely at \mathcal{Y}_{max}^{rat} . And for this value of Σ , the minimum in the corresponding curve from Landau theory is amplified the most within the dimensional approximation. This is in line with the observation that for $\Sigma \approx -3$ the corresponding minimas from the dimensional approximation and from the local functional approach are located close to \mathcal{Y}_{min}^{rat} and have similar depths. Upon further decreasing the value of $\Sigma = \text{sgn}(th_b) \xi_t / \xi_h$, on one hand the minimum of $\vartheta_{\parallel+}^{(4)}(\mathcal{Y}, \Sigma)$ becomes deeper, but on the other hand it is less amplified. As it turns out, the latter effect is stronger and thus leads to the observed behavior. Recall (see Secs. 5.1 and 5.2) that the depth of the minimum of $\vartheta_{\parallel+}^{(4)}$ along the critical isotherm is about $10\vartheta_{\parallel+}^{(4)}(0, 0)$ and the depth of the minimum for $d = 3$ along the critical isochore is about twice the corresponding value at $\mathcal{Y} = 0$. Moreover it becomes by a factor of ten deeper along the critical isotherm. Therefore for large negative values of $\Sigma \rightarrow -\infty$ the depths of the minima of the curves as obtained by the local functional approach and by the dimensional approximation differ by a factor of ~ 2 , see Fig. 5.3.

5.4. Derjaguin approximation

Within the Derjaguin approximation, which is valid for $\Delta = D/R \rightarrow 0$, where D is the surface-to-surface between two spheres and R is their radius, the results of $\vartheta_{\parallel}^{(d)}$ can be used in order to obtain the scaling functions $\vartheta_{\circ\circ}^{(d, d_\circ)}$ and $\Theta_{\circ\circ}^{(d, d_\circ)}$ of the critical Casimir force between two d_\circ -dimensional spherical particles and of the corresponding potential. For $d_\circ = 3$ see Eqs. (3.27) and (3.28), respectively. Because in the following only the case $d_\circ = 3$ is considered this dependence will not be written explicitly.

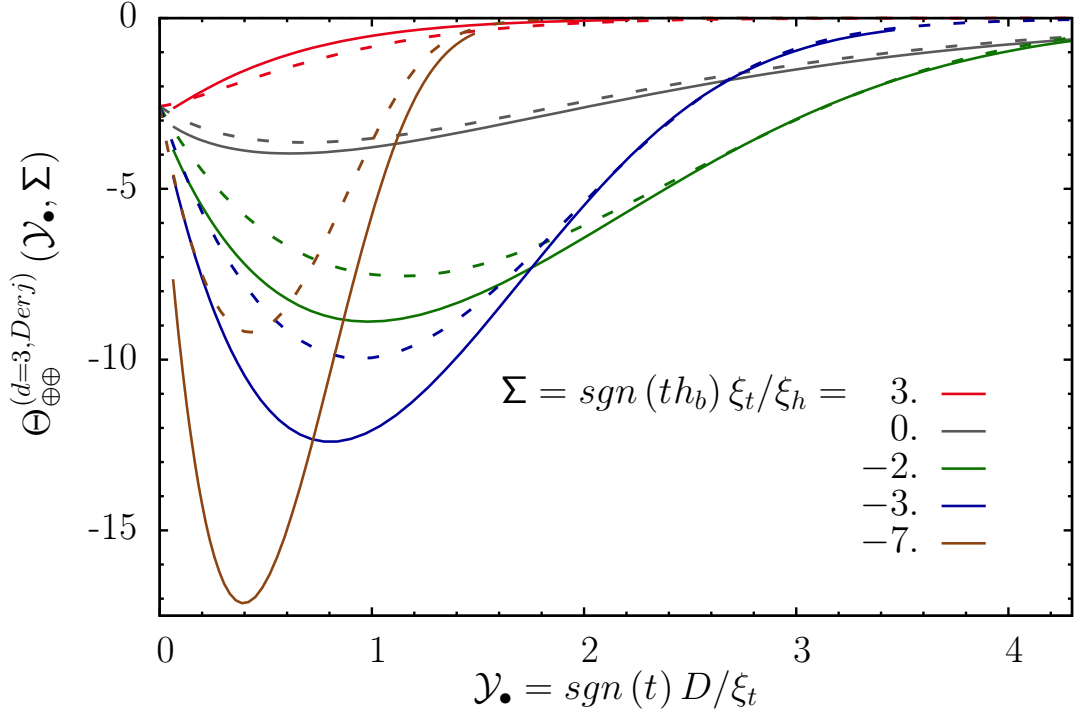


Figure 5.5.: Comparison of the scaling function $\Theta_{\oplus\oplus}^{(d=3, Derj)}$ of the potential of the critical Casimir force [Eq. (3.26)] between two spheres with $(+, +)$ boundary conditions in spatial dimension $d = 3$ within the Derjaguin approximation, Eq. (3.28). The input scaling functions $\vartheta_{\parallel+}^{(3)}$ of the critical Casimir force in the film are from the local functional approach (full lines, see also Sec. 5.2) and from dimensional approximation, Eq. (5.6), with $d' = 4$ (dashed lines, see also Sec. 5.3). The scaling variables are $\mathcal{Y}_\bullet = \text{sgn}(t) D/\xi_t$ and $\Sigma = \text{sgn}(th_b) \xi_t/\xi_h$, where D is the surface-to-surface distance between the spheres and ξ_t and ξ_h are the true bulk correlation lengths, Eq. (3.10), of the reduced temperature deviation $t = (T - T_{c,b})/T_{c,b}$ from the upper critical temperature $T_{c,b}$ and of the bulk ordering field h_b . The Derjaguin approximation corresponds to the limit $\Delta = D/R \rightarrow 0$, where R is the radius of the spheres. The resulting scaling function does not depend on Δ . $\Sigma = \text{sgn}(th_b) \xi_t/\xi_h = \text{const}$ [Eq. (3.19b)] corresponds to thermodynamic paths along which the relative (to each other) influence of the two control parameters t and h_b does not vary. $\Sigma = 0$ and $|\Sigma| = \infty$ correspond to the critical isochore ($h_b = 0$) and the critical isotherm ($t = 0$), respectively. Thermodynamic paths corresponding to values $\Sigma \gg 1$ lie close to the critical isotherm, and therefore the scaling function $\Theta_{\oplus\oplus}^{(d=3, Derj)}$ attains only in a small range of values of $\mathcal{Y}_\bullet = \text{sgn}(t) L/\xi_t$ large values, compare, e.g., the brown curves and the green curves corresponding to $\Sigma = -7$ and $\Sigma = -2$, respectively. As it has been observed in the film geometry (see also Fig. 5.3) the dimensional approximation works well only for not too large values of $\Sigma = \text{sgn}(th_b) \xi_t/\xi_h$ and for large values of $\mathcal{Y}_\bullet = \text{sgn}(t) L/\xi_t$.

$d = 3$ comparison

The scaling functions $\Theta_{\oplus\oplus}^{(d=3,Derj)}$ resulting from the scaling functions $\vartheta_{\parallel\pm}^{(d=3)}$ obtained by using the local functional approach (Sec. 5.2) and the dimensional approximation (Sec. 5.3), are shown in Fig. 5.5 for various fixed values of $\Sigma = \text{sgn}(th_b) \xi_t/\xi_h$ as functions of $\mathcal{Y}_\bullet = \text{sgn}(t) D/\xi_t$. ξ_t and ξ_h are the bulk correlation lengths [Eq. (3.10)] associated to the reduced temperature deviation $t = (T - T_{c,b})/T_{c,b}$ from the upper bulk critical temperature $T_{c,b}$ and to the bulk ordering field h_b . The observed gross features in that comparison are similar to the ones for the film geometry. For $\Sigma < 1.5$ the curves $\Theta_{\oplus\oplus}^{(3,Derj)}(\mathcal{Y}_\bullet)$ exhibit a minimum (on the scale of Fig. 5.5) which becomes deeper upon decreasing the value of Σ . The depth of the minimum as well as its deepening is more pronounced within the results of the local functional approach than for the curves obtained from the dimensional approximation. For both approaches the position of the minimum is similar. For $\Sigma \approx 2$ this position attains its largest value which is $\mathcal{Y}_\bullet \simeq 1$. Whereas in the film geometry for $\Sigma \approx -3$ the results of both approaches are similar, for the sphere-sphere geometry already at this values of $\Sigma = \text{sgn}(th_b) \xi_t/\xi_h$ the results of both approaches deviate quantitatively. This can be due to the integration over the scaling function $\vartheta_{\parallel\pm}^{(3)}$ in order to obtain $\Theta_{\oplus\oplus}^{(3,Derj)}$ [Eq. (3.28)], in which the quantitative differences add. As for the film geometry, within the dimensional approximation the minimum becomes shallower again for large negative values of Σ , see the discussion in Sec. 5.3.

Comparison with full calculations

The preliminary results obtained from numerical calculations in the full geometry for the scaling function $\vartheta_{\oplus\oplus}^{(d=4)}$ of the critical Casimir force between two spheres both with (+) boundary conditions are now available [285]. In Fig. 5.6, for $\mathcal{Y}_\bullet = D/\xi_t = 1$ and the various values $\Delta = D/R = 2.0, 1.0,$ and 0.5 the resulting curves $\vartheta_{\oplus\oplus}^{(4)}(\Lambda) = \vartheta_{\oplus\oplus}^{(4)}(\Delta = \text{const}, \mathcal{Y}_\bullet = \text{const}, \Lambda)$ as function of $\Lambda = \text{sgn}(h_b) L/\xi_h$ are compared with the corresponding curve obtained from the Derjaguin approximation. These curves exhibit similar characteristics. For $\Lambda > 0$ the curves $\vartheta_{\oplus\oplus}^{(4)}(\Lambda)$ monotonically approach 0 upon increasing the value of Λ . The minima of these curves are located at values $\Lambda_{min} \simeq -5 \dots -7$ and the values $|\vartheta_{\oplus\oplus}^{(d=4)}|$ at the minima are about $3 \dots 7$ times larger than the corresponding value at $\Lambda = 0$. For decreasing the value of Δ the position Λ_{min} becomes slightly more negative. The variation of the strength $|\vartheta_{\oplus\oplus}^{(d=4)}|$ upon changing the value of $\Delta = D/R$ exhibits different trends for different values of $\Lambda = \text{sgn}(h_b) L/\xi_h$. For $\Lambda = 0$ the strength weakens upon decreasing the value of Δ , whereas for mediate and large negative values of Λ the strength of $|\vartheta_{\oplus\oplus}^{(d=4)}|$ increases upon decreasing the value of $\Delta = D/R$. In particular, the minimum of the curves $\vartheta_{\oplus\oplus}^{(4)}(\Lambda)$ becomes deeper upon decreasing the value of Δ . The curve corresponding to $\Delta = 0.5$ does not exhibit clearly these features. This may be due to numerical artifacts. The numerical calculations for such small surface-to-surface distances are tedious and subtle. In order to obtain a better understanding of the dependence of $\vartheta_{\oplus\oplus}^{(d=4)}$ on the value of $\Delta = D/R$ the more accurate

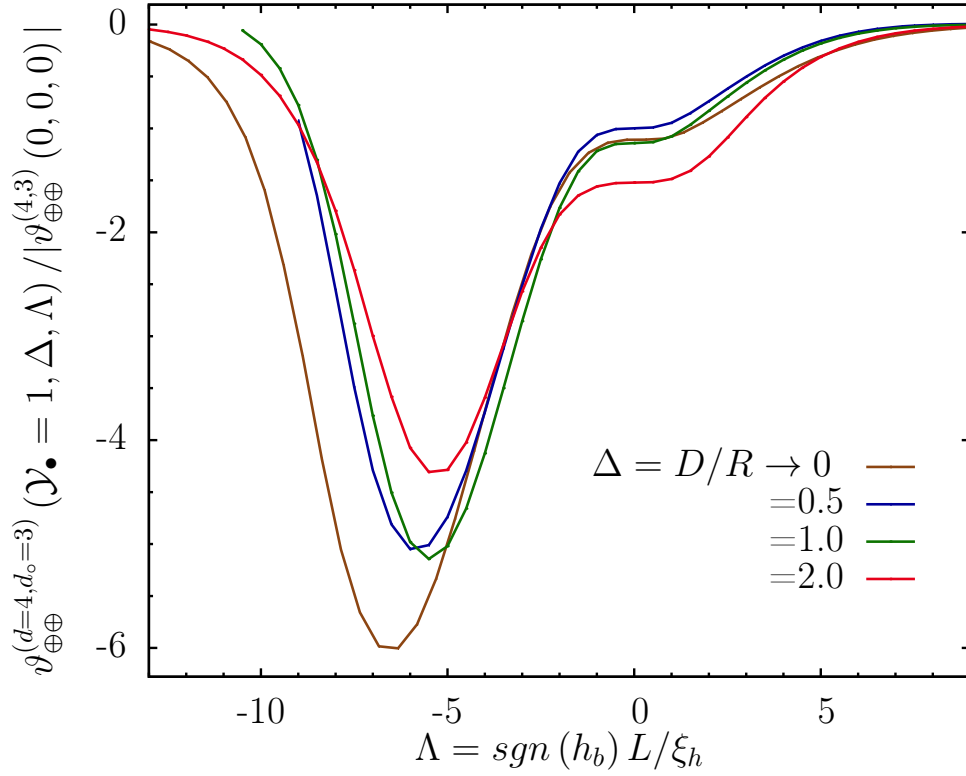


Figure 5.6.: The scaling functions $v_{\oplus\oplus}^{(d=4, d_o=3)}$ of the critical Casimir force between two three-dimensional (hyper-)spheres both with (+) boundary conditions in spatial dimension $d = 4$ as functions of $\Lambda = \text{sgn}(h_b) L / \xi_h$ at the fixed value $\mathcal{Y}_\bullet = \text{sgn}(t) D / \xi_t = 1$. ξ_t and ξ_h are the true bulk correlation lengths, Eq. (3.10), of the reduced temperature deviation $t = (T - T_{c,b}) / T_{c,b}$ from the upper critical temperature $T_{c,b}$ and of the bulk ordering field h_b . R is the radial extent of the (hyper-)spheres which are in one dimension infinitely large and D is their surface-to-surface distance. For $\Delta = D/R \neq 0$ the preliminary results are from Ref. [285]. $\Delta \rightarrow 0$ corresponds to the Derjaguin approximation, Eq. (3.27). The gross feature of these curves is the same, i.e., a pronounced minimum at negative bulk field, i.e., $\Lambda < 0$.

results need to be obtained. Further, the preliminary results of the full calculations for $\Delta > 0.1$ reveal that indeed for decreasing the value of $\Delta = D/R$ the curves approach the corresponding curves as obtained by the Derjaguin approximation. However, a quantitative agreement could not be achieved. This is in contrast to the sphere-plane geometry where for $\Delta < 0.3$ already quantitative agreement is observed [54, 55, 56, 231]. Because in the case of the sphere-sphere geometry there are two curved surfaces the influence of which are approximated within the Derjaguin approximation, instead of one such surface in the plane-sphere geometry it is reasonable that in the latter case the Derjaguin limit is approached already for larger values of Δ than in the former case. For $(d_o = 4)$ -dimensional spheres in spatial dimension $d = 4$ the results for the full geometry are available [222]. There, a non-monotonic dependence of the value of $v_{\oplus\oplus}^{(d=4, d_o=4)}$ on its variables has been observed.

6. Effective model

In an effective approach the presence of the solvent enters via the effective pair potential $V(r = D + 2R)/(k_B T) = U(r = D + 2R)$ acting between the large colloidal particles (Sec. 4.1). D is the surface-to-surface distance between the colloidal particles with radius R . For the present study of monodisperse colloidal particles immersed in a near-critical solvent two contributions to this effective potential are relevant. The background interaction potential between the colloids, which is present also away from the critical temperature $T_c^{(s)}$ of the solvent, consists of a hard core repulsion for center-to-center distances $r < 2R$ and a soft, repulsive tail U_{rep} for $D = r - 2R > 0$, see Eq. (4.1). The latter prevents aggregation due to omnipresent effectively attractive dispersion forces. Upon approaching the critical temperature $T_c^{(s)}$ of the solvent the critical Casimir forces emerge and their corresponding potential $V_c = k_B T U_c$, Eq. (3.26), adds to the background contribution. Therefore the effective pair-potential between the solute particles is given by

$$U(r) = \begin{cases} \infty, & D < 0 \\ U_{rep} + U_c^{(d=3)} = A \exp(-\kappa D) + (R/D) \Theta_{\oplus\oplus}^{(d=3)}(\mathcal{Y}_\bullet, \Delta, \Sigma) & D > 0. \end{cases} \quad (6.1)$$

For a particular experimental realization the strength A and the range κ^{-1} of the softly repulsive interaction are material dependent constants [Eq. (4.1)]. In Eq. (6.1) $\Theta_{\oplus\oplus}^{(d=3)}$ is the scaling function of the critical Casimir force, Eq. (3.26), which depends on the scaling variables $\mathcal{Y}_\bullet = \text{sgn}(t) D/\xi_t$, $\Delta = D/R$, and $\Sigma = \text{sgn}(th_b) \xi_t/\xi_h$. ξ_t and ξ_h are the bulk correlation lengths, Eqs. (3.10), associated with the reduced temperature deviation $t = (T_c^{(s)} - T)/T_c^{(s)}$ from the lower critical temperature of the solvent and the bulk ordering field h_b conjugated to the order parameter. In the case of binary liquid mixtures the bulk field $h_b \sim (\mu_a - \mu_b) - (\mu_a - \mu_b)_c$ is related to the deviation of the difference $(\mu_a - \mu_b)$ of the chemical potentials $\mu_{a,b}$ from the critical value of this difference. Additional interaction which would account for effectively attractive dispersion forces are not considered. Effectively, dispersion forces can be switched off by using index-matched colloidal suspensions. As will be discussed in Ch. 7, the presence of attractive dispersion forces does not change the conclusions of the present study. For dilute suspensions many-body effects of the critical Casimir forces can be neglected. However, such effects are important for determining the structure of the clusters formed. For capturing the *onset* of aggregation in the homogeneous solution the critical Casimir pair potential $U_c^{(d=3)}$ is sufficient. From the general expressions for the effective ($N \geq 2$)-body interactions presented in Ref. [9] one cannot deduce easily a condition, for which circumstances many-body ($N > 2$) interactions can be neglected. One may expect that for such low number densities ρ of the colloids for which the mean distance $\rho^{-1/d}$ between the colloids

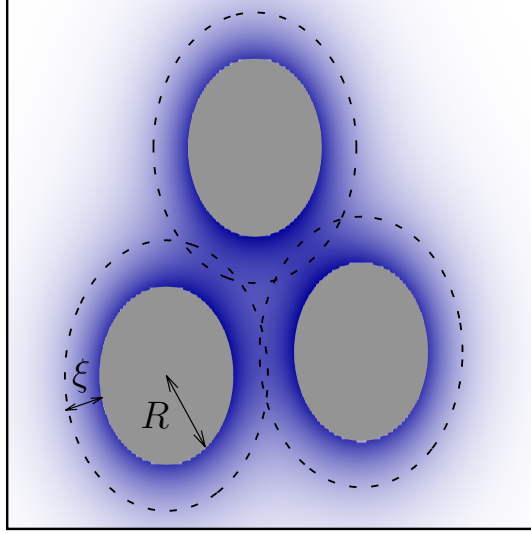


Figure 6.1.: Sketch of three colloidal particles (gray circles) with radii R immersed in a near-critical solvent. The disturbance of the order parameter profile around the particles is drawn as blue shaded area. The order parameter profile is disturbed on the scale of the bulk correlation length ξ (dashed lines indicate the spheres with radii $R + \xi$). For the three particles at contact, i.e., their center-to-center distance $r = 2R$, the regions of each particle in which the order parameter profile is disturbed have a common overlap if $\xi/R > \sqrt{4/3} - 1 \simeq 0.155$.

is large compared with the range of the critical Casimir forces, i.e., $\varrho^{-1/d} > 2R + \xi$, the approximation of pairwise additive critical Casimir forces is valid. However, from the general expressions it is not evident, that the range of the effective pair-potential and the mean-distance enter the condition for the validity of the pairwise approximation. Another criterion depends only on the properties of the order parameter profile. This profile is influenced by the presence of the colloidal particles on the scale of the bulk correlation ξ , see Fig. 6.1. Therefore, one can expect that three-body interactions become important, when the volumes of disturbance of three colloidal particles overlap. For three particles in contact, this is the case for $\xi/R > \sqrt{\frac{4}{3}} - 1 \simeq 0.155$ as has been shown by simple geometrical arguments in Ref. [286] in a different context.

6.1. Range of parameters

The effective pair-potential U given in Eq. (6.1) can be written in terms dimensionless parameters,

$$U(r = D + 2R) = \begin{cases} \infty & x < 0 \\ s \left\{ a \exp(-x) + (1/x) \Theta_{\oplus\oplus}^{(3,Derj)}(x/\zeta, \Sigma) \right\} & x > 0, \end{cases} \quad (6.2)$$

where $s = \kappa R$, $a = A/s$, $\zeta = \text{sgn}(t) \kappa \xi_t$, and $x = \kappa D = \kappa r - 2s$. (The amplitude a should not be confused with the acronym for the preferentially adsorbed phase.) This parametrization has the advantage, that the shape of U is determined by a , ζ , and Σ , while s tunes the overall strength of the potential without affecting its shape. The ratio of the competing length scales of repulsion and of the critical Casimir force are measured by ζ , which is typically varied experimentally; a is usually kept constant and provides a measure of the repulsion, while Σ [Eq. (3.19)] depends solely on the thermodynamic state of the solvent.

In the following the ranges of the values of the parameters entering into the effective potential, Eq. (6.2), and of the scaling variable Σ which correspond to possible experimental realizations are discussed. The radius R of colloidal particles typically varies between $0.1\mu m$ and $1\mu m$. In the experiments reported in the present context so far colloidal suspensions had been stabilized by electrostatic repulsion, with the value of the strength parameter A ranging over several orders of magnitudes, i.e., from $A \simeq 10^2$ up to $10^5 \dots 10^6$ (see, e.g., Refs. [44, 45, 79, 80]). The value of κ^{-1} can be tuned by salting the solution. Due to screening effects, an increased amount of ions in the solution leads to a decrease of κ^{-1} . Although the coupling between the charge density and fluctuations of the order parameter is not yet fully understood, there is experimental [287] and theoretical [288, 289, 290, 291, 292] evidence that critical adsorption and critical Casimir forces can be altered significantly by adding ions to the binary liquid mixture. Such subtle mechanisms are not taken into account within the effective potential, Eq. (6.2), discussed here. Therefore it is applicable only for not too small values of the screening length, i.e., for $\kappa^{-1} \gtrsim 10nm$. For binary liquid mixtures the correlation length amplitude $\xi_+^{(0)}$ is of the order of few Ångstrom. The relevant experiments have been carried out at room temperature due to $T_c^{(s)} \approx 300K$. In those experiments deviations from the critical temperature as small as $T - T_c^{(s)} \sim 10mK$ have been resolved [44, 45], which corresponds to a correlation length ξ_t of a couple of tens of nm .

It is more difficult to assess the experimentally relevant range of the scaling variable Σ , which is a function of the bulk ordering field h_b . Often the amplitude $\xi_h^{(0)}$ of the correlation length $\xi_h(h_b)$ is not known. However, one may use the equation of state, Eq. (3.20), which relates Σ to the scaling variable X associated with the order parameter Φ , Eq. (3.19). In terms of the parameters of the potential given in Eq. (6.2), for $t > 0$ one has $X = m_0 \zeta^{-1/\nu}$ with

$$m_0 = \text{sgn}(\Phi) \left(\zeta_+^{(0)} \right)^{1/\nu} |\mathcal{B}_t/\Phi|^{1/\beta} \quad (6.3)$$

where $\zeta_+^{(0)} = \kappa \xi_+^{(0)}$. \mathcal{B}_t and $\xi_+^{(0)}$ are the non-universal amplitudes of the bulk order parameter and the bulk correlation length, see Eqs. (3.9) and (3.10), respectively. For example, in binary liquid mixtures the order parameter Φ is proportional to the deviation of the concentration c_a of the component a from its critical value $c_{a,c}^{(s)}$, $\Phi = \mathcal{A}(c_a - c_{a,c}^{(s)})$ (note that \mathcal{B}_t is proportional to \mathcal{A}), which can be easily controlled by changing the mass or the volume fraction of one of the components of the mixture. The experiments reported in Refs. [44, 45] provide indications concerning the size of the critical region in

the thermodynamic direction orthogonal to the temperature axis for the binary liquid mixture of water and lutidine near the consolute point of its phase segregation. These measurements revealed the occurrence of critical Casimir forces within the range of the lutidine mass fraction ω_L deviating from its critical value $\omega_{L,c}$ up to $|\omega_L - \omega_{L,c}| \simeq 0.04$. From the experimental data in Refs. [293, 294, 72] one finds for the water-lutidine mixture $\mathcal{B}_{t,\omega} \approx 1.0$, see Appendix C.1. The index ω refers to the specific choice of the order parameter, i.e., $\Phi_\omega(t \rightarrow 0^-) \equiv \omega_L - \omega_{L,c} \equiv \mathcal{B}_{t,\omega} |t|^\beta$. Fitting the experimentally determined coexistence curve [71, 79, 80] yields a somewhat smaller value $\mathcal{B}_{t,\omega} = 0.765$ which we adopt in the following. Therefore the difference $|\omega_L - \omega_{L,c}| \simeq 0.04$ corresponds to $|\mathcal{B}_t/\Phi| = 19$, which for, e.g., $\zeta_+^{(0)} = 0.02$ translates into $|m_0| \simeq 17$ [Eq. (6.3)], where the values of the critical exponents of the three-dimensional Ising universality class as given in Eq. (3.15b) have been used. The critical composition corresponds to $m_0 = \pm\infty$. Accordingly, for the temperature differences accessible in these experiments, i.e., for $(T - T_c^{(s)})/T_c^{(s)} \approx 3 \times 10^{-5}$, one has for the scaling variable $|X| \approx 0.26$, corresponding to $|\Sigma| \approx 6.6$.

As discussed before, the effective pair potential given in Eq. (6.2) is applicable only for sufficiently large distances $D \gtrsim \kappa^{-1}$ because it takes only the interactions of the double-layers into account and neglects possible short-ranged contributions to effective van-der-Waals interactions. Furthermore, the critical Casimir potential takes its universal form, Eq. (3.26), only in the scaling limit, i.e., for distances D which are sufficiently large compared with the correlation length amplitude $\xi_+^{(0)} \approx 0.25nm$. Analogously also ξ_t and ξ_h must be sufficiently large compared with microscopic scales. Later on, in order to circumvent the unphysical divergence $\sim x^{-1}$ in $U(D \rightarrow 0)$ [see Eq. (6.2)] for small distances D a linear extrapolation shall be considered, as far as necessary:

$$U(D < D_0) = A \exp(-\kappa D) + U_{c,0} + (D - D_0) U'_{c,0}, \quad (6.4)$$

where $D_0 \simeq \xi_0$, $U_{c,0} = U_c(D = D_0)$, and $U'_{c,0} = (\partial U_c / \partial D)_{D=D_0}$.

6.2. Shapes of the effective potential

By varying the thermodynamic state of the solvent the range and the strength of the attractive critical Casimir forces are changed. This variable attraction combined with the repulsive background contribution results in a broad variety of possible shapes of the effective potential given by Eq. (6.2). Examples of various shapes of this effective potential, as obtained for different values of the parameters a , ζ , and Σ , are shown in Fig. 6.2, where the reduced potential is plotted $u = U/s$ versus the reduced distance $x = \kappa D$. Depending on the values of the parameters, the critical Casimir forces compensate the repulsion for all values of D or only within certain regimes. Compensation for all values of D occurs if the strength a of the repulsion is not too strong. This is illustrated by the blue curve in Fig. 6.2 corresponding to the parameter values $a = 10$, $\zeta = 2.5$, and $\Sigma = -4.2$. Recall that negative values of Σ , Eq. (3.19b), correspond to solvent compositions which are poor in the species preferred by the colloids. For different choices

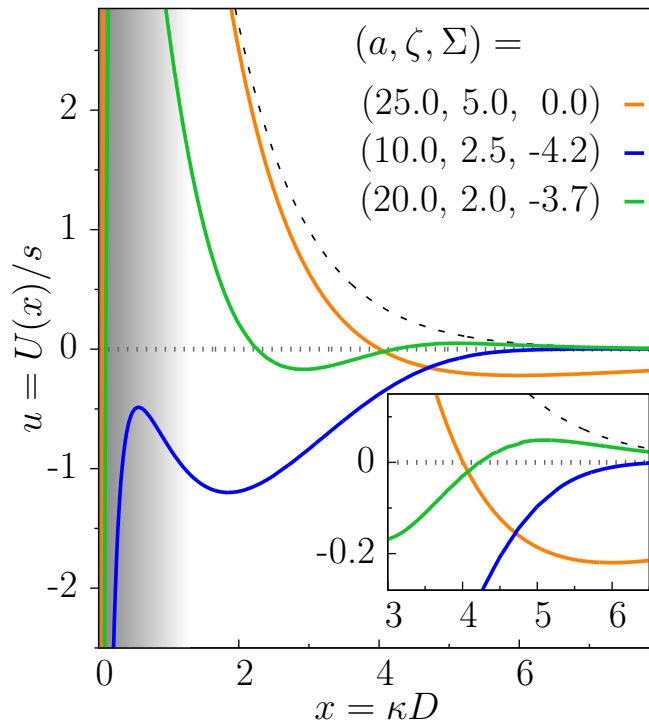


Figure 6.2.: Exemplary shapes of the effective pair potential given by Eq. (6.2). The dashed line represents the purely repulsive part of the potential for $a = 20$. The potentials considered here are physically appropriate for $x = \kappa D \gtrsim 1$. At smaller values of x (grayish area) additional (effective) forces can occur. In particular, the occurrence of a first minimum at contact, i.e., at $D = 0$, depends on microscopic details, which are not taken into account by Eq. (6.2).

of the values of the parameters, the potential may exhibit local minima of different kind. A minimum at distances smaller than the one corresponding to the repulsive barrier shall be referred to as the primary minimum, whereas a minimum at distances larger than the one corresponding to the repulsive barrier as a secondary minimum [16, 70]. For larger values of a , a secondary attractive minimum (i.e., $u < 0$) can occur (in addition to the primary global minimum for $D \rightarrow 0$, which will be discussed below), while for small distances D the potential maintains a repulsive part, as for the orange and green curves in Fig. 6.2. Since $s = \kappa R$ can vary between ca. 10 and 100 a shallow minimum in u can correspond to a deep potential well in U . For suitably chosen parameters, such as for the green curve ($a = 20$, $\zeta = 2$, $\Sigma = -3.7$) in Fig. 6.2, the potential may be repulsive at large distances $D \rightarrow \infty$ and may have an attractive secondary minimum. Thus the critical Casimir forces provide a mechanism for realizing short-ranged attractive and long-ranged repulsive interaction pair potentials as studied for example in Refs. [266, 295] in related contexts. These studies have shown that such potentials give rise to complex phase behaviors of colloidal suspensions.

The issue of the contact value $U(D = 0)$ and the possibility of the occurrence of a primary minimum at small values of D is subtle and, as pointed out in Sec. 6.1, cannot be discussed in general in terms of the effective potential U given by Eq. (6.2). However, U captures the occurrence of the potential barrier for $D \simeq \kappa^{-1}$ and its reduction due to the attractive critical Casimir forces which is sufficient for the focus of the present study, i.e., concerning the influence of the universal critical Casimir forces. The short-ranged interactions acting at distances $D \ll \kappa^{-1}, \xi$ (with $\xi \gg \xi_+^{(0)}$) depend sensitively on materials properties. But for the following reason they do not affect our consideration of the stability of colloidal suspensions. In the case of large values of a , the repulsion is strong enough such that the critical Casimir forces cannot significantly reduce the associated potential barrier. Therefore within experimental observation times only the pair-interaction potential U considered in Eq. (6.2) is relevant for determining the phase behavior and the coagulation process. The influence of attractive short-ranged forces could be observed only for very long waiting-times because the time scale for passing the barrier is $\sim \exp(U)$, see Sec. 4.4. On the other hand in the case of small values of a the critical Casimir forces fully compensate the repulsion. The estimates for the values of the parameters for which the repulsive barrier disappears and thus rapid coagulation sets in can be obtained from the effective potential U given in Eq. (6.2). However, in order to be able to determine the detailed process of coagulation a truly microscopic description is needed. This is beyond the scope of the present study devoted to *universal* features. As long as no additional microscopic forces compete with the considered effective potential, Eq. (6.2) provides a description which is sufficient for the present purpose.

7. Structure and stability

7.1. Structure

The diversity of possible shapes of the effective pair potential given in Eq. (6.2), see Fig. 6.2, leads to a variety of radial distribution functions $g(r)$. In Figs. 7.1 and 7.2 the results for the hypernetted-chain closure are shown. The results obtained using the Percus-Yevick closure are almost the same, differing mostly in that, for the same value of ζ , the amplitude of the resulting $g(r)$ is slightly smaller than the one within the hypernetted-chain closure. For temperatures far away from the critical temperature of the solvent (i.e., for $\zeta = \kappa\xi_t \ll 1$), the colloids are effectively hard spheres with an effective diameter $\sigma > 2R$ due to the soft repulsive background contribution U_{rep} . Accordingly, for such values of ζ , $g(r)$ has the corresponding characteristics of a fluid of hard spheres, such as the rather broad first peak for small values of D . Due to the emerging attractive critical Casimir forces, for increasing $\zeta \sim |t|^{-\nu}$, i.e., for decreasing the temperature deviation $|t| = \left|1 - T/T_c^{(s)}\right|$ within the homogeneous phase of the solvent, the radial distribution function $g(r)$ is enhanced close to the surfaces of the colloids. This implies an enhanced short-ranged order.

In the case that the effective potential exhibits a repulsive barrier at small values of D and is attractive throughout large distances (denoted by (la) in the following), upon increasing ζ the positions of the extrema of $g(r)$ move towards smaller values of D (especially for intermediate values of ζ) and the value of $g(r)$ at the maxima (minima) increases (decreases); the latter occurs mostly for larger values of ζ , see Fig. 7.1.

In contrast, in the case of effective potentials which are repulsive at large distances (denoted by (lr) in the following), a new first peak at small values of D emerges and increases with increasing ζ while the former first peak decreases and finally disappears, see Fig. 7.2. For the brown curve, corresponding to $\zeta = 2.5$, in Fig. 7.2 the emergence of a new peak at $D/R \simeq 0.1$ is seen. The broad former first peak is located at larger distances $D/R \simeq 0.25$. A similar trend is seen for the other extrema at larger values of D . However, since in that range of D the amplitude of $g(r)$ is already quite small, the actual changes of the shape of $g(r)$ cannot be described in such simple terms.

In homogeneous, i.e., not phase separated systems, the (newly emerged or shifted) first peak in $g(r)$ can become significantly larger in the (lr) case than in the (la) case, see Figs. 7.2 and 7.1, respectively, and note the different scales. The reason for this difference can be understood as follows. To a large extent the height of the first maximum in $g(r)$ depends on the depth of the attraction well of the effective potential. Indeed, for comparable potential well depths the first peak in $g(r)$ is only slightly larger in the (lr) case than in the (la) case. However, for equally deep potential wells the overall

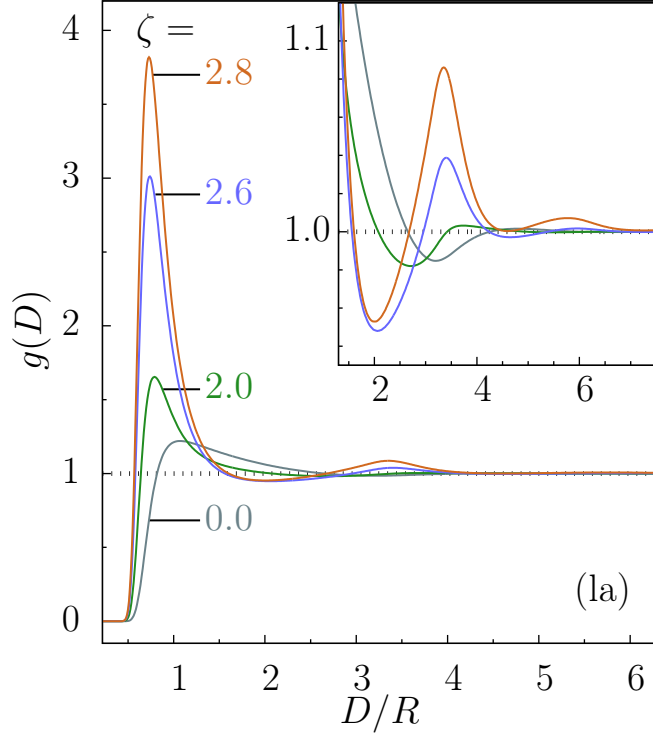


Figure 7.1.: The radial distribution function $g(r)$ as obtained from the HNC closure (Eq. (4.7)) for four values of $\zeta \sim |t|^{-\nu}$ and for a volume fraction $\eta = 0.04$ of the colloids. The parameters of the corresponding effective potential (attractive at large distances (la), Eq. (6.2)) are $a = 100$ for the strength of the repulsion, $m_0 = -100$ for the reduced composition (Eq. (6.3)), and $s = \kappa R = 10$; κ^{-1} is the range of the soft repulsion, R is the radius of the colloids, and $D = r - 2R$ is the surface-to-surface distance. The sequence of curves corresponds to the generic isochoral thermodynamic path realized in experiments. For these values of the parameters, upon decreasing the reduced temperature t , i.e., increasing ζ , a single attractive minimum develops in the effective potential. This increasing attraction due to the critical Casimir force leads to the enhancement of $g(r)$ close to the surface of the colloid. This peak suggests that the formation of colloid dimers is favored. The inset provides an enlarged view of the vicinity of the second maximum of $g(r)$.

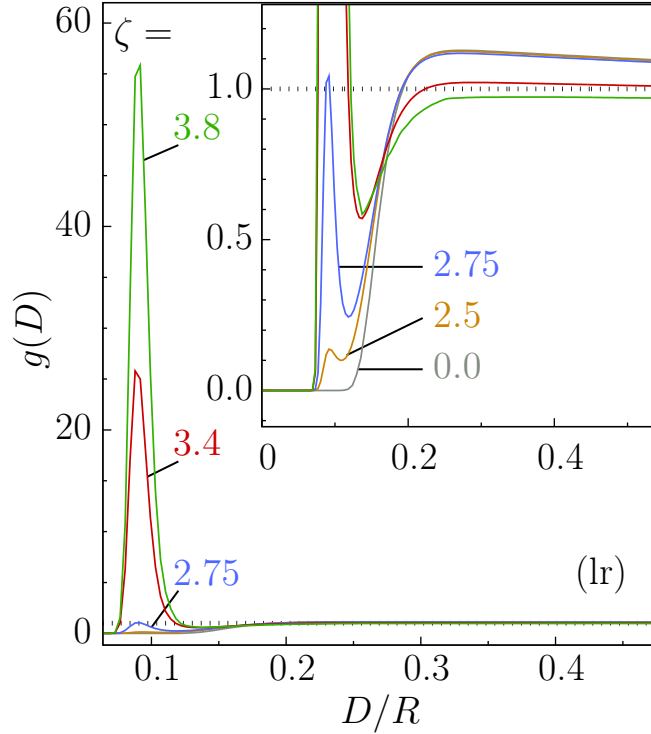


Figure 7.2.: The radial distribution function $g(r)$ as obtained from the HNC closure (Eq. (4.7)) for various values of $\zeta \sim |t|^{-\nu}$ and for a volume fraction $\eta = 0.04$ of the colloids. The parameters of the corresponding effective potential (repulsive at large distances (lr), Eq. (6.2)) are $a = 40$ for the strength of the repulsion, $m_0 = -3$ for the reduced composition (Eq. (6.3)), and $s = \kappa R = 50$; κ^{-1} is the range of the soft repulsion, R is the radius of the colloids, and $D = r - 2R$ is the surface-to-surface distance. For these values of the parameters, upon decreasing the reduced temperature t , i.e., increasing ζ , an attractive minimum develops in the effective potential at intermediate values of D while repulsion remains at small and large values of D . Due to this attraction a peak develops upon decreasing t . For a comparable potential well depth this peak is higher and narrower than in the case without a long-ranged repulsion (compare Fig. 7.1).

attraction is stronger in the (la) case due to the attraction throughout large distances (which gives rise to a larger compressibility χ_T which is proportional to the integral of $g(r) - 1$). Accordingly, the systems interacting via (la) effective potentials can phase separate for shallower potential wells. Systems with potential well depths corresponding to large first peaks in $g(r)$ (as the ones shown for the (lr) potentials in Fig. 7.2) and with a (la) character would already be phase separated. In this sense, the repulsion occurring at larger values of D enhances the stability (w.r.t. phase separation) even of colloidal suspensions exhibiting large peaks in $g(r)$ in homogeneous systems. In order to illustrate this point, notice that the compressibility corresponding to the blue curve ($\zeta = 2.6$) in Fig. 7.1 turns out to be approximately the same as the one corresponding to the green curve ($\zeta = 3.8$) in Fig. 7.2, although for the latter system the peak in $g(r)$ is nearly 20 times larger.

7.2. Stability

In the following the stability ratio $W = W(a, s, \zeta, \Sigma)$ [Eq. (4.19)] for the effective potential given in Eq. (6.2) within the one-phase region is considered. Since the stability ratio W depends exponentially on the potential, in the calculation of W one can afford to omit the use of a cut-off at small distances D . The main contribution to W stems from the maximum of the potential. The use of a cut-off would only slightly change the value of W but it would require an additional specification which is not necessary for this analysis.

In Fig. 7.3 the contour lines $W = 1$ are plotted in the space spanned by the parameters a and $z = \Sigma/\zeta = 1/(\kappa\xi_h)$ for various values of ζ . Changing Σ for fixed ζ and s corresponds to moving along an isotherm in the thermodynamic space of the system. In order to have the contour lines on the same scale, it is useful to introduce the reduced variable $\Sigma/\zeta = 1/(\kappa\xi_h)$ as abscissa. For $W = 1$ the time scales of diffusion and pairing of two particles are comparable, see Eq. (4.20). For a given value of ζ , in the region $W > 1$ above the corresponding contour line the suspension initially equilibrates into a (metastable) fluid state. If the potential has its global minimum at $D = 0$, e.g., due to van-der-Waals forces, aggregates may form eventually at long times; these time scales depend on the value of W . On the other hand, for $W < 1$ rapid coagulation sets in.

The overall characteristics of the shape of contour lines $W = 1$ remains the same for different (but fixed) values of ζ and s (see Fig. 7.3). Upon decreasing Σ towards slightly negative values (i.e., for a binary solvent upon decreasing the amount of the component preferred by the colloids relative to the critical composition) the colloidal stability remarkably decreases, i.e., the contour line $W = 1$ is shifted to larger values of the parameter a of the repulsion strength. For even more negative values of Σ , the system is driven far away from criticality, so that the attraction due to the critical Casimir forces weakens and stability is favored again. For the curves $a = a(z = \Sigma/\zeta = 1/(\kappa\xi_h))$, which are given by $W(a, s, \zeta, \Sigma = z\zeta) = 1$ for fixed s and fixed ζ , the position z_{max} of their maximum does hardly vary with ζ . However the amplitude of $a(z)$ and in particular the maximum value $a_{max} = a(z_{max})$ exhibit a significantly nonmonotonic dependence

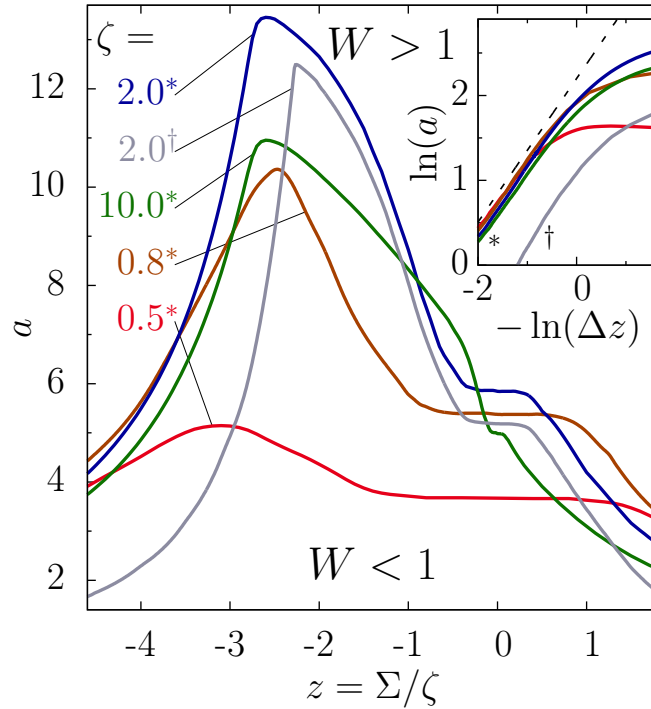


Figure 7.3.: Contour lines of constant stability ratio $W = 1$ (Eq. (4.19)) for the effective pair potential given in Eq. (6.2) as function of a and Σ for various (fixed) values of ζ . The star and the dagger superscripts correspond to $s = 10$ and $s = 50$, respectively. For values $W < 1$ (the region below the corresponding contour line) the colloids coagulate rapidly. For a binary solvent with compositions which are smaller, i.e., slightly poorer in the component preferred by the colloids, than the critical composition, i.e., for $\Sigma \lesssim 0$, this region ($W < 1$) broadens towards larger values of the parameter a of the repulsion strength. The logarithmic plot in the inset shows, that for rather large negative values of Σ the contour lines decay according to a power law as function of $\Delta z = z_m - z$. The slope of the dashed line is 0.84; $z_m = -2.6$ approximates the position of the maxima of the contour lines.

on $\zeta \sim |t|^{-\nu}$. The value of a_{max} is largest for $\zeta \simeq 2$. This behavior reflects the fact that for $(+, +)$ boundary conditions (i.e., equal surface fields on both surfaces) as considered here the critical Casimir forces are not strongest at $T_c^{(s)}$ and $h_b = 0$, but slightly within the one-phase region and for small negative values of h_b .

The contour lines corresponding to a fixed value of s and various values of ζ merge to a single curve for large negative and large positive values of Σ/ζ . Interestingly, within the plotted range of large negative values of $z = \Sigma/\zeta$ the (common) decay of the contour lines can be described by a power law $\sim (z_m - z)^{-p} = \Delta z^{-p}$ (see the double logarithmic plot in the inset of Fig. 7.3, where $z_m = -2.6$ approximates the various $z_{max}(\zeta)$ and $p \simeq 0.84$). In the limit of strong bulk fields, i.e., $|h_b| \rightarrow \infty$, the critical Casimir forces are vanishingly small. In this limit, $W = 1$ for hard spheres without a soft repulsive contribution and therefore $[a(|z| \rightarrow \infty)]_{W=1} \rightarrow 0$. The leveling off of the contour lines $W = 1$ close to $\Sigma = 0$ is a consequence of the choice of the abscissa $\sim h_b^{\nu/(\delta\beta)}$. As a function of h_b the contour lines exhibit no leveling off around $z = 0$.

The potential under consideration as given in Eq. (6.2) is proportional to the parameter s . Thus with increasing (decreasing) values of s the region $W < 1$ of aggregation shrinks (widens), because the repulsive barrier in U becomes larger (smaller). However, since the repulsive barrier contributes exponentially to W , the boundary of the region $W < 1$ is mostly determined by the sheer occurrence of the repulsive barrier (which, however, is independent of s) and therefore the dependence of the contour line $W = 1$ on s is weak. This is seen in Fig. 7.3 by comparing the blue and gray curves, which are for $\zeta = 2$ the contour lines $W = 1$ for $s = 10$ and $s = 50$, respectively. Note, that this weak dependence of the stability region on the parameter $s = \kappa R$ is in contrast to the strong dependence on s of the two-phase region of the effective colloidal system, as discussed in Sec. 8.4, see especially Fig. 8.3. For the two-phase region not only the existence but also the actual strength of the attraction is important, and therefore it is sensitive to the value of s , because $U \sim s$.

The contour lines in Fig. 7.3 of constant stability ratio $W = 1$ can be compared with the contour lines in Fig. 8.3 of constant critical temperature $T_c^{(eff)}$ (or $\zeta_c^{(eff)}$) delimitating the ‘‘liquid’’-‘‘gas’’ coexistence of the effective one-component colloidal system. In both figures the contour lines are plotted in the plane spanned by the parameter a , measuring the strength of the repulsion of the effective pair potential, and the scaling variable Σ (or Σ rescaled by the fixed value of ζ). The gross features of these contour lines are similar but the values of a are rather different. (Note the different scales for a in these two figures.) For example, for the same value of $s = \kappa R = 10$, at the temperature corresponding to $\zeta = 2$ strong coagulation (i.e., $W < 1$) occurs for $a \lesssim 13$, whereas at the comparable temperature corresponding to $\zeta = 3$ the colloidal suspension starts to phase separate already for a much stronger repulsion, i.e., for $a \lesssim 300$, see the blue curves in Fig. 8.3 in Sec. 8.4. Notice, however, that phase separation occurs at relatively high packing fractions $\eta \gtrsim 0.06$ of the colloidal particles, see Sec. 8.4 whereas aggregation occurs also for very small packing fractions of the colloidal particles.

The experimentally relevant case of the variation of the stability ratio W with temperature at constant order parameter is shown in a semi-logarithmic plot in Fig. 7.4

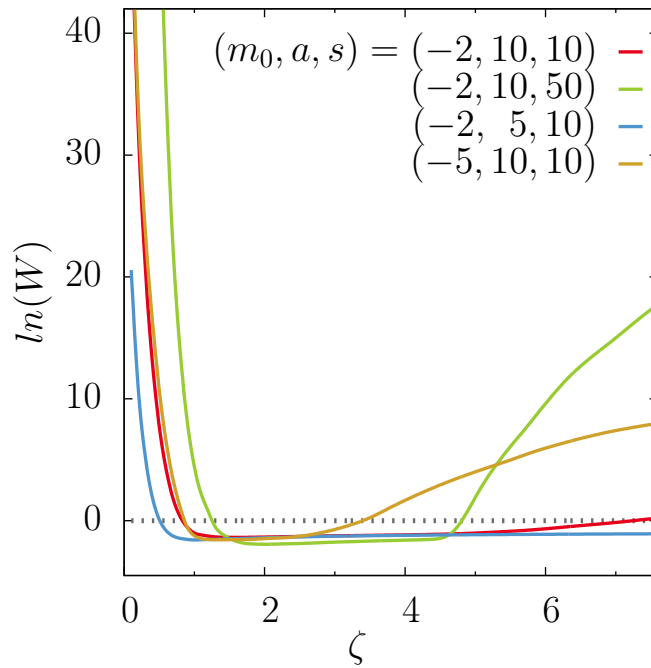


Figure 7.4.: Semi-logarithmic plot of the stability ratio W , Eq. (4.19), for the typical experimental situation of varying the reduced temperature $|t| \sim \zeta^{-1/\nu}$ at fixed composition $(c_a - c_{a,c}^{(s)}) \sim m_0^{-1}$, Eq. (6.3). The steep decrease of $\ln(W)$ towards negative values upon increasing ζ , i.e., for $t \rightarrow 0$, suggests that coagulation sets in within a narrow temperature interval. The increase of W for large values of ζ occurs for strongly repulsive contributions to the effective potential [$a = 10$, Eq. (6.2)]; $s = \kappa R$, where κ^{-1} is the range of the repulsive “background” potential and R is the radius of the colloids.

in terms of $\zeta \sim |t|^{-\nu}$ and the parameter m_0 which is related to the order parameter, Eq. (6.3). The steep decrease of W upon increasing $\zeta \lesssim 1$ indicates that coagulation (i.e., W crossing the value 1 from above) is expected to set in above the critical temperature within a rather narrow temperature interval. For the plots in Fig. 7.4 the chosen values of the parameter allow one to focus on the region of the onset of coagulation. As one can infer from the stability diagram, Fig. 7.3, $a = 10$ corresponds to a relatively strong repulsion in the sense that for this value the range of values of Σ for which $W < 1$ holds and thus coagulation occurs is rather narrow. This implies that one finds $W < 1$ only for intermediate values of ζ . Such a case is represented by the red curve in Fig. 7.4 which corresponds to $m_0 = -2$, $a = 10$, and $s = 10$. There is a clear increase of W for $\zeta \gtrsim 4.5$; for larger ζ , W becomes even larger than 1. The effect of varying m_0 , a , or s relative to the red curve can be inferred from the brown, blue, and green curves, respectively. Since the height of the potential barrier is proportional to s [see Eq. (6.2)], stability is significantly enhanced for larger values of s , see the green curve corresponding to $s=50$ in Fig. 7.4. The value of ζ , for which $\ln(W)$ turns from positive to negative (negative to positive) is larger (smaller) than the corresponding one for $s = 10$. For the composition corresponding to $m_0 = -5$, which is closer to the critical composition [see Eq. (6.3)], the region of values of ζ for which $W < 1$ is smaller than for $m_0 = -2$, see the brown curve in Fig. 7.4. Upon decreasing a , the value of ζ for which $\ln(W)$ changes from being positive to being negative becomes smaller, see the blue curve corresponding to $a = 5$. For such small values of a , $\ln(W)$ remains negative upon increasing ζ , also for values of the parameters m_0 and s not shown in Fig. 7.4.

In summary, along the thermodynamic paths considered (and typically realized in experiments) the range of the attraction due to the critical Casimir forces grows steadily with increasing ζ , but the amplitude of the critical Casimir forces is a nonmonotonic function of ζ . The critical Casimir force attains its maximal strength for an intermediate value of ζ . Therefore, upon increasing ζ the repulsive barrier in the effective pair potential is at first reduced; for sufficiently small values of a it can even disappear altogether. For even larger values of ζ , the potential barrier may grow again (or emerge) because the amplitude of the critical Casimir force decreases again. This latter barrier is located at smaller values of D than the one which is present for small values of ζ . The nonmonotonic dependence of the maximal strength of the critical Casimir force on temperature results in a nonmonotonic behavior of $W = W(\zeta)$. Although, as stated above, a repulsive barrier may emerge again, it is likely that aggregates, which have formed for intermediate values of ζ , will not break up. This might be due to either specific microscopic interactions or due to the secondary minimum in the effective pair potential, which is still quite deep. Also in the case in which for all values of ζ a repulsive barrier remains, coagulation can appear, due to a deep secondary minimum. This case will be discussed in the next section 7.3.

7.3. Comparison with experiments

For dilute suspensions, the second virial coefficient B_2 , Eq. (4.14), provides information about the strength of the radially symmetric attraction between spherical particles [262]. In Refs. [79, 80] the second virial coefficient B_2 has been determined for latex particles immersed in a mixture of 2,6-lutidine and water by using light scattering. In order to be able to compare these experimental data with the corresponding values for B_2 as resulting from the effective pair potential $U(r)$ given in Eq. (6.1) the amplitude A of the repulsive contribution $U_{rep}(r) = A \exp(-\kappa D)$ has to be specified. For the reported experiments, the repulsion is due to screened electrostatic interactions and A is given by Eq. (4.2). The reported experimental values [80] $\Upsilon = 5.7 \mu C/cm^2$ and $2R = 555 nm$ [80] are adopted and the values $\xi_+^{(0)} = 0.25 nm$ and $T_c^{(s)} = 310 K$ as typical for water-lutidine mixtures (see, e.g., Ref. [45]) are used. The relative permittivity ϵ as function of the mass fraction ω_L of lutidine can be obtained by using the Clausius-Mossotti relation [296], see Appendix C.2. In Ref. [80] no precise value of the Debye screening length κ^{-1} is given; it is stated that $\kappa^{-1} \approx (7 \dots 10) nm$. Therefore the values of B_2 have been calculated theoretically for several values of κ .

Within their analysis, for temperatures far away from $T_c^{(s)}$ (i.e., $|T - T_c^{(s)}| \gtrsim 3K$) the authors of Ref. [80] obtained values for B_2 which would correspond to a system of hard spheres of a radius of $4200 nm$. These extremely large, unexpected values (they actually used particles of diameter $555 nm$) cannot be easily explained by a soft, repulsive interaction [80]. In order to circumvent this non-trivial effect, the theoretical and experimental values of B_2 normalized by the corresponding values $(B_2)_{reg}$ far away from $T_c^{(s)}$ are compared. For the normalization of the experimental data, the mean values corresponding to the three largest temperature differences $|T - T_c^{(s)}|$ which have been reported are used. For $(B_2)_{reg}$ in the theoretical curves the values as obtained by taking in the effective potential, Eq. (6.2), for $x > 0$ only the soft, repulsive term into account (i.e., taking $\zeta = \kappa \xi_t = 0$) are used, so that $(B_2)_{reg}/v_{HS} = 5.15, 5.33, 5.53,$ and 6.37 for $\kappa^{-1}[nm] = 4, 4.5, 5,$ and 7 , respectively, where $v_{HS} = (4\pi/3) R^3$ is the volume of the hard spheres (HS).

In Fig. 7.5, for the critical composition, i.e., $\Sigma = 0$, the variation of B_2 upon approaching the critical temperature $T_c^{(s)}$ for the effective pair potential in Eq. (6.2) with the experimental data given in Fig. 4 of Ref. [80] are compared. Although a rather simple form for the background repulsive potential has been adopted, for $\kappa^{-1} = 4.5 nm$ one obtains a fair agreement, in the sense that the qualitative trend of the steep decrease is captured, whereas a quantitative agreement for the whole range of ξ_t has not been achieved. Yet due to large error bars of the experimental data and large differences between not normalized experimental and theoretical values of B_2 (the origin of which is unclear) one cannot claim that this value of κ^{-1} is the actual experimental one. Rather κ^{-1} has to be considered in that case as an effective fitting parameter which accounts for differences between the experimentally realized and the model background potential in order to match the model with the experimental data. Furthermore, the sensitivity of the results to uncertainties in the other parameters has not been checked. Both from

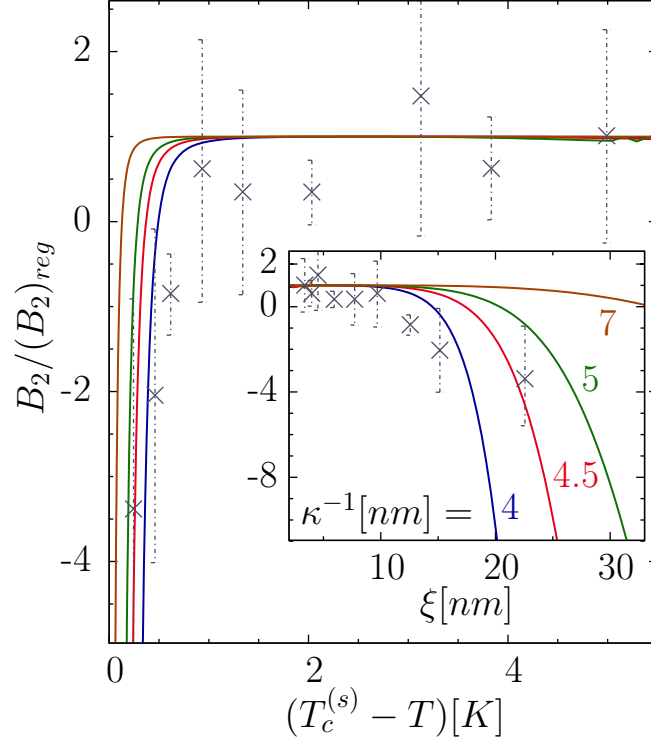


Figure 7.5.: The value of the second virial coefficient B_2 [Eq. (4.14)] normalized by its value $(B_2)_{reg}$ far away from $T_c^{(s)}$ as function of the temperature deviation from the critical temperature $T_c^{(s)}$ of the solvent and at its critical composition ($\Sigma = 0$). The same data in the inset but as function of the correlation length $\xi_t = \xi_+^{(0)} \left| 1 - T/T_c^{(s)} \right|^{-\nu}$ of the solvent. The experimental values (symbols) for latex particles immersed in the critical water-lutidine mixture are taken from Fig. 4 of Ref. [80]. The lines correspond to the values obtained from the effective pair potential given in Eq. (6.2). The values of a and s were obtained by using Eq. (4.2) for A and the values $\Upsilon = 5.7 \mu C/cm^2$ and $2R = 555 nm$ as given in Ref. [80]. The values of κ are similar to the range reported in Ref. [80]. The values $\xi_+^{(0)} = 0.25 nm$ and $T_c^{(s)} = 310 K$ has been adopted. For the critical mass fraction $\omega_{L,c} = 0.287$ of lutidine [80] one obtains $\epsilon = 22.3$ (Appendix C.2). For further details see the main text.

experiment and theory it is evident that the attraction close to the critical temperature increases significantly, resulting in a steep decrease of B_2 towards large negative values.

In Ref. [80] the variation of B_2 as function of $|T - T_c^{(s)}|$ is reported also for a mass fraction ω_L of lutidine larger than its critical value $\omega_{L,c} \simeq 0.287$, see Fig. 7.6. In general, for off-critical compositions the strength and the range of the critical Casimir force results from the interplay of the two bulk correlation lengths $\xi_t \sim |t|^{-\nu}$ and $\xi_h \sim |h_b|^{-\nu/(\beta\delta)}$, see Sec. 3.4 and Ch. 5. For $\omega_L = 0.35 > \omega_{L,c}$ the binary solvent is poorer in the component preferred by the kind of colloids used (i.e., water) than at the critical composition. In such a case the interplay of ξ_t and ξ_h is rather complex due to the occurrence of capillary condensation which leads to bridging between two colloids. In particular, at the same temperature the critical Casimir force can become stronger upon moving away from the critical composition. But at off-critical compositions it is in general shorter ranged than at the critical composition. Moreover, at off-critical compositions the critical Casimir force emerges as function of temperature only closer to the critical temperature as compared with the corresponding thermodynamic path at the critical composition. In Fig. 7.6 the reduced experimental data for B_2 corresponding to the mass fraction $\omega_L = 0.35 > \omega_{L,c} = 0.287$ are compared with the theoretical curves obtained within the present effective model; for $\omega_L = 0.35$ one has $(B_2)_{reg}/v_{HS} = 5.35, 5.55, 5.96,$ and 6.40 for $\kappa^{-1}[nm] = 4.5, 5, 6,$ and $7,$ respectively. As can be inferred from Fig. 7.6 for $\kappa^{-1} = 4.5nm$ the total attraction (within the present effective model), in terms of B_2 , is stronger for $\omega_L = 0.35$ than for the critical composition $\omega_{L,c}$, i.e., for the same value of ξ_t , B_2 is more negative. For the theoretical curves corresponding to $\kappa^{-1}[nm] = 5$ and 6 the aforementioned interplay of ξ_t and ξ_h manifests itself more clearly. For the off-critical composition the attraction due to the critical Casimir forces sets in only for larger values of ξ_t but becomes more rapidly stronger with increasing ξ_t so that, for large values of ξ_t , B_2 is more negative for $\omega_L = 0.35$ than for $\omega_{L,c}$. At the critical composition, B_2 starts to decrease (due to the attractive critical Casimir forces) already for smaller values of ξ_t than for $\omega_L = 0.35$.

For the experimental data (within the large error bars and the reported temperature range) no dependence of the value of B_2 as function of $|T - T_c^{(s)}|$ on the composition is observed. (Reference [80] provides the values of B_2 as function of $|T - T_{cx}^{(s)}|$ but lacks an absolute value for the coexistence temperature $T_{cx}^{(s)}$. $T_{cx}^{(s)}$ is the temperature at which the solvent undergoes a first-order phase segregation for $\omega_L = 0.35 \neq \omega_{L,c}$, see Ch. 8, especially Fig. 8.1. $T_{cx}^{(s)} - T_c^{(s)} = 0.145K$ is adopted as obtained from $|\omega_L - \omega_{L,c}| = \mathcal{B}_{t,\omega} |t|^\beta$ with $\mathcal{B}_{t,\omega} = 0.765$.) This finding is in contrast to the behavior of the measured effective particle-wall interaction potentials of Ref. [297], for which a dependence on the composition of the water-lutidine mixture has been observed. At present it remains unclear whether the dependence of B_2 on ω_L could not be resolved experimentally or whether the data from these experiments happen to lie in that crossover regime in which the curves $B_2(T_c^{(s)} - T)$ happen to be close to each other for the critical and the off-critical mixture, see the inset in Fig. 7.6.

For the same system the authors of Ref. [80] used for the measurement of B_2 , in

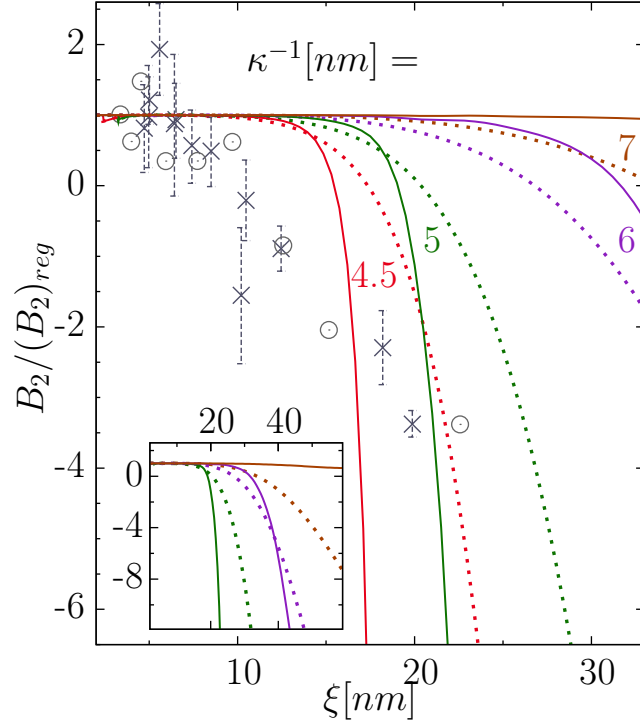


Figure 7.6.: The variation of the second virial coefficient B_2 (Eq. (4.14)) as function of the correlation length $\xi_t = \xi_+^{(0)} \left| 1 - T/T_c^{(s)} \right|^{-\nu}$ of the solvent upon approaching the critical temperature $T_c^{(s)}$ for an off-critical composition of the binary solvent. The inset shows the same for a larger range of ξ_t . The experimental values (\times) are taken from Fig. 2 of Ref. [80] and the four theoretical curves are obtained by using the effective potential in Eq. (6.2). The values $\kappa^{-1}[\text{nm}] = 7, 6, 5,$ and 4.5 , correspond to $m_0 = -10.6, -13.5, -18.0,$ and -21.3 , respectively (Eq. (6.3)). For the lutidine mass fraction $\omega_L = 0.35 \gtrsim \omega_{L,c}$ the solvent is poor in the component preferred by the colloids. Therefore the critical Casimir force is stronger than for the critical composition. Thus B_2 can be expected to decrease more rapidly than for $\omega_L = \omega_{L,c}$. This is indeed the case for the theoretical curves. For the experimental data of Ref. [80] no dependence on ω_L is seen; the dotted curves and the experimental data (\circ) correspond to the critical composition as shown in Fig. 7.5. B_2 is normalized in the same way as in Fig. 7.5. The order parameter amplitude used here is $\mathcal{B}_{t,\omega} = 0.765$, see Appendix C.1 and Eq. (3.17). By making use of the Clausius-Mossotti relation [296] one obtains $\epsilon = 19.3$ (see Eq. (4.2) and Appendix C.2). The values of the other parameters are the same as in Fig. 7.5.

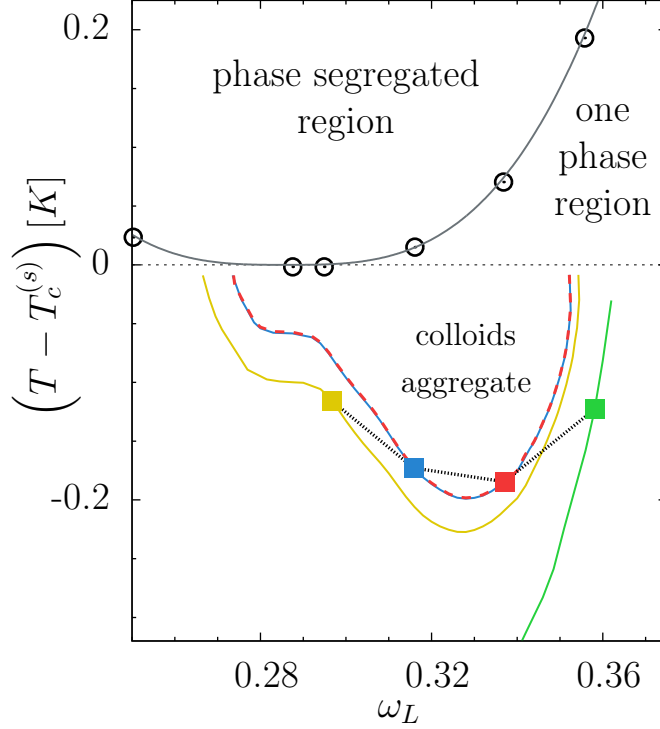


Figure 7.7.: Comparison of the values of B_2 (Eq. (4.14)) at the thermodynamic state points of the solvent for which immersed colloids aggregate. The four experimentally obtained state points (squares; the straight black dotted lines in between are a guide to the eye) are taken from Fig. 1 (middle) of Ref. [76]. The isolines of constant B_2 (full colored lines; for visibility of the blue line the red one is dashed, both lines nearly coincide) each belonging to one of the state points (squares), are calculated within the present model [Eq. (6.2)]. For the three state points closest to the critical composition $\omega_{L,c}$ (yellow, blue, and red) one has $B_2 < 0$ corresponding to an effectively attractive colloidal suspension. To a certain extent the B_2 -isolines resemble the possible shape of the line of the onset of aggregation. For the state point with the largest deviation $\omega_L - \omega_{L,c}$ (green) one has $B_2 > 0$ within the model used here, suggesting that in this case there are effectively attractive forces other than the critical Casimir forces which drive the aggregation. For further details see the main text. In order to obtain the theoretical values of B_2 the following values have been adopted $\xi_+^{(0)} = 0.25nm$, $\kappa^{-1} = 6nm$, $T_c^{(s)} = 307K$, and $\omega_{L,c} = 0.286$ and the experimentally given values $2R = 378nm$ and $\Upsilon = 3.85\mu C/cm^2$ have been used. The repulsion strength A is obtained from Eq. (4.2) with ϵ depending on the mass fraction ω_L of lutidine [296], see Appendix C. The experimentally determined coexistence points (circles) on the binodal of phase segregation with a lower critical point agree well with the relation $|\omega_L - \omega_{L,c}| = \mathcal{B}_{t,\omega} |t|^\beta$, where $\beta = 0.3256$ and $\mathcal{B}_{t,\omega} = 0.765$ (gray line); in accordance with a lower critical point the reduced temperature is $t = (T_c^{(s)} - T) / T_c^{(s)}$.

Ref. [76] the aggregation phenomena of immersed colloids have been studied. The corresponding given experimental values of the parameters, and especially Eq. (4.2) for the repulsion strength parameter A can be used, in order to investigate these state points within the present model.

First, it is worthwhile to mention that for the parameters corresponding to these experiments, the repulsive barrier for small values of $x = \kappa D$ is of the order of tens of $k_B T$. Therefore, it seems that the observed aggregation is due to the very deep secondary minimum emerging at a certain distance D_{min} . This is a different mechanism than the one discussed in Sec. 7.2, where the aggregation due to the disappearance of the repulsive barrier at short distances D has been considered. While in the latter case the colloids would stick together with their surfaces at contact, in the former case they are close but not at contact. With $\kappa D_{min} \approx 1$ and $s = \kappa R \approx 10 \dots 100$, from the effective potential given in Eq. (6.2) it follows that the colloids are a surface-to-surface distance $D/R \approx 10^{-1} \dots 10^{-2}$ apart. In Ref. [76] the mean surface-to-surface distance has not been estimated, but in experiments performed for a similar system Ref. [73] it has been found that in the flocculated and sedimented aggregates the average interparticle distance is about three times the mean radius of the polydisperse colloids. This is in stark contrast with the present theoretical estimates. Other experimental reports do not specify the average interparticle distance occurring in the aggregates. In Refs. [84, 85] it is stated, that the sediment is less dense than expected for a tight packing of spheres and in Ref. [93] the aggregates are characterized as being compact, not fractal. The authors of Ref. [83] argue that for their system the aggregates are indeed crystalline. The possibility, that the flocculated colloidal particles form a bona fide, thermodynamically stable, liquid-like or crystalline phase cannot be addressed within the effective, one-component approach used here, because within this approach the reliable prediction of the occurrence of a phase transition can be made only if the colloidal number density is sufficiently large, see Ch. 8 whereas in the experiments referred to above the packing fraction is as small as $\eta \approx 10^{-6} \dots 10^{-3}$.

Next, the issue is addressed whether a relation can be established which connects the onset of the reversible aggregation to a threshold of a specific quantity which is both theoretically and experimentally accessible. To do so following Refs. [79, 80] the second virial coefficient B_2 is considered and it is analyzed whether the values of B_2 corresponding to thermodynamic state points of the solvent, at which the aggregation of colloids sets in, are similar. For such state points, as determined experimentally and reported in Fig. 1 (middle) of Ref. [76], the corresponding values of B_2 within the present effective model (Ch. 6) for the four values of ω_L are $B_2 / (\frac{4\pi}{3} R^3) = -67$ (red square), -65 (blue square), -23 (yellow square), and 5.4 (green square) (Fig. 7.7). In Fig. 7.7 the isolines of constant B_2 for these values of B_2 are shown (using the same color code). According to the present model, which takes into account only the repulsive electrostatics and the attractive critical Casimir forces, for the state point with the largest deviation $\omega_L - \omega_{L,c}$ (green) one has $B_2 > 0$ which corresponds to an effectively repulsive colloidal system. Either the employed approximate scaling function of the critical Casimir force is not valid in that region of the thermodynamic space, or for this region of the thermodynamic space of the solvent other effectively attractive forces than

the critical Casimir forces drive the observed aggregation. The values of B_2 for the three other state points are similar to each other, for two of them (the blue one and the red one) the corresponding isolines are even hardly distinguishable. The similarity of these values of B_2 as obtained within the present model suggests that for these thermodynamic states the aggregation is indeed driven by the critical Casimir forces and that B_2 can serve (to a certain extent, see below) as an indicator for the structural instability.

According to the B_2 -isolines, for the critical composition $\omega_{L,c}$ and slightly smaller compositions the structural instability is also expected to occur at temperatures $T \approx T_c^{(s)} - 0.05K$, see Fig. 7.7. However, for such values of ω_L no aggregation has been observed in the reported experiments, although such temperature deviations are within the experimentally accessible resolution. Besides the possibility that B_2 can indeed not serve as a quantitative indicator for the aggregation, there are further possible reasons for this mismatch and the quantitative disagreement between the yellow B_2 -isoline on one hand and the red and blue B_2 -isolines on the other hand. One reason could be the simplified choice for the background potential which is used in the present study. Furthermore, there are several experimental parameters for which only estimates could be used. Within their analysis, the authors of Ref. [75] conclude that for calculating the electrostatic potentials one should not use the bare surface charge density as given by the manufacturer. Rather, the dissociation of the colloidal surface in the solvent has to be taken into account. In the present analysis the nominal value for the surface charge has been used due to the lack of more detailed data. The authors of Ref. [78] point this out, too, and reveal the role of impurities as another important factor. They determined the aggregation line in “fresh” mixtures and in the same mixture but one or several days later. While the aggregation phenomenon as such was reproducible, the values of the thermodynamic variables of the solvent at which the aggregation sets in varied strongly within one and the same sample.

In the same reference, a dependence of the aggregation line on the volume fraction η of colloids is observed, whereas in Ref. [83] it is stated that the shape of the region in thermodynamic space where aggregates are forming does neither depend on the colloidal concentration nor on the colloidal radius. In Ref. [76] a dependence of the time scale of the aggregation process on η is reported. The present analysis does not capture such a dependence.

In conclusion, the results suggest that the critical Casimir force plays an important role in order to explain the aggregation phenomenon in this region of the phase diagram of the solvent. Yet, in order to be able to determine all relevant mechanisms and forces and in order to obtain quantitative agreement between the experiments and the theoretical results, for both further efforts are needed to provide more precise values of the relevant quantities.

Despite the complexity of the considered systems and of the aggregation process described above, in Refs. [87, 88, 89] the simple criterion $\kappa\xi_t = \zeta = 1$ for aggregation is discussed. Besides the criticism raised in Ref. [88], in the present analysis quantitative support for this criterion is found. The discussed phenomena occur for values $\zeta \sim 1$, which can be expected because for $\kappa^{-1} \gg \xi_t$ the electrostatic repulsion and for $\kappa^{-1} \ll \xi_t$ the attractive critical Casimir forces dominate. Thus for $\kappa^{-1} \sim \xi_t$ phenomena which are

related to the emergence of the critical Casimir forces are expected to occur. However, there is no indication, that in general $\zeta = 1$ acts as a threshold value. Actually, for off-critical mixtures rather the competition of the three length scales κ^{-1} , ξ_t , and ξ_h is of importance and the repulsion strength amplitude A has a (minor) influence.

Finally, in Fig. 7.7 experimental data for the binodal of the water-lutidine mixture are shown, which nicely agree with the functional form $\omega_L - \omega_{L,c} = \pm \mathcal{B}_{t,\omega} |t|^\beta$ (gray line), where $\beta = 0.3256$ and $\mathcal{B}_{t,\omega} = 0.765$. This shows that the present description, which is symmetric w.r.t. $\omega_L = \omega_{L,c}$, is sufficient for the phase space region of interest here.

8. Thermodynamics

In this chapter colloidal suspensions with phase-separating solvents are considered, which are structural stable. That is, the corresponding effective pair potentials between the colloidal solute particles, as given by Eq. (6.2) and discussed in Ch. 6, are repulsive at short distances (i.e., the repulsion strength $a = A/(\kappa R)$ is sufficiently large).

8.1. General discussion

This Section is concerned with the thermodynamics of actually ternary colloidal suspensions with binary solvents such as water-lutidine mixtures which exhibit a closed-loop two-phase region of demixed phases (each being rich in one of the two species). The focus is on that region of this miscibility gap which is close to the lower critical point. For fixed pressure, their thermodynamic states can be characterized by the temperature T and the concentration c_a of one of the species with the critical point $(T_c^{(s)}, c_{a,c}^{(s)})$ and the liquid-liquid phase coexistence curve $T_{cx}^{(s)}(c_a)$ in the absence of colloids. Upon adding colloidal particles to such a solvent, for fixed pressure the thermodynamic space of the system becomes three-dimensional spanned by T , c_a , and, e.g., by the colloidal number density ϱ (see Fig. 8.1; one can also choose, instead, the fugacity of the colloids). Accordingly, the closed-loop phase coexistence curve $T_{cx}^{(s)}(c_a)$ becomes a two-dimensional, tubelike manifold $T_{cx}(c_a, \varrho)$ with $T_{cx}(c_a, \varrho = 0) = T_{cx}^{(s)}(c_a)$. It contains a line \mathcal{C}_c of critical points $(T_c(\varrho), c_{a,c}(\varrho))$ which is the extension of the critical point of the solvent in the absence of colloids, i.e., $(T_c(\varrho = 0), c_{a,c}(\varrho = 0)) = (T_c^{(s)}, c_{a,c}^{(s)})$. For fixed temperature $T = \text{const}$, the set of pairs $\left[\left(c_a^{(1)}, \varrho^{(1)} \right), \left(c_a^{(2)}, \varrho^{(2)} \right) \right]$ of coexisting states given by $T = T_{cx}(c_a, \varrho)$ forms a curve $\mathcal{C}_{cx}(T)$ in the (c_a, ϱ) plane, the shape of which depends on the considered value of T (see Figs. 8.1(a) and (b)). In the phase diagram, two coexisting states are connected by a straight, so-called tie line (see Fig. 8.1). (If one chooses the fugacity of the colloids instead of ϱ , one also obtains a tubelike manifold T_{cx} of phase coexistence. However, in this case the horizontal tie lines lie in the plane of constant fugacity, i.e., parallel to the (T, c_a) -plane, because the coexisting phases share a common fugacity of the colloids.)

As stated above, the two-phase loop of the pure solvent (i.e., for $\varrho = 0$, bounded by $T_{cx}^{(s)}(c_a)$) extends into the three-dimensional thermodynamic space of the actual colloidal suspension ($\varrho \neq 0$). Due to the presence of additional interactions and degrees of freedom one expects that the shape of this two-phase region (bounded by $T_{cx}(c_a, \varrho)$) is not a straight but a distorted tube. The actual shape of $T_{cx}(c_a, \varrho)$ is expected to depend

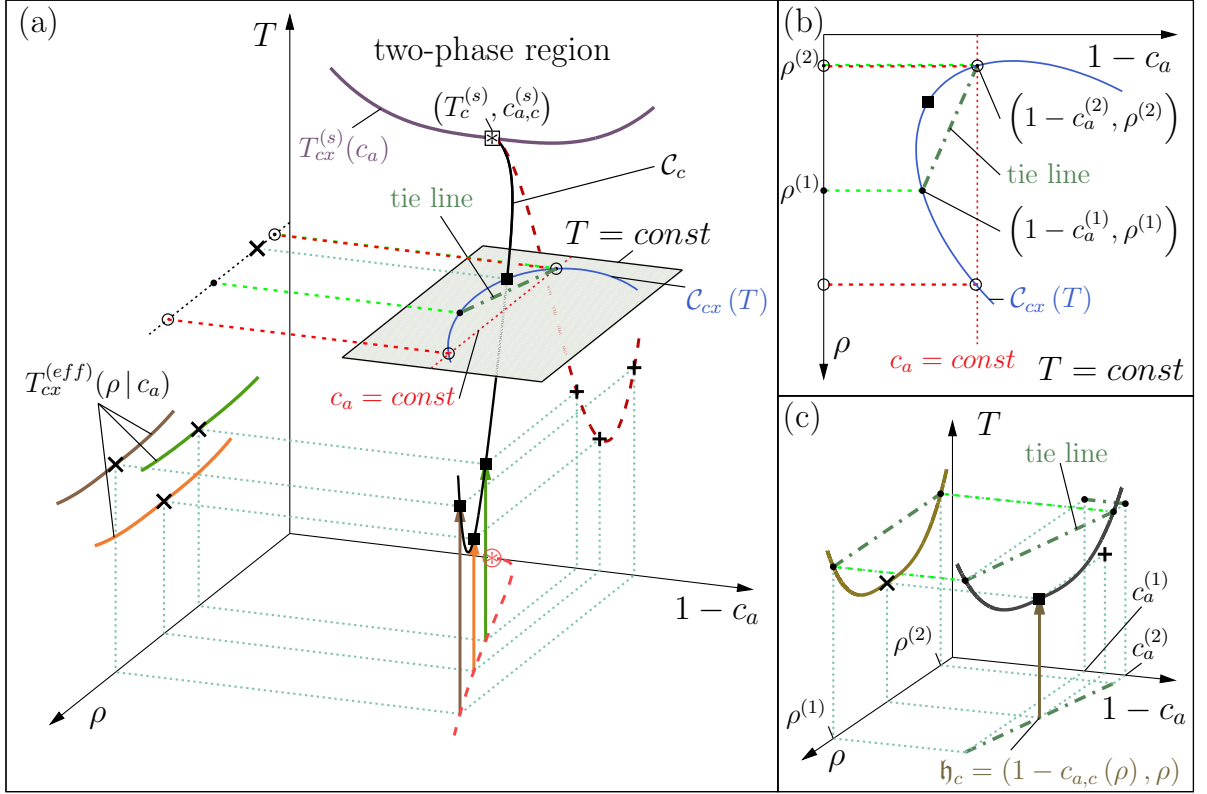


Figure 8.1.: Sketch of the phase diagram for colloids immersed in a binary liquid mixture, the latter exhibiting a closed-loop miscibility gap. The focus is on the region around the lower critical point $\boxtimes (T_c^{(s)}, c_{a,c}^{(s)}, \rho = 0)$ (see the lavender phase separation curve $T_{cx}^{(s)}(c_a)$ in the $(T, c_a, \rho = 0)$ plane). For fixed pressure corresponding to a liquid state of the system, the thermodynamic space of the pure solvent is two-dimensional; here the representation in terms of the temperature T and the concentration c_a is chosen. Upon adding colloids at fixed pressure the thermodynamic space becomes three-dimensional; here the colloidal number density ρ as additional thermodynamic variable is used. The miscibility gap of the pure solvent in the $(T, c_a, \rho = 0)$ -plane extends to a two-phase region in the three-dimensional thermodynamic space and is bounded by a two-dimensional manifold $T_{cx}(c_a, \rho)$ of coexisting states (not shown). The tube-like shape of $T_{cx}(c_a, \rho)$ is not straight but bent and twisted. Its actual form is expected to depend sensitively on all interactions (i.e., the solvent-solvent, the solvent-colloid, and the colloid-colloid interactions). Each state on $T_{cx}(c_a, \rho)$ coexists with another one, both being connected by a horizontal and straight, so-called tie line (green dash-dotted line). There is a line \mathcal{C}_c (black curve) of critical points (some of which are shown as black squares) embedded in $T_{cx}(c_a, \rho)$ which is the extension of the critical point $(T_c^{(s)}, c_{a,c}^{(s)}, \rho = 0)$. \mathcal{C}_c is given by the states for which the tie line has zero length. The projections of \mathcal{C}_c (with selected critical points \blacksquare) onto the planes (ρ, c_a) and (T, c_a) (with $+$ as the projection of \blacksquare) are indicated as red dashed curves. For $\rho \rightarrow 0$ the bending of the curve \mathcal{C}_c can be inferred from scaling arguments (Eq. (8.1)). For colloidal suspensions interacting via an effective potential which consists of a soft repulsion and the critical Casimir attraction, the results of the effective approach suggest that, for intermediate values of ρ , \mathcal{C}_c bends up again (see Sec. 8.4). This bending is due to the specific properties of the critical Casimir forces and is indicated in panel (a). Effective colloidal models render coexistence

curves $T_{cx}^{(eff)}(\varrho|c_a)$ which are explicit functions of ϱ only and depend parametrically on the overall concentration c_a (see panel (a) for three examples; the three vertical arrows indicate thermodynamic paths describing the approach of the corresponding critical point ■ upon raising temperature). For suitable effective models and within a certain region of the thermodynamic space (see main text), the critical points (\times), $(T_c^{(eff)}(c_a), \varrho_c(c_a))$, of the coexistence curves $T_{cx}^{(eff)}(\varrho|c_a)$ are expected to approximate the projection of \mathcal{C}_c onto the (T, ϱ) -plane. Within the effective approach a unique value c_a is taken throughout the whole system. In contrast, all three panels show that in general for $T = const$ the coexisting phases (i.e., the points connected by a tie-line) differ both in ϱ and c_a . Thus the effective approach has a limited applicability for determining the phase diagram. Experimentally, upon increasing temperature one is able to determine a (in general nonplanar) coexistence curve [black line in panel (c)] in the three-dimensional thermodynamic space. In panel (c), for a selected critical value $\mathfrak{h}_c = (1 - c_{a,c}(\varrho), \varrho)$ [i.e., \mathfrak{h}_c is a point on the red dashed line in the (ϱ, c_a) -plane] such a curve (black line), its projection onto the (T, ϱ) -plane (mustard line), as well as a selected tie line and its three projections are shown. Note that the tie line is not parallel to the ϱ -axis. This means that the coexisting phases differ with respect to c_a , in contrast to the aforementioned assumption of an unique value of c_a for the effective one-component description. Thus the mustard curve in panel (c) will in general differ from the corresponding curve $T_{cx}^{(eff)}(\varrho|c_a)$ in panel (a), even if the associated critical points are the same.

sensitively on all interactions present in the ternary mixture, i.e., among the colloidal particles, between the colloidal and the solvent particles, and among the solvent particles. The relevance of the solvent-solvent interaction for the effective potential and, accordingly, for the phase behavior of the effective colloidal system has been demonstrated recently by Monte Carlo studies in which various kinds of model solvents have been used [298]. It is reasonable to expect that this relevance transfers also to the phase behavior of the full multi-component system. Such distortions of the phase diagram relative to that of the underlying binary mixture do occur for ternary mixtures of molecular fluids. For example, in Ref. [299] experimental studies of molecular ternary mixtures containing various kinds of lutidines are reported. These studies show that the upper and lower critical temperature for a closed-loop phase diagram can be tuned by varying only the concentration of the third component and that the two-phase loop can even disappear upon adding a third component. Similar experimental results are reported in Refs. [300, 301]. Such complex phase diagrams can also be generated by adding colloidal particles to the binary solvent, as can be inferred from corresponding experimental studies [82, 81, 83]. In contrast to the molecular ternary mixtures, for the latter kind of ternary mixtures a decrease of the lower critical temperature upon adding colloids as a third component is reported.

Theoretical studies of bona fide ternary mixtures have so far been concerned with, e.g., lattice gas models [302, 303, 304] and (additive or non-additive) mixtures of hard spheres, needles, and polymers [305, 306]. In these studies the constituents are of comparable size, i.e., their size ratios are less than ten. The peculiarity of the kind of mixtures considered here lies in the fact that the sizes of their constituents differ by a few orders

of magnitude. This property distinguishes them significantly from mixtures of molecular fluids. In contrast to molecular ternary mixtures, in colloidal suspensions the colloidal particles influence the other two components not only by direct interactions but also via strong entropic effects. This is the case because their surfaces act as confinements to fluctuations of the concentration of the solvent and they also generate an excluded volume for the solvent particles. The importance of considering the colloidal suspension as a truly ternary mixture has been already pointed out in Ref. [98].

8.2. Scaling of the critical point shift

For dilute suspensions, i.e., for $\varrho \rightarrow 0$, the shape of the line \mathcal{C}_c of the critical points can be estimated by resorting to phenomenological scaling arguments similar to the ones given by Fisher and Nakanishi [171] for a critical medium confined between two parallel plates separated by a distance L , see Sec. 3.3 and in particular Eq. (3.23). For a dilute suspension, the mean distance $\varrho^{-1/d}$ between colloidal particles plays a role analogous to L . Close to the critical point of the solvent, due to $\xi_t \sim |t|^{-\nu}$ one can identify the two relevant scaling variables $w^{(1)} \propto |t|^{-\beta\delta} h_b$ and $w^{(2)} \propto |t|^\nu \varrho^{-1/d}$ and propose the scaling property $\mathfrak{f}(T, \Delta\mu, \varrho) \simeq |t|^{2-\alpha} \mathfrak{f}(w^{(1)}, w^{(2)})$ of the free energy density, compare with Eqs. (3.6). The difference $\Delta\mu = \mu_a - \mu_b \sim h_b$ of the chemical potentials $\mu_{a,b}$ of the two components a and b of the solvent acts as a symmetry breaking bulk field. It turns out that the scaling variable $w^{(3)} \propto |t|^\nu R$ associated to the radius R of the solute particles is an irrelevant scaling variable, compare Eq. (3.5) and the discussion thereafter. The critical points are given by singularities in \mathfrak{f} occurring at certain points $(w_c^{(1)}, w_c^{(2)})$. This implies that the critical point $(T_c(\varrho), h_{b,c}(\varrho))$ shifts according to

$$T_c(\varrho) - T_c^{(s)} \sim \varrho^{1/(\nu d)} \quad \text{and} \quad h_{b,c}(\varrho) \sim \varrho^{\beta\delta/(\nu d)} \quad (8.1a)$$

so that

$$c_{a,c}(\varrho) - c_{a,c}^{(s)} \sim \varrho^{\beta/(d\nu)} \quad (8.1b)$$

with $[1/(\nu d)]_{d=3} \simeq 0.53$ and $[\beta/(d\nu)]_{d=3} \simeq 0.17$, compare Eq. (3.15b). This states that in the presence of colloids the critical point occurs when the bulk correlation lengths ξ_t and ξ_h [Eq. (3.10)] of the solvent become comparable with the mean distance $\varrho^{-1/d}$ between the colloids. Eqs. (8.1) valid in the limit $\varrho \rightarrow 0$ have been derived by resorting to scaling arguments for a slab. In a slab of width L a dimensional crossover occurs from the spatial dimension d to $(d-1)$ for the limiting cases $L \rightarrow \infty$ and $L \rightarrow 0$, respectively, see Sec. 3.3. In contrast, for the considered case of a bulk system consisting of colloidal particles in a (near-critical) binary liquid mixture there is no limit, in which the fluctuations would be restricted to a dimension lower than $d = 3$. Regardless of the density ϱ of the colloidal particles they cannot lower the dimension, due to their strictly finite size. Therefore no dimensional crossover is expected.

8.3. Effective one-component approach

Integrating out the degrees of freedom associated with the smallest components of the solution (here two) provides a manageable effective description of colloidal suspensions. This kind of approach is commonly used, for instance, recently for studying large particles immersed in various kinds of model solvents [298] or in order to describe a binary mixture of colloids immersed in a phase separating solvent [307]. However, this effective description has only a limited range of applicability for investigating the phase behavior of colloidal suspensions. For example, it fails in cases in which the influence of a set of colloids on the solvent cannot be neglected or the (pure) solvent undergoes a phase separation on its own, as considered here. In the effective approach, the concentration c_a of one of the solvent species, averaged over the whole sample, enters as a unique parameter into the effective interaction potential between the large particles, see the dependence on Σ in Eqs. (3.26) and (6.2). However, generically (e.g., due to the adsorption preferences of the colloids) the concentrations $c_a^{(i)}$ are different in the two coexisting phases $i = 1, 2$ (see Fig. 8.1) and thus, for a proper description, one would have to allow this parameter, and hence the effective potential, to vary in space. Experiments have revealed¹ [75, 76, 84, 85] that for suspensions very dilute in colloids with a phase separated solvent, basically all colloidal particles are populating the phase rich in the component preferred by the colloids (with concentration $c_a^{(1)}$). In this case the actual effective attractive interaction among the particles will be weaker than implied by the effective potential in which only the *overall* concentration $c_a < c_a^{(1)}$ enters as a parameter. Recall that the critical Casimir forces depend non-monotonously on c_a and are strongest for $c_a \lesssim c_{a,c}^{(s)}$, see Ch. 5. Thus for $c_a^{(2)} < c_a < c_a^{(1)}$ the critical Casimir forces differ for each concentration and are – for the typical situation considered here – in general weakest for $c_a^{(1)}$; $c_a^{(2)}$ is the concentration in the other coexisting phase. Within the effective approach for the colloids, one obtains, e.g., by means of density functional theory, coexistence curves $T_{cx}^{(eff)}(\varrho | c_a)$ which depend parametrically on the solvent composition $c_a \approx c_{a,c}^{(s)}$ [or equivalently, by making use of Eq. (3.20), on Σ as in Eq. (6.2)]. Since the effective potential corresponding to this specific value of c_a is used both for the one-phase region as well as for both phases within the two-phase region, this implies that the tacitly assumed corresponding physical situation is such that the composition c_a is fixed throughout the system as an *external constraint*. In particular the two coexisting phases do not differ in their values of the concentration of the solvent particles but only in their colloidal densities $\varrho^{(1)}$ and $\varrho^{(2)}$. Thus within the effective approach for determining the phase behavior one of the essential features, i.e., the tendency of the solvent to phase separate, is suppressed. Accordingly, it is not possible to construct the full coexistence manifold $T_{cx}(c_a, \varrho)$ on the basis of the curves $T_{cx}^{(eff)}(\varrho | c_a)$ alone. Rather, the effective approach is adequate as long as to a large extent the phase segregation involves only the colloidal

¹ In these references also exceptions to the described behavior are discussed which, however, are not relevant for the region of the thermodynamic space considered here. For high temperatures $T > T_c^{(s)}$ (recall that $T_c^{(s)}$ is a lower critical point) the colloids may populate the meniscus formed by the two coexisting phases of the solvent, and for compositions rather different from the critical one the colloids are homogeneously distributed in both coexisting phases (as long as they are soluble at all).

degree of freedom, i.e., the values of ϱ differ in the two phases, but the values of c_a are nearly the same. Therefore the approximation $T_{cx}(c_a, \varrho) \approx T_{cx}^{(eff)}(\varrho | c_a)$ is valid in a region of the thermodynamic space in which the actual tie lines happen to be almost orthogonal to the c_a -axis (see Fig. 8.1). For the phase diagram in terms of the variables T , c_a , and the fugacity of the colloids this latter condition implies that the tie lines have to be sufficiently short.

For temperatures corresponding to the one-phase region of the pure solvent and for an intermediate range of values of the colloidal number ϱ the effective one-component approach might work well. On one hand ϱ should be *large enough* so that the competition between the configurational entropy and the potential energy due to the effective forces can drive a phase separation. On the other hand ϱ has to be *small enough* so that the approximation of using an effective pair potential between the colloids is valid and the influence of the colloids on the phase behavior of the solvent is subdominant. Given such values of ϱ and T , the reduced second virial coefficient B_2^* [Eq. (4.15)] is an appropriate measure for the strength of the attraction and a useful indicator of the occurrence of a phase separation into a colloidal-rich (“liquid”) and a colloidal-poor (“gas”) phase. According to the discussion above, for values of the thermodynamic variables (i.e., the values of T and ϱ , and for the prescribed value of c_a) which are approximately the same as in the one-component approach, the ternary mixture is expected to exhibit a phase separation. According to the extended law of corresponding states due to VLNF the corresponding critical point should occur when B_2^* reaches the critical value $B_{2,c}^* \simeq -1.212$ [Eq. (4.15)] of Baxter’s model. While the extended law of corresponding states due to VLNF provides an empirical estimate for the values of parameters for which there is a critical point, within density functional theory these parameters as well as the shape of the phase coexistence curve can be calculated. Within the effective approach only its dependence on the colloidal density number ϱ for globally fixed values of c_a can be determined.

8.4. Phase diagrams

Generically, in experiments the solvent composition and hence the associated quantity m_0 [Eq. (6.3)] is fixed and $\zeta \sim |t|^{-\nu}$ is varied. In Fig. 8.2(a) for a solvent exhibiting a lower critical point and for the parameter choices $aT/T_c^{(s)} = 100$, $s = 10$, $m_0 = -100$, -20 , and -6 , and $\zeta_0 = 0.01$, 0.05 , and 0.1 [Eq. (6.2)] the coexistence curves $T_{cx}^{(eff)}(\varrho | c_a)$ and the spinodals of the colloidal “liquid”-“gas” phase transition as function of the colloid packing fraction $\eta = (4\pi/3)R^3\varrho$ as obtained by the density functional theory presented in Eq. (4.21) are shown. [Note that in accordance with Eq. (4.2) and (6.2) in the product aT the explicit dependence on T drops out.] For the corresponding free energy F_{RPA} given in Eq. (4.22) the effective colloidal system phase separates if $\tilde{U}_{a,0} < \left(\tilde{U}_{a,0}\right)_c = -21.3$. This condition is satisfied provided the attractive part of the interaction potential is sufficiently strong. Recall, that for the effective potential considered here attraction occurs for $T/T_c^{(s)} = 1 \pm (\zeta/\zeta_0)^{-1/\nu} \rightarrow 1$ [see Eq. (6.2)]. For a solvent exhibiting a lower (upper)

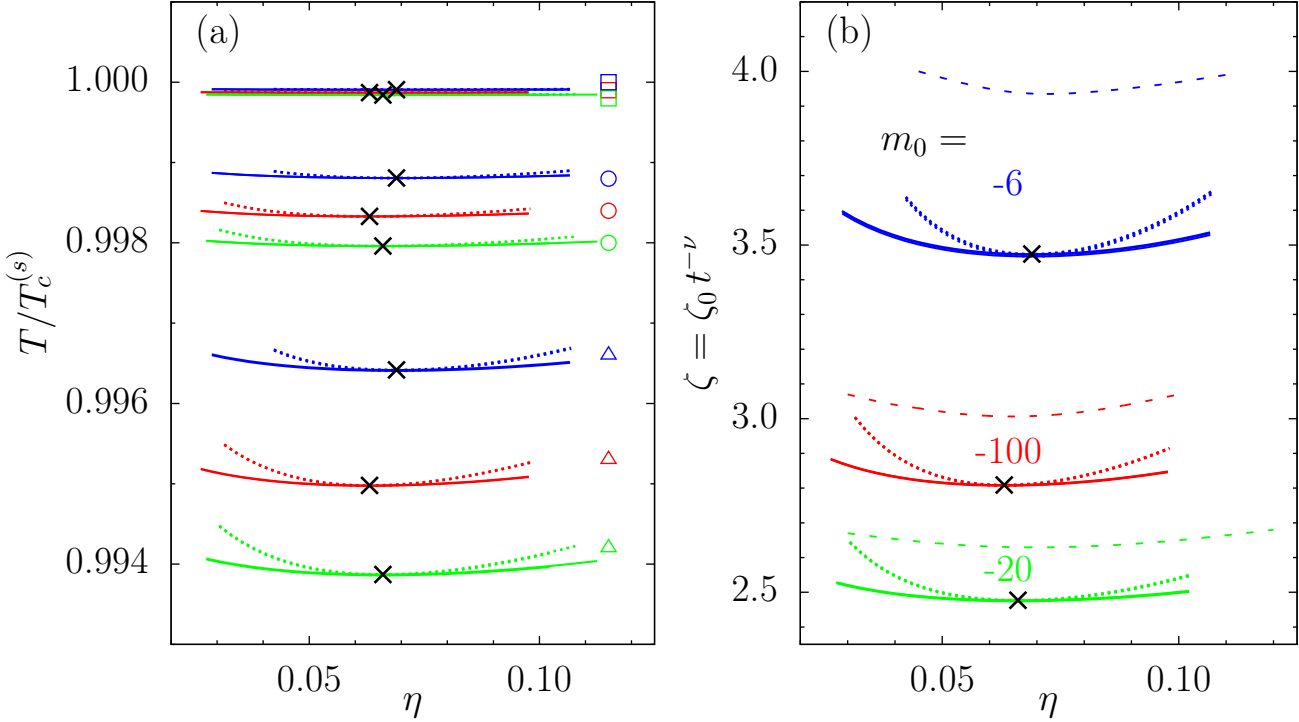


Figure 8.2.: (a) Phase coexistence curves $T_{cx}^{(eff)}(\varrho|c_a)$ (full lines), spinodals (mean-field divergence of χ_T , dotted lines), and the critical points $T_c^{(eff)}$ (crosses) of an effective, one-component system of large particles [Eq. (6.2)] as obtained by density functional theory according to Eq. (4.21). The curves correspond to a solvent with a lower critical temperature $T_c^{(s)}$ and to various fixed solvent compositions c_a [$m_0 = -100$ (red), -20 (green), -6 (blue)]. The other parameters are taken as $\zeta_0 = 0.01$ (\square), 0.05 (\circ), and 0.1 (\triangle), $s = 10$, and $aT/T_c^{(s)} = 100$. Close to the phase separation, the dominant temperature dependence is that of the critical Casimir forces encoded in $\zeta(t = 1 - T/T_c^{(s)}) = \text{sgn}(t) \kappa \xi_t(t) = \text{sgn}(t) \zeta_0 |t|^{-\nu}$. Therefore, in terms of ζ [see panel (b)] the curves in (a) for different values of ζ_0 fall de facto on top of each other, independent of whether the solvent has an upper or a lower critical point. Within the integral equation approach only the spinodals have been determined [Percus-Yevick: dashed lines in (b), see the main text]. According to Eq. (6.3), $(c_a - c_{a,c}^{(s)})^{-1} \sim m_0 = \pm\infty$ corresponds to the critical composition $c_{a,c}^{(s)}$. For solvent compositions which are somewhat poor in the component preferred by the colloids, i.e., for intermediate negative values of $m_0 \simeq -20$, the critical Casimir forces are strongly attractive. Therefore, for them small correlation lengths suffice to bring about phase separation; accordingly the binodals occur at small values of $\zeta \sim |t|^{-\nu}$. Here only thermodynamic states of the solvent which are in the one-phase region, i.e., $t > 0$, are considered.

critical point the lower (upper) sign holds in the one-phase region of the solvent, within which the effective approach is applicable. In this temperature limit the variation of a [Eq. (4.2) and (6.2)] with T is subdominant and thus the dependence of F_{RPA} on $T/T_c^{(s)}$ and ζ_0 reduces to a dependence on ζ only. Accordingly, as can be inferred from the comparison of Figs. 8.2(a) and 8.2(b), in terms of ζ for each value of m_0 the coexistence curves $T_{cx}^{(eff)}(\rho | c_a)$ for different values of ζ_0 fall de facto on top of each other. The difference between these curves is of the order of $(\zeta_0/\zeta)^{1/\nu}$ [because $T/T_c^{(s)} = 1 \pm (\zeta/\zeta_0)^{-1/\nu}$], which for the three values of ζ_0 used in Fig. 8.2 is about the thickness of the lines shown in Fig. 8.2(b). In terms of this presentation it does not matter whether the solvent exhibits a lower or an upper critical point. Although spinodals are mean-field artifacts (Sec. 4.3), they are presented also because they provide some indication about the location of the binodal which encloses the former. Furthermore the spinodals carry the advantage that the isothermal compressibility χ_T is the property of only one thermodynamic state. Therefore, in contrast to the calculation of the binodal (which depends on two coexisting phases), the calculation of the spinodal does not suffer from the non-uniqueness of the effective potential in the case of phase coexistence. As discussed in Ch. 4, based on formally exact relations the phase behavior can in principle be calculated from the correlation functions obtained within the integral equation approach. Within the so-called compressibility route [Eq. (4.13)] the spinodals, i.e., the loci of the mean-field divergence of χ_T , are directly accessible. On the other hand, the binodals, i.e., the loci of two thermodynamic states which at the same temperature have different packing fractions but the same pressure, are directly accessible via the so-called virial route [Eq. (4.12)]. Because the calculation of the binodals (the spinodals) via the compressibility route (virial route) requires thermodynamic integration, which is (in particular in the present context) subtle, these calculations have not been performed. The spinodals calculated by the compressibility route are shown as dashed curves in Fig. 8.2(b). For the region of the thermodynamic space where the integral equation approach renders solutions for the correlation functions, the calculations failed to find binodals, i.e., along the pressure isotherms $p(\eta; T = \text{const})$ as calculated via the virial route there are no two states with $\eta_1 \neq \eta_2$ and $p(\eta_1; T) = p(\eta_2; T)$. These observations can be explained by the thermodynamic inconsistency of this integral equation approach. Due to the approximate bridge function, the binodals as obtained by two different routes need not to coincide. The same observations are found within the hypernetted-chain approximation within which the spinodals are shifted w.r.t. to the Percus-Yevick results to slightly smaller values of ζ . Although within the integral equation approach the binodals could not be determined, at least the loci of the obtained spinodals are similar to the ones obtained from density functional theory.

Since the critical Casimir forces are strongest for slightly off-critical compositions $m_0^{-1} \sim (c_a - c_{a,c}^{(s)}) \lesssim 0$ the binodals (and spinodals) are shifted to smaller values of ζ upon decreasing $|m_0|$ down to $m_0 \simeq -20$. With a further decrease of $|m_0|$ the system moves too far away from the critical point of the solvent so that the critical Casimir force weakens and the spinodals shift again to larger values of ζ .

The critical value η_c of the packing fraction is rather small, i.e., $\eta_c \approx 0.07$ (see Fig. 8.2),

because the effective hard sphere diameter σ which results from the soft repulsion U_{rep} is larger than $2R$. In terms of $\eta_\sigma = (\sigma/(2R))^3\eta$ (defined after Eq. (4.22)) the critical value assumes its RPA-value $\eta_{\sigma,c}^{(RPA)} = 0.129$. In Refs. [9, 308], the phase diagrams of hard particles in the presence of smaller ones have been considered. The presence of the smaller particles leads to an attractive depletion force between the larger particles. Within an effective one-component approach fluid-fluid transitions have been found by means of Monte Carlo simulations. For size ratios $0.1 \dots 0.8$ the critical packing fraction η_c of the large particles is about $\eta_c \simeq 0.25$ [308]. These binary hard-sphere mixtures are different from colloidal suspensions considered here as well as the physical origin of the attractive effective interaction potential between the large particles. However, on the level of the effective one-component system, considering both systems as hard particles interacting in addition via an attractive potential one can compare the resulting phase diagrams. Because the results of the Monte-Carlo simulations are more reliable than the random-phase approximation, one may conclude, that the reported critical packing fractions in Fig. 8.2 are too small. Indeed, the random phase approximation works well if the range of the attractive interaction is much larger than the range of the repulsive interaction [262]. In the present case, the range of attraction is rather small compared with the radius R of the colloidal particles. In such cases, however, the Percus-Yevick closure works usually well. Therefore it is interesting to note, that the spinodals obtained via the random phase approximation and the Percus-Yevick closure are quite similar. The binodals shown in Fig. 8.2 are rather flat compared with, e.g., the ones for hard spheres interacting via a short-ranged, attractive temperature independent potential and described also by Eq. (4.22). In the present system, the deviation from the critical temperature T_c which leads to a range of η for the coexisting phases as large as shown in Fig. 8.2, is about 1%, whereas for a system of hard spheres with an attraction the corresponding temperature deviation is a few percent. For smaller values of ζ_0 the binodals are flatter and the differences of the critical temperatures for different values of m_0 are smaller [see Fig. 8.2(a)]. The requirement $\eta^{-1/3} > (4\pi/3)^{1/3} (2 + \zeta/s)$ (see Ch. 6) concerning the validity of the pairwise approximation for the critical Casimir forces is fulfilled for the whole range of values for η and ζ shown in Fig. 8.2; e.g., for $s = 10$ and $\zeta = 4$ the above condition is $\eta < 0.3$. On the other hand, the other requirement, $\zeta < 0.154s$ is clearly not fulfilled in this range of the the values of ζ .

The sketch of the phase diagram in Fig. 8.1 and the calculated coexistence curves in Fig. 8.2 correspond to using the background potential with fixed parameters s and a . In order to investigate the dependence of the locus of the phase separation on properties of the background potential, in the following the critical temperature $T_c^{(eff)} = T_c^{(eff)}(\Sigma, a, s, \zeta_0, T_c^{(s)}, \pm)$ of the effective colloidal system as function of its arguments (\pm is taken to be $-$ and $+$ for a lower and an upper critical point, respectively) is discussed. According to the discussion above, to this end it is sufficient to determine $\zeta_c^{(eff)}(\Sigma, a, s)$. In Fig. 8.3 for fixed values of s and for specific values of $\zeta_c^{(eff)}$ the contour lines $a = a(\Sigma; s; \zeta_c^{(eff)})$ are shown. That is, for a colloidal system with a background potential characterized by certain values of a and s , from the plot in Fig. 8.3 one can read off the value of the difference of the chemical potentials of the

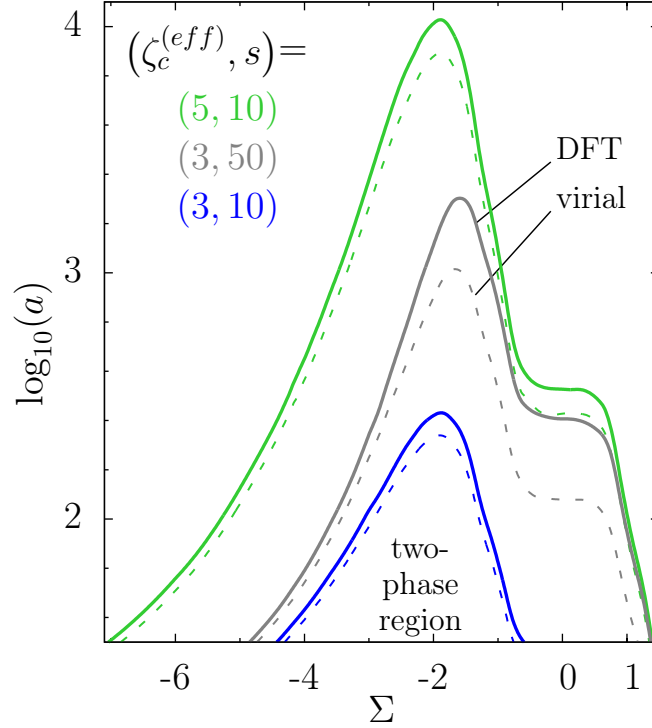


Figure 8.3.: Attraction due to critical Casimir forces can induce a “liquid”-“gas” phase separation of the colloids. Within the effective approach described by Eq. (6.2) the dominant temperature dependence is that of the Casimir scaling function encoded in $\zeta = \kappa \xi_t(t) \sim |t|^{-\nu}$. The full curves correspond to density functional theory [Eq. (4.21)] and show for which values of Σ and a corresponding to the solvent composition and the repulsive strength of the background potential, respectively, a given temperature (in terms of ζ) is the critical one $T_c^{(eff)}$ or $\zeta_c^{(eff)}$. The contour lines $a(\Sigma; s; \zeta_c^{(eff)})$ depend parametrically on $s = \kappa R$ where κ^{-1} is the range of the background repulsion and R is the radius of the colloids. Systems, with their parameters being located in the area below the contour line $\zeta_c^{(eff)}$, are phase separated at this temperature. This two-phase region expands to larger values of a with increasing ζ . For a fixed value $\zeta_c^{(eff)}$, $a(\Sigma; s; \zeta_c^{(eff)})$ is largest for compositions slightly poor in the component preferred by colloids, i.e., $\Sigma \lesssim 0$. In addition, the corresponding contour lines based on the extended law of corresponding states due to VLNF $B_2^*(\zeta = \tilde{\zeta}_c^{(eff)}, \Sigma, a; s) = B_{2,c}^*$ for the reduced second virial coefficient [Eq. (4.15)] are plotted as dashed lines. It is satisfactory to see that both approaches provide comparable results.

two components of the solvent (which is related to Σ) for which $T_c^{(eff)}$ has a prescribed value. The full curves are calculated within the density functional approach [Eq. (4.21)] and are compared with the ones corresponding to the simple prediction [Eqs. (4.14) and (6.2)] $B_2^*(\zeta = \tilde{\zeta}_c^{(eff)}, \Sigma, a; s) = B_{2,c}^* = -1.212$, which also yields a relation $\tilde{\zeta}_c^{(eff)} = \tilde{\zeta}_c^{(eff)}(\Sigma, a; s)$. Both approaches differ only slightly. For given values of $\zeta_c^{(eff)}$ and Σ the extended law of corresponding states due to VLNF predicts a smaller critical value of a than obtained from density functional theory. The largest deviations occur for slightly negative values of Σ , for which the critical Casimir forces are more attractive. For all values of the parameters shown in Fig. 8.3 (i.e., $a \gtrsim 30$), at small distances D the corresponding potentials exhibit repulsive barriers $\gtrsim 30k_B T$. For smaller values of a , i.e., $a \lesssim 15$, this potential barrier disappears and the colloidal particles may form aggregates, as discussed in Ch. 7 and see in particular Fig. 7.3.

The contour lines $a = a(\Sigma; s; \zeta_c^{(eff)})$ attain their largest values for slightly negative values of Σ , i.e., for $\Sigma \simeq -2$. This again reflects the asymmetry of the strength of the critical Casimir forces with respect to the bulk ordering field h_b in the presence of symmetry breaking surface fields. In Fig. 8.3, for all parameter pairs (a, Σ) below each contour line, characterized by $\zeta_c^{(eff)}$, the corresponding system at the temperature belonging to the value $\zeta_c^{(eff)}$ is phase separated. This two-phase region widens with increasing values of ζ and it significantly expands to larger values of a , which is in line with the fact that the critical Casimir forces become stronger upon approaching $T_c^{(s)}$. For $s = 10$, upon increasing $\zeta_c^{(eff)}$ from 3 to 5 the largest critical value of a increases by two orders of magnitude (compare the corresponding blue and green curves in Fig. 8.3). The two-phase region can be markedly increased upon increasing s (compare the blue and gray curves in Fig. 8.3 corresponding to $\zeta_c^{(eff)} = 3$ with $s = 10$ and $s = 50$, respectively) because for the phase separation the strength of the attraction is important; due to $U \sim s$ [Eq. (6.2)] the latter can be easily tuned by varying s .

For the experimental studies reported in Refs. [82, 81] colloidal mixtures consisting of silica spheres, water, and 2-butoxyethanol or lutidine have been used; with a radius $R \approx 11nm$ the colloidal particles have been rather small. Thus, a priori, the effective approach, developed in Ch. 6 and discussed in Sec. 8.3, is not expected to apply. Nonetheless, one can try to do so and estimate the critical temperature for solutions containing such small particles by using the general scaling arguments presented in Sec. 8.2. At the critical temperature, the dimensionless scaling variable $w^{(3)} = w_0^{(3)} |t|^\nu R$ associated with the radius of the colloids takes on a certain value $w_c^{(3)}$ with $w_c^{(3)}/w_0^{(3)} = \left| \left(T_c^{(s)} - T_c(\varrho) \right) / T_c^{(s)} \right|^\nu R \equiv |t_c|^\nu R$ (where $w_0^{(3)}$ is a non-universal amplitude). On one hand the value of $w_c^{(3)}/w_0^{(3)}$ depends on the specific components of the colloidal suspension via the non-universal amplitude $w_0^{(3)}$. On the other hand, see Sec. 8.2, it depends on ϱ [or equivalently on h_b , see Eq. (8.1)], via $w_c^{(3)}$ with $w_c^{(3)}$ as function of $w_c^{(2)}$ [or $w_c^{(1)}$]. Thus, the value of $w_c^{(3)}/w_0^{(3)}$ varies along the line \mathcal{C}_c of critical points. Because $T_c(\varrho \rightarrow 0) \rightarrow T_c^{(s)}$ one has $w_c^{(3)}(\varrho \rightarrow 0) \sim \left| 1 - T_c(\varrho) / T_c^{(s)} \right|^\nu R \rightarrow 0$.

However, there are no general theoretical estimates concerning which values $w_c^{(3)} \neq 0$ are attained for $\varrho \neq 0$. This lack of knowledge can be overcome by resorting to the results obtained from the effective approach. Still this leaves open the issue, to which extent the non-universal amplitude $w_0^{(3)}$ depends on the kind of colloids used. Within the present analysis the dependence on the kind of solvent used is taken into account by adopting the corresponding values for the non-universal parameters. Concerning the kind of colloids, at least two main influences of the colloids on the solvent, i.e., the excluded volume and the strong adsorption of one of the components, are taken into account via R and the boundary conditions for the solvent order parameter at the colloid surfaces [i.e., $h_s = \infty$ in Eqs. (3.29)], respectively. The non-universal amplitude may depend on the direct colloid-solvent interaction, e.g., via a non-universal amplitude related to a finite surface field $h_s < \infty$. The direct interactions between the colloids can be expected to enter the non-universal amplitude, too. Softly repulsive colloid-colloid interactions may be taken into account by using an effective HS diameter σ [see, e.g., Eq. (4.17)] instead of $2R$ (which, in turn corresponds to a non-universal amplitude $w_0^{(3)}$ proportional to $\sigma/(2R)$). For the solvents used, the relevant parameters are $\xi_0 \approx 0.25nm$ and $\zeta_0 \sim 0.03$. Choosing $s = 10$ (see Sec. 6.1 and Fig. 8.2(a)) renders $R = \xi_0 s / \zeta_0 \approx 85nm$. This value of R is sufficiently large so that the aforementioned effective approach can be considered to be reliable. From Fig. 8.2(a) the corresponding shift $|t_c| \sim 0.001$ can be read off which leads to $w_c^{(3)}/w_0^{(3)} \simeq 1.094nm$. By using this latter mean-field estimate and demanding, that the such obtained value applies approximately to the experiments reported in Refs. [82, 81] for the experimental value $R \approx 11nm$ of the radius of the colloidal particles one thus obtains the shift $|t_c| = \left(w_0^{(3)}R/w_c^{(3)}\right)^{-1/\nu} \simeq 0.234$. With the critical temperature $T_c^{(s)} \approx 320K$ of the solvent [82, 81], this leads to $T_c(\varrho) = (1 - t_c)T_c^{(s)} \approx 310K$. Indeed, for such a temperature phase separation in the ternary mixture has been observed although even lower critical temperatures $T_c \approx 300K$ have been reported [82, 81]. As stated above such an agreement for even small colloids could not have been anticipated from the outset.

9. Conclusions

9.1. Outlook

In order to make a further progress in the understanding of the role of critical Casimir forces for aggregation phenomena, advances concerning static and dynamical issues are needed. In order to obtain more reliable quantitative results in the spatial dimension $d = 3$, the dependence of the critical Casimir forces on the bulk ordering field h_b should be tested with Monte-Carlo simulation data. It is tempting to test the reliability of the local functional approach both within the sphere-plane geometry and in the film geometry for finite positive surface fields. In $d = 3$, for both cases the results can be compared with corresponding Monte-Carlo simulation data provided by Refs. [227] and [212, 213], respectively. Because the local functional approach is formulated for general d , its results can also be compared with corresponding exact results in $d = 2$. Concerning finite surface fields, within the present specifications [Eqs. (3.32) and (3.34)] the local functional approach is limited to positive, not too asymmetric boundary fields, because it fails to describe properly an interface. Yet, it is worthwhile to test to which extent this approach captures the deviations from the strong adsorption limit. Because the formalism of the local functional approach is the same as for mean-field theory, i.e., the minimization of a suitable functional, it seems plausible that a ‘rescaling’ property of quantities in films subject to finite surface fields onto corresponding fixed point values, as observed for $d = 4$ [214], can be found within the local functional approach also for $d = 3$. Such a property could help to analyze experimental data and to allude to which extent substrates used in experiments fulfill the strong adsorption limit. If in different situations the local functional approach proves to yield results similar to Monte Carlo simulations, it is a versatile tool for quantitative comparisons of theoretical predictions with experimental data, because the local functional approach is substantially less computational demanding than Monte Carlo simulations. With the `f3dm`-library a powerful tool for numerical minimization of functionals in complex geometries is available [309], see also Ref. [231]. For $h_b = 0$, in various studies the rich crossover behavior of the critical Casimir force between two plates with asymmetric finite surface fields has been revealed. However, in that crossover regime the strength of the critical Casimir force is notable smaller than for the strong adsorption limit. In order to increase the strength of the critical Casimir force in this crossover regime of finite surface fields, slightly off-critical compositions of the critical medium could be used, because for these the critical Casimir forces are stronger than for the critical composition. In $d = 3$ and for weak surface fields (and $h_b = 0$), both theoretical results [212, 213] and experimental data [46] for the critical Casimir force are available, but

a quantitative comparison is lacking. Such a comparison would be needed in order to make use of the tunability of critical Casimir forces via surface fields in potential applications. To this end also a deeper understanding of the relation between the scaling variables associated to the surfaces and experimentally accessible, microscopic quantities is required. Insights to this issue could be gained from the microscopic and the surface field-mixing considerations presented in Refs. [249] and [184], respectively, as well as from a comparison of the universal scaling functions of the critical Casimir force with effective potentials between solute particles obtained from microscopic calculations. For a near-critical model solvent (composed of particles interacting between each other via a hard core repulsion and an attractive square well potential), effective interaction potentials between two spherical particles which interact with the solvent particles (in addition to the hard core repulsion) via attractive or repulsive square well potentials with various interaction strengths have been obtained by Monte Carlo simulations [310].

The study of the *process* of aggregation of colloidal particles due to the critical Casimir forces and of the structure of the resulting clusters demands a dynamical description. Even the critical dynamics of the order parameter profile in a fixed configuration of confinement is already a challenge by its own, see, e.g., Refs. [311, 231, 312] and references therein. Inter alia, each bulk universality class splits up into several dynamical universality classes and the relaxation time $\tau_{rx} \sim |t|^{-\nu z}$ diverges upon approaching the bulk critical temperature. τ_{rx} describes the temporal persistence of order parameter fluctuations and z is the universal dynamical critical exponent. Further, for the detailed description of the clustering, the non-additivity of the critical Casimir forces as well as hydrodynamic interactions, which are non-additive, too, have to be taken into account. Within mean-field theory, for two spherical particles in front of a planar wall, the many-body contribution to the total critical Casimir force can reach up to 25% [313]. Thus, for the precise description of the aggregation of colloidal particles in near critical solvents one is faced with the collective motion of solute particles which interact between each other via long-ranged many-body forces mediated by two coupled, slowly relaxing fields. Because the theoretical analysis of the reported experimental data of turbidity measurements requires a dynamical approach and in several experimental studies dynamical structure factors have been reported, it seems to be justified to address this challenging problem theoretically and with suitable computer simulations. (For a list of experimental studies see Ch. 2.) For the static structure factor, the approach reported in Ref. [188], which has been concerned for critical films with ordinary-ordinary boundary conditions, provides a starting point. It needs to be checked to which extent this approach can be applied to symmetry breaking boundary conditions and to non-planar boundaries.

Recently, it has been shown, that the critical Casimir force between a colloidal particle with (+) boundary condition and a patterned substrate of stripes with (+) and (-) boundary conditions can change its sign as function of the distance between the particle and the substrate. For certain realizations this leads to a stable levitation of the colloidal particle above the substrate, which is purely due to the critical Casimir effect, and the height can be tuned sensitively with temperature [55]. In the work only the critical composition (i.e., $h_b = 0$) has been considered. For a given (experimental) pattern it

may help to use the bulk field as additional tunable parameter of the critical Casimir force, in order to adjust the conditions of stable levitation at a desired height.

Concerning the thermodynamic properties of colloidal suspensions with near-critical solvents a multicomponent theory (beyond the effective approach) is needed, as discussed in Ch. 8. One of the challenges thereby is to construct a suitable theory, which accounts for all relevant degrees of freedom, i.e., the ones of the solvent particles and the ones of the large solute particles *and* takes care about the sizes of the particles of different species, which differ by several orders of magnitude. Standard theories of mixtures, which treat the different species on the same level, encounter problems in such cases as has been observed in calculations of the effective potential between two large solute particles [314]. The results obtained from the Ornstein-Zernicke approach (within the RPA-closure), which treats both components on the same footing, underestimate extremely the strength of the effective potential compared with the results of a density functional approach using the insertion method [19], within which one large solute particle acts as an external potential. However, concerning bulk thermodynamic properties the density functional approach may be faced with similar problems as the Ornstein-Zernicke approach, because in the corresponding calculations the large solute particles cannot be treated anymore as an external potential. To which extent such a failure arises and how it can be circumvented needs to be investigated. Further, the proper treatment of the attractive interactions among the small particles of the solvent is a subtle issue, even for calculating the free energy of solvation for a big particle [22, 23]. The large size difference of the particles of the different species obviously enters into the total entropy and the interaction energy between particles of different kinds. But furthermore, this size difference has also entropic effects on the total interaction energy of the (smaller) particles of the solvent. This coupling has been revealed in a density functional treatment of a binary mixture of hard particles and particles which interact among each other via a softly-repulsive pair potential [315]. It is straightforward to extend this density functional to a mixture of several species of ‘soft’ particles. Such a mixture of ‘soft’ particles can exhibit a fluid-fluid demixing transition and may serve as a toy model for a phase-separating solvent. In the binary mixture of hard particles and ‘soft’ particles, depletion forces between the hard particles due to the presence of the latter may drive a phase separation. This kind of phase transition is well studied, see e.g., Ref. [315] and references therein, and has been recently studied in the presence of a fixed matrix of quenched hard particles [316]. For the binary Asakura-Oosawa model (within which the particles of one kind do not interact with each other and the particles of the other kind expose a hard core repulsion) and particles of similar sizes, differences in the phase diagrams obtained from the effective one-component description and of the full binary mixture have been revealed by Monte-Carlo simulations [317].

Within field-theoretical methods, microscopic structures, such as packing effects of hard particles, get lost. Nonetheless, suitable coarse-grained field theories are promising to have the potential to allude to the generic features of colloidal mixtures with phase-separating solvents. A systematic coarse-graining scheme, within which microscopic and mesoscopic fluctuations can be incorporated has been recently developed [318, 295] and applied to ionic systems [319]. It is reasonable to assume that the considered colloidal

suspensions, consisting of spherical solute particles and a phase-separating solvent, belong to the Ising universality class. If it is so, the critical behavior of these suspensions would be given by the same description of the singular bulk free energy, Eq. (3.5), and the same effective field theory, Eq. (3.29), as the critical solvent. The difference would be, that the corresponding order parameter Φ will be a function of both the concentration c_a of the solvent as well as the density of the colloidal particles, $\Phi = \Phi(c_a, \varrho)$. An analogous effect has been explored in near-critical solvents containing ions. For such mixtures, the critical field is a combination of the concentration of the solvent and the density of the ions [288]. This issue could be also further explored within the concepts of field-mixing and complete scaling (for the case of simple fluids, see, e.g., Ref. [118] and references therein).

More complex colloidal suspensions offer a broad field of activity for further research, for example a mixture of colloidal species with different adsorption preferences for the solvent particles. According to Gibbs' phase rule, for such a four-component system (a binary mixture of colloids in a binary solvent) at constant pressure a two-dimensional manifold of critical points embedded in a three-dimensional manifold of coexisting states in the (then four-dimensional) thermodynamic space can be expected. Recently, such a mixture was studied experimentally [307]. In this study, concerning the effective interaction potential of the critical Casimir forces between the colloids the attractive $(+, +)$ boundary conditions and the repulsive $(+, -)$ boundary conditions were realized for colloidal particles of the same kind and for particles of different kind, respectively. In line with an effective density functional approach, upon approaching the critical temperature of the solvent there are indications that these two kinds of particles phase separate. Another kind of more complex colloidal suspensions is provided by non-spherical solute particles immersed in near-critical solvent. Such particles may have rod-like shapes or can be so-called Janus particles. The latter have different adsorption preferences at opposing sides. A study of Janus-cylinders within the effective approach has explored not only the possibility of a phase segregation in colloidal-rich and colloidal-poor phases, but also that in the nematic phase the critical Casimir forces induce an orientational order, such that the faces of the Janus-particles with the same adsorption preference face each other [320]. The addition of ions to near-critical colloidal suspensions offers further perspectives. It has been shown both theoretically [288, 289, 290, 291, 292] and experimentally [287] that the strength of and even the sign of the effective force between solute particles in near-critical solvents is sensitive to the amount of added salt and that the ions couple to the fluctuations of the order parameter associated to the solvent. Therefore, it can be expected, that the presence of ions modifies the phase behavior of such mixtures, although certain bulk critical properties of the pure solvent (without colloids) are hardly affected by salt [287, 297]. Recently the large scale structure of a solvent containing impurities has been analyzed by means of general properties of the direct correlation function [321]. It has been shown that only impurities of anions and cations which differ sufficiently in their sizes alter the large scale structure of the solvent. If such impurities are present, the solvent becomes non-uniform upon increasing its bulk correlation length. If it turns out that such conditions can be realized in experiments, the effective force between two solute particles in such a structured liquid solvent is of

interest and how the presence of the (molecular) aggregates influences the assembly of immersed larger colloidal particles.

In general, a flexible confinement is of interest. In such a case there is an interplay between the flexible confinement the shape of which determines the effective force acting between the boundaries with this effective force which in turn affects the shape of the boundary. Such conditions could be met in colloidal suspensions which are dense in colloidal particles. If the particles are jammed or in a glassy state, the effect of this non-trivial confinement to the critical behavior of the binary liquid solvent could be investigated or, in turn, whether the attractive critical Casimir forces could induce a glassy state to dense colloidal particles. Experiments have been reported which addressed the structure of silica hydrogels [322] and the influence of a fractal network of silica particles on the demixing of the 2,6-lutidine-water mixture, which served as solvent [323]. In Ref. [324] scattering methods have been used to investigate silica particles immersed in 2,6-lutidine-water mixture. A structural arrest of the solute particles and a glass transition has been reported. Related to those issues, it seems worthwhile to study critical phenomena of binary liquid mixtures confined by porous media [325]. Measurements of the specific heat in such a confinement has been reported in Ref. [326]. In the non-equilibrium state of granular matter [327] there are also fluctuations on large spatial scales, the confinement of which results in Casimir-like effective forces [328, 329]. The mutual interplay between geometry and phase transitions has been studied also in Ref. [330], addressing complete wetting of a flexible substrate.

Within the scope of nanofluids, i.e., fluids containing nanometer-sized structures, such as hard particles or soft entities, near-critical solvents open new perspectives. Nanofluids raise fundamental questions for basic research and are exploited in a wide array of applications [331]. On one hand, it is intriguing to observe and investigate critical phenomena with nanometer sized particles. On the other hand, critical phenomena offer a richness in order to tune the properties of nanofluidic devices. For example, the shape of a nanometer-sized droplet or film (formed by a binary liquid mixture) will be altered by critical fluctuations, as well as the self-assembly of immersed nano-particles. A wealth of phenomena can be expected by exposing near-critical nanofluids to confinement. The implications and the potential of wetting phenomena in the broader field of nanofluidics have been recently emphasized [332].

9.2. Summary

In the present study colloidal suspensions with the solvent which phase separates has been explored theoretically. In typical experimental realizations such a solvent is a binary liquid mixture which exhibits a miscibility gap. Close to its critical demixing point long-ranged fluctuations of the corresponding order parameter emerge. These critical fluctuations drive the divergence of the bulk correlation length ξ and the system becomes scale invariant (Sec. 3.2). Exposing the near-critical medium to boundaries perturbs the fluctuating order parameter near the confining surfaces on the scale of

ξ and restricts the spectrum of its thermal fluctuations (Sec. 3.3). These restrictions result in a modified critical behavior, for example, in confined geometries the critical temperature is shifted w.r.t. the bulk. Since these alterations depend on the spatial configuration of the confinements they result in an effective force between the confining surfaces which is called the critical Casimir force (Sec. 3.4). Colloidal particles act as cavities in the fluctuating, near-critical solvent and thus the critical Casimir forces act between these solute particles in addition to regular background forces (Sec. 4.1). For colloidal particles with the same adsorption preferences to one of the two species forming the binary liquid mixture, the so-called (+, +) boundary conditions apply and the critical Casimir forces are attractive. This attraction due to the critical Casimir forces can be easily controlled by the reduced temperature deviation $t = (T_c^{(s)} - T)/T_c^{(s)}$ from the lower critical temperature $T_c^{(s)}$ of the solvent and provides a versatile mechanism in order to manipulate the collective behavior of colloidal particles with number density ρ . For certain circumstances, the presence of the solvent can be treated in an implicit way via parameters in an effective contribution to the pair potential of the colloids. Standard liquid state theory can be applied to such effective, one-component systems of colloidal particles in order to describe their structure (Sec. 4.2), their thermodynamic properties (Sec. 4.3), and their stability (Sec. 4.4). The present study has elaborated on the limitations of the applicability of this effective approach to colloidal suspensions with phase-separating solvents. The main results of this thesis concern the dependence of the critical Casimir forces on the composition of the solvent (Ch. 5), the structure and stability of dilute colloidal particles in near-critical solvents (Ch. 7), and the phase behavior of colloidal suspensions with phase-separating solvents (Ch. 8), and can be summarized as follows.

For spatial dimensions $d = 4$ and $d = 3$ the critical Casimir forces in a slab with (+, +) boundary conditions have been calculated (Secs. 5.1 and 5.2, respectively) and have been discussed in terms of the corresponding universal scaling function¹ $\vartheta^{(d)}$, Eq. (3.25). For spatial dimension $d = 4$, mean-field theory (Sec. 3.5.1) is exact and $\vartheta^{(d=4)}$ has been calculated for the whole range of the thermodynamic control parameters t and h_b , where h_b is the bulk field conjugated to the order parameter Φ . For the case of a binary liquid mixture h_b is related to the difference of the chemical potentials of the two species. In Figs. 5.1 and 5.2 the variation of $\vartheta^{(d=4)}$ along specific thermodynamic paths is shown. The critical Casimir forces are weakest for temperatures corresponding to the bulk coexistence region and compositions rich in the preferential phase, i.e., for $t \leq 0$ and $h_b \geq 0$. Upon turning from the positive branch of the critical isotherm ($t = 0, h_b > 0$) to the positive branch of the critical isochor ($t > 0, h_b = 0$) and further to the negative branch of the critical isotherm ($t = 0, h_b < 0$), the critical Casimir force becomes significantly stronger. For binary liquid mixtures the latter corresponds to compositions $c_a \lesssim c_{a,c}^{(s)}$ which are slightly poorer in the component adsorbed by the colloidal particles than the critical composition $c_{a,c}^{(s)}$. Capillary condensation occurs for

¹In the summary, in favor of an easier reading, the indices \parallel_{\pm}^{\pm} and $\oplus\oplus$ indicating the film geometry and the sphere-sphere geometry, respectively, with (+, +) boundary conditions, as they are present in the main text, have been dropped.

$t < 0$ and at bulk fields $h_b^{(cx)}(L) < 0$. For thermodynamic state points for which in the bulk the $(-)$ phase is present, whereas in the film predominantly the $(+)$ phase is present, i.e., for $t < 0$ and $h_b^{(cx)} < h_b < 0$, the effective force between the two walls is strongest. Upon crossing $h_b^{(cx)}$ the effective force exhibits a jump to significantly smaller values in the predominantly $(-)$ phase then in the predominantly $(+)$ phase. For the experimentally relevant case, spatial dimension $d = 3$, the (semi-empirical) local functional approach (Sec. 3.5.2) has been evaluated for temperatures $t > 0$ (corresponding to the bulk one-phase region) and for bulk fields $h_b \neq 0$. In $d = 3$ the critical Casimir force exhibits the same qualitative features as in $d = 4$, see Fig. 5.3. The increase of the strength $|\vartheta^{(d)}|$ of the scaling function of the critical Casimir force upon turning from the critical isochor towards the critical isotherm is even stronger in $d = 3$ than in $d = 4$. An approximation, Eq. (5.6), is proposed and discussed in order to estimate the dependence of the critical Casimir force on the bulk field h_b in spatial dimension d from available results for spatial dimension d' . This approximation is applied to $d = 3$ and $d' = 4$. As can be inferred from Fig. 5.3, for not too strong bulk fields this approximation compares well with the results obtained from the local functional approach. The comparison with available data [185] for the critical Casimir force in $d = 2$ and $d' = 4$ the approximation underestimates extremely the strength of the critical Casimir force. For the comparison along an isotherm, $t = const > 0$, see Fig. 5.4. The quantitative mismatch for $d = 2$ and $d' = 4$ can be expected, because for $d' = 4$ the approximation given in Eq. (5.6) can be seen as the lowest order contribution of an expansion in $\epsilon = 4 - d$ of the dependence of $\vartheta^{(d)}$ on h_b . By making use of the Derjaguin approximation [Eq. (3.27) and (3.28)], the critical Casimir force between two spherical particles which are close to each other can be obtained from the results corresponding to the film geometry. In Fig. 5.5 the scaling functions $\Theta_{Derj}^{(d=3)}$ of the corresponding potential resulting from the functions $\vartheta^{(3)}$ obtained by using both the local functional approach and the dimensional approximation are compared. The quantitative differences between corresponding results of the two approaches are larger for $\Theta_{Derj}^{(d=3)}$ than for $\vartheta^{(3)}$ in the film geometry. For $d = 4$, preliminary results of numerical calculations of the critical Casimir force in the full sphere-sphere geometry are available [285]. In Fig. 5.6, these results for the critical Casimir force at fixed temperature $t > 0$ and for different particle separations D as function of the bulk field h_b are compared with the corresponding curve obtained from the Derjaguin approximation. These curves exhibit the same gross features, which are the monotonic decay towards zero for increasing values $h_b \geq 0$ and a pronounced minimum for slightly negative bulk fields. The results of the Derjaguin approximation, which corresponds to $D \rightarrow 0$, are in line with the general trends observed from the preliminary data for the critical Casimir force upon decreasing the distance D .

In Ch. 6, a generic effective one-component description for colloidal particles immersed in a near-critical solvent is introduced and discussed. Within this approach the presence and influence of the solvent enters through the parameters of the effective pair potential between the monodisperse colloidal particles of radius R . The considered effective pair potential, Eq. (6.1), consists of the critical Casimir contribution, Eq. (3.26), plus a regular background potential. For the latter a generic, softly repulsive contribution,

Eq. (4.1), with strength A and acting on a length scale κ^{-1} is adopted. In Sec. 6.1, the ranges of the values of the parameters entering into the effective potential which correspond to possible experimental realizations are discussed. The competition between the repulsive and the tunable attractive contributions to the effective pair potential leads to a variety of possible shapes of this potential, see Fig. 6.2.

Concerning the structure of the effective one-component colloidal system, the Ornstein-Zernicke equation (4.3) has been solved numerically by making use of the Percus-Yevick and the hypernetted-chain closure [Eqs. (4.9) and (4.10), respectively]. In Figs. 7.1 and 7.2 the radial distribution function $g(r)$ for two different, experimentally realizable parameter sets ($a = A/s, s = \kappa R, m_0$) and various temperatures [in terms of $\zeta = \kappa\xi(t, h_b = 0)$] is shown. $m_0^{-1} \sim c_a - c_{a,c}^{(s)}$ is related to the composition of the solvent [Eq. (6.3)]. Close to the surface of a colloidal particle ($r \gtrsim 2R$) a peak develops upon approaching the critical temperature $T_c^{(s)}$ (i.e., for increasing values of ζ), reflecting the increasing attraction due to the critical Casimir force. This indicates the presence of a pronounced short-ranged order and that the formation of colloidal dimers is favored. Concerning the structural stability of colloidal suspensions with near-critical solvents, two different mechanisms have been identified, see Secs. 7.2 and 7.3. The solute particles may stick together in contact with each other due to attractive short-ranged surface forces. The stability ratio $W \sim \tau_{pair}/\tau_{diff}$ [Eqs. (4.19) and (4.20)] is a measure for the strength of a repulsive barrier which prevents such kind of coagulation. The time scales τ_{pair} and τ_{diff} are related to the pairing of two colloids and to the diffusion of a single particle, respectively. Rapid coagulation is expected to set in for $W < 1$. The emergence of the attractive critical Casimir forces can reduce and diminish a present repulsive barrier. Within the described effective model, W has been calculated. In Fig. 7.3 the contour lines $W = 1$ are shown for various temperatures (in terms of ζ) and various values of $s = \kappa R$ in the space spanned by the parameter $a = A/s$ of the strength of the background repulsion and by the bulk ordering field h_b [in terms of $z = 1/(\kappa\xi(t = 0, h_b))$]. This shows that the critical Casimir force can lead to rapid coagulation. The coagulation region extends to larger values of a for $h_b \lesssim 0$ because the critical Casimir forces are stronger for compositions of the solvent slightly poor in the component preferred by the colloids. The variation of W with temperature at fixed solvent composition, as it is typically realized in experiments, is shown in Fig. 7.4. W rapidly decreases to $W < 1$ upon approaching the critical temperature via the disordered phase. This implies that the aggregation should set in within a narrow temperature interval. For cases in which a repulsive barrier remains ($W > 1$), clustering of the solute particles can appear, too, because of a deep attractive minimum in the effective pair potential. For such situations, the results obtained from the effective model has been compared with experimental data in Sec. 7.3 thereby concentrating on the second virial coefficient B_2 , Eq. (4.14). In Figs. 7.5 and 7.6, for the critical and for an off-critical composition, respectively, the variation of the second virial coefficient B_2 upon decreasing the distance t from the critical temperature $T_c^{(s)}$ of the solvent as obtained within the effective model is compared with experimental data [80]. For both, the theoretical results and the experimental data, upon decreasing t the virial coefficient B_2 decreases towards large negative

values. Due to extremely large experimental values of $|B_2|$ also far away from $T_c^{(s)}$, the origin of which is not clear, the quality of the quantitative comparison is limited. For the off-critical composition, the critical Casimir force can become stronger than at the critical composition. However, it attains a relevant strength only closer to the critical temperature $T_c^{(s)}$ of the solvent and for the same temperature t it has in general a shorter spatial range than for the critical composition. Therefore, for the same value of t , the total attraction due to the critical Casimir forces can either be smaller or larger for an off-critical composition compared with the critical one. Accordingly, as can be seen in Fig. 7.6, B_2 can be less or more negative, respectively. For the experimental data of Ref. [80] there is no visible dependence on the composition of the solvent, which could be due to this crossover behavior. The issue whether a relationship can be established between the onset of aggregation and a specific quantity which is accessible both theoretically and experimentally has been addressed. To this end, for thermodynamic state points at which in experiments [76] aggregation sets in B_2 has been calculated within the effective model. For the state point farthest from the critical point, within the present approach, the critical Casimir forces cannot be the driving force. Regarding the other state points, to a certain extent the corresponding B_2 -isolines agree with each other and with the possible shape of the aggregation line, see Fig. 7.7. Concerning the quantitative discrepancies various possible explanations have been discussed, see Sec. 7.3.

A general discussion of the phase behavior of a ternary mixture consisting of colloidal particles and a binary solvent which exhibits a miscibility gap is given in Sec. 8.1 and it is illustrated in the sketches in Fig. 8.1. For such suspensions dilute in colloidal particles, scaling arguments for the shift of the critical temperature for $\varrho \rightarrow 0$ are given in Eq. (8.1). In Sec. 8.3 the relationship between the full description and the one which is based on an effective, one-component colloidal fluid is discussed in detail. For certain regions of the three-dimensional thermodynamic space (T, c_a, ϱ) of a ternary mixture, the effective one-component model is applicable for obtaining the onset of phase separation (see Sec. 8.3). Both within density functional theory (and applying the random phase approximation), Eq. (4.21), and the integral equation approach (Secs. 4.2 and 4.3), for particles interacting via the effective pair potential given in Eq. (6.2) the phase coexistence curve and the spinodal (i.e., the loci where within mean-field theory the isothermal compressibility χ_T diverges) have been calculated. In Fig. 8.2 the coexistence curves for various values of $c_a - c_{a,c}^{(s)} \sim m_0^{-1}$ are shown. Both approaches yield similar results for the spinodals, although the spinodals as obtained by using the density functional theory approach are narrower and are located slightly further away from the critical temperature $T_c^{(s)}$ of the solvent than the ones obtained from the integral equation approach. In Fig. 8.3 the dependence of the critical temperature of the effective one-component system (expressed in terms of $\zeta_c^{(eff)}$) on the parameters $a = A/s$ and $s = \kappa R$ of the background potential and on the bulk field h_b of the solvent is shown. For a given value of a , $\zeta_c^{(eff)}$ is smallest for slightly negative values of h_b . The critical temperature has been calculated within density functional theory and compared with the simple prediction $B_2^* = B_{2,c}^*$ as suggested by Vliegenthart and Lekkerkerker [267] and Noro and Frenkel [268]; B_2^* is the reduced second virial coefficient, Eqs. (4.14) and (4.15), and $B_{2,c}^*$

is the critical value of Baxter's model. Both approaches yield good agreement. In an experimentally study [82, 81] a shift of the critical temperature $|T_c(\varrho) - T_c^{(s)}| \sim 20\text{K}$ in the presence of rather small ($R = 11\text{nm}$) colloidal particles with number density ϱ w.r.t. the critical temperature $T_c^{(s)} = T_c(\varrho = 0)$ of the solvent has been observed. By making use of the results obtained from the effective model and of general scaling arguments this order of magnitude of the shift can be estimated.

These results show that the critical Casimir forces can induce reversible structural instabilities to colloidal particles immersed in near-critical solvents. The phase behavior of such suspensions has been discussed and it has been stressed that concerning the full phase diagram of these colloidal suspensions the separation of length scales associated with the solvent and with the solute particles does not hold. That is, a full description of the multicomponent mixture, beyond the effective one-component colloidal description, is needed which takes the degrees of freedom of *both* the solvent and the solute colloidal particles into account. In Sec. 9.1 potential approaches in order to address open issues are sketched and possible directions for future research related to the topics of this thesis are drawn.

Acknowledgments

During and before the time in which I have worked on this thesis I received support from many people who I thank.

I am grateful to Prof. Dr. S. Dietrich for giving me the opportunity to graduate in his group on such an interesting subject. The discussions with him and his advises contributed to the outcome of this study. He created a pleasant and productive environment, which I enjoyed and for which I thank him.

Prof. Dr. C. Holm I thank for refereeing my thesis.

I am pleased to thank Dr. habil. Ania Maciołek. Serdecznie dziękuję, nauczyłaś mnie bardzo dużo. Pracowałem i pracuję chętnie razem z tobie. I am glad for having her as adviser, for her enthusiasm and patience. The instructive discussions with her put forward my knowledge and the progress of this work.

It is a pleasure to thank Prof. Dr. R. Evans for his interest in this work, the time he spent, and his hospitality during my visit in Bristol. He deepened my understanding of liquids enormously and made me aware of the their subtleness. The discussions with him have been enlightening and inspiring. Without him I would not have the understanding of the present subject as I have it know.

I benefited from many helpful discussions with Prof. Dr. R. Roth and it has been always nice to meet him.

I acknowledge fruitful discussions with Prof. Dr. R. K. P. Zia and Prof. Dr. A. Ciach.

Dr. M. Tröndle has always a helping hand. It was a pleasure to share the room with him and to exchange views with him, on physics but not only. He introduced me to computational techniques.

I am glad to have met Dr. S. Kondrat. The collaboration with him his productive and one has a good time with him. I thank him for his invitation to London and his hospitality during my short visit.

I thank the present and old members of the ‘Theory of Inhomogeneous Condensed Matter’ group for discussions and the nice atmosphere.

Dr. U. Nellen, Dr. L. Helden, and Dr. S. Buzzaccaro provided me with insights to their experiments.

Im organisatorischen Bereich waren Fr. Geigle und das EDV Team stets hilfreich, sowie das freundliche Team der MPI-Stuttgart Bibliothek.

Ein Dank geht an die Familie und Freunde. Meine Eltern unterstützten mich in unterschiedlicher Weise, wie auch meine Frau Cindy, die die deutsche Zusammenfassung gründlich durchlas und es sich aussuchte, mit mir zu leben.

Und eine besondere Erwähnung dürfen Max und Leo genießen, die für unbeschreibliche Erkenntnisse und Erfahrungen sorgen.

Den Schlusspunkt setzen die Stuttgarter Kickers, “unsere Fans sind unsere Kraft”.

A. Bulk critical properties within Landau theory

Within Landau theory for bulk critical phenomena (which is a mean-field approximation) the singular part of the (reduced) bulk free energy density f_{sgl} is the Hamiltonian density h given in Eq. (3.29b) and the order parameter in the bulk attains a constant value. It is appropriate to introduce the reduced quantities [222]

$$M = \sqrt{\frac{g}{6}}\Phi \quad \text{and} \quad H = \sqrt{\frac{g}{6}}h_b, \quad (\text{A.1})$$

In terms of these, the equation of state is

$$\frac{\partial f_{sgl}}{\partial \Phi} = \tau\Phi + \frac{g}{3!}\Phi^3 - h_b = (6/g)^{1/2} \{ \tau M + M^3 - H \} \stackrel{!}{=} 0, \quad (\text{A.2})$$

and accordingly the bulk order parameter is [222, 333]

$$\Phi_b(\tau, h_b, g) = \begin{cases} \text{sgn}(h_b) (2\tau/f - f/g) & D \geq 0 \\ \text{sgn}(h_b) 2b^{1/2}/g \cos \left[\frac{1}{3} \arccos(-ab^{-3/2}) - \pi/3 \right] & D < 0 \end{cases} \quad (\text{A.3})$$

where $a = 3g^2|h_b|$, $b = 2g|\tau|$, $D = a^2 + \text{sgn}(\tau)b^3$, and $|f| = \left| -a + \sqrt{D} \right|^{1/3}$ with $\text{sgn}(f) = \text{sgn}(-a + \sqrt{D})$. In particular $M_b(\tau, H) = \sqrt{\frac{g}{6}}\Phi_b(\tau, h_b, g)$ attains the values

$$M_b(\tau, H=0) = \begin{cases} 0 & \tau > 0 \\ \pm |\tau|^{1/2} & \tau < 0 \end{cases} \quad \text{and} \quad M_b(\tau=0, H) = \text{sgn} H |H|^{1/3}. \quad (\text{A.4})$$

In general, $M(\tau, H) = M_b(-|\tau|, H=0) G_{\pm}(\Sigma = \text{sgn}(\tau H) \xi_t/\xi_h)$ where the scaling function G_{\pm} depends on the sign of τ and is

$$G_{\pm}(\Sigma) = \begin{cases} \text{sgn}(\Sigma) \sqrt{8} \cos \left[\arccos(-0.5|\Sigma/U_{\pm}|^3) / 3 - \pi/3 \right], & |\Sigma| < \frac{\text{sgn}(-\tau)}{2^{1/6}} \\ \text{sgn}(\Sigma \tilde{g}_{\pm}(\Sigma)) \sqrt{1/6} \left(2 \text{sgn}(\tau) |\tilde{g}_{\pm}(\Sigma)|^{-1/3} - |\tilde{g}_{\pm}(\Sigma)|^{1/3} \right), & \text{else} \end{cases} \quad (\text{A.5})$$

where $\tilde{g}_{\pm}(\Sigma) = -2^{1/2} |\Sigma/U_{\pm}|^3 + [2 |\Sigma/U_{\pm}|^6 + \text{sgn}(\tau) 2^3]^{1/2}$ and $U_{\pm} = \xi_{\pm}^{(0)}/\xi_{+}^{(0)}$ depends on the sign of τ . From Eq. (A.4) the mean-field values for the critical exponents $(\beta)_{MFT} = 1/2$ and $(\delta)_{MFT} = 3$ can be read off [compare their definition Eq. (3.9), the values given in Eq. (3.15a), and the scaling relations in Eqs. (3.14)]. Within mean-field theory the bulk

correlation length $\xi(t, h_b)$ is given by $\xi^2 = 1/f^{(2)}$, where $f^{(2)} \equiv \partial^2 f_{sgl}/\partial\Phi^2$ [139, 222, 32]. Accordingly,

$$\xi = [\tau + (g/2)\Phi^2]^{-1/2} = [\tau + 3M^2]^{-1/2}, \quad (\text{A.6})$$

and in particular

$$\xi_+ = \xi(t > 0, h_b = 0) = \tau^{-1/2} \quad (\text{A.7a})$$

$$\xi_- = \xi(t < 0, h_b = 0) = (-2\tau)^{-1/2} \quad (\text{A.7b})$$

$$\xi_h = \xi(t = 0, h_b \leq 0) = 3^{-1/2} |H|^{-1/3}. \quad (\text{A.7c})$$

From Eqs. (A.7) the value $(U_\xi)_{MFT} = \sqrt{2}$ of the universal amplitude ratio within mean-field theory is obtained, compare (3.16), as well as $(\nu)_{MFT} = 1/2$ and $[\nu/(\beta\delta)]_{MFT} = 1/3$, compare Eq. (3.10). Further one obtains the non-universal amplitude $\xi_h^{(0)} = (9g/2)^{-1/6}$ and the mean-field relation $\mathcal{B}_t \xi_t^{(0)} = \sqrt{6/g}$, which is specific to the Landau model. Combining Eqs. (A.3) and (A.6) one obtains the scaling function I [Eq. (3.11)] within mean-field theory.

$$I(\Sigma) = U_\pm [3|G_\pm(\Sigma)|^2 + \text{sgn}(\tau)]^{-1/2}. \quad (\text{A.8})$$

Finally the result $\varsigma/(k_B T) = 4\sqrt{2}g^{-1} \left(\xi_t^{(0)}\right)^{-3} |t|^{3/2}$ [334, 335] for the surface tension $\varsigma = \varsigma_0 |t|^\mu$, where $\mu = (d-1)\nu$ [Eqs. (3.13) and (3.14)] within Landau theory is reported. The universal ratio R_σ [Eq. (3.16)] is within Landau theory $R_\sigma = \frac{\varsigma_0}{k_B T} \left(\xi_t^{(0)}\right)^{d-1} \stackrel{MFT}{=} 4\sqrt{2}/g$ and $\mu = (d-1)\nu \stackrel{MFT}{=} 3/2$.

B. The critical Casimir force within the local functional approach

Here, the results of this approach for values $h_b \neq 0$ and $t > 0$ are evaluated. The following expressions are given formally for general values of t , however for $t < 0$ the validity of these expressions is subtle because for values $h_b < 0$ and $t < 0$ the order parameter profile $\Phi(z)$ may attain values which correspond to instable or metastable bulk values, $|\Phi(z)| < |\Phi(t, h_b)|$. The integrand of the functional depends solely on bulk quantities and accordingly may be ill defined for such values of the order parameter profile. In particular, the used linear parametric model is not suitable to describe metastable states. This issue has been not investigated within the present study, because the range of values $t > 0$ has been sufficient for studying critical Casimir forces in colloidal suspensions. Integrating once the Euler-Lagrange equation $(\partial \mathbf{f} / \partial \Phi) = \frac{d}{dz} (\partial \mathbf{f} / \partial \Phi')$ for the functional given in Eq. (3.31) yields

$$\Phi' \frac{\partial \mathbf{f}}{\partial \Phi'} - \mathbf{f} = E(L), \quad (\text{B.1})$$

where the constant of integration $E(L)$ depends on the width L , and the boundary conditions are

$$\left. \frac{\partial \mathbf{f}}{\partial \Phi'} \right|_{z=-L/2} = \frac{\partial \mathbf{f}_1}{\partial \Phi_1} \quad \text{and} \quad - \left. \frac{\partial \mathbf{f}}{\partial \Phi'} \right|_{z=L/2} = \frac{\partial \mathbf{f}_2}{\partial \Phi_2}. \quad (\text{B.2})$$

It can be shown [257] that $E(L) = f_C^{(\parallel)} / (k_B T \mathcal{S})$, compare Eq. (3.24). Inserting the specifications of \mathbf{f} as given in Eqs. (3.32) and (3.34) the general Eq. (B.1) reads

$$\hat{G}(\Phi' \Lambda(\Phi, t, h_b)) = 1 + E(L) / \mathcal{W}(\Phi; t, h_b), \quad (\text{B.3})$$

where $\hat{G}(x) = x \frac{d\mathcal{G}}{dx} - \mathcal{G}(x)$. For symmetric boundary conditions $c_1, c_2 > 0$ and $h_{s,1}, h_{s,2} > 0$ the order parameter profile has a minimum $\Phi_{min} = \Phi(z_{min})$ located at z_{min} . In particular $\Phi'(z_{min}) = 0$ and, because $\hat{G}(0) = 0$ [206], from Eq. (B.3) and the note after Eq. (B.2) it follows that

$$f_C^{(\parallel)} / (k_B T \mathcal{S}) = E(L) = -\mathcal{W}(\Phi_{min}; t, h_b). \quad (\text{B.4})$$

The scaling function $\vartheta_{\parallel\pm}^{(d)}$ is obtained from Eq. (B.4) together with the scaling expressions in Eqs. (3.25) and (3.35),

$$\vartheta_{\parallel\pm}^{(d)}(\mathcal{Y}, \Sigma) = -A_1 |\mathcal{Y}|^d U_{\pm}^d \Psi_{min}^{(1+\delta)} \tilde{Y}_{\pm}(\Psi_{min}, \Sigma) \quad (\text{B.5})$$

with the universal amplitude $A_1 = R_\chi Q_c / (\delta + 1)$, compare with Eqs. (3.14) and (3.16), and $U_\pm (\mathcal{Y} > 0) = 1$ and $U_\pm (\mathcal{Y} < 0) = U_\xi = \xi_+^{(0)} / \xi_-^{(0)}$. Concerning values $\mathcal{Y} < 0$ be aware of the subtleness discussed at the beginning of this appendix.

An implicit equation determining Φ_{min} is obtained by applying the inverse function $\hat{\mathcal{G}}^{-1}$ on Eq. (B.3) and integrating it from $-L/2$ to z_{min} , i.e.,

$$z_{min} + L/2 = \int_{\Phi_{min}}^{\Phi_1} d\Phi \frac{\Lambda(\Phi, t, h_b)}{\hat{\mathcal{G}}^{-1}(1 - \mathcal{W}(\Phi_{min}; t, h_b) / \mathcal{W}(\Phi; t, h_b))}, \quad (\text{B.6})$$

where $\Phi' < 0$ for the range of integration and $\hat{\mathcal{G}}^{-1}(\hat{\mathcal{G}}(x)) = |x|$ has been used. Using the scaling forms given in Eq. (3.35) and applying the strong adsorption limit for which $z_{min} = 0$ and $\Phi_1 = \infty$ one obtains

$$A_2 |\mathcal{Y}| = \int_{\Psi_{min}}^{\infty} du \frac{u^{-(1+\nu/\beta)} \left[\tilde{Z}_\pm(u) / \tilde{Y}_\pm(u, \Sigma) \right]^{1/2}}{\hat{\mathcal{G}}^{-1} \left(1 - (\Psi_{min}/u)^{1+\delta} \tilde{Y}_\pm(\Psi_{min}, \Sigma) / \tilde{Y}_\pm(u, \Sigma) \right)}. \quad (\text{B.7})$$

Adopting the linear parametric model (Sec. 3.5.3) allows to evaluate Eqs. (B.4) and (B.6) quantitatively. Within the parametric model the excess free energy density and the bulk correlation length are given by Eqs. (3.39) and (3.40), respectively, and the integrated Euler-Lagrange equation (B.6) becomes

$$z_{min} + L/2 = \int_{\mathfrak{z}_{min}}^{\mathfrak{z}_1} d\hat{\mathfrak{z}} \frac{\Phi'_{(t)}(\hat{\mathfrak{z}}) [t/k(\hat{\mathfrak{z}})]^{-\nu-\beta} \sqrt{a(\hat{\mathfrak{z}})/w(\hat{\mathfrak{z}}; \mathfrak{z}_b)}}{\hat{\mathcal{G}}^{-1} \left[1 - \left(\frac{k(\hat{\mathfrak{z}})}{k(\mathfrak{z}_{min})} \right)^{2-\alpha} \frac{w(\mathfrak{z}_{min}; \mathfrak{z}_b)}{w(\hat{\mathfrak{z}}; \mathfrak{z}_b)} \right]}, \quad (\text{B.8})$$

where \mathfrak{z}_{min} and \mathfrak{z}_1 are given by Φ_{min} and Φ_1 , respectively, and $\Phi'_{(t)}(\mathfrak{z}) = (\partial\Phi/\partial\mathfrak{z})_{t=const} = [t/k(\mathfrak{z})]^\beta [m'(\mathfrak{z}) - \beta m(\mathfrak{z}) k'(\mathfrak{z}) / k(\mathfrak{z})]$, compare Eqs. (3.36). For $t > 0$ one has $0 \leq \mathfrak{z}_{min} \leq \mathfrak{z}_1 \leq \mathfrak{z}_c$ and for $t < 0$ one has $\mathfrak{z}_c \leq \mathfrak{z}_{min} \leq \mathfrak{z}_1 \leq \mathfrak{z}_x$.

In the strong adsorption limit $\Phi_1 = [t/k(\mathfrak{z}_1)]^\beta m(\mathfrak{z}_1) \rightarrow \infty$. Accordingly $\mathfrak{s}_1 \rightarrow \infty$ and $\mathfrak{z}_1 \rightarrow \mathfrak{z}_c$ such that $k(\mathfrak{z}_1) \rightarrow 0$ and $t = \mathfrak{s}_1 k(\mathfrak{z}_1) = const$. Therefore Eq. (B.8) becomes with the approximation $\hat{\mathcal{G}}^{-1}(x) \simeq \sqrt{x}$ [see after Eqs. (3.34) and (5.2)]

$$|\mathcal{Y}| = \frac{2U_\pm}{\xi_+^{(0)}} \int_{\mathfrak{z}_{min}}^{\mathfrak{z}_c} d\hat{\mathfrak{z}} \frac{|k(\hat{\mathfrak{z}})|^\nu [m'(\hat{\mathfrak{z}}) - \beta m(\hat{\mathfrak{z}}) k'(\hat{\mathfrak{z}}) / k(\hat{\mathfrak{z}})] \sqrt{a(\hat{\mathfrak{z}})/w(\hat{\mathfrak{z}}; \mathfrak{z}_b)}}{\hat{\mathcal{G}}^{-1} \left[1 - \left(\frac{k(\hat{\mathfrak{z}})}{k(\mathfrak{z}_{min})} \right)^{2-\alpha} \frac{w(\mathfrak{z}_{min}; \mathfrak{z}_b)}{w(\hat{\mathfrak{z}}; \mathfrak{z}_b)} \right]}, \quad (\text{B.9})$$

where $U_\pm = \xi_+^{(0)} / \xi_\pm^{(0)}$ depending on the sign of \mathcal{Y} and the non-universal metric factor $\xi_+^{(0)} = [k(0)]^\nu [2a(0)/p(0)]^{1/2}$ [compare with Eq. (3.41)] cancels with the non-universal metric factors of the integrand such that the right hand side is universal. From Eq. (B.4) together with Eqs. (3.14), (3.25), (3.36), and (3.39) the scaling function $\vartheta_{\parallel\pm}^{(d)} = - \left(\xi_+^{(0)} / U_\pm \right)^d |y|^d |k(\mathfrak{z}_{min})|^{-d\nu} w(\mathfrak{z}_{min}; \mathfrak{z}_b)$ of the critical Casimir force is obtained.

In order to show the universality of the rhs explicitly, note that \mathcal{A}/A_+ is universal, where A_+ is the non-universal amplitude associated to the specific heat [Eqs. (3.8) and (3.6)]. Therefore

$$\vartheta_{\parallel\pm}^{(d)} = -\frac{Q_+}{\alpha U_{\pm}^d} |\mathcal{Y}|^d |k(\mathfrak{z}_{min})|^{-d\nu} w(\mathfrak{z}_{min}; \mathfrak{z}_b) / (A_+), \quad (\text{B.10})$$

with the universal the universal amplitude ratio $Q^+ = \alpha A_+ (\xi_0^+)^d$, Eq. (3.16). For the linear parametric model [257],

$$A_+^{(lin)} = -\frac{l_0 m_0}{2b^2} (2 - \alpha) (1 - \alpha) \left\{ \frac{2\beta (b^2 - 1)}{b^2 (2 - \alpha)} - \frac{2\beta - 1 - (4\beta - 1)/b^2}{(1 - \alpha)} - \frac{1 - 2\beta}{b^2 \alpha} \right\}. \quad (\text{B.11})$$

C. Properties of water lutidine mixtures

The binary liquid mixture water-2,6 lutidine has a lower critical temperature $T_c^{(s)} \simeq 307\text{K}$ and a critical mass fraction $\omega_{L,c} = 0.28 \dots 0.29$ [67, 336, 293]. The reported values in literature vary slightly, for a discussion see Ref. [45].

C.1. The non-universal amplitude of the order parameter

For the mixture of 2,6-lutidine and water the amplitude \mathcal{B}_t of the bulk order parameter $\Phi(t \rightarrow 0^-) = \mathcal{B}_t |t|^\beta$, Eq. (3.9), can be estimated from the refractive indices $n_{1,2}$ of the two coexisting phases 1 and 2 near the lower critical point [293]. The refractive index difference $\Delta n = n_1 - n_2$ is related to the difference in the volume fraction $\Delta\varphi_a = \varphi_a^{(1)} - \varphi_a^{(2)}$ of the component a in the two phases according to [293] $\Delta\varphi_a = k(T)\Delta n$. The coefficient $k(T)$ can be expressed [294] in terms of the refractive indices $n_{1,2}$ and the refractive indices $n_{a,b}$ of the pure components a and b : $k = 3(n_1 + n_2)[(A_a - A_b)(n_1^2 + 2)(n_2^2 + 2)]^{-1}$, where $A_{a,b} = (n_{a,b}^2 - 1)/(n_{a,b}^2 + 2)$. The refractive indices of pure water and pure 2,6-lutidine are [72] $n_W = 1.33$ and $n_L = 1.49$, respectively. For the lutidine-water mixture the resulting value of $k = k(T)$ varies by less than 0.4% within the reported temperature range [293] $T - T_{c,b} < 15\text{K}$. Thus to a good approximation one can take $k(T) \simeq k_0 \simeq 6.35$ independent of T . According to Ref. [293] for $T - T_{c,b} < 0.5\text{K}$ the two-phase coexistence in terms of the refractive index is well described by the power law $\Delta n = A(T - T_{c,b})^\beta$ with $T_{c,b} = (307.258 \pm 0.001)\text{K}$, $A = (0.0471 \pm 0.0001)\text{K}^{-\beta}$, and $\beta = 0.338 \pm 0.003$. Thus for $\Delta\varphi \simeq B_\varphi |t|^\beta$ one obtains the amplitude $B_\varphi = k_0 (T_{c,b})^\beta A \simeq 2.073$. The mass fraction ω_a in terms of the volume fraction φ_a is given by

$$\omega_a = \varrho_{m,a}\varphi_a [\varrho_{m,a}\varphi_a + \varrho_{m,b}\varphi_b]^{-1} = \Omega\varphi_a [(\Omega - 1)\varphi_a + 1]^{-1}, \quad (\text{C.1})$$

where $\varrho_{m,a}$ and $\varrho_{m,b}$ are the mass densities of the components a and b , respectively, and $\Omega = \varrho_{m,a}/\varrho_{m,b}$. Accordingly $\Delta\omega_a(t \rightarrow 0^-) = \omega_a^{(1)} - \omega_a^{(2)} = B_\omega |t|^\beta$, where the amplitude is given by $B_\omega = \Omega [(\Omega - 1)\varphi_{a,c} + 1]^{-2} B_\varphi = \Omega [1 + (\Omega^{-1} - 1)\omega_{a,c}]^2 B_\varphi$; $\omega_{a,c}$ is the critical mass fraction of the component a . With the mass densities [72] $\varrho_{m,W} = 0.995\text{g/cm}^3$ and $\varrho_{m,L} = 0.911\text{g/cm}^3$ of pure water and pure lutidine, respectively, and the critical mass fraction [71] $\omega_{L,c} \simeq 0.29$ one obtains $B_\omega \simeq 2.0$. For the symmetric coexistence curve, as assumed here, the order parameter defined by the mass fraction is

$\Phi_\omega (t < 0, h_b = 0) = \omega_a^{(1)} - \omega_{a,c} = 0.5\Delta\omega_a$, rendering the value $\mathcal{B}_{t,\omega} = 0.5 \times B_\omega \simeq 1.0$. Fitting the experimentally determined coexistence curve [71, 79, 80] yields a somewhat smaller value $\mathcal{B}_{t\omega} = 0.765$ which is adopted in the main text.

C.2. Permittivity

By using the Clausius-Mossotti relation [104, 296], which both for pure systems and for mixtures expresses the permittivity in terms of the polarizabilities of the constituting atoms, the relative (to vacuum) permittivity ϵ of a binary liquid mixture can be expressed [296] in terms of the volume fraction φ_a of component a and the relative permittivities $\epsilon_{a,b}$ of the two components a and b : $f(\epsilon) = v_f(\varphi_a f(\epsilon_a) + (1 - \varphi_a) f(\epsilon_b))$, where $f(\epsilon) = (\epsilon - 1) / (\epsilon + 2)$ and v_f is the fractional volume change upon mixing for which $v_f = 1$ [104] is adopted. The volume fraction φ_a expressed in terms of the mass fraction ω_a is, compare with Eq. (C.1), $\varphi_a = \omega_a \varrho_{m,b} / [(1 - \omega_a) \varrho_{m,a} + \omega_a \varrho_{m,b}]$, where $\varrho_{m,a}$ ($\varrho_{m,b}$) is the mass density of component a (b); For the mass density and the relative permittivity of pure lutidine (of pure water) the values [72] $\varrho_{m,L} = 0.911g/cm^3$ ($\varrho_{m,W} = 0.995g/cm^3$) and [104] $\epsilon_L = 7.33$ ($\epsilon_W = 81$), respectively, are adopted.

Technical tools

Numerical calculations have been done using computer programs written in the programming language C with the aid of the GNU Scientific Library (GSL) [337] and by using the Computing software Mathematica [333]. The figures have been mostly done with the powerful graphing utility gnuplot [338] and some with the drawing program xfig [339]. The editors emacs [340] and kile [341] have been used. The text has been written in the document markup language LaTeX [342]. Helpful hereby has been Ref. [343], which has an extended reference list.

References

- [1] W. B. Russel, D. A. Saville, and W. R. Schowalter, *Colloidal Dispersions*, Cambridge University Press, Cambridge, 1989.
- [2] H. R. Kruyt, editor, *Colloid Science: Irreversible systems*, Elsevier Publishing Company, Amsterdam, 1952.
- [3] W. Ostwald, *Die Welt der vernachlässigten Dimensionen: eine Einführung in die moderne Kolloidchemie; mit besonderer Berücksichtigung ihrer Anwendungen*, Steinkopff, Dresden, 12 ed., 1944.
- [4] T. Graham, *Liquid Diffusion Applied to Analysis*, *Phil. Trans. Roy. Soc. London* **151**, 183 (1861).
- [5] R. J. Hunter, *Foundations of colloid science*, Clarendon Press, Oxford, 2001.
- [6] H. Staudinger, *Organische Kolloidchemie*, Vieweg, Braunschweig, 1940.
- [7] C. N. Likos, *Effective interactions in soft condensed matter physics*, *Phys. Rep.* **348**, 267 (2001).
- [8] L. Belloni, *Colloidal interactions*, *J. Phys.: Condens. Matt.* **12**, R549 (2000).
- [9] M. Dijkstra, R. van Roij, and R. Evans, *Phase diagram of highly asymmetric binary hard-sphere mixtures*, *Phys. Rev. E* **59**, 5744 (1999).
- [10] W. G. McMillan and J. E. Mayer, *The Statistical Thermodynamics of Multicomponent Systems*, *J. Chem. Phys.* **13**, 276 (1945).
- [11] A. Yethiraj, *Tunable colloids: control of colloidal phase transitions with tunable interactions*, *Soft Matter* **3**, 1099 (2007).
- [12] D. M. Herlach, I. Klassen, P. Wette, and D. Holland-Moritz, *Colloids as model systems for metals and alloys: a case study of crystallization*, *J. Phys.: Condens. Matt.* **22**, 153101 (2010).
- [13] V. J. Anderson and H. N. W. Lekkerkerker, *Insights into phase transition kinetics from colloid science*, *Nature (London)* **416**, 811 (2002).
- [14] D. Frenkel, *Playing Tricks with Designer "Atoms"*, *Science* **296**, 65 (2002).
- [15] D. Babič, C. Schmitt, and C. Bechinger, *Colloids as model systems for problems in statistical physics*, *Chaos* **15**, 026114 (2005).

- [16] J. N. Israelachvili, *Intermolecular & Surface Forces*, Academic Press, London, 1998.
- [17] S. Asakura and F. Oosawa, *On Interaction between Two Bodies Immersed in a Solution of Macromolecules*, *J. Chem. Phys.* **22**, 1255 (1954).
- [18] A. Vrij, *Polymers at Interfaces and the Interactions in Colloidal Dispersions*, *Pure Appl. Chem.* **48**, 471 (1976).
- [19] R. Roth, R. Evans, and S. Dietrich, *Depletion potential in hard-sphere mixtures: Theory and applications*, *Phys. Rev. E* **62**, 5360 (2000).
- [20] D. J. Ashton, J. Liu, E. Luijten, and N. B. Wilding, *Monte Carlo cluster algorithm for fluid phase transitions in highly size-asymmetrical binary mixtures*, *J. Chem. Phys.* **133**, 194102 (2010).
- [21] J. Largo and N. B. Wilding, *Influence of polydispersity on the critical parameters of an effective-potential model for asymmetric hard-sphere mixtures*, *Phys. Rev. E* **73**, 036115 (2006).
- [22] R. Evans, J. R. Henderson, and R. Roth, *Nonanalytic curvature contributions to solvation free energies: Influence of drying*, *J. Chem. Phys.* **121**, 12074 (2004).
- [23] M. C. Stewart and R. Evans, *Wetting and drying at a curved substrate: Long-ranged forces*, *Phys. Rev. E* **71**, 011602 (2005).
- [24] R. Evans, private communication.
- [25] R. Evans, *Fluids adsorbed in narrow pores: phase equilibria and structure*, *J. Phys.: Condens. Matt.* **2**, 8989 (1990).
- [26] S. Dietrich, Wetting phenomena, in *Phase Transitions and Critical Phenomena*, edited by C. Domb and J. L. Lebowitz, vol. 12, p. 1, Academic Press, London, 1988.
- [27] C. Bauer, T. Bieker, and S. Dietrich, *Wetting-induced effective interaction potential between spherical particles*, *Phys. Rev. E* **62**, 5324 (2000).
- [28] C. Domb, *The critical point : A historical introduction to the modern theory of critical phenomena*, Taylor & Francis, London, 1996.
- [29] M. E. Fisher, The theory of critical point singularities, in *Fenomeni critici: Corso 51, Varenna sul Lago di Como, 27.7. - 8.8.1970*, edited by M. S. Green, Proceedings of the International School of Physics “Enrico Fermi”, p. 1, London [among others], 1971, Academic Press.
- [30] H. E. Stanley, *Introduction to Phase transitions and Critical Phenomena*, The international Series of Monographs on Physics, Clarendon Press, Oxford, 1971.

-
- [31] W. Gebhardt and U. Krey, *Phasenübergänge und kritische Phänomene*, Vieweg, Braunschweig, 1980.
- [32] J. J. Binney, N. J. Dowrick, A. J. Fischer, and M. E. J. Newman, *The Theory of Critical Phenomena: An introduction to the renormalization group*, Clarendon Press, Oxford, 1992.
- [33] T. Andrews, *The Bakerian Lecture: On the Continuity of the Gaseous and Liquid States of Matter*, *Phil. Trans. Roy. Soc. London* **159**, 575 (1869).
- [34] M. v. Smoluchowski, *Molekular-kinetische Theorie der Opaleszenz von Gasen im kritischen Zustande, sowie einiger verwandter Erscheinungen*, *Ann. Phys. (Berlin)* **330**, 205 (1908).
- [35] A. Einstein, *Theorie der Opaleszenz von homogenen Flüssigkeiten und Flüssigkeitsgemischen in der Nähe des kritischen Zustandes*, *Ann. Phys. (Berlin)* **338**, 1275 (1910).
- [36] N. Goldenfeld, *Lectures on phase transitions and the renormalization group*, Addison-Wesley, Reading, Mass. [among others], 1992.
- [37] J. L. Cardy, *Scaling and renormalization in Statistical physics*, vol. 5 of *Cambridge lecture notes in physics*, Cambridge University Press, Cambridge, 1996.
- [38] M. E. Fisher, *Quantum Corrections to Critical-Point Behavior*, *Phys. Rev. Lett.* **16**, 11 (1966).
- [39] R. B. Griffiths, *Dependence of Critical Indices on a Parameter*, *Phys. Rev. Lett.* **24**, 1479 (1970).
- [40] M. E. Fisher, S.-k. Ma, and B. G. Nickel, *Critical Exponents for Long-Range Interactions*, *Phys. Rev. Lett.* **29**, 917 (1972).
- [41] M. E. Fisher and P. G. de Gennes, *Phénomènes aux parois dans un mélange binaire critique*, *C. R. Acad. Sci., Paris, Ser. B* **287**, 207 (1978).
- [42] M. Krech, *The Casimir effect in critical systems*, World Scientific, Singapore, 1994.
- [43] A. Gambassi, *The Casimir effect: From quantum to critical fluctuations*, *J. Phys.: Conf. Ser.* **161**, 012037 (2009).
- [44] C. Hertlein, L. Helden, A. Gambassi, S. Dietrich, and C. Bechinger, *Direct measurement of critical Casimir forces*, *Nature (London)* **451**, 172 (2008).
- [45] A. Gambassi, A. Maciołek, C. Hertlein, U. Nellen, L. Helden, C. Bechinger, and S. Dietrich, *Critical Casimir effect in classical binary liquid mixtures*, *Phys. Rev. E* **80**, 061143 (2009).

- [46] U. Nellen, L. Helden, and C. Bechinger, *Tunability of critical Casimir interactions by boundary conditions*, *EPL* **88**, 26001 (2009).
- [47] R. Garcia and M. H. W. Chan, *Critical Fluctuation-Induced Thinning of ^4He Films near the Superfluid Transition*, *Phys. Rev. Lett.* **83**, 1187 (1999).
- [48] A. Ganshin, S. Scheidemantel, R. Garcia, and M. H. W. Chan, *Critical Casimir Force in ^4He Films: Confirmation of Finite-Size Scaling*, *Phys. Rev. Lett.* **97**, 075301 (2006).
- [49] R. Garcia and M. H. W. Chan, *Critical Casimir Effect near the $^3\text{He} - ^4\text{He}$ Tricritical Point*, *Phys. Rev. Lett.* **88**, 086101 (2002).
- [50] M. Fukuto, Y. F. Yano, and P. S. Pershan, *Critical Casimir Effect in Three-Dimensional Ising Systems: Measurements on Binary Wetting Films*, *Phys. Rev. Lett.* **94**, 135702 (2005).
- [51] S. Rafai, D. Bonn, and J. Meunier, *Repulsive and attractive critical Casimir forces*, *Physica A* **386**, 31 (2007).
- [52] D. C. Prieve, *Measurement of colloidal forces with TIRM*, *Adv. Colloid Interface Sci.* **82**, 93 (1999).
- [53] H. H. von Grünberg, L. Helden, P. Leiderer, and C. Bechinger, *Measurement of surface charge densities on Brownian particles using total internal reflection microscopy*, *J. Chem. Phys.* **114**, 10094 (2001).
- [54] M. Tröndle, S. Kondrat, A. Gambassi, L. Harnau, and S. Dietrich, *Normal and lateral critical Casimir forces between colloids and patterned substrates*, *EPL* **88**, 40004 (2009).
- [55] M. Tröndle, S. Kondrat, A. Gambassi, L. Harnau, and S. Dietrich, *Critical Casimir effect for colloids close to chemically patterned substrates*, *J. Chem. Phys.* **133**, 074702 (2010).
- [56] M. Tröndle, O. Zvyagolskaya, A. Gambassi, D. Vogt, L. Harnau, C. Bechinger, and S. Dietrich, *Trapping colloids near chemical stripes via critical Casimir forces*, *Mol. Phys.* **109**, 1169 (2011).
- [57] A. Gambassi and S. Dietrich, *Critical Casimir forces steered by patterned substrates*, *Soft Matter* **7**, 1247 (2011).
- [58] C. P. Royall, D. G. A. L. Aarts, and H. Tanaka, *Bridging length scales in colloidal liquids and interfaces from near-critical divergence to single particles*, *Nature Physics (London)* **3**, 636 (2007).

- [59] H. B. G. Casimir, *On the attraction between two perfectly conducting plates*, Proc. R. Acad. Sci. Amsterdam **51**, 793 (1948); online available at the KNAW Digital Library, <http://www.dwc.knaw.nl/DL/publications/PU00018547.pdf>.
- [60] S. K. Lamoreaux, *Demonstration of the Casimir Force in the 0.6 to 6 μ m Range*, Phys. Rev. Lett. **78**, 5 (1997); **81**, 5475 (1998).
- [61] A.-F. Bitbol, K. S. Ronia, and J.-B. Fournier, *Universal amplitudes of the Casimir-like interactions between four types of rods in fluid membranes*, EPL **96**, 40013 (2011).
- [62] H. Lehle and M. Oettel, *Importance of boundary conditions for fluctuation-induced forces between colloids at interfaces*, Phys. Rev. E **75**, 011602 (2007).
- [63] M. Napiórkowski and J. Piasecki, *Casimir force induced by an imperfect Bose gas*, Phys. Rev. E **84**, 061105 (2011).
- [64] M. Napiórkowski and J. Piasecki, *The Bulk Correlation Length and the Range of Thermodynamic Casimir Forces at Bose-Einstein Condensation*, J. Stat. Phys. **147**, 1145 (2012).
- [65] M. Kardar and R. Golestanian, *The “friction” of vacuum, and other fluctuation-induced forces*, Rev. Mod. Phys. **71**, 1233 (1999).
- [66] D. Dantchev, F. Schlesener, and S. Dietrich, *Interplay of critical Casimir and dispersion forces*, Phys. Rev. E **76**, 011121 (2007).
- [67] J. D. Cox and E. F. G. Herington, *The coexistence curve in liquid-liquid binary systems*, Trans. Faraday Soc. **52**, 926 (1956).
- [68] W. C. K. Poon and M. D. Haw, *Mesoscopic structure formation in colloidal aggregation and gelation*, Adv. Colloid Interface Sci. **73**, 71 (1997).
- [69] H. Stechemesser and B. Dobiáš, editors, *Coagulation And Flocculation*, vol. 126 of *Surfactant Science Series*, Taylor & Francis, Boca Raton, 2005.
- [70] N. M. Kovalchuk and V. M. Starov, *Aggregation in colloidal suspensions: Effect of colloidal forces and hydrodynamic interactions*, Adv. Colloid Interface Sci. **179**, 99 (2012).
- [71] D. Beysens and D. Estève, *Adsorption Phenomena at the Surface of Silica Spheres in a Binary Liquid Mixture*, Phys. Rev. Lett. **54**, 2123 (1985).
- [72] Y. Jayalakshmi, J. S. V. Duijneveldt, and D. Beysens, *Behavior of density and refractive index in mixtures of 2,6-lutidine and water*, J. Chem. Phys. **100**, 604 (1994).

- [73] V. Gurfein, D. Beysens, and F. Perrot, *Stability of colloids and wetting phenomena*, *Phys. Rev. A* **40**, 2543 (1989).
- [74] J. S. van Duijneveldt and D. Beysens, *Adsorption on colloids and flocculation: The influence of salt*, *J. Chem. Phys.* **94**, 5222 (1991).
- [75] P. D. Gallagher and J. V. Maher, *Partitioning of polystyrene latex spheres in immiscible critical liquid mixtures*, *Phys. Rev. A* **46**, 2012 (1992).
- [76] P. D. Gallagher, M. L. Kurnaz, and J. V. Maher, *Aggregation in polystyrene-sphere suspensions in near-critical binary liquid mixtures*, *Phys. Rev. A* **46**, 7750 (1992).
- [77] M. L. Broide, Y. Garrabos, and D. Beysens, *Nonfractal colloidal aggregation*, *Phys. Rev. E* **47**, 3768 (1993).
- [78] T. Narayanan, A. Kumar, E. S. R. Gopal, D. Beysens, P. Guenoun, and G. Zalczer, *Reversible flocculation of silica colloids in liquid mixtures*, *Phys. Rev. E* **48**, 1989 (1993).
- [79] M. L. Kurnaz and J. V. Maher, *Interaction of dilute colloidal particles in a mixed solvent*, *Phys. Rev. E* **51**, 5916 (1995).
- [80] M. L. Kurnaz and J. V. Maher, *Measurement of the second virial coefficient for the interaction of dilute colloidal particles in a mixed solvent*, *Phys. Rev. E* **55**, 572 (1997).
- [81] Y. Jayalakshmi and E. W. Kaler, *Phase Behavior of Colloids in Binary Liquid Mixtures*, *Phys. Rev. Lett.* **78**, 1379 (1997).
- [82] S. R. Kline and E. W. Kaler, *Colloidal Interactions in Water/2-Butoxyethanol Solvents*, *Langmuir* **10**, 412 (1994).
- [83] R. D. Koehler and E. W. Kaler, *Colloidal Phase Transitions in Aqueous Nonionic Surfactant Solutions*, *Langmuir* **13**, 2463 (1997).
- [84] H. Gröll and D. Woermann, *Stability of colloidal suspensions in a binary liquid mixture in the vicinity of its binodal curve*, *Ber. Bunsenges. Phys. Chem.* **101**, 814 (1997).
- [85] B. Rathke, H. Gröll, and D. Woermann, *Stability of Dilute Colloidal Silica Suspensions in the Vicinity of the Binodal Curve of the System 2-Butoxyethanol/Water*, *J. Colloid Interface Sci.* **192**, 334 (1997).
- [86] H. Guo, T. Narayanan, M. Sztuchi, P. Schall, and G. H. Wegdam, *Reversible Phase Transition of Colloids in a Binary Liquid Solvent*, *Phys. Rev. Lett.* **100**, 188303 (2008).

- [87] D. Bonn, J. Otwinowski, S. Sacanna, H. Guo, G. Wegdam, and P. Schall, *Direct Observation of Colloidal Aggregation by Critical Casimir Forces*, *Phys. Rev. Lett.* **103**, 156101 (2009); see also the comment in Ref. [88] and the reply in Ref. [89].
- [88] A. Gambassi and S. Dietrich, *Colloidal Aggregation and Critical Casimir Forces*, *Phys. Rev. Lett.* **105**, 059601 (2010); comment on Ref. [87], for reply see Ref. [89].
- [89] D. Bonn, G. Wegdam, and P. Schall, *Bonn, Wegdam, and Schall Reply:*, *Phys. Rev. Lett.* **105**, 059602 (2010); reply on the comment in Ref. [88].
- [90] S. J. Veen, O. Antoniuk, B. Weber, M. A. C. Potenza, S. Mazzoni, P. Schall, and G. H. Wegdam, *Colloidal Aggregation in Microgravity by Critical Casimir Forces*, *Phys. Rev. Lett.* **109**, 248302 (2012).
- [91] D. Beysens, J.-M. Petit, T. Narayanan, A. Kumar, and M. L. Broide, *Adsorption and wetting phenomena for colloids in liquid mixtures*, *Ber. Bunsenges. Phys. Chem.* **98**, 382 (1994).
- [92] A. Kumar and D. Beysens, *Phase transitions at interfaces: Flocculation of charge stabilised colloids in liquid mixtures*, *Physica A* **224**, 68 (1996).
- [93] D. Beysens and T. Narayanan, *Wetting-Induced Aggregation of Colloids*, *J. Stat. Phys.* **95**, 997 (1999).
- [94] Z. Király, L. Turi, I. Dékány, K. Bean, and B. Vincent, *Van der Waals attraction between Stöber silica particles in a binary solvent system*, *Colloid Polym. Sci.* **274**, 779 (1996).
- [95] S. Buzzaccaro, R. Rusconi, and R. Piazza, *"Sticky" Hard Spheres: Equation of State, Phase Diagram, and Metastable Gels*, *Phys. Rev. Lett.* **99**, 098301 (2007).
- [96] S. Buzzaccaro, J. Colombo, A. Parola, and R. Piazza, *Critical Depletion*, *Phys. Rev. Lett.* **105**, 198301 (2010).
- [97] R. Piazza, S. Buzzaccaro, A. Parola, and J. Colombo, *When depletion goes critical*, *J. Phys.: Condens. Matt.* **23**, 194114 (2011).
- [98] T. J. Sluckin, *Wetting phenomena and colloidal aggregation in binary mixtures*, *Phys. Rev. A* **41**, 960 (1990).
- [99] E. A. Boucher, *Critical wetting, flocculation of silica particles in near-critical lutidine-water mixtures and related phenomena*, *J. Chem. Soc., Faraday Trans.* **86**, 2263 (1990).
- [100] P. Attard, C. P. Ursenbach, and G. N. Patey, *Long-range attractions between solutes in near-critical fluids*, *Phys. Rev. A* **45**, 7621 (1992).

- [101] H. Löwen, *Solvent-Induced Phase Separation in Colloidal Fluids*, *Phys. Rev. Lett.* **74**, 1028 (1995).
- [102] R. R. Netz, *Colloidal Flocculation in Near-Critical Binary Mixtures*, *Phys. Rev. Lett.* **76**, 3646 (1996).
- [103] B. M. Law, J.-M. Petit, and D. Beysens, *Adsorption-induced reversible colloidal aggregation*, *Phys. Rev. E* **57**, 5782 (1998).
- [104] J. M. Petit, B. M. Law, and D. Beysens, *Adsorption-Induced Aggregation of Colloidal Particles in Binary Mixtures: Modeling the Pair Free Energy*, *J. Colloid Interface Sci.* **202**, 441 (1998).
- [105] R. Okamoto and A. Onuki, *Charged colloids in an aqueous mixture with a salt*, *Phys. Rev. E* **84**, 051401 (2011).
- [106] P. J. Mohr, B. N. Taylor, and D. B. Newell, *CODATA recommended values of the fundamental physical constants: 2006*, *J. Phys. Chem. Ref. Data* **37**, 1187 (2008); published also in *Rev. Mod. Phys.* **80**, 633 (2008), for online updates see <http://physics.nist.gov/constants>.
- [107] P. Becker, *History and progress in the accurate determination of the Avogadro constant*, *Rep. Prog. Phys.* **64**, 1945 (2001).
- [108] P. M. Chaikin and T. C. Lubensky, *Principles of condensed matter physics*, Cambridge University Press, Cambridge, 1995.
- [109] C. J. Thompson, *Mathematical statistical mechanics*, A series of books in applied mathematics, LinkMacmillan, New York, 1972.
- [110] L. D. Landau and E. M. Lifschitz, *Statistische Physik*, vol. 5 of *Lehrbuch der theoretischen Physik*, Akademie Verlag, Berlin, 1979.
- [111] R. B. Griffiths and J. C. Wheeler, *Critical Points in Multicomponent Systems*, *Phys. Rev. A* **2**, 1047 (1970).
- [112] P. H. V. Konynenburg and R. L. Scott, *Critical Lines and Phase Equilibria in Binary Van Der Waals Mixtures*, *Phil. Trans. Roy. Soc. London, Ser. A* **298**, 495 (1980).
- [113] B. Widom, *Theory of Phase Equilibrium*, *J. Phys. Chem.* **100**, 13190 (1996).
- [114] J. S. Walker and C. A. Vause, *Theory of closed-loop phase diagrams in binary fluid mixtures*, *Phys. Lett. A* **79**, 421 (1980).
- [115] J. S. Walker and C. A. Vause, *Lattice theory of binary fluid mixtures: Phase diagrams with upper and lower critical solution points from a renormalization-group calculation*, *J. Chem. Phys.* **79**, 2660 (1983).

- [116] T. Narayanan and A. Kumar, *Reentrant phase transitions in multicomponent liquid mixtures*, *Phys. Rep.* **249**, 135 (1994).
- [117] N. G. Almarza, *Closed-loop liquid-vapor equilibrium in a one-component system*, *Phys. Rev. E* **86**, 030101 (2012).
- [118] C. E. Bertrand, J. F. Nicoll, and M. A. Anisimov, *Comparison of complete scaling and a field-theoretic treatment of asymmetric fluid criticality*, *Phys. Rev. E* **85**, 031131 (2012).
- [119] J. Leys, P. Losada-Pérez, G. Cordoyiannis, C. A. Cerdeiriña, C. Glorieux, and J. Thoen, *Temperature, concentration, and frequency dependence of the dielectric constant near the critical point of the binary liquid mixture nitrobenzene-tetradecane*, *J. Chem. Phys.* **132**, 104508 (2010).
- [120] P. Ehrenfest, *Phasenumwandlungen im ueblichen und erweiterten Sinn, klassifiziert nach den entsprechenden Singularitaeten des thermodynamischen Potentials (Phase conversions in a general and enhanced sense, classified according to the specific singularities of the thermodynamic potential)*, *Proc. R. Acad. Sci. Amsterdam* **36**, 153 (1933); online available at the [KNAW Digital Library](http://www.dwc.knaw.nl/DL/publications/PU00016385.pdf), <http://www.dwc.knaw.nl/DL/publications/PU00016385.pdf>.
- [121] K. Binder, C. Billotet, and P. Mirolid, *On the theory of spinodal decomposition in solid and liquid binary mixtures*, *Z. Phys. B* **30**, 183 (1978).
- [122] K. Binder, *Spinodal Decomposition in Confined Geometry*, *J. Non-Equilib. Thermodyn.* **23**, 1 (1998).
- [123] M. E. Fisher, *The theory of equilibrium critical phenomena*, *Rep. Prog. Phys.* **30**, 615 (1967).
- [124] J. G. Brankov, D. M. Danchev, and N. S. Tonchev, *Theory of critical phenomena in finite-size systems: Scaling and quantum effects*, vol. 9 of *Series in modern condensed matter physics*, World Scientific, Singapore, 2000.
- [125] B. Widom, *Equation of State in the Neighborhood of the Critical Point*, *J. Chem. Phys.* **43**, 3898 (1965).
- [126] L. P. Kadanoff, W. Götze, D. Hamblen, R. Hecht, E. A. S. Lewis, V. V. Palciauskas, M. Rayl, J. Swift, D. Aspnes, and J. Kane, *Static Phenomena Near Critical Points: Theory and Experiment*, *Rev. Mod. Phys.* **39**, 395 (1967).
- [127] B. Widom, *Surface Tension and Molecular Correlations near the Critical Point*, *J. Chem. Phys.* **43**, 3892 (1965).
- [128] M. E. Fisher, *The renormalization group in the theory of critical behavior*, *Rev. Mod. Phys.* **46**, 597 (1974); **47**, 543 (1975).

- [129] F. J. Wegner, *Corrections to Scaling Laws*, *Phys. Rev. B* **5**, 4529 (1972).
- [130] A. Pelissetto and E. Vicari, *Critical phenomena and renormalization-group theory*, *Phys. Rep.* **368**, 549 (2002).
- [131] J. V. Sengers and M. R. Moldover, *Two-scale-factor universality near the critical point of fluids*, *Phys. Lett. A* **66**, 44 (1978).
- [132] V. Privman, P. C. Hohenberg, and A. Aharony, Universal critical-point amplitude relations, in *Phase Transitions and Critical Phenomena*, edited by C. Domb and J. L. Lebowitz, vol. 14, p. 1 and p. 364, Academic Press, London, New York, 1991.
- [133] H. Nakanishi and M. E. Fisher, *Multicriticality of Wetting, Prewetting, and Surface Transitions*, *Phys. Rev. Lett.* **49**, 1565 (1982).
- [134] S. Dietrich, *Structures in fluids induced by interfaces*, *J. Phys.: Condens. Matt.* **8**, 9127 (1996).
- [135] K. Binder and P. C. Hohenberg, *Phase Transitions and Static Spin Correlations in Ising Models with Free Surfaces*, *Phys. Rev. B* **6**, 3461 (1972).
- [136] K. Binder and P. C. Hohenberg, *Surface effects on magnetic phase transitions*, *Phys. Rev. B* **9**, 2194 (1974).
- [137] H. W. Diehl, *The Theory of Boundary Critical Phenomena*, *Int. J. Mod. Phys. B* **11**, 3503 (1997).
- [138] K. Binder, Critical behaviour at surfaces, in *Phase Transitions and Critical Phenomena*, edited by C. Domb and J. L. Lebowitz, vol. 8, p. 2, Academic Press, London, 1983.
- [139] H. W. Diehl, Field-theory of surface critical behaviour, in *Phase Transitions and Critical Phenomena*, edited by C. Domb and J. L. Lebowitz, vol. 10, p. 75, Academic Press, London, 1986.
- [140] T. C. Lubensky and M. H. Rubin, *Critical phenomena in semi-infinite systems. II. Mean-field theory*, *Phys. Rev. B* **12**, 3885 (1975).
- [141] A. J. Bray and M. A. Moore, *Critical behaviour of semi-infinite systems*, *J. Phys. A: Math.* **10**, 1927 (1977).
- [142] T. W. Burkhardt and H. W. Diehl, *Ordinary, extraordinary, and normal surface transitions: Extraordinary-normal equivalence and simple explanation of $|T - T_c|^{2 - \alpha}$ singularities*, *Phys. Rev. B* **50**, 3894 (1994).
- [143] H. W. Diehl and M. Smock, *Critical behavior at supercritical surface enhancement: Temperature singularity of surface magnetization and order-parameter profile to one-loop order*, *Phys. Rev. B* **47**, 5841 (1993); **48**, 6740 (1993).

- [144] D. L. Mills, *Surface Effects in Magnetic Crystals near the Ordering Temperature*, *Phys. Rev. B* **3**, 3887 (1971).
- [145] M. I. Kaganov and A. N. Omelyanchuk, *Phenomenological Theory of Phase Transitions in a Thin Ferromagnetic Plate*, *J. Exp. Theor. Phys. (JETP)* **34**, 895 (1972); English translation of *Zh. Éksp. Teor. Fiz.* **61**, 1679 (1971).
- [146] S. Alvarado, M. Campagna, and H. Hopster, *Surface Magnetism of Ni(100) near the Critical Region by Spin-Polarized Electron Scattering*, *Phys. Rev. Lett.* **48**, 51 (1982).
- [147] H. W. Diehl and S. Dietrich, *Scaling laws and surface exponents from renormalization group equations*, *Phys. Lett. A* **80**, 408 (1980).
- [148] H. W. Diehl and S. Dietrich, *Field-theoretical approach to static critical phenomena in semi-infinite systems*, *Z. Phys. B* **42**, 65 (1981).
- [149] P. Kumar, *Magnetic phase transition at a surface: Mean-field theory*, *Phys. Rev. B* **10**, 2928 (1974); **12**, 3984 (1975).
- [150] S. Leibler and L. Peliti, *Magnetisation profile in the presence of a surface magnetic field*, *J. Phys. C: Solid State Phys.* **15**, L403 (1982).
- [151] E. Brézin and S. Leibler, *Critical adsorption: The renormalization-group approach*, *Phys. Rev. B* **27**, 594 (1983).
- [152] U. Ritschel and P. Czerner, *Near-Surface Long-Range Order at the Ordinary Transition*, *Phys. Rev. Lett.* **77**, 3645 (1996).
- [153] P. Czerner and U. Ritschel, *Near-surface long-range order at the ordinary transition: scaling analysis and Monte Carlo results*, *Physica A* **237**, 240 (1997).
- [154] A. Ciach and U. Ritschel, *Critical adsorption in systems with weak surface field: The renormalization-group approach*, *Nucl. Phys. B* **489**, 653 (1997).
- [155] G. Flöter and S. Dietrich, *Universal amplitudes and profiles for critical adsorption*, *Z. Phys. B* **97**, 213 (1995).
- [156] A. Hanke and S. Dietrich, *Critical adsorption on curved objects*, *Phys. Rev. E* **59**, 5081 (1999).
- [157] T. Bieker and S. Dietrich, *Wetting of curved surfaces*, *Physica A* **252**, 85 (1998); **259**, 466 (1998).
- [158] M. Tröndle, L. Harnau, and S. Dietrich, *Critical adsorption and critical Casimir forces for geometrically structured confinements*, *J. Chem. Phys.* **129**, 124716 (2008).

- [159] M. Sprenger, F. Schlesener, and S. Dietrich, *Critical adsorption at chemically structured substrates*, *Phys. Rev. E* **71**, 056125 (2005).
- [160] M. Sprenger, *Kritische Phänomene auf chemisch strukturierten Substraten*, PhD thesis, University Stuttgart, Stuttgart, 2006, online available at OPUS the publication server of the University of Stuttgart, <http://elib.uni-stuttgart.de/opus/volltexte/2006/2804/>.
- [161] F. Parisen Toldin and S. Dietrich, *Critical Casimir forces and adsorption profiles in the presence of a chemically structured substrate*, *J. Stat. Mech.: Theory Exp.* **2010**, P11003 (2010).
- [162] L. D. Gelb, K. E. Gubbins, R. Radhakrishnan, and M. Sliwinska-Bartkowiak, *Phase separation in confined systems*, *Rep. Prog. Phys.* **62**, 1573 (1999).
- [163] K. Binder, J. Horbach, R. Vink, and A. De Virgiliis, *Confinement effects on phase behavior of soft matter systems*, *Soft Matter* **4**, 1555 (2008).
- [164] K. Binder, *Phase Transitions in Reduced Geometry*, *Annu. Rev. Phys. Chem.* **43**, 33 (1992).
- [165] S. Dietrich, *New physical phases induced by confinement*, *J. Phys.: Condens. Matt.* **10**, 11469 (1998).
- [166] A. J. Archer, R. Evans, R. Roth, and M. Oettel, *Solvent mediated interactions close to fluid-fluid phase separation: Microscopic treatment of bridging in a soft-core fluid*, *J. Chem. Phys.* **122**, 084513 (2005).
- [167] C. Gögelein, M. Brinkmann, M. Schröter, and S. Herminghaus, *Controlling the Formation of Capillary Bridges in Binary Liquid Mixtures*, *Langmuir* **26**, 17184 (2010).
- [168] V. Privman, Finite-size scaling theory, in *Finite Size Scaling and Numerical Simulation of Statistical Systems*, edited by V. Privman, p. 1, World Scientific, Singapore, 1990.
- [169] G. Caginalp and M. E. Fisher, *Wall and boundary free energies, II. General domains and complete boundaries*, *Commun. Math. Phys.* **65**, 247 (1979); see also M. E. Fisher and G. Caginalp, *Wall and boundary free energies, I. Ferromagnetic scalar spin systems*, *Commun. Math. Phys.* **56**, 11 (1977).
- [170] K. Binder, D. Landau, and M. Müller, *Monte Carlo Studies of Wetting, Interface Localization and Capillary Condensation*, *J. Stat. Phys.* **110**, 1411 (2003).
- [171] M. E. Fisher and H. Nakanishi, *Scaling theory for the criticality of fluids between plates*, *J. Chem. Phys.* **75**, 5857 (1981).

- [172] H. Nakanishi and M. E. Fisher, *Critical point shifts in films*, *J. Chem. Phys.* **78**, 3279 (1983).
- [173] R. Evans and U. M. B. Marconi, *Phase equilibria and solvation forces for fluids confined between parallel walls*, *J. Chem. Phys.* **86**, 7138 (1987).
- [174] A. O. Parry and R. Evans, *Influence of wetting on phase equilibria: A novel mechanism for critical-point shifts in films*, *Phys. Rev. Lett.* **64**, 439 (1990).
- [175] A. O. Parry and R. Evans, *Novel phase behaviour of a confined fluid or Ising magnet*, *Physica A* **181**, 250 (1992).
- [176] K. Binder, D. P. Landau, and A. M. Ferrenberg, *Character of the Phase Transition in Thin Ising Films with Competing Walls*, *Phys. Rev. Lett.* **74**, 298 (1995).
- [177] K. Binder, D. P. Landau, and A. M. Ferrenberg, *Thin Ising films with competing walls: A Monte Carlo study*, *Phys. Rev. E* **51**, 2823 (1995).
- [178] M. C. Stewart and R. Evans, *Phase behavior and structure of a fluid confined between competing (solvophobic and solvophilic) walls*, *Phys. Rev. E* **86**, 031601 (2012).
- [179] E. V. Albano and K. Binder, *Phase Coexistence in Nanoscopically Thin Films Confined by Asymmetric Walls*, *J. Stat. Phys.* **135**, 991 (2009).
- [180] E. Carlon and A. Drzewiński, *Effect of Gravity and Confinement on Phase Equilibria: A Density Matrix Renormalization Approach*, *Phys. Rev. Lett.* **79**, 1591 (1997).
- [181] E. Carlon and A. Drzewiński, *Critical point shift in a fluid confined between opposing walls*, *Phys. Rev. E* **57**, 2626 (1998).
- [182] L. Pang, D. P. Landau, and K. Binder, *Phase transitions in thin films with competing surface fields and gradients*, *Phys. Rev. E* **84**, 041603 (2011).
- [183] A. Maciołek, A. Ciach, and A. Drzewiński, *Crossover between ordinary and normal transitions in two dimensional critical Ising films*, *Phys. Rev. E* **60**, 2887 (1999).
- [184] A. Maciołek, R. Evans, and N. B. Wilding, *Effects of weak surface fields on the density profiles and adsorption of a confined fluid near bulk criticality*, *J. Chem. Phys.* **119**, 8663 (2003).
- [185] A. Maciołek, A. Drzewiński, and R. Evans, *Near-critical confined fluids and Ising films: Density-matrix renormalization-group study*, *Phys. Rev. E* **64**, 056137 (2001).
- [186] M. Krech and S. Dietrich, *Free energy and specific heat of critical films and surfaces*, *Phys. Rev. A* **46**, 1886 (1992).

- [187] M. Krech and S. Dietrich, *Specific heat of critical films, the Casimir force, and wetting films near critical end points*, *Phys. Rev. A* **46**, 1922 (1992).
- [188] R. Klimpel and S. Dietrich, *Structure factor of thin films near continuous phase transitions*, *Phys. Rev. B* **60**, 16977 (1999).
- [189] E. A. G. Jamie, R. P. A. Dullens, and D. G. A. L. Aarts, *Fluid–fluid demixing of off-critical colloid–polymer systems confined between parallel plates*, *J. Phys.: Condens. Matt.* **24**, 284120 (2012).
- [190] M. N. Barber, Finite-size scaling, in *Phase Transitions and Critical Phenomena*, edited by C. Domb and J. L. Lebowitz, vol. 8, p. 145, Academic Press, London, New York, 1983.
- [191] E. Brézin, *An investigation of finite size scaling*, *J. Phys. (Paris)* **43**, 15 (1982).
- [192] M. Krech and S. Dietrich, *Finite-size scaling for critical films*, *Phys. Rev. Lett.* **66**, 345 (1991); *ibid.* **67**, 1055 (1991).
- [193] M. Krech, *Fluctuation-induced forces in critical fluids*, *J. Phys.: Condens. Matt.* **11**, R391 (1999).
- [194] A. Maciołek and S. Dietrich, *Critical Casimir effect in ^3He - ^4He films*, *EPL* **74**, 22 (2006).
- [195] M. Krech, *Casimir forces in binary liquid mixtures*, *Phys. Rev. E* **56**, 1642 (1997).
- [196] A. Maciołek, A. Gambassi, and S. Dietrich, *Critical Casimir effect in superfluid wetting films*, *Phys. Rev. E* **76**, 031124 (2007).
- [197] R. Evans and J. Stecki, *Solvation force in two-dimensional Ising strips*, *Phys. Rev. B* **49**, 8842 (1994).
- [198] J. Rudnick, R. Zandi, A. Shackell, and D. Abraham, *Boundary conditions and the critical Casimir force on an Ising model film: Exact results in one and two dimensions*, *Phys. Rev. E* **82**, 041118 (2010).
- [199] A. Maciołek, A. Drzewiński, and P. Bryk, *Solvation force for long-ranged wall-fluid potentials*, *J. Chem. Phys.* **120**, 1921 (2004).
- [200] O. Vasilyev, A. Gambassi, A. Maciołek, and S. Dietrich, *Monte Carlo simulation results for critical Casimir forces*, *EPL* **80**, 60009 (2007).
- [201] O. Vasilyev, A. Gambassi, A. Maciołek, and S. Dietrich, *Universal scaling functions of critical Casimir forces obtained by Monte Carlo simulations*, *Phys. Rev. E* **79**, 041142 (2009); **80**, 039902 (2009).

- [202] M. Hasenbusch, *Thermodynamic Casimir effect for films in the three-dimensional Ising universality class: Symmetry-breaking boundary conditions*, *Phys. Rev. B* **82**, 104425 (2010).
- [203] Z. Borjan and P. J. Upton, *Order-Parameter Profiles and Casimir Amplitudes in Critical Slabs*, *Phys. Rev. Lett.* **81**, 4911 (1998).
- [204] Z. Borjan and P. J. Upton, *Off-Critical Casimir Effect in Ising Slabs with Symmetric Boundary Conditions in $d = 3$* , *Phys. Rev. Lett.* **101**, 125702 (2008).
- [205] M. E. Fisher and P. J. Upton, *Universality and interfaces at critical end points*, *Phys. Rev. Lett.* **65**, 2402 (1990).
- [206] M. E. Fisher and P. J. Upton, *Fluid interface tensions near critical end points*, *Phys. Rev. Lett.* **65**, 3405 (1990).
- [207] R. Okamoto and A. Onuki, *Casimir amplitudes and capillary condensation of near-critical fluids between parallel plates: Renormalized local functional theory*, *J. Chem. Phys.* **136**, 114704 (2012).
- [208] P. Nowakowski and M. Napiórkowski, *Scaling of solvation force in two-dimensional Ising strips*, *Phys. Rev. E* **78**, 060602 (2008).
- [209] P. Nowakowski and M. Napiorkowski, *Properties of the solvation force of a two-dimensional Ising strip in scaling regimes*, *J. Phys. A: Math.* **42**, 475005 (2009).
- [210] D. B. Abraham and A. Maciołek, *Casimir Interactions in Ising Strips with Boundary Fields: Exact Results*, *Phys. Rev. Lett.* **105**, 055701 (2010).
- [211] Z. Borjan, *Crossover behaviors in the Ising strips with changeable boundary conditions: Exact variational results*, *EPL* **99**, 56004 (2012).
- [212] M. Hasenbusch, *Thermodynamic Casimir force: A Monte Carlo study of the crossover between the ordinary and the normal surface universality class*, *Phys. Rev. B* **83**, 134425 (2011).
- [213] O. Vasilyev, A. Maciołek, and S. Dietrich, *Critical Casimir forces for Ising films with variable boundary fields*, *Phys. Rev. E* **84**, 041605 (2011).
- [214] T. F. Mohry, A. Maciołek, and S. Dietrich, *Crossover of critical Casimir forces between different surface universality classes*, *Phys. Rev. E* **81**, 061117 (2010).
- [215] F. M. Schmidt and H. W. Diehl, *Crossover from Attractive to Repulsive Casimir Forces and Vice Versa*, *Phys. Rev. Lett.* **101**, 100601 (2008).
- [216] H. W. Diehl and F. M. Schmidt, *The critical Casimir effect in films for generic non-symmetry-breaking boundary conditions*, *New J. Phys.* **13**, 123025 (2011).

- [217] M. Sprenger, F. Schlesener, and S. Dietrich, *Forces between chemically structured substrates mediated by critical fluids*, *J. Chem. Phys.* **124**, 134703 (2006).
- [218] A. Drzewiński, A. Maciołek, and A. Ciach, *Effect of bulk magnetic field on critical Ising films*, *Phys. Rev. E* **61**, 5009 (2000).
- [219] A. Maciołek, A. Drzewiński, and A. Ciach, *Crossover between ordinary and normal transitions in the presence of a bulk field*, *Phys. Rev. E* **64**, 026123 (2001).
- [220] A. Drzewiński, A. Maciołek, and R. Evans, *Influence of Capillary Condensation on the Near-Critical Solvation Force*, *Phys. Rev. Lett.* **85**, 3079 (2000).
- [221] A. Drzewiński, A. Maciołek, and A. Barasiński, *Solvation forces in Ising films with long-range boundary fields: density-matrix renormalization-group study*, *Mol. Phys.* **109**, 1133 (2011).
- [222] F. Schlesener, A. Hanke, and S. Dietrich, *Critical Casimir Forces in Colloidal Suspensions*, *J. Stat. Phys.* **110**, 981 (2003).
- [223] A. Hucht, *Thermodynamic Casimir Effect in ^4He Films near T_λ : Monte Carlo Results*, *Phys. Rev. Lett.* **99**, 185301 (2007).
- [224] M. Hasenbusch, *Specific heat, internal energy, and thermodynamic Casimir force in the neighborhood of the λ transition*, *Phys. Rev. B* **81**, 165412 (2010).
- [225] A. Hanke, F. Schlesener, E. Eisenriegler, and S. Dietrich, *Critical Casimir Forces between Spherical Particles in Fluids*, *Phys. Rev. Lett.* **81**, 1885 (1998).
- [226] F. Soyka, O. Zvyagolskaya, C. Hertlein, L. Helden, and C. Bechinger, *Critical Casimir Forces in Colloidal Suspensions on Chemically Patterned Surfaces*, *Phys. Rev. Lett.* **101**, 208301 (2008).
- [227] M. Hasenbusch, *Thermodynamic Casimir forces between a sphere and a plate: Monte Carlo simulation of a spin model*, *Phys. Rev. E* **87**, 022130 (2013).
- [228] S. Kondrat, L. Harnau, and S. Dietrich, *Critical Casimir interaction of ellipsoidal colloids with a planar wall*, *J. Chem. Phys.* **131**, 204902 (2009).
- [229] T. W. Burkhardt and E. Eisenriegler, *Casimir Interaction of Spheres in a Fluid at the Critical Point*, *Phys. Rev. Lett.* **74**, 3189 (1995).
- [230] B. Derjaguin, *Untersuchungen über die Reibung und Adhäsion, IV, Theorie des Anhaftens kleiner Teilchen*, *Kolloid Zeitschrift* **69**, 155 (1934).
- [231] M. Tröndle, *Statics and dynamics of critical Casimir forces*, PhD thesis, University Stuttgart, Stuttgart, 2012, online available at [OPUS](http://opus.uni-stuttgart.de/opus/volltexte/2012/7202/) the publication server of the University of Stuttgart, <http://opus.uni-stuttgart.de/opus/volltexte/2012/7202/>.

- [232] L. Onsager, *Crystal Statistics. I. A Two-Dimensional Model with an Order-Disorder Transition*, *Phys. Rev.* **65**, 117 (1944).
- [233] P. Christe and M. Henkel, *Introduction to conformal invariance and its applications to critical phenomena*, vol. 16 of *Lecture notes in physics: Monographs*, Springer, Berlin [among others], 1993.
- [234] K. G. Wilson, *Renormalization Group and Critical Phenomena. I. Renormalization Group and the Kadanoff Scaling Picture*, *Phys. Rev. B* **4**, 3174 (1971); *Renormalization Group and Critical Phenomena. II. Phase-Space Cell Analysis of Critical Behavior*, *ibid.* **4**, 3184 (1971).
- [235] J. Zinn-Justin, *Quantum Field Theory and Critical Phenomena*, vol. 123 of *International Series of Monographs on Physics*, Clarendon Press, Oxford, 4 ed., 2002.
- [236] K. Binder and E. Luijten, *Monte Carlo tests of renormalization-group predictions for critical phenomena in Ising models*, *Phys. Rep.* **344**, 179 (2001).
- [237] M. Hasenbusch, *Monte carlo studies of the three-dimensional Ising model in equilibrium*, *Int. J. Mod. Phys. C* **12**, 911 (2001).
- [238] K. Binder, *Applications of Monte Carlo methods to statistical physics*, *Rep. Prog. Phys.* **60**, 487 (1997).
- [239] K. Binder, Monte carlo investigations of phase transitions and critical phenomena, in *Phase Transitions and Critical Phenomena*, edited by C. Domb and J. L. Lebowitz, vol. 5b, Academic Press, London, 1976.
- [240] S. Fisk and B. Widom, *Structure and Free Energy of the Interface between Fluid Phases in Equilibrium near the Critical Point*, *J. Chem. Phys.* **50**, 3219 (1969).
- [241] Z. Borjan and P. J. Upton, *Local-functional theory of critical adsorption*, *Phys. Rev. E* **63**, 065102 (2001).
- [242] L. V. Mikheev and M. E. Fisher, *Exact variational analysis of layered planar Ising models*, *Phys. Rev. Lett.* **70**, 186 (1993).
- [243] L. V. Mikheev and M. E. Fisher, *Two-dimensional layered Ising models: Exact variational formulation and analysis*, *Phys. Rev. B* **49**, 378 (1994).
- [244] P. Schofield, *Parametric Representation of the Equation of State Near A Critical Point*, *Phys. Rev. Lett.* **22**, 606 (1969).
- [245] B. D. Josephson, *Equation of state near the critical point*, *J. Phys. C: Solid State Phys.* **2**, 1113 (1969).
- [246] A. Parola and L. Reatto, *Hierarchical reference theory of fluids and the critical point*, *Phys. Rev. A* **31**, 3309 (1985).

- [247] V. L. Ginzburg, *Some remarks on phase transitions of the second kind and the microscopic theory of ferroelectric materials*, Sov. Phys. Solid State **2**, 1824 (1960); English translation of Fiz. Tver. Tela **2**, 2031 (1960).
- [248] J.-C. Tolédano and P. Tolédano, *The Landau theory of phase transitions*, World Scientific, Singapore, New Jersey, Hong Kong, 1987.
- [249] J. Kuipers and E. M. Blokhuis, *Wetting and drying transitions in mean-field theory: Describing the surface parameters for the theory of Nakanishi and Fisher in terms of a microscopic model*, J. Chem. Phys. **131**, 044702 (2009).
- [250] E. Eisenriegler and M. Stapper, *Critical behavior near a symmetry-breaking surface and the stress tensor*, Phys. Rev. B **50**, 10009 (1994).
- [251] H. Au-Yang and M. E. Fisher, *Wall effects in critical systems: Scaling in Ising model strips*, Phys. Rev. B **21**, 3956 (1980).
- [252] M. E. Fisher, S.-Y. Zinn, and P. J. Upton, *Trigonometric models for scaling behavior near criticality*, Phys. Rev. B **59**, 14533 (1999); **64**, 149901 (2001).
- [253] S.-Y. Zinn and M. E. Fisher, *Scaling for interfacial tensions near critical endpoints*, Phys. Rev. E **71**, 011601 (2005).
- [254] H. B. Tarko and M. E. Fisher, *Theory of critical point scattering and correlations. III. The Ising model below T_c and in a field*, Phys. Rev. B **11**, 1217 (1975).
- [255] D. J. Wallace and R. K. P. Zia, *Parametric models and the Ising equation of state at order epsilon 3*, J. Phys. C: Solid State Phys. **7**, 3480 (1974).
- [256] P. Schofield, J. D. Litster, and J. T. Ho, *Correlation Between Critical Coefficients and Critical Exponents*, Phys. Rev. Lett. **23**, 1098 (1969).
- [257] Z. Borjan, *Application of local functional theory to surface critical phenomena*, PhD thesis, University of Bristol, Bristol, 1999.
- [258] M. E. Fisher and S.-Y. Zinn, *The shape of the van der Waals loop and universal critical amplitude ratios*, J. Phys. A: Math. **31**, L629 (1998).
- [259] J.-L. Barrat and J.-P. Hansen, *Basic concepts for simple and complex liquids*, Cambridge University Press, Cambridge, 2003.
- [260] H. Tanaka, *Viscoelastic phase separation in soft matter and foods*, Faraday Discuss. **158**, 371 (2012).
- [261] L. S. Ornstein and F. Zernike, *Accidental deviations of density and opalescence at the critical point of a single substance*, Proc. R. Acad. Sci. Amsterdam **17**, 793 (1914); online available at the KNAW Digital Library, <http://www.dwc.knaw.nl/DL/publications/PU00012727.pdf>.

- [262] J. P. Hansen and I. R. McDonald, *Theory of simple liquids*, Academic Press, 1976.
- [263] M. J. Gillan, *A new method of solving the liquid structure integral equations*, *Mol. Phys.* **38**, 1781 (1979).
- [264] C. Caccamo, *Integral equation theory description of phase equilibria in classical fluids*, *Phys. Rep.* **274**, 1 (1996).
- [265] J. Brader, *Solution of the Ornstein–Zernike Equation in the Critical Region*, *Int. J. Thermophys.* **27**, 394 (2006).
- [266] A. J. Archer and N. B. Wilding, *Phase behavior of a fluid with competing attractive and repulsive interactions*, *Phys. Rev. E* **76**, 031501 (2007).
- [267] G. A. Vliegenthart and H. N. W. Lekkerkerker, *Predicting the gas–liquid critical point from the second virial coefficient*, *J. Chem. Phys.* **112**, 5364 (2000).
- [268] M. G. Noro and D. Frenkel, *Extended corresponding-states behavior for particles with variable range attractions*, *J. Chem. Phys.* **113**, 2941 (2000).
- [269] R. J. Baxter, *Percus–Yevick Equation for Hard Spheres with Surface Adhesion*, *J. Chem. Phys.* **49**, 2770 (1968).
- [270] M. A. Miller and D. Frenkel, *Competition of Percolation and Phase Separation in a Fluid of Adhesive Hard Spheres*, *Phys. Rev. Lett.* **90**, 135702 (2003).
- [271] J. D. Weeks, D. Chandler, and H. C. Andersen, *Role of Repulsive Forces in Determining the Equilibrium Structure of Simple Liquids*, *J. Chem. Phys.* **54**, 5237 (1971).
- [272] H. C. Andersen, J. D. Weeks, and D. Chandler, *Relationship between the Hard-Sphere Fluid and Fluids with Realistic Repulsive Forces*, *Phys. Rev. A* **4**, 1597 (1971).
- [273] J. Jansen, C. de Kruif, and A. Vrij, *Attractions in sterically stabilized silica dispersions: III. Second virial coefficient as a function of temperature, as measured by means of turbidity*, *J. Colloid Interface Sci.* **114**, 492 (1986).
- [274] S. Xu and Z. Sun, *Progress in coagulation rate measurements of colloidal dispersions*, *Soft Matter* **7**, 11298 (2011).
- [275] N. Fuchs, *Über die Stabilität und Aufladung der Aerosole*, *Z. Phys.* **89**, 736 (1934); *Theory of coagulation*, *Z. Phys. Chem. Abt. A* **171**, 199 (1934).
- [276] E. P. Honig, G. J. Roeberson, and P. H. Wiersema, *Effect of hydrodynamic interaction on the coagulation rate of hydrophobic colloids*, *J. Colloid Interface Sci.* **36**, 97 (1971).

- [277] L. A. Spielman, *Viscous interactions in Brownian coagulation*, *J. Colloid Interface Sci.* **33**, 562 (1970).
- [278] R. Evans, *The nature of the liquid-vapour interface and other topics in the statistical mechanics of non-uniform, classical fluids*, *Adv. Phys.* **28**, 143 (1979).
- [279] R. Roth, *Fundamental measure theory for hard-sphere mixtures: a review*, *J. Phys.: Condens. Matt.* **22**, 063102 (2010).
- [280] J. M. Brader, R. Evans, and M. Schmidt, *Statistical mechanics of inhomogeneous model colloid-polymer mixtures*, *Mol. Phys.* **101**, 3349 (2003).
- [281] Y. Rosenfeld, *Free-energy model for the inhomogeneous hard-sphere fluid mixture and density-functional theory of freezing*, *Phys. Rev. Lett.* **63**, 980 (1989).
- [282] R. Roth, R. Evans, A. Lang, and G. Kahl, *Fundamental measure theory for hard-sphere mixtures revisited: the White Bear version*, *J. Phys.: Condens. Matt.* **14**, 12063 (2002).
- [283] H. Hansen-Goos and R. Roth, *Density functional theory for hard-sphere mixtures: the White Bear version mark II*, *J. Phys.: Condens. Matt.* **18**, 8413 (2006).
- [284] An unknown referee has drawn the attention to this issue in the report to Ref. [344].
- [285] S. Kondrat, 2012, preliminary data.
- [286] A. P. Gast, C. K. Hall, and W. B. Russel, *Polymer-induced phase separations in nonaqueous colloidal suspensions*, *J. Colloid Interface Sci.* **96**, 251 (1983).
- [287] U. Nellen, J. Dietrich, L. Helden, S. Chodankar, K. Nygard, J. Friso van der Veen, and C. Bechinger, *Salt-induced changes of colloidal interactions in critical mixtures*, *Soft Matter* **7**, 5360 (2011).
- [288] A. Ciach and A. Maciolek, *Distribution of ions near a charged selective surface in critical binary solvents*, *Phys. Rev. E* **81**, 041127 (2010).
- [289] F. Pousaneh and A. Ciach, *The origin of the attraction between like charged hydrophobic and hydrophilic walls confining a near-critical binary aqueous mixture with ions*, *J. Phys.: Condens. Matt.* **23**, 412101 (2011).
- [290] F. Pousaneh, A. Ciach, and A. Maciolek, *Effect of ions on confined near-critical binary aqueous mixture*, *Soft Matter* **8**, 3567 (2012).
- [291] M. Bier, A. Gambassi, M. Oettel, and S. Dietrich, *Electrostatic interactions in critical solvents*, *EPL* **95**, 60001 (2011).
- [292] M. Bier, A. Gambassi, and S. Dietrich, *Local theory for ions in binary liquid mixtures*, *J. Chem. Phys.* **137**, 034504 (2012).

- [293] M. A. Handschy, R. C. Mockler, and W. J. O'Sullivan, *Coexistence curve of 2,6-lutidine + water, near its lower critical point*, *Chem. Phys. Lett.* **76**, 172 (1980).
- [294] D. T. Jacobs, D. J. Anthony, R. C. Mockler, and W. J. O'Sullivan, *Coexistence curve of a binary mixture*, *Chem. Phys.* **20**, 219 (1977).
- [295] A. Ciach, *Universal sequence of ordered structures obtained from mesoscopic description of self-assembly*, *Phys. Rev. E* **78**, 061505 (2008).
- [296] R. F. Kayser, *Wetting of a binary liquid mixture on glass*, *Phys. Rev. B* **34**, 3254 (1986).
- [297] U. Nellen, *Kolloidale Wechselwirkungen in binären Flüssigkeiten*, PhD thesis, University Stuttgart, Stuttgart, 2011, online available at OPUS the publication server of the University of Stuttgart, <http://elib.uni-stuttgart.de/opus/volltexte/2011/6825>.
- [298] N. Gnan, E. Zaccarelli, P. Tartaglia, and F. Sciortino, *How properties of interacting depletant particles control aggregation of hard-sphere colloids*, *Soft Matter* **8**, 1991 (2012).
- [299] R. J. L. Andon and J. D. Cox, *896. Phase relationships in the pyridine series. Part I. The miscibility of some pyridine homologues with water*, *J. Chem. Soc.* **1952**, 4601 (1952).
- [300] B. V. Prafulla, T. Narayanan, and A. Kumar, *Light scattering near a double critical point: Evidence for crossover behavior*, *Phys. Rev. A* **45**, 1266 (1992).
- [301] B. V. Prafulla, T. Narayanan, and A. Kumar, *Double-critical-point phenomena in three-component liquid mixtures: Light-scattering investigations*, *Phys. Rev. A* **46**, 7456 (1992).
- [302] D. Mukamel and M. Blume, *Ising model for tricritical points in ternary mixtures*, *Phys. Rev. A* **10**, 610 (1974).
- [303] J. Sivardière and J. Lajzerowicz, *Spin-1 lattice-gas model. II. Condensation and phase separation in a binary fluid*, *Phys. Rev. A* **11**, 2090 (1975).
- [304] J. Sivardière and J. Lajzerowicz, *Spin-1 lattice-gas model. III. Tricritical points in binary and ternary fluids*, *Phys. Rev. A* **11**, 2101 (1975).
- [305] M. Schmidt, H. Löwen, J. M. Brader, and R. Evans, *Density functional theory for a model colloid-polymer mixture: bulk fluid phases*, *J. Phys.: Condens. Matt.* **14**, 9353 (2002).
- [306] M. Schmidt, *Density functional for ternary non-additive hard sphere mixtures*, *J. Phys.: Condens. Matt.* **23**, 415101 (2011).

- [307] O. Zvyagolskaya, A. J. Archer, and C. Bechinger, *Criticality and phase separation in a two-dimensional binary colloidal fluid induced by the solvent critical behavior*, *EPL* **96**, 28005 (2011).
- [308] M. Dijkstra, J. M. Brader, and R. Evans, *Phase behaviour and structure of model colloid-polymer mixtures*, *J. Phys.: Condens. Matt.* **11**, 10079 (1999).
- [309] S. Kondrat and M. Tröndle, *F3DM - a numerical library for the 3d finite element method*, unpublished documentation for the F3DM library and tools.
- [310] N. Gnan, E. Zaccarelli, and F. Sciortino, *Tuning effective interactions close to the critical point in colloidal suspensions*, *J. Chem. Phys.* **137**, 084903 (2012).
- [311] A. Gambassi and S. Dietrich, *Critical Dynamics in Thin Films*, *J. Stat. Phys.* **123**, 929 (2006).
- [312] M. Marcuzzi, A. Gambassi, and M. Pleimling, *Collective non-equilibrium dynamics at surfaces and the spatio-temporal edge*, *EPL* **100**, 46004 (2012).
- [313] T. G. Mattos, L. Harnau, and S. Dietrich, *Many-body effects for critical Casimir forces*, *J. Chem. Phys.* **138**, 074704 (2013).
- [314] A. J. Archer and R. Evans, *Solvent-mediated interactions and solvation close to fluid-fluid phase separation: A density functional treatment*, *J. Chem. Phys.* **118**, 9726 (2003).
- [315] M. Schmidt, A. R. Denton, and J. M. Brader, *Fluid demixing in colloid-polymer mixtures: Influence of polymer interactions*, *J. Chem. Phys.* **118**, 1541 (2003).
- [316] M. A. Annunziata and A. Pelissetto, *Colloids and polymers in random colloidal matrices: Demixing under good-solvent conditions*, *Phys. Rev. E* **86**, 041804 (2012).
- [317] F. Lo Verso, R. L. C. Vink, D. Pini, and L. Reatto, *Critical behavior in colloid-polymer mixtures: Theory and simulation*, *Phys. Rev. E* **73**, 061407 (2006).
- [318] A. Ciach, W. T. Gózdź, and G. Stell, *Field theory for size- and charge-asymmetric primitive model of ionic systems: Mean-field stability analysis and pretransitional effects*, *Phys. Rev. E* **75**, 051505 (2007).
- [319] O. Patsahan and I. Mryglod, *The method of collective variables: a link with the density functional theory*, *Condens. Matter Phys.* **15**, 24001 (2012).
- [320] M. Labbé-Laurent, *Janus-Teilchen in kritischen Flüssigkeiten*, Master's thesis, University Stuttgart, Stuttgart, 2012.
- [321] M. Bier and L. Harnau, *The Structure of Fluids with Impurities*, *Z. Phys. Chem.* **226**, 814 (2012).

- [322] F. Ferri, B. J. Frisken, and D. S. Cannell, *Structure of silica gels*, *Phys. Rev. Lett.* **67**, 3626 (1991).
- [323] B. J. Frisken, F. Ferri, and D. S. Cannell, *Effect of dilute silica gel on phase separation of a binary mixture*, *Phys. Rev. Lett.* **66**, 2754 (1991).
- [324] X. Lu, S. G. J. Mochrie, S. Narayanan, A. R. Sandy, and M. Sprung, *Temperature-dependent structural arrest of silica colloids in a water-lutidine binary mixture*, *Soft Matter* **6**, 6160 (2010).
- [325] R. L. C. Vink, *Critical behavior of soft matter fluids in bulk and in random porous media: from Ising to random-field Ising universality*, *Soft Matter* **5**, 4388 (2009).
- [326] V. Voronov and V. Buleiko, *Experimental investigation of the behavior of the specific heat in finite systems in the vicinity of the critical mixing point*, *J. Exp. Theor. Phys. (JETP)* **86**, 586 (1998); English translation of *Zh. Éksp. Teor. Fiz.* **113**, 1071 (1998).
- [327] T. P. C. van Noije, M. H. Ernst, E. Trizac, and I. Pagonabarraga, *Randomly driven granular fluids: Large-scale structure*, *Phys. Rev. E* **59**, 4326 (1999).
- [328] R. Brito, R. Soto, and U. Marconi, *Casimir forces in granular and other non equilibrium systems*, *Granular Matter* **10**, 29 (2007).
- [329] M. R. Shaebani, J. Sarabadani, and D. E. Wolf, *Nonadditivity of Fluctuation-Induced Forces in Fluidized Granular Media*, *Phys. Rev. Lett.* **108**, 198001 (2012).
- [330] N. R. Bernardino and S. Dietrich, *Complete wetting of elastically responsive substrates*, *Phys. Rev. E* **85**, 051603 (2012).
- [331] G. A. Pilkington and W. H. Briscoe, *Nanofluids mediating surface forces*, *Adv. Colloid Interface Sci.* **179**, 68 (2012).
- [332] M. Rauscher and S. Dietrich, *Wetting Phenomena in Nanofluidics*, *Annu. Rev. Material Res.* **38**, 143 (2008).
- [333] Wolfram Research, Mathematica (®), <http://www.wolfram.com/mathematica/>.
- [334] E. Brézin and S. Feng, *Amplitude of the surface tension near the critical point*, *Phys. Rev. B* **29**, 472 (1984).
- [335] M. Tröndle, *Critical Casimir forces in a film: stripes vs. homogeneous wall - MFT results*, unpublished notes, 2012.
- [336] C. A. Grattoni, R. A. Dawe, C. Y. Seah, and J. D. Gray, *Lower critical solution coexistence curve and physical properties (density, viscosity, surface tension, and interfacial tension) of 2,6-lutidine + water*, *J. Chem. Eng. Data* **38**, 516 (1993).
- [337] Gnu Scientific Library, <http://www.gnu.org/software/gsl/>.

- [338] Gnuplot, <http://www.gnuplot.info/>.
- [339] Drawing program xfig, <http://www.xfig.org/>.
- [340] Gnu emacs text editor, <http://www.gnu.org/software/emacs/>.
- [341] Kile - an integrated latex environment, <http://kile.sourceforge.net/>.
- [342] Comprehensive TeX Archive Network, <http://www.ctan.org>.
- [343] E. Niedermair and M. Niedermair, *LATEX: das Praxisbuch*, Franzis, Poing, 3. ed., 2006.
- [344] T. F. Mohry, A. Maciołek, and S. Dietrich, *Phase behavior of colloidal suspensions with critical solvents in terms of effective interactions*, *J. Chem. Phys.* **136**, 224902 (2012).

T. F. Mohry:

Phase behavior of colloidal suspensions with critical solvents

